

# **ANALYSIS AND EVALUATION OF A REUSABLE ENGINE PACKAGING SYSTEM**



Submitted as a requirement for the degree of  
Master of Engineering

by

Nabih M. Tawfik

Supervisor

Associate Professor Michael Sek

Victoria University of Technology  
Faculty of Engineering and Science  
Department of Mechanical Engineering

August 1997

## ABSTRACT

The research work presented in this thesis is concerned with evaluating a newly designed reusable engine packaging system which has been proposed by the Holden Engine Company for transporting engines manufactured in Australia to the Opel Company in Germany.

A description of the experimental analysis carried out in order to obtain the data required to validate the Finite Element (FE) model is given. The selection of material properties and boundary conditions for modelling the engine rack prototype was undertaken prior to comparing the FE model with the set of obtained experimental data.

Simulated environmental conditions were used to predict the response of the rack in terms of engine displacement at the points of contact with the rack and the energy transfer to the engine due to a parameterised shock.

The measurements, theoretical analysis and simulation studies described in this project illustrate a general procedure that may be used to evaluate new engine packaging system designs or modifications to existing design.

## Acknowledgments

I am indebted to many people for their help and support throughout this study. First of all, I would like to express my gratefulness to Associate Professor Michael Sek, the principal supervisor of this research, for the continuous guidance and encouragement that he has given me over the period in which the research has been carried out.

Also I would like thank the following people for their generous support and assistance during this project : from Holden's Engine Company - Graham Docker, Robert Restuccia and Garry Stevens, from the Department of Mechanical Engineering at Victoria University - Professor Geoffrey Lleonart, Associate Professor Kevin Duke, Dr Jimmin He, Vincent Rouillard, Ben Bruscella, David Ip, Denise Colledge, Marlene Schutt and my office colleagues Clyde Lindridge, Robert Winduss and Horst Heilmayr.

Finally, I would like to express my deep appreciation to my wife Amar, my children Benjamin, Carol and Claire for their generous support and encouragement which provided me with faith and persistence to complete this research.

# Contents

<b>1. Introduction</b>	<b>1</b>
<b>2. Literature Review</b>	<b>8</b>
<b>2.1 Shock and Vibration</b>	<b>8</b>
2.1.1 Shock and Vibration in Transportation Environment	8
2.1.2 Transportation Hazards	19
2.1.3 Experimental Analysis	37
2.1.4 Frequency Response Function Method	38
<b>2.2 Finite Element Method</b>	<b>42</b>
2.2.1 The Finite Element Method	42
2.2.2 Finite Element Static and Dynamic Analysis	43
2.2.3 Structural Static Analysis	45
2.2.4 Modal	46
2.2.5 Natural Frequency	46
2.2.6 Harmonic Response	47
2.2.7 Transient Dynamics	48
2.2.8 Finite Element Damping	49
2.2.9 Response Spectrum	50
<b>2.3 Finite Element Verification and Validation</b>	<b>56</b>
2.3.1 Finite Element Verification	56
2.3.2 The Finite Element Validation	59
2.3.3 Identification of Differences between Finite Element Analysis and Experiment Data	61
2.3.4 Methods of Model Updating	64
<b>3. Aims</b>	<b>73</b>
<b>4. Results and Discussion of Finite Element Analysis</b>	<b>74</b>
<b>4.1 Experimental Evaluation</b>	<b>74</b>
4.1.1 Excitation Signal	75
4.1.2 Excitation of the Structure	77

4.1.3 Experimental Equipment	79
4.1.4 Experiment Setup and Results	80
<b>4.2 FEA Modelling Strategy</b>	<b>89</b>
4.2.1 Type of Elements	90
4.2.2 Size and Number of Elements	90
4.2.3 Finite Element Analysis	90
4.2.4 Material Properties Selection	92
4.2.5 Finite Element Natural Frequency	98
4.2.6 Finite Element Mode Shapes	100
4.2.7 Finite Element Frequency Response Function	104
<b>4.3 Comparisons and Validation</b>	<b>111</b>
4.3.1 Comparisons of Natural Frequencies	111
4.3.2 Comparison of FRF's	113
4.3.3 Displacement Comparisons	117
<b>4.4 Summarising Remarks</b>	<b>122</b>
<b>5. Results and Discussion of Dynamic Analysis</b>	<b>124</b>
<b>5.1 Natural Frequency</b>	<b>126</b>
5.1.1 Natural Frequency Analysis	126
<b>5.2 Harmonic Response</b>	<b>132</b>
5.2.1 Harmonic Response Analysis	133
<b>5.3 Random Vibration</b>	<b>138</b>
5.3.1 Spectral Response	138
5.3.2 Spectral Response Analysis	140
5.3.3 Spectral Response in Vertical Direction only	140
5.3.4 Spectral Response in Three Orthogonal Directions	144
<b>5.4 Transient Dynamic</b>	<b>148</b>
5.4.1 Simulated Half-Sine Shock	148
5.4.2 Transient Response Analysis	152
<b>5.5 Summarising Remarks</b>	<b>166</b>

<b>6. Conclusions and Recommendations</b>	<b>168</b>
6.1 Conclusions	168
6.2 Recommendations	170
<b>References</b>	<b>171</b>
<b>Appendices</b>	<b>182</b>

## List of Figures

Figure 1-1 Layout of the engine rack	3
Figure 1-2 Engine rack stacked in three tiers	4
Figure 1-3 Collapsed engine racks	5
Figure 2-1 Examples of shocks time functions and their FT (amplitude spectra)	14
Figure 2-2 Vibration acceleration envelope for : land, sea, and air	20
Figure 2-3 Commercial transport random vibration spectra	21
Figure 2-4 Cargo environment for highway transport	23
Figure 2-5 Route comparison leaf spring truck vertical vibration	24
Figure 2-6 Sample truck vibration test profiles	25
Figure 2-7 Vertical vibration level in trucks	26
Figure 2-8 Cargo environments for rail transport	29
Figure 2-9 Vibration acceleration spectra envelope for railcars	30
Figure 2-10 Vibration levels in rail shipments	30
Figure 2-11 Longitudinal impact in railcars	31
Figure 2-12 Lateral impact in railcars	31
Figure 2-13 Cargo environments for sea transport	34
Figure 2-14 Cargo environments for air transport	36
Figure 2-15 System with input signal $a(t)$ and output signal $b(t)$	39
Figure 2-16 Finite element model	58
Figure 2-17 Transient contact force	58
Figure 2-18 Transient contact velocity response	59
Figure 4-1 Schematic diagram to the test arrangement	81
Figure 4-2 Prototype No H4185 layout	82
Figure 4-3 Experimental FRF (H5,1)	83
Figure 4-4 Experimental FRF (H6,1)	83
Figure 4-5 Experimental FRF (H7,1)	84
Figure 4-6 Experimental FRF (H8,1)	84
Figure 4-7 Experimental FRF (H5,1)	85
Figure 4-8 Experimental FRF (H6,1)	85
Figure 4-9 Experimental FRF (H7,1)	86
Figure 4-10 Experimental FRF (H8,1)	86

Figure 4-11 Prototype No H4185	94
Figure 4-12 Prototype No H4185 layout	95
Figure 4-13 FE model arrangement	98
Figure 4-14 Engine rack mode shapes from : Mode 1 to 4	100
Figure 4-15 Engine rack mode shapes from : Mode 5 to 8	101
Figure 4-16 Engine rack mode shapes from : Mode 8 to 12	102
Figure 4-17 Engine rack mode shapes from : Mode 13 to 16	103
Figure 4-18 Engine rack mode shapes for : Mode 17	104
Figure 4-19 FE arrangement to obtain FRF of the engine rack	106
Figure 4-20 Finite element FRF (H224,333)	107
Figure 4-21 Finite element FRF (H265,333)	107
Figure 4-22 Finite element FRF (H380,333)	108
Figure 4-23 Finite element FRF (H411,333)	108
Figure 4-24 Finite element FRF (H224,333)	109
Figure 4-25 Finite element FRF (H265,333)	109
Figure 4-26 Finite element FRF (H380,333)	110
Figure 4-27 Finite element FRF (H411,333)	110
Figure 4-28 Comparison of the natural frequency of experimental vs FEA	112
Figure 4-29 FRF overlay experimental and FE (H7,1) and (H224,333)	113
Figure 4-30 FRF overlay experimental and FE (H6,1) and (H265,333)	113
Figure 4-31 FRF overlay experimental and FE (H8,1) and (H380,333)	114
Figure 4-32 FRF overlay experimental and FE (H5,1) and (H411,333)	114
Figure 4-33 FRF overlay experimental and FE (H7,1) and (H224,333)	115
Figure 4-34 FRF overlay experimental and FE (H6,1) and (H265,333)	116
Figure 4-35 FRF overlay experimental and FE (H8,1) and (H380,333)	116
Figure 4-36 FRF overlay experimental and FE (H5,1) and (H411,333)	117
Figure 5-1 FEM used for simulation	125
Figure 5-2 Mode shapes of the loaded rack : Mode 1 to 4	127
Figure 5-3 Mode shapes of the loaded rack : Mode 5 to 8	128
Figure 5-4 Mode shapes of the loaded rack : Mode 9 to 12	129
Figure 5-5 Mode shapes of the loaded rack : Mode 13 to 16	130
Figure 5-6 Mode shapes of the loaded rack : Mode 17 to 20	131
Figure 5-7 FE harmonic response loading simulation	132

Figure 5-8 Harmonic response displacement magnitude at node 224	133
Figure 5-9 Harmonic response displacement magnitude at node 265	133
Figure 5-10 Harmonic response displacement magnitude at node 380	134
Figure 5-11 Harmonic response displacement magnitude at node 411	134
Figure 5-12 Harmonic response displacement magnitude at node 224	135
Figure 5-13 Harmonic response displacement magnitude at node 265	135
Figure 5-14 Harmonic response displacement magnitude at node 380	136
Figure 5-15 Harmonic response displacement magnitude at node 411	136
Figure 5-16 Commercial transport random vibration PSD	139
Figure 5-17 Commercial transport random vibration PSD	140
Figure 5-18 Various shock pulses	150
Figure 5-19 Acceleration spectrum of a shock signals (5 g,70 ms, e=0.2)	151
Figure 5-20 Acceleration spectrum of a shock signal (36 g, 10 ms, e=0.3)	152
Figure 5-21 Displacement response at node 224 to a shock (36 g, 10 ms, e=0.3)	153
Figure 5-22 Acceleration response at node 224 to a shock (36 g, 10 ms, e=0.3)	153
Figure 5-23 Displacement response of node 224 to 5 g,70 ms, e=0.2	154
Figure 5-24 Displacement response of node 224 to 36g, 10 ms, e=0.3	154
Figure 5-25 Displacement energy transferred at node 224	158
Figure 5-26 Displacement energy transferred at node 265	158
Figure 5-27 Displacement energy transferred at node 380	159
Figure 5-28 Displacement energy transferred at node 411	159
Figure 5-29 Displacement ESD values transferred through node 224	161
Figure 5-30 Displacement ESD values transferred through node 265	161
Figure 5-31 Displacement ESD values transferred through node 380	162
Figure 5-32 Displacement ESD values transferred through node 411	162
Figure 5-33 Maximum displacement response at node 224	163
Figure 5-34 Maximum displacement response at node 265	163
Figure 5-35 Maximum displacement response at node 380	164
Figure 5-36 Maximum displacement response at node 411	164

## List of Tables

Table 2-1 Cargo - handling field test result: Peak Acceleration (g)	18
Table 2-2 PC based finite element packages	43
Table 2-3 PC based finite element packages comparison	44
Table 4-1 Characteristics summary of excitation signals	77
Table 4-2 Receptance relationships for H5,1	87
Table 4-3 Receptance relationships for H6,1	87
Table 4-4 Receptance relationships for H7,1	88
Table 4-5 Receptance relationships for H8,1	88
Table 4-6 Natural frequency comparison of different type of elements	96
Table 4-7 The FE predicted natural frequencies	99
Table 4-8 Receptance at resonant modes for the FEM	111
Table 4-9 Comparison of the natural frequency of experimental vs FEA	112
Table 4-10 Receptance comparison : Node 7 vs 224	118
Table 4-11 Receptance comparison : Node 6 vs 265	119
Table 4-12 Receptance comparison : Node 8 vs 380	120
Table 4-13 Receptance comparison : Node 5 vs 411	121
Table 5-1 The first 20 natural frequencies	126
Table 5-2 Modes and displacement relationship at nodes of contact	137
Table 5-3 Spectral Value	141
Table 5-4 Seismic excitation factors and mass participation factors	141
Table 5-5 Maximum displacements amplitude due to vertical excitation	142
Table 5-6 Nodal displacement at natural frequencies	143
Table 5-7 Maximum nodal and plate stress for vertical excitation	143
Table 5-8 Spectral Value	144
Table 5-9 Seismic excitation factors and mass participation factors	145
Table 5-10 Maximum displacements amplitude due to three orthogonal excitation directions	145
Table 5-11 Nodal maximum displacement at natural frequencies	146
Table 5-12 Maximum nodal and plate stress for X, Y, and Z	147
Table 5-13 Displacement energy transferred at nodes 224, 265, 380 and 411	156
Table 5-14 Maximum energy at contact nodes	160

Table 5-15 ESD values at natural frequencies	165
Table 5-16 Nodal displacement at natural frequencies	165

## Symbols and Abbreviations

$\{F(t)\}$	Time dependent load vector
$\{F\}$	Matrix of forces at each node, can include concentrated force
$[K]$	Stiffness matrix
$[M]$	Mass matrix
$\{r\}$	Influence vector
$\{R\}$	Load vector
$\{P\}$	Force applied at model at any time
$\{x\}_i$	Modal displacement for $i^{\text{th}}$ mode
$\{x\}$	Displacement vector, at each node
$\{\ddot{x}\}$	Acceleration vector, at each node
$\{\dot{x}\}$	Velocity vector
$t$	Time
$F_0$	Force amplitude at a known frequency $\omega$
$m$	Number of modes
$N$	Number of degrees of freedom
$n$	Number of coordinates
$X$	Experimental
$U$	Updated
$f$	Frequency in Hz
$A$	Analytical
SRSS	Square Root of Sum of the Squares
CQC	Complete Quadratic Combination
$S$	Spectral value from the associated spectral tables
$L_i$	Seismic excitation factor for $i^{\text{th}}$ mode
$Y_i$	Displacement amplitude for $i^{\text{th}}$ mode
$S_i$	Spectral value for $i^{\text{th}}$ mode
$L_j$	Seismic excitation factor for $i^{\text{th}}$ mode
$H(\omega)$	Frequency Response Function
PSD	Power Spectral Density
$S(\omega)$	PSD input
ASTM	American Society for Testing and Material

CSIRO	Commonwealth Scientific and Industrial Research Organisation
E	Modulus of elasticity (Young's modulus)
FFT	Fast Fourier Transform
FE	Finite Element
FEM	Finite Element Model
FEA	Finite Element Analysis
FRF	Frequency Response Function
IMAC	International Modal Analysis Conference.
RMS	Root Mean Squares
HEC	Hoden Engine Company
J	Torsion constant
G	Shear modulus
LVT	Load vs time table
Grms	Measure of the overall acceleration level of the PSD spectrum.
$F_2$	The higher - frequency point on the PSD plot (Hz)
$F_1$	The lower - frequency point on the PSD plot (Hz)
ESD	Energy Spectral Density
PSD	Power Spectral Density
$PSD_2$	The PSD value at frequency $F_2$
$PSD_1$	The PSD value at frequency $F_1$ .
dB	Logarithmic scale.
$S_{AA}(f)$	Instantaneous Autospectrum of A
$S_{BB}(f)$	Instantaneous Autospectrum of B
$S_{AB}(f)$	Cross spectrum from A & B
$S_{BA}(f)$	Cross spectrum from B & A
$G_{AA}(f)$	Average autospectrum
$G_{AB}(f)$	Average cross spectrum from A to B
$G_{BB}(f)$	Average autospectrum
$\Delta t$	Discrete time step
$[I(\omega)]$	Inertance matrix
$[I]$	Unit matrix
$I_{ij}(\omega)$	Inertance FRF
$\alpha_{ij}(\omega)$	Receptance FRF

$[\alpha(\omega)]$	Receptance matrix
$\{\phi\}$ $[\Phi]$	Mass normalised eigenvector, matrix
$\lambda, [\lambda]$	Eigenvalue, diagonal eigenvalue matrix
$i, j$	Coordinate indices
$\omega$	Natural Frequency = $2\pi f$ where $f$ is frequency in Hz
$\omega_1$	Lowest natural frequency of the structure
$\omega_2$	Maximum natural frequency of interest in structure.
$\alpha$ & $\beta$	Constants determined by choosing the damping ratios ( $\xi_1, \xi_2$ )
$\phi$	Phase angle
$\sigma$	Population standard deviation
$\omega_i$	Circular frequency for $i^{\text{th}}$ mode
$\{\phi\}_i$	Eigenvector for $i^{\text{th}}$ mode
$\rho_{ij}$	Coefficient dependent on modal damping and frequencies
$I_{11}$	Second moment of area about 1 axis
$I_{22}$	Second moment of area about 2 axis
$\rho$	Mass density
$\nu$	Poisson's ratio
$\alpha_{ij}$	Receptance
$\omega_r$	Natural frequency of $r^{\text{th}}$ mode
$\eta_r$	Damping loss factor of $r^{\text{th}}$ mode
$\bar{\omega}$	Undamped natural frequency
$[\bar{\phi}]$	Mass normalised mode shapes
$\gamma^2$	Coherence

# 1. Introduction

Holden Engine Company (HEC) in Australia, is exporting approximately 600 fully assembled engines per day to the Opel car company in Germany and the Vauxhall car company in England. Consequently, the HEC is obliged to comply with all legislation applying to the packaging system it uses to protect its products in the countries to which it exports.

In recent years, the countries which comprise the European Union have progressed significantly towards reducing the amount of waste generated from disposable packaging material. According to Lox (1992), by the year 2000, these countries expect to be removing 90% by weight of all the packaging materials in their waste stream and recycling 60% by weight of each type of packaging material.

Current legislation in Germany is aimed at converting 80% of the country's annual 11 million tonnes of packaging and other waste into valuable products and secondary raw material, Rummler and Schutt (1993). In order to achieve this objective, the German government has adopted policies aimed at reducing packaging waste and at encouraging the return of used packaging material for re-processing. Laws covering "take back obligation" have been introduced, and in some instances, mandatory deposits are imposed in order to provide an incentive for packaging to be returned to its place of origin, Cutter (1990). A waste tax law has imposed a tax on any material incinerated or dumped in landfills. This tax is in addition to the cost of disposal.

The Opel car company in Germany requires its suppliers to comply with the following guidelines, that all packaging must be:

- restricted to be the minimum amount required for protection,
- reusable and/or made from reusable/recyclable material,
- returnable, with a supplier's responsibility to take back all packaging.

A preliminary investigation of the current method of packaging and shipping engines from HEC in Australia to Opel in Germany has been conducted by the HEC Quality Assurance Department, Bird and Freeman (1993). Currently, fully assembled engines

are enclosed in plastic engine bags, packaged into corrugated fibreboard boxes, stacked on non-returnable wooden pallets and transported in steel shipping containers. This method of packaging costs \$2.3 million per year, based on four engines per box, plus \$5.3 million per year for shipping and insurance. The existing system is responsible for producing approximately 80,000 corrugated fibreboard boxes and 80,000 wooden pallets per year that require disposal. The waste generated exclusively by the HEC in the European market is about 1600 tonnes per year. In addition to the environmental issues associated with the existing method of packaging, the corrugated fibreboard boxes often collapse and result in damage. It is estimated that 3% to 5% of exported engines are damaged in shipment.

The CSIRO Food Research Laboratory in New South Wales, Sharp (1992), has investigated the current method of engine packaging for export by the HEC. The investigation concluded that the unsatisfactory performance of the existing packaging system could be caused by the following factors:

- Unseasoned hardwood which is used as part of the packaging may contain up to 50% moisture. During the voyage this moisture migrates into the fibreboard, depriving the carton and its internal supporting members of their strength.
- Collapse of the cartons allows the upper pallets to rest directly on the engines in the lower layer, causing mechanical damage to unprotected engine components. This collapse can also tear the plastic engine bags, thus permitting moisture in the atmosphere within the container to reach any exposed cast iron or alloy components, causing them to corrode.

In order to overcome the problems associated with the existing packaging system, the HEC has proposed a new reusable system composed of collapsible steel racks. These steel racks will be loaded with engines and transported to their overseas destination, where the engines will be removed and the racks are knocked down and stacked for the return journey to Australia.

Figure 1-1 shows the layout of the rack developed by HEC design group, Tawfik (1992). The racks shown in Figure 1-2 enable engines to be stacked in three tiers in a

20 ft container. This represents a 50% improvement in storage and shipping costs compared to the current corrugated packaging system. The rack can be collapsed by a ratio of 4:1 to improve volumetric efficiency of transportation on return to Australia as shown in Figure 1-3.

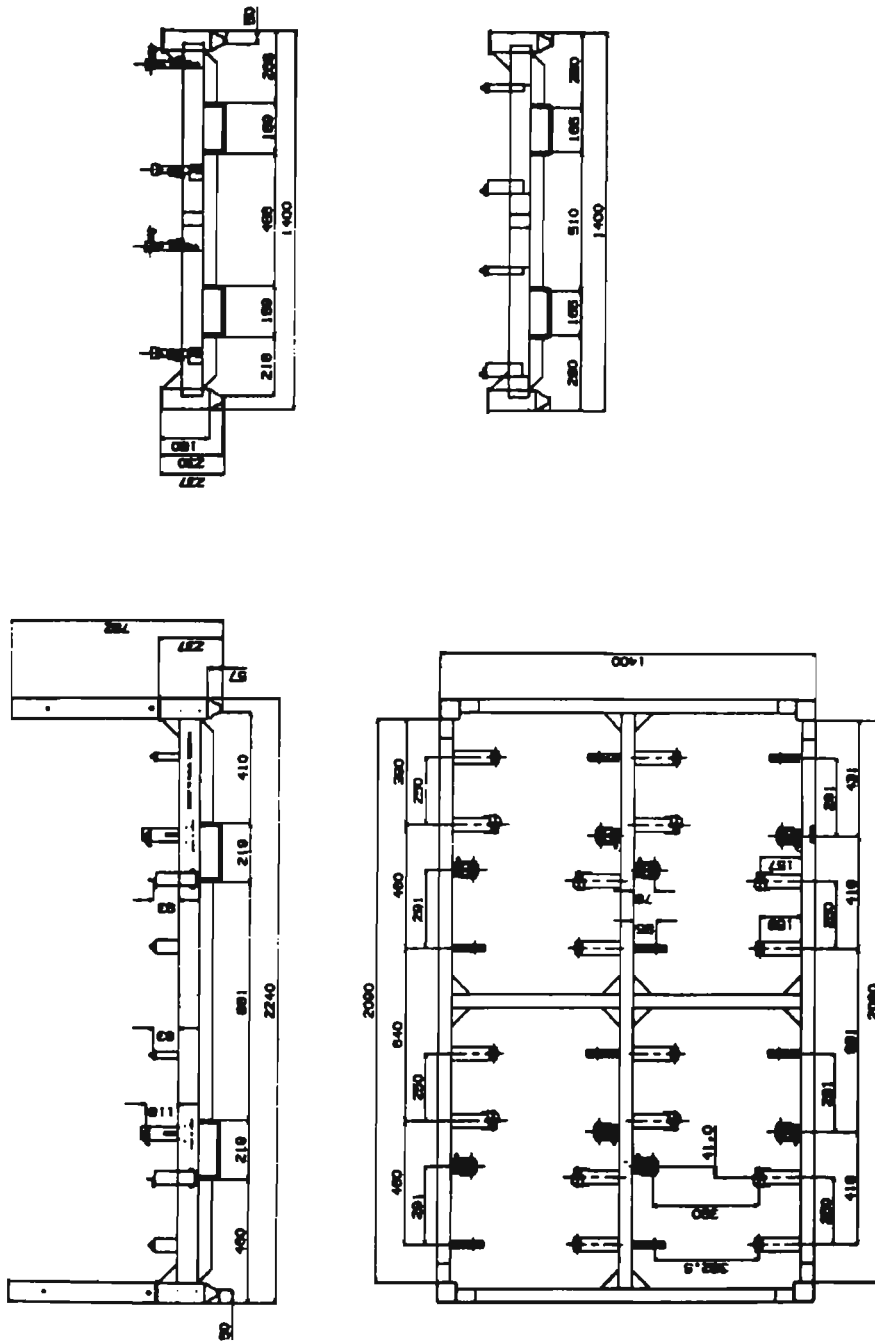


Figure 1-1 Layout of the engine rack

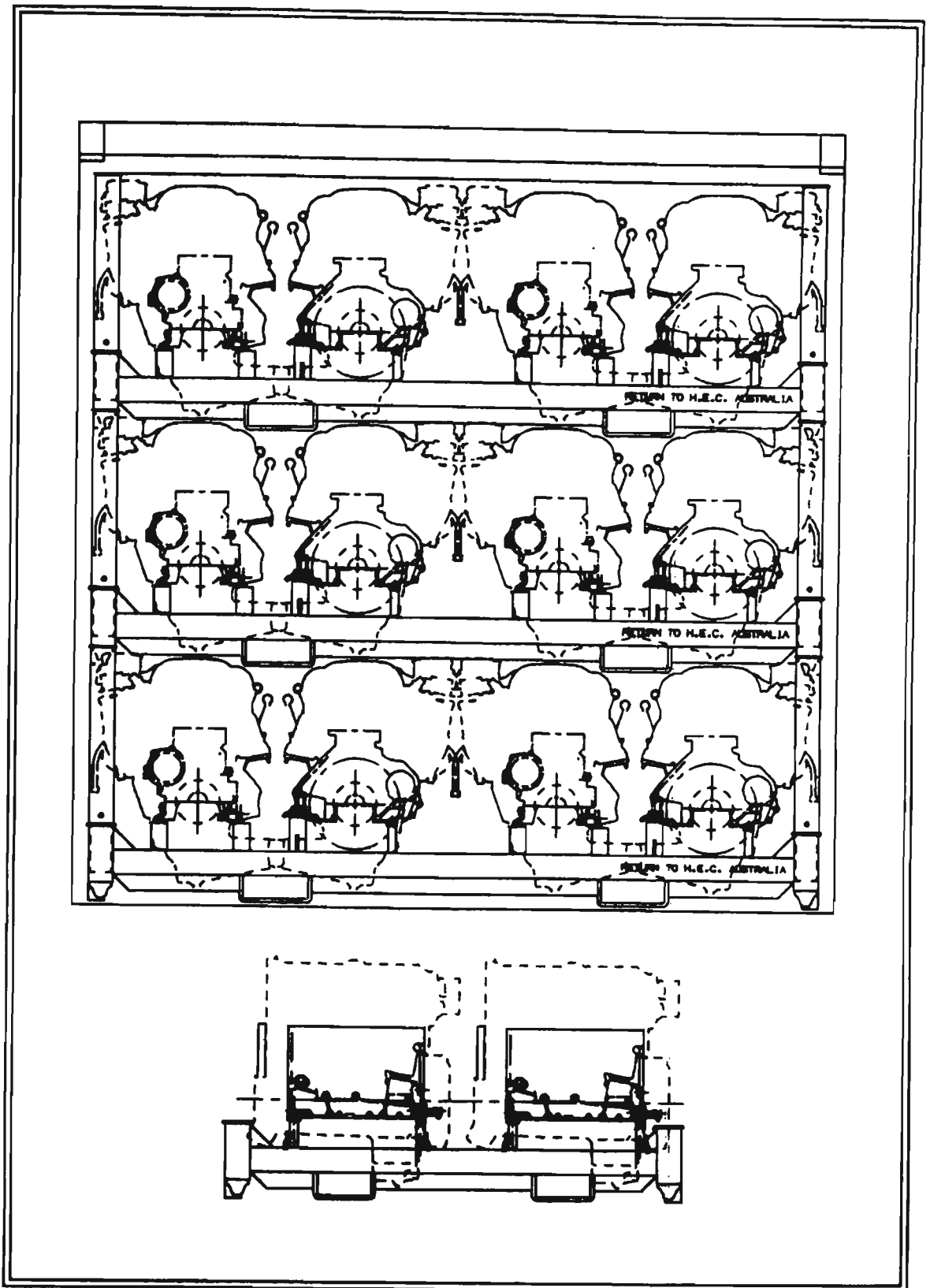


Figure 1-2 Engine rack stacked in three tiers

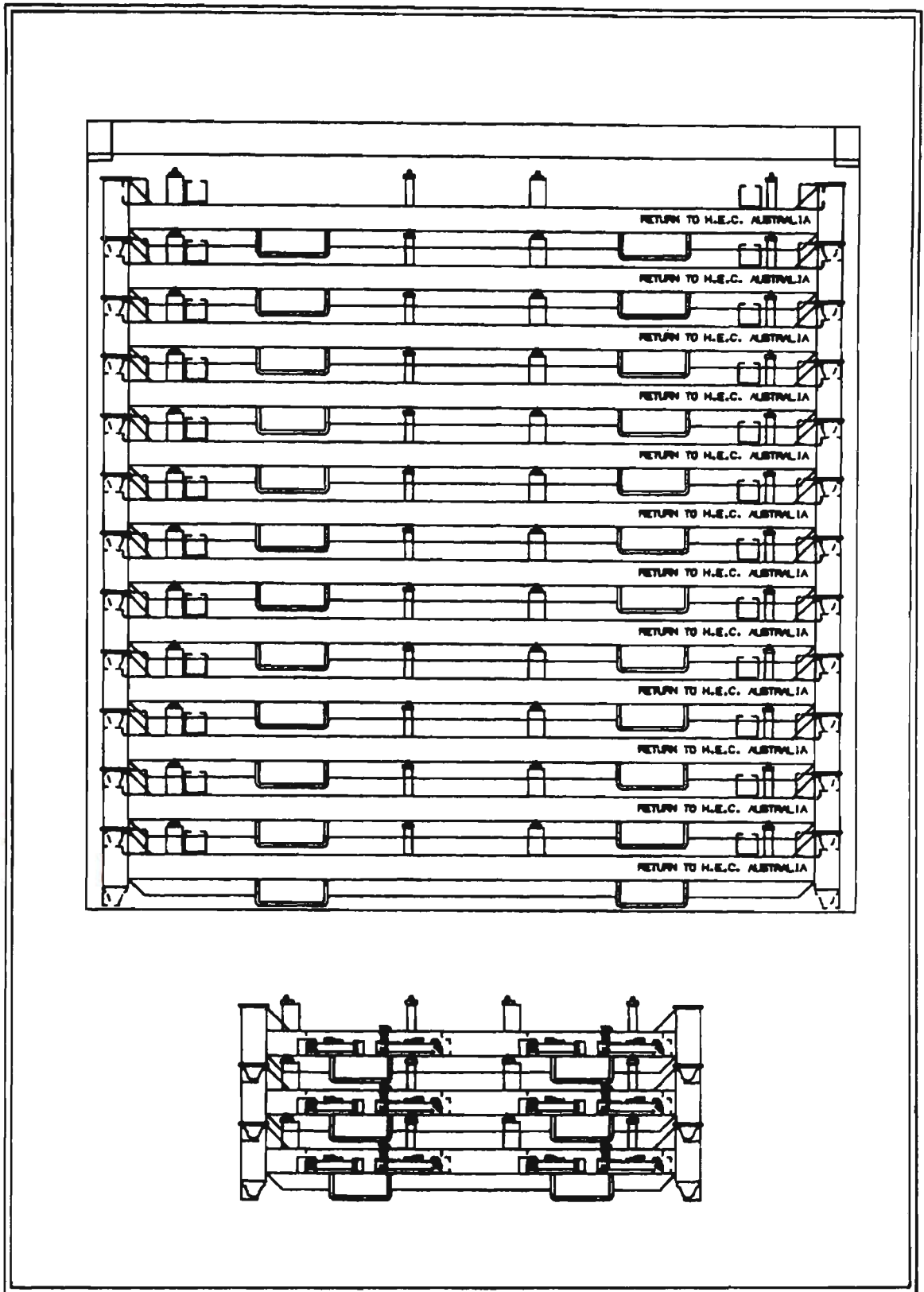


Figure 1-3 Collapsed engine racks

Environmental concerns directed the HEC's interest in establishing guidelines for the design, construction and handling of this reusable engine packaging system. The HEC will have to commit an estimated \$4.5 million to produce 7000 racks.

Although a prototype of the proposed system has been manufactured, no comprehensive analysis or testing has been undertaken to prove the design. The Packaging Centre at Victoria University of Technology, Richmond (1992) has performed a limited in scope empirical investigation of the effects of shock loading on engine and rack stability. No detailed analysis of the effects of static or dynamic loading on the rack structure has yet been undertaken.

Shocks are mainly encountered during handling operations. A shock is defined as a rapid transfer of energy which takes place in a relatively short time. Random vibrations encountered during transportation are principally caused by a moving vehicle in contact with the ground being subjected to excitation due to surface unevenness, engine vibration, wheel and tyres unbalance or load distribution. Vibration and shocks cause dynamic loads on the rack and its contents. The interaction between transportation environment and the packaged engine is controlled by the dynamic characteristics of the system. In certain circumstances inappropriate dynamic characteristics may lead to the loss or functional failure of the packaging system.

The dynamic characteristic of the loaded engine rack and similar structures are often predicted using finite element methods at the design stage or during design modifications. Whilst finite element modelling may produce reliable static and dynamic predictions for simple structures, in most cases there is a need to validate its performance against data obtained from experimental testing under simulated environmental conditions.

Validation of dynamic characteristics predicted by the FEM, such as the natural frequencies and frequency response functions, can be accomplished by a comparison of the predicted parameters with experimental results of prototype testing using experimental modal analysis, Ewins (1995). When validation is not satisfactory, modification of the FEM such as the selection of element type, the size of meshing,

material properties, boundary conditions, may be considered. If the dynamic characteristics predicted by FEA compare well with the experimentally determined parameters, then the FEM can be used to predict the behaviour of the prototype rack and its contents in the simulated environmental condition.

In order to gain a deeper understanding of the performance of the proposed reusable engine package system, this study will involve a theoretical analysis and experimental evaluation of the loading induced in the system by the transportation environment. A special feature of the research program will be the emphasis placed on the investigation of the interaction between the rack structure and the engine under dynamic excitation. The key to ensuring that the new packaging system provides reliable protection for the engine against the hazards of the transportation environment lies in developing effective engineering techniques that can be applied to improve the design of the system. To date it appears that few such studies have been attempted and a successful outcome will have considerable direct application to several other rigid packaging systems.

## **2. Literature Review**

The aim of the first section of this literature review is to highlight and expose the environment hazards that the engine rack and its content may be subjected to during transportation and storage. The second section of this literature review will illustrate that the finite element method can be used to predict the rack response to known environmental input. The third section will demonstrate methods used to update and validate the finite element model in preparation for the use in environment simulation.

### **2.1 Shock and Vibration**

#### **2.1.1 Shock and Vibration in Transportation Environment**

During transportation, handling and storage of a product at any or all points between the manufacturer and consumer, products encounter mechanical shocks, generally in handling operations due to drops and impacts, Tevelow (1983) and Schlue (1966). A mechanical shock occurs when an object undergoes a sudden change in velocity. Such a shock may be characterised by a the rapid increase in acceleration in a short period of time. In some cases a package may reach an acceleration of 150 g or more.

Product also receives vibrations from the transportation vehicle, which may be from internal sources such as engine rotation, wheel imbalance etc., or external sources such as pavement irregularities, uncoordinated drivers etc.

Foley et al ( 1973b) describe the source of shocks and vibration in the road transportation environment as the vehicle travels over the road, the surface and its irregularities create an excitation input at the individual tyres that may be vertical, have a side thrust, or be in the direction of motion, as in braking. Major vibration modes are excited in ascending order of frequency band as bouncing and pitching of :

- the sprung mass of the main cargo frame work and body on the suspension system.
- the unsprung axle system on the tyres.

Subsequently, also in order of increasing frequency, tyre excitations, engine and related drives, frame bending modes, and various chassis, floor, and body panel resonances are excited.

It has been noted that shocks are encountered mainly in handling operations, and compressive forces during transportation and storage. The shock levels, their shapes and their respective duration are the required data to represent and evaluate the severity of the shock parameter. Shock data are collected by installing a self-contained acceleration recording unit inside the package, and sending this test package through the distribution system. By recording the shock pulse that occurs during drops and impacts, the drop height of the package can be estimated. The accelerometers and recording unit sense and record acceleration versus time. The majority of shock waveforms have approximately a half-sine shape. Vibration levels and their respective frequency spectra are the required data to represent a random vibration parameter such as mean values, variances etc. Data on transport vibration is collected by installing accelerometers and data recorders on the decks of trucks, trains, ships, aircraft, etc. The accelerometers measure acceleration versus time, but procedures such as spectral analysis, Fourier transforms, etc. are then employed to transform the time domain data into frequency domain. A typical frequency range could reach as low as 0.2 Hz at sea and over 100 Hz on truck/rail and peak acceleration from 0.2 to 1 g, Foley (1973b).

### **Damaging Effect of Random Vibration Environment**

In a transport environment all vehicles moving in contact with the ground are subjected to random excitations due to surface unevenness, engine vibration, tyre unbalance or load distribution, Schiff (1990). If a vehicle moves in such conditions with constant velocity then the excitation most likely is stationary and the dynamic response parameters of the vehicle can be obtained either in the time or frequency domain. If the vehicle moves with a variable

velocity, the base excitation becomes nonstationary and the dynamic response is determined by the modes of the vehicle structure and the acceleration magnitude at the particular frequency. In such a case, it is the natural frequency and damping of the structure that will determine what acceleration magnitude will be experienced. Environment excitation consists of accelerations covering a broad band of frequencies, which is commonly expressed as a Power Spectral Density (PSD).

The PSD of the random vibration environment and the acceleration response spectrum of the shock environment have specific values at the structure's natural frequency, and these values determine the deformations and stresses that occur in the structure.

If the environmental excitation must pass through other structures before reaching the structure under investigation, the acceleration spectrum will usually be altered, often significantly. Because of the intervening structure, acceleration magnitudes at specific frequencies may be amplified or attenuated when arriving at the structure being analysed than they were in the original environment.

Crowford (1992) explains that the deformations that a structure undergoes are proportional to the acceleration imposed on it and the stresses in the structure are related to the accelerations (or strain) through the elastic modulus. Therefore, in the linear range of material elasticity, the stresses in the structure are directly related to the accelerations imposed on the structure, which in turn are determined by the natural frequencies of the structures as well as the acceleration environment and other associate structures.

### **Power Spectral Density (PSD)**

A true measurement of the PSD require that the amplitude increments and frequency increments be quite small;  $\Delta x \rightarrow 0$  and  $\Delta f \rightarrow 0$ , respectively, Tevelow (1983). A random vibration record  $x(t)$  of length T seconds.

$$PSD = \lim_{T \rightarrow \infty} \lim_{B \rightarrow 0} \frac{1}{TB} \int_0^T x_B^2(t) dt \quad 2.1$$

where  $x_B^2$  is the square of the amplitudes within the band  $\Delta f = B$  displayed at interval  $B$  across the frequency domain,  $f$ .

For a given vibration record, the PSD may be estimated from measurements of the squared instantaneous signal amplitude in a narrow bandwidth plotted at the centre frequency of that band. The PSD is obtained from data record as follows:

- Use of narrow band pass filter of bandwidth  $B$  in Hz that scans the frequency spectrum.
- Squaring the instantaneous amplitude of the filtered signal.
- Averaging this squared value over the record sampling time.
- Dividing this mean squared value by filter bandwidth  $B$ .

A display of this value (i.e.  $g^2 / \text{Hz}$ ) across the analysis frequency range is defined as the PSD of the signal.

The PSD is the limiting mean-square value (e.g. of acceleration, velocity, displacement or other random variable) per unit bandwidth, i.e. the limit of the mean-square value in a given rectangular bandwidth divided by the bandwidth, as the bandwidth approaches to zero.

### **Fast Fourier Transform Analysis**

Fourier Transformation (FT) concept is based on converting information from the time domain into the frequency domain or vice versa to present the information in such a way that it is easy to interpret and facilitate the analysis. The FT which is performed in practice is the so called Discrete Fourier Transform (DFT). The Fast Fourier Transform (FFT) is just an algorithm which computes the DFT with a greatly reduced number of arithmetical operations compared to a direct computation.

The development of the microprocessor has resulted in availability of digital signal analysers that simplify and speed up the analysis of vibration data records, Tevelow (1988). An average power spectrum is obtained as follows:

1. The analyser takes  $N$  samples of the analog record at operator selected fixed time intervals and stores it as one record.
2. The information is transferred to frequency domain using a Fourier Transform.
3. The transform is multiplied by its conjugate value (analogue to the amplitude squaring process used in computation of power, as in PSD).
4. The result is stored.
5. A new record is entered; steps 1 to 3 are repeated and the result added to the previous result.
6. Steps 1 to 5 are repeated for a fixed number of records, the summed spectrum is then divided by the number of records to get the average estimated PSD for the collection.
7. The average estimated PSD is displayed as function of frequency

### **Damaging Effects of Transients**

Broch (1980), Hoppman (1988), Robert (1988) and Sheldon (1988) point out that a shock occurs when two or more bodies suddenly collide. The characteristic of this impact is the generation of a relatively large force, and in a short duration in relation to the natural frequency of the system and it may last for a time which corresponds to several cycles of the system natural frequency. This force is the source of the energy generation in the system which causes the plastic deformation of material and ultimately rupture.

In designing a device to withstand shock, the strength of the equipment is indicated by the response of the structure to shock from rough handling, impact etc. This response may be expressed in term of the deflection of a member relative to another member, or by the magnitude of the dynamic loading. i.e. the energy that constitutes a shock (force, acceleration, velocity or displacement).

To estimate the effect of shock on a particular system it is necessary to obtain a time history, duration, and the specific shape of the shock. All have an effect on the structure response, or when the purpose is to formulate a laboratory test as a means to simulate an environmental condition. The structure response can be calculated from the time history by either of the Fourier spectrum analysis or shock spectrum analysis.

### **Parameters of the Shock**

Broch (1980) demonstrated that transient vibration and mechanical shocks are, like random vibrations occurred relatively often.

Shocks and transient vibrations may be described in term of force, acceleration, velocity or displacement and for a complete description it is necessary to obtain an exact time history record of the quantity in question.

In many cases the ultimate goal is not the waveform itself, but rather a means to estimate the effect that the corresponding shock or transient vibration would have on a certain mechanical system. A more useful method of description might then be found in the form of Fourier transform. If the time function representing a shock is  $f(t)$  then its Fourier Transform (FT) is given by :

$$F(f) = \int_{-\infty}^{\infty} f(t) e^{-j2\pi ft} dt \quad 2.2$$

Figure 2-1 show various shock time functions and the amplitudes of their Fourier spectra. It can be seen that in general a shock pulse contains energy spread over all frequencies from zero to infinity and that the spectra are continuous with no discrete frequency components.

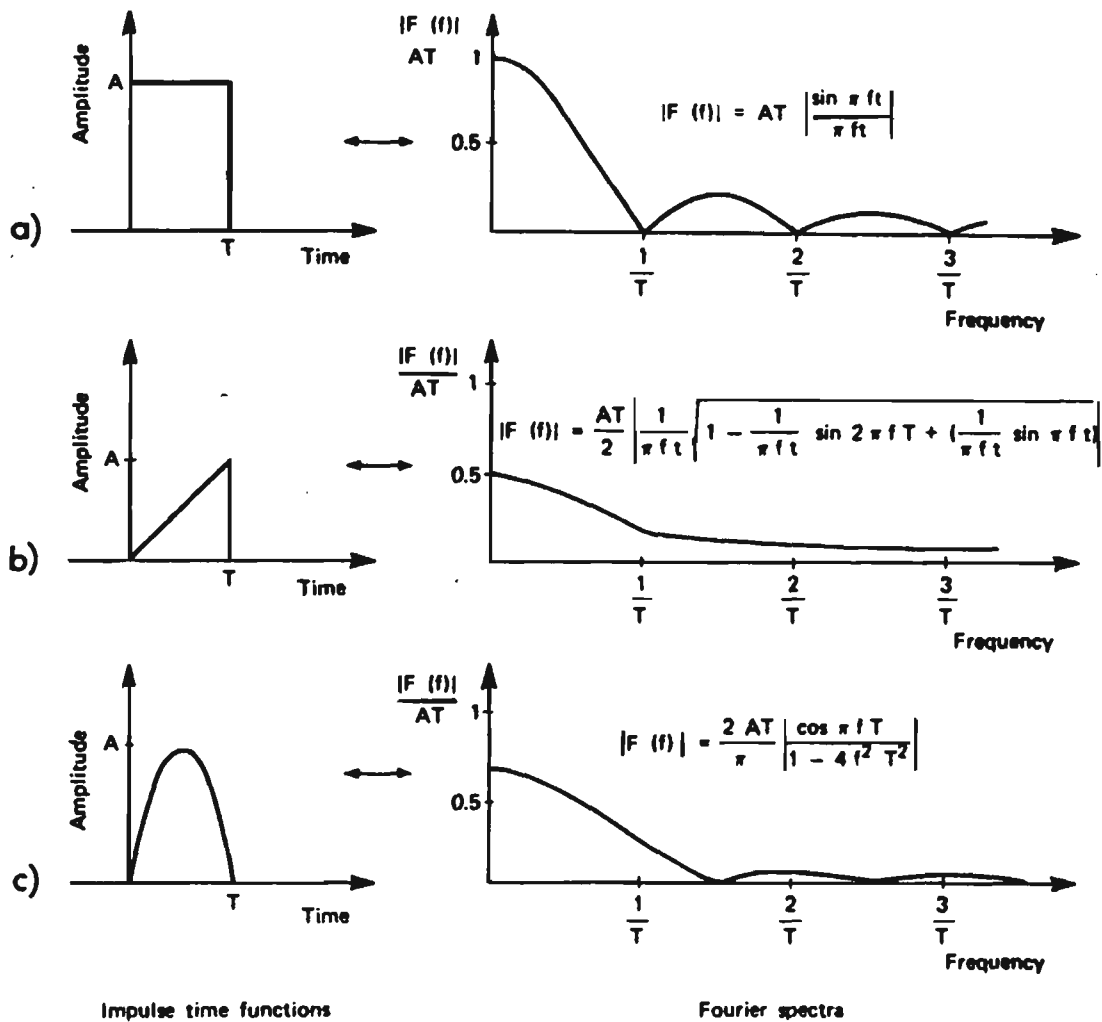


**Figure 2-1 Examples of shocks time functions and their FT (amplitude spectra)**

- (a) rectangular shock pulse.
- (b) final peak sawtooth shock pulse.
- (c) half - sine shock pulse.

### Shock Response and Shock Spectra

A shock is a transmission of kinetic energy to a system, the transition taking place in a relatively short time compared with the natural period of oscillation of the system, Broch

(1980). A rectangular shock pulse may contain one or two shocks depending upon the natural period of oscillation of the system influenced by it and the duration of pulse.

Spectral decomposition are the most widely used procedure for the analysis of shock data.

The two most common forms of spectral decomposition used are:

- Fourier spectrum
- shock spectrum

The Fourier spectrum is simply the forward Fourier transform of time history. It can be calculated for either the excitation or the response time history. When dealing with shock data, it is often difficult to measure the response of the system under service conditions and the analysis is limited to the excitation time history. Generally the Fourier spectrum is used to the input shock and the frequency response function of the system in order to get information about the system response. The response being calculated in the frequency domain, the inverse Fourier transformation operation produces the response time history of the system. Shock Response Spectrum is the spectral decomposition, which has proven to be of considerable value with respect to the comparison of shock motions, to the design of equipment to withstand shocks, and to the formulation of laboratory tests as a means to simulate environmental conditions.

Various types of shock spectra are used depending upon the intended application of information obtained. These may be the initial shock spectrum which is obtained from the maximum response while the shock pulse is still acting, or residual shock spectrum which is obtained from the maximum response after the pulse has occurred.

Selection between the Fourier and the shock spectrum methods of spectral decomposition is based on the application of the data. Fourier analysis is used to describe input data, response data or, if the both are measured simultaneously, it can be used to describe the frequency response function of the system. Once two of the three items are known the third can be calculated.

Typically, the input time history and frequency response function are known and the response time history is to be determined.

On the other hand, the application of shock spectral analysis is used to predict peak response levels from input measurements, with only limited knowledge of the system response properties.

Also Ewins (1995) noted in case of a transient excitation, there is an additional constraint imposed by the requirement that the response signals must have died away by the end of sample time. For lightly damped structures this will result in rather long sample times being required and this in turn poses a problem because it has a direct influence on the frequency range that can be covered. For example, if it is decided that a sample length of 2 seconds is necessary in order to ensure that the response has died away, and have a 512-point transform, then the minimum time interval possible between successive points on the digitised time histories will be approximately 4 ms. This in turn means that the frequency resolution of the spectrum will be 0.5 Hz and highest frequency on that spectrum will be as low as 250 Hz and it will not be possible to measure the FRF at higher frequencies than this. Such restriction may well clash with the demands of test and quite elaborate action may be required to remove it, for example by using an exponential window or by using a zoom facility

The transfer function of a structure may be determined by applying a transient force to the structure and noting the response. This is analogous to the commonly used method of applying a sinusoidal varying force whose frequency can be varied over wide range and noting the sinusoidal varying motion at the frequency of the force application.

### **Damaging Effects due to Stacking**

According to Schlue (1966) the intensity of the static compressive forces is generally associated with warehousing and storage stacking. These static compressive loads are a result of stacking one container on top of another up to some reasonable height. Stacking height can

vary considerably depending on available headroom, storage equipment, stability, or regarding maximum stack height.

The dynamic compressive loads result from transportation are more difficult to establish. Load amplification can occur as result of vibrations at critical resonant frequencies and can result in high dynamic loads at the bottom containers, even for low stacking heights in vehicles. In addition there is a load resulting from, for example, ship low frequency motions (pitching and rolling) and aircraft response to updraughts or gusts. Other sources of dynamic loading include railcar coupling, mechanical handling equipment such as squeeze clamps on lift trucks, slings, and cargo nets, and compression due to strapping.

As early as 1964 the USA army research, Lambert stated that stacking may subject the cargo and the cargo container, to severe loading conditions, as the dynamic and static loads are resisted by each succeeding lower unit of cargo in the stack. The same consideration as regards stacking and dynamic loading must be given in the horizontal plane, since vertical accelerations will also cause a load build up on the end unit unless load dividing measures are taken. Effects of cargo stacking are most distressing in sea transport.

### **Damaging Effect due to Handling**

Ostrem (1965) reported on the data required to evaluate the shipping shock and vibration environment including both the in-transit environment and the handling environment. The in-transit environment includes those motions resulting from movement on transport vehicles. The handling environment dominated by those motions resulting from operations such as physical handling, loading and unloading and movement with storage or warehouse areas. The data describing cargo handling shock and vibration have been reported in terms of peak acceleration, drop heights, or shock spectra.

Data reported in terms of peak acceleration provide information on the relative severity of the shocks occurring during shipping but do not provide information on the input shock excitation. Data reported in terms of drop height are considered of most use because of the

standard drop height test, (ASTM D5276-92, ASTM D4169). Data reported in terms of shock spectra are of most use for describing the shock environment.

McAleese (1962) conducted an extensive measurement program on peak acceleration. A number of shipping containers of various shapes and weight were prepared and equipped with commercial impact recorders. The containers were shipped via truck, ship and air. Table 2-1 shows the measured field data in terms of peak accelerations. The laboratory tests attempted to correlate instrument peak acceleration reading with drop height showed wide variation.

**Table 2-1 Cargo - handling field test result: Peak Acceleration (g)**

Note, Data presented are ranges, followed by means (in parentheses)

Container Shape	Container weight (kg)			
Length: Width: Height	Small 30 - 40	Medium Small 70 - 110	Medium 110 - 230	Large 230 - 700
Average (3:2:2)	1-45 (12)	1-40 (10)	1-7.5 (4)	1-13 (6.5)
Long (3:1:1)	1-15 (9)	1-11 (6)	1-10 (6)	1-4 (5)
Tall (1:1:2)	1-23 (9)	1-12 (7)	1-15 (5)	1-5 (3)

Goodwin, Goyal (1997), Bull et al (1963), Harrison (1963), Dagele (1963) investigated the drop height of various sizes, weight, and shapes of packages to define drop height parameters in a study of shipments via air freight and another via railway express. The data recorded for 49 trips involving 13 packages (862 drops were recorded above 75 mm), the data collected shows that only 5 percent of the packages received drops above 500 mm. Other data shows that 5 percent of packages had drops over 200 mm and one percent over 400 mm. While in

sorting operation a higher drops occurred during operation, with 5 percent being dropped over 400 mm and 5 percent of the drops were over 600 mm.

Singh and Voss (1992) have investigated the effect of drops, tosses and kicks encountered during transportation environment and the effect of weight and volume on the packages shipped. The study provided a broader insight into the dynamic events that occur in the transportation environment and accounted for the variation of drops, tosses and kicks

Singh and Voss concluded that the highest drop observed was 1070 mm for small size packages. The size of the package had no significant effect on the drop heights. Lighter weight and smaller size packages experienced higher drop heights. Weight in general also did not have a significant effect on the medium/large size package drop heights. The 95 % of the drop occurred at 760 mm or less for the small/light package, 600 mm for small/medium packages, 450 mm for the medium/light package, 600 mm for the medium/medium packages, 660 mm for the medium/heavy package and 450 mm for the large/heavy packages.

### **2.1.2 Transportation Hazards**

Lambert, as early as (1964) suggested the following guidelines to identify the transportation hazard and the data required to determine and evaluate this hazard.

- Certain data can be established in the field of transportation shock and vibration that will be helpful tool for analytical comparison. The first step is to obtain and use acceleration inputs to a transportation system that are independent of the operational characteristics, such as the physical state of the right way, impact speed, sea state and landing rate. From this point, other factors can be presented that are determined wholly or in part by the mechanical makeup and operational characteristics of the transportation system and that are peculiar to the specific system.
- It is recognised that some combination of factors such as forces, accelerations and frequencies that would classify and standardise the required strength of a broad range of cargo would be a most useful tool to initiate better comparison of transportation shock and vibration data.

A comparison of the vibration environment for various transportation modes are summarised by envelope curves of acceleration as plotted in Figure 2-2 and published by Ostrem and Godshall (1979). The data presented show the maximum vibration levels for general cargo which may be located at any position and any orientation. Also data permits a comparison of the various modes and it shows that trucks impose the severest vibration loads on cargo with railcar next, followed by ship and aircraft.

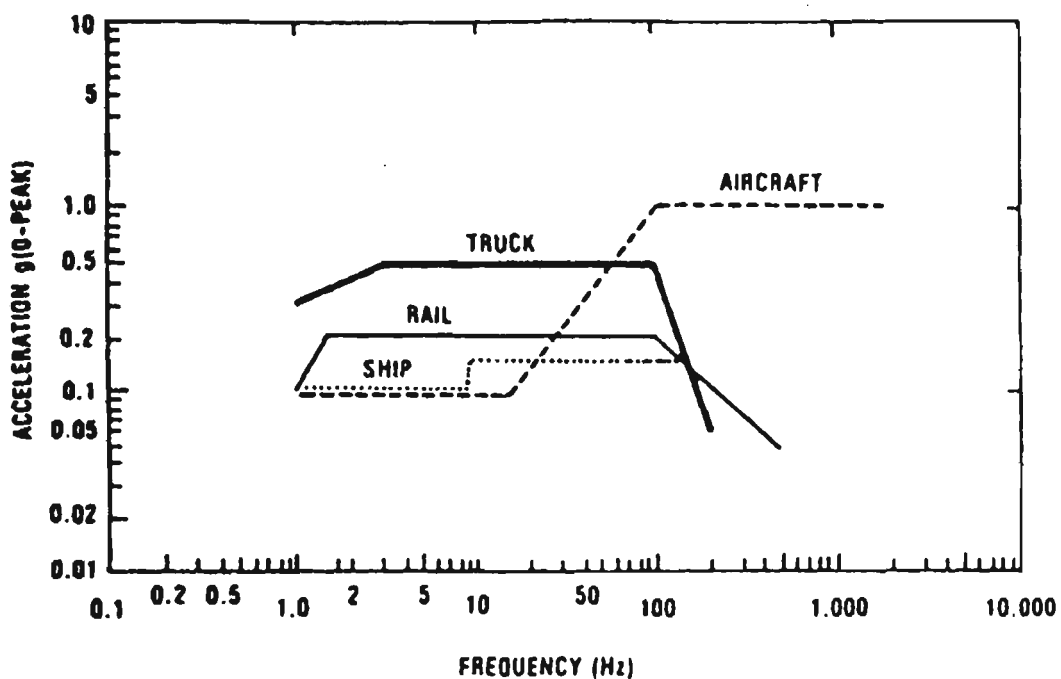


**Figure 2-2 Vibration acceleration envelope for : land, sea, and air transportation**

Reports obtained later, ASTM D4728 (1997), do not contradict these levels of vibration but do indicate that Ostrem and Godshall selections are quite conservative, that is, test levels would be set too high.

The PSD shown in Figure 2-3 shows a typical random vibration PSD log-log scale to which a package would be exposed during its transportation. The graph illustrates that there are

relative differences in vibration intensity and frequency content for various types of commercial transportation. The graph has evolved from a compilation of field measurements made by several organisations over a period of time. Also this graph shows average vibration intensities measured under various loading conditions, suspension types, road conditions, weather condition, travel speed, etc. and it does not represent the environment that exist in any specific transportation, ASTM D4728 ( 1997).

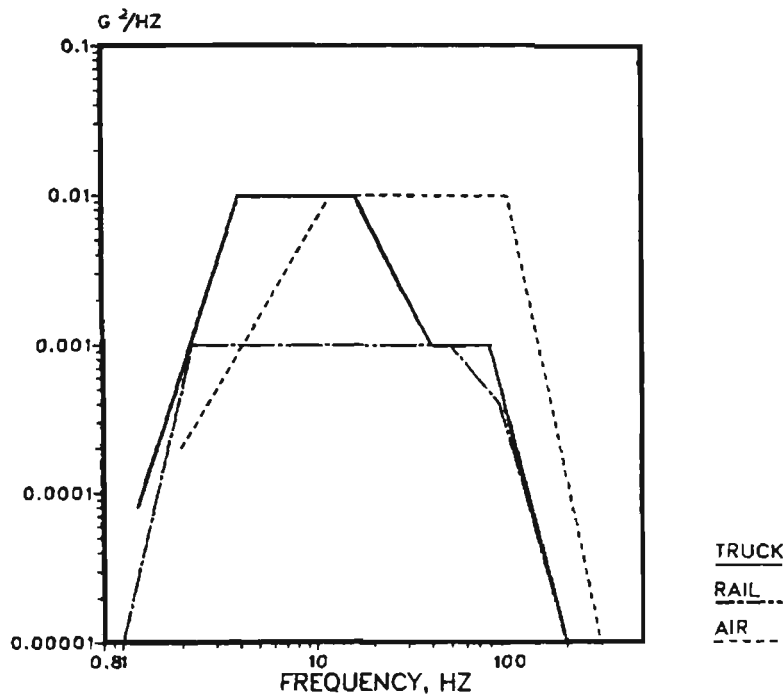


**Figure 2-3 Commercial transport random vibration spectra**

Schiff (1990) discussed the truck imposed random vibration condition PSD shown in Figure 2-3 as follows:

The PSD is usually specified in term of initial and final values at the low and high frequency ends of the spectrum; plateau values where the PSD is constant over a frequency range; and slopes in units of dB per octave over frequency ranges where the PSD is increasing or decreasing with increasing frequency. The dimensionless slope  $m$  between two points on log - log PSD plot is given by

$$m = \ln ( PSD_2 / PSD_1 ) / \ln( F_2 / F_1 ) \quad 2.3$$

The slope  $m'$  in units of dB per octave is given by

$$m' = 3m \text{ dB / octave} \quad 2.4$$

The slopes  $m$  and  $m'$  is either positive or negative.

The mean PSD value  $\overline{PSD}$  between  $F_1$  and  $F_2$  is

$$\overline{PSD} = [ ( PSD_1 ) / ( 1 + m ) ] [ F_2 ( F_2 / F_1 )^m - F_1 ] \quad 2.5$$

In the case of plateau of constant PSD value,  $m = 0$  the above eq. becomes

$$\overline{PSD} = PSD_1 ( F_2 - F_1 ) \quad 2.6$$

The value of  $G_{rms}$  over the entire PSD spectrum is

$$G_{rms} = \left( \sum \overline{PSD} \right)^{\frac{1}{2}} \quad 2.7$$

Where  $\sum$  is the sum of all of the PSD segments in the spectrum  $G_{rms}$  is a measure of the overall acceleration level of the PSD spectrum.

## Road Transportation Hazards

In the effort of defining and quantifying the damaging level to the packaging during truck transportation research has defined the mechanical damage to packages or products in shipment to be attributed to vibration and shocks encountered in the transportation environment. The level of damage can be also influenced by the temperature and humidity. Performance testing of the packaging systems in the laboratory is becoming a commonly used tool in the optimisation of packaging. This is subjecting a packaging system to the excitation that is similar to that experienced by packaging in the real transport environment.

Lambert (1964) recommendations for designing a suitable packaging system for highway transportation were:

- The product and its packaging system should be capable of sustaining the loading incident to a 1,000 mile road trip over a paved highway in condition described by AASHO-SI.
- For all shocks and vibration, the stresses in the restraining system should not exceed the yield strength of the material, nor should they exceed one - half the yield strength of the material under static load conditions (as published by the American Society for Testing and Materials [ASTM])
- Envelopes of maximum values recorded during transportation are shown in Figure 2-4. It was recommended that the vibration time for design purposes be consistent with a 5,000 mile trip. It was also recommended that the packaging system items be designed to withstand 30 shock applications.

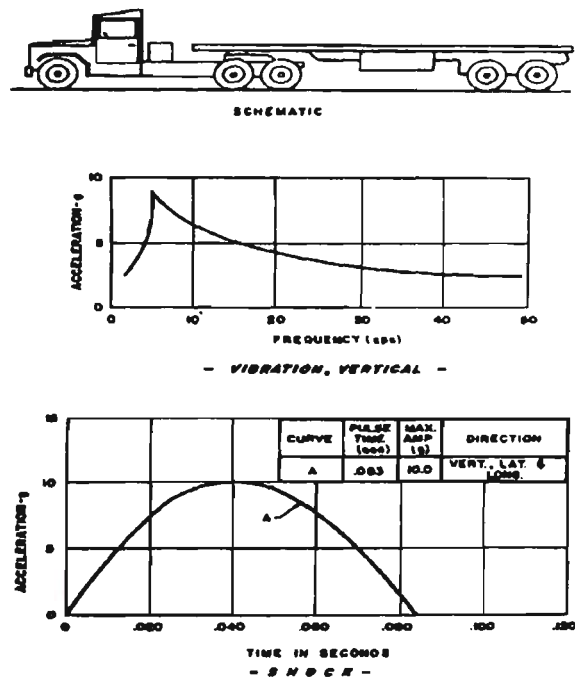


**Figure 2-4 Cargo environment for highway transport**

The major vibration modes associated with truck and road transport environment are bounce, pitching, and frame bending, Glotzbach et al (1977). Bounce is an oscillation resulting in an up and down motion. Pitching creates a rocking motion which may be longitudinal or side to side. These are rigid body motions. Frame bending describes the flexure of the vehicle body such that the ends of the frame are moving up or down, at the time in the same direction, while the center of the vehicle is moving in the opposite direction. Figure 2-5 shows the various vibration intensities attributed to different road conditions by a single truck/payload combination. In this particular study, a single truck was instrumented and driven over various routes. Each condition was reduced to PSD format and plotted, ASTM (1994).

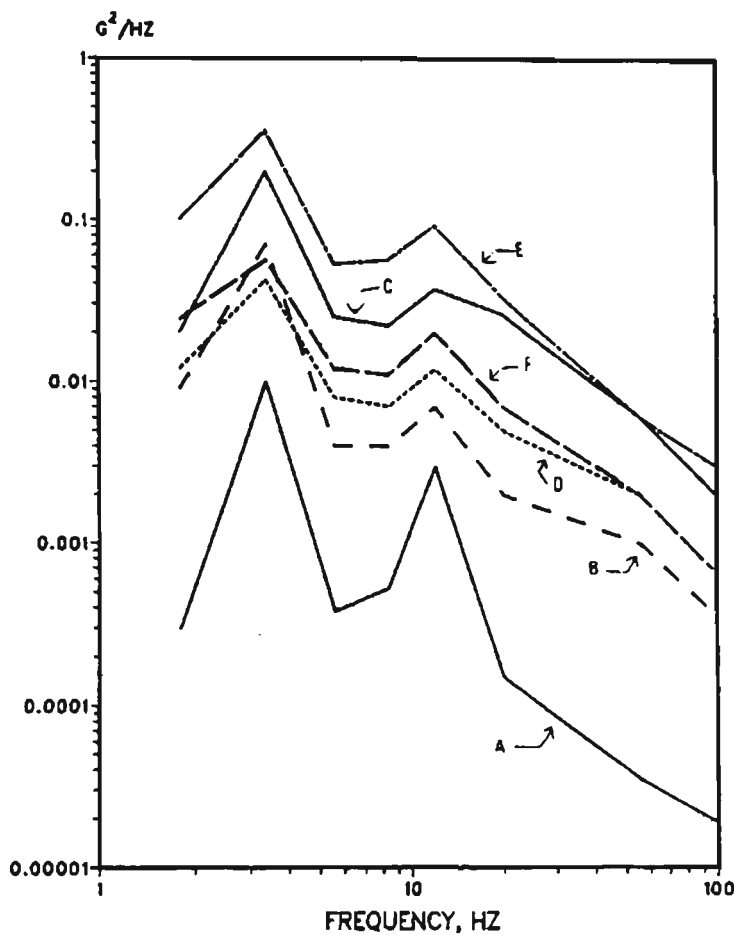


**Figure 2-5 Route comparison leaf spring truck vertical vibration**

The description of the routes and surfaces conditions corresponding to the spectra in Figure 2-5 are:

- A Production area: speeds less than 30 km/h, rough roads.

- B City Roads: speeds between 16 - 22 km/h extremely rough, cracks and railroad tracks.
- C Expressway : Concrete highway, indicative of Interstate Highway, speeds over 90 km/h.
- D Suburban Roads : speeds less than 30 km/h, sharp turn and numerous stops.
- E Main Suburban Roads : Asphalt road with many pitched area, railroad tracks, numerous stop, average speeds between 55 - 70 km/h and
- F Secondary Suburban Roads: Two lane, asphalt, lots of bumps, slow speeds less than 35 km/h.

Later edition of ASTM D4728 (1995) has superseded the data in ASTM D4728 (1991).

Figure 2-6 Illustrates the difference that may exist due to truck trailer suspension and trailer loading travelling on interstate expressways at 88 km/h, Singh (1992).

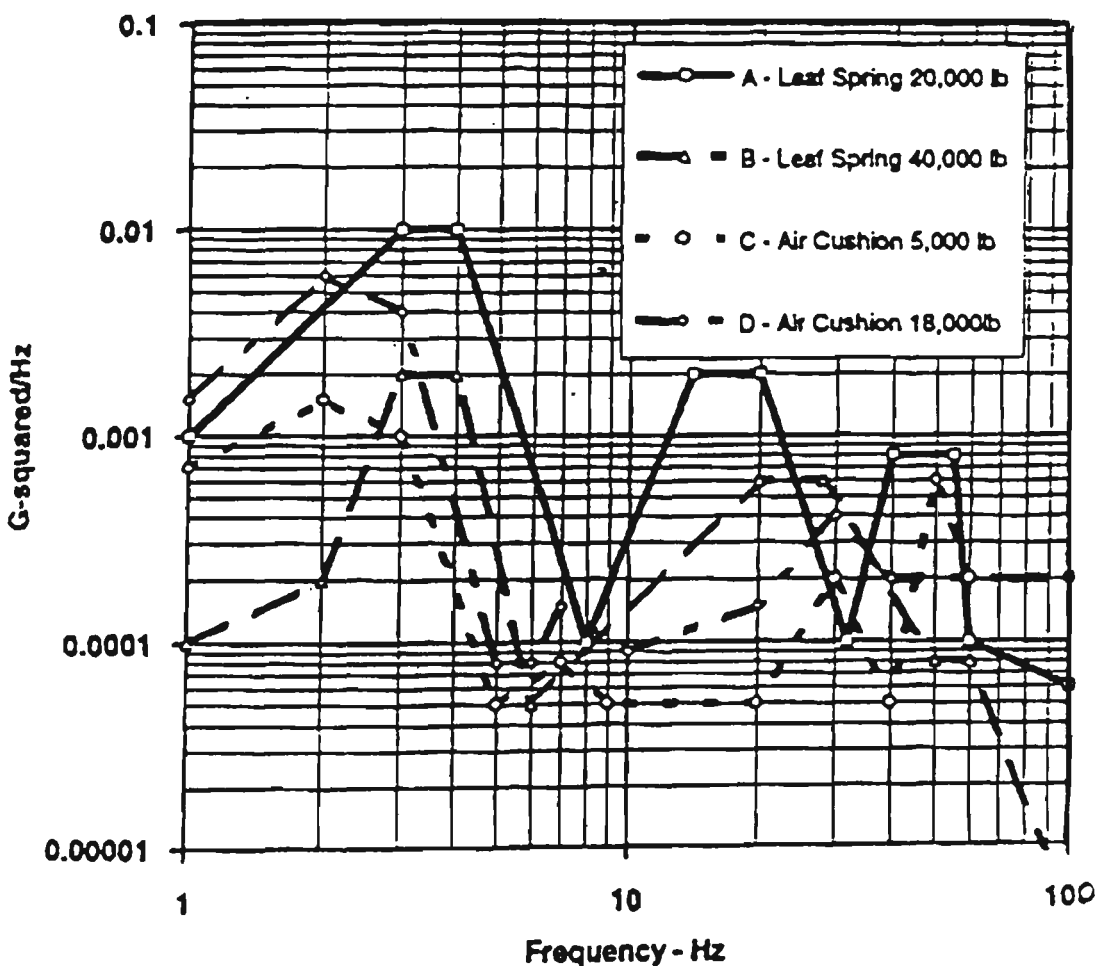
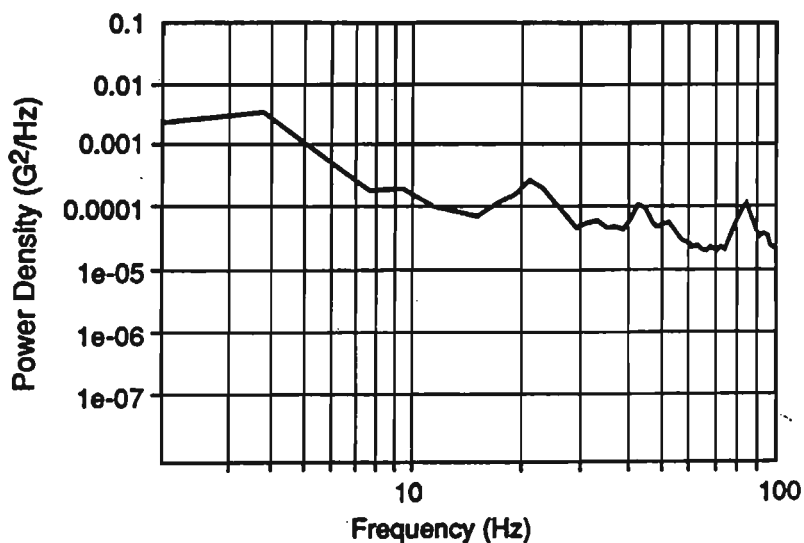


Figure 2-6 Sample truck vibration test profiles

Singh et al (1995) conducted a study to develop test methods that could be used to simulate and measure the shock and vibration levels that occur in truck shipments containing steel racks used to transport engines by measuring specific routes that were used to transport the racks with engines from the production plant to the assembly plant. The data was collected at several locations on the floor of the vehicles and on the racks themselves to determine the severity of shock and vibration input from truck trailers. The corresponding vibration test duration and the number of impacts are based on recommendations provided in ASTM D4169 (1991), D4728 and D4003 (1991). The results in Figure 2-7 shows the vertical vibration spectrum measured at the rear during truck shipments. The vertical vibration spectra measured can be used to simulate vertical vibration during truck shipments.



**Figure 2-7 Vertical vibration level in trucks**

According to Singh vertical vibration levels are severe in truck shipments, with high PSD values of the trailer bed corresponding to 4 Hz. There were virtually no impacts of any significant severity measured in lateral and longitudinal directions for truck shipments.

Based on the data collected, Singh's conclusions were:

- The vertical vibration levels in truck shipments are more severe at frequencies below 20 Hz. The vertical vibration level in truck shipments are highest at 4 Hz.
- The impacts occurring in the longitudinal and lateral direction for truck shipments were negligible.

Rouillard et al (1996) presented an analysis of spectral and statistical characteristics of actual road surface elevation records. A loaded truck experiences vertical acceleration mainly due to suspension, road, vehicle speed and road surface characteristics, which may vary greatly between and during journeys, the statistical parameters used to describe road surface profiles are much less sensitive to change with respect to time. The paper presents an analysis of the spectral and statistical characteristic of actual road surface elevation, and the deviation of the road profile distribution from the Gaussian distribution. It also shows that roads of different roughness seem to retain their spectral distribution. In addition, a statistical parameters guide for use in the classification of road profiles was developed. A method in which a random vibration controller was used to simulate road profile spectra by controlling the displacement instead of the acceleration of a shaker table was described. This technique uses a physical model of the vehicle suspension to account for the dynamic characteristics of the vehicle.

The following are the main advantages claimed for this technique.

- Once a wide range of road profiles have been analysed and universally classified, only these road categories and the suspension characteristics of particular road vehicles will be required to physically simulate the complete process in the laboratory.
- Suitable adjustable mechanical devices may be easily designed and built to represent the dynamic behaviour of a wide range of road transport vehicles as well as provide the necessary compliance during impact between a test package and shaker table.
- Mean vehicle speed may be taken into consideration by simply shifting the PSD along the frequency axis.

The technique can be further improved by employing systems that will enable the generation of non-Gaussian random signals and allow the spectral characteristics, both shape and RMS, to be varied as a function of time. This is to account for variations in road surface characteristics and vehicle velocity which occur during a single journey. Furthermore, the presence of exceptional and transient phenomena such as potholes and other major road surface defects can be taken into account by superposition of the actual dimension of the “defect” onto steady-state signals. Rouillard's conclusions were as follows:

- simulation of road transport processes can be better achieved by synthesising road profiles instead of accelerating vehicle loading trays.
- The spectral shape of a section of road profiles was found to be independent of road roughness and the distribution of the profiles was found to deviate from the Gaussian distribution.
- A range of spectral and statistical parameters were considered for the universal classification of road profiles. Only the parameters describing these categories and the vehicle suspension characteristics are required to simulate the transportation process.
- The compliance of the loading tray can be modelled with a physical device to more accurately simulated the package-loading tray interaction, especially during impacts.
- The use of digital signal processors (DSPs) together with a time-domain adaptive filter-control technique was recommended for the accurate reproduction of stationary and non-stationary demand signals.

### **Rail Transportation Hazard**

A suggestion for planning a packaging system suitable for rail transportation was put forward by Lambert (1964), his recommendations were as follows:

- The cargo and its packaging systems should be capable of withstanding a transportation shock environment simulated by three successive rail impacts in both car directions of 16 kilometre per hour for sensitive cargoes and 13 km per hour for general cargoes.
- The stresses in the packaging system should be less than one-half the yield strength of the material in the static state. The combined static and dynamic stresses must not exceed the yield strength of the material in any packaging system during the dynamic portion of the impact loading.
- The cargo and its packaging system should be able to withstand without failure a transportation vibration environment equivalent to one produced by over the road movement in a 150 - car train.

- Lambert's envelopes of the maximum environmental values are shown in Figure 2-8. These values were recorded while using standard commercial rail cars impacted at 16 km per hour.

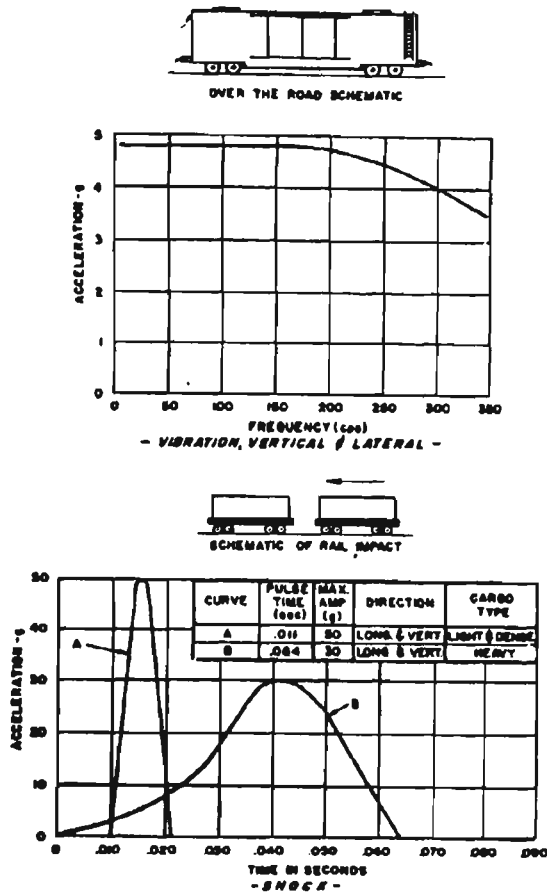
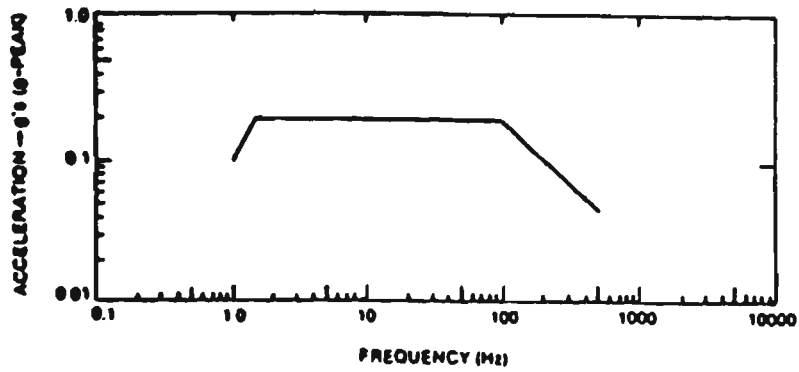


Figure 2-8 Cargo environments for rail transport

Tevelow (1983) found the acceleration in the vertical axis was the most severe train vibration with lateral and longitudinal vibration much less for normal ride conditions. Worn wheel, track roughness, track joints, track misalignment and roadbed unevenness produce discrete excitations and each contributes to higher than normal levels of vibration.

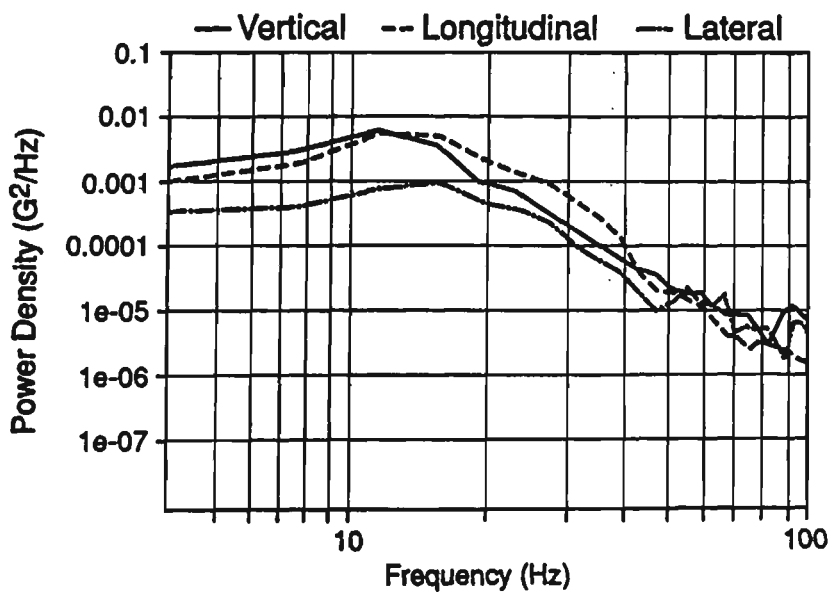
Ostrem and Godshall (1979) define the vibration acceleration spectra envelope for rail cars under extreme conditions Figure 2-9 showing that the acceleration is flat at 0.2 g (0 - peak) from 1.5 to 100 Hz, dropping to 0.1 g at 1.0 Hz and to 0.04 g at 500 Hz.



**Figure 2-9 Vibration acceleration spectra envelope for railcars**

Singh et al (1995) conducted a study aimed at developing a test method that could be used to simulate and measure the shock and vibration levels that occur in rail shipments containing steel racks used to transport engines by measuring specific routes that were used to transport the racks with engines from the production plant to the assembly plant. The data was collected at several locations on the floor of the rail boxcars and on the racks themselves to determine the severity of shock and vibration input from rail boxcars.

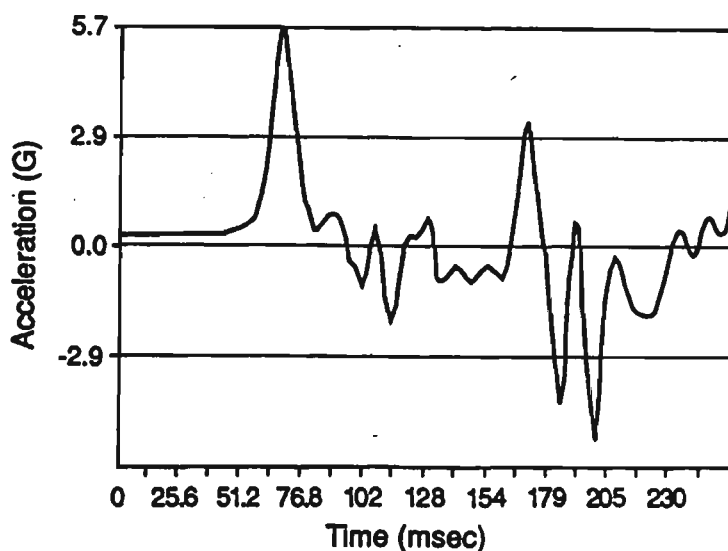
The corresponding vibration test duration and the number of impacts are based on recommendations provided in ASTM D4169 (1991), D4728 and D4003 (1991). Figure 2-10 shows the vertical, lateral and longitudinal vibration spectra for the rail shipments.



**Figure 2-10 Vibration levels in rail shipments**

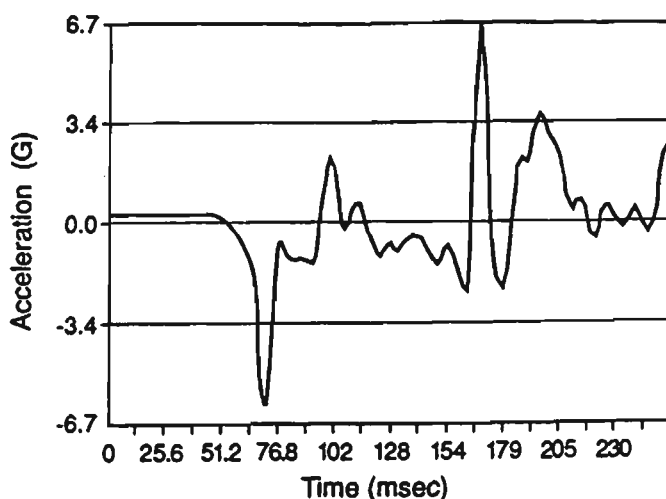
Based on this data it is evident that the vertical vibration levels are significant in rail shipments. The data in the lateral and longitudinal spectra show extremely low energy levels and do not play a significant role in the design criteria of the steel racks.

Figure 2-11 shows a brief time history of one of the most severe impact peaks of 5.7 g with a duration of 14 ms in the longitudinal direction that occurred in the boxcars during rail shipments as a result of coupling.



**Figure 2-11 Longitudinal impact in railcars**

Figure 2-12 shows lateral impact peak of 6.7 g with duration of 7 ms.



**Figure 2-12 Lateral impact in railcars**

When comparing the data for the steel rack impact levels in the longitudinal and lateral direction, the impact levels in the steel racks were generally found to be lower in the lateral direction than in longitudinal direction. The longitudinal impact level shows a high acceleration peak at 5.7 g compared to 6.7 g in the lateral direction. The most severe impact in the lateral direction, however, had a higher peak acceleration than that in longitudinal direction, but occurred for only half the duration and therefore was not as severe. The impacts in both the lateral and the longitudinal directions are severe and should be used as a criteria for testing racks designed for rail shipments.

Based on the data collected, the following conclusions were made:

- The vertical vibration levels are less severe in rail shipments, and highest at 11 Hz.
- The impacts occurring in the longitudinal direction are more severe than those in the lateral direction for rail shipments.

Singh and Marcondes (1992) have investigated the vibration level in commercial truck shipments as a function of suspension and payload. The data was presented in the form of power density spectra for various trucks suspension systems, road surfaces and trailers sizes used for commercial shipments. The data was used as a means of simulating real life shipments on electro-hydraulic vibration tables with random vibration capability. To measure the vibration levels in the different trailer systems piezoelectric accelerometers were attached to the floor of the trailer. A total of six trailers ( four with leaf spring, one with air ride suspension and a panel van ) were monitored for a total of over 16000 km.

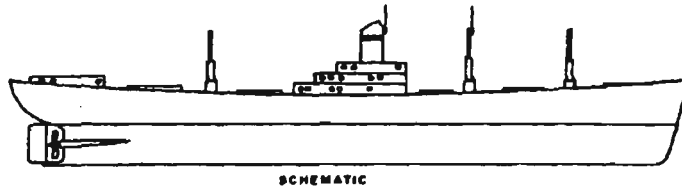
Singh and Marcondes conclusions were:

- Leaf spring suspension trailers have high vibration levels between 3 and 4 Hz. Fully loaded trailers have lower vibration levels than partially loaded trailers.
- Air ride trailers have significant lower vibration levels compared to leaf spring trailers. The suspension frequency is about 2 Hz. The vibration levels increase with an increase in load.
- Panel vans show significant vibration levels at higher frequencies.
- The most severe vibration levels recorded in all cases were vertical and occurred at the rear of the trailers.

## Sea Transportation Hazards

Stacking and packaging guidelines for sea transport were recommended by Lambert (1964) and are as follows:

- For sea transportation, the cargo and its packaging system should be capable of sustaining an environment occasioned by a seaway-induced loading on a transport ship
- Stacking is critical in sea transport, and subject the shipment to severe loading conditions as the dynamic and static loads are resisted by each succeeding lower unit of cargo in the stack. The same consideration as regards stacking and dynamic loading must be considered in the horizontal plane, since longitudinal accelerations will also cause a load build up on the end unit unless load dividing measures are taken.
- Figure 2-13 presents guidance as to the nature of the sea-induced accelerations on the cargo. The data are a plot of an envelope of the maximum values of the vibrations in the frequency range of 0 to 15 Hz. Also shown is a time-history envelope of the maximum shock environment measured.



SCHMATIC

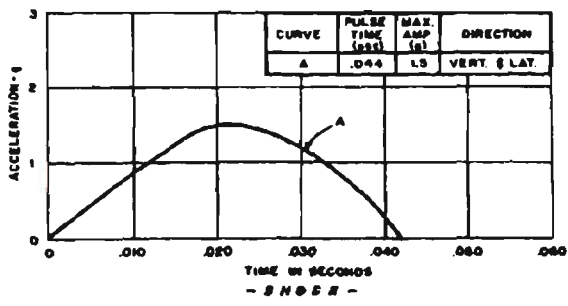
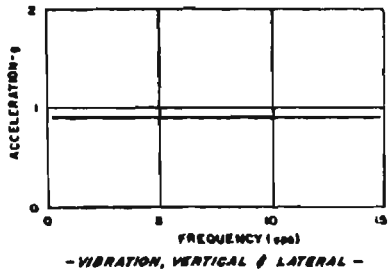


Figure 2-13 Cargo environments for sea transport

Shipboard vibrations originate from the ship's on board machinery and interaction with the sea. The ship's engines drive shafts, gearing and propellers initiate low level excitation. In addition, resonances may be excited as harmonics of the shaft frequency and blade passing frequency.

A ship at sea is subject to external influences of wind and wave which produce a variety of movements, generally periodic in nature. The instantaneous position or motion of the ship is therefore the consequence of a combination of the following types of rigid body movements:

- Pitching
- Rolling
- Yawing
- Heaving
- Fore - and - off acceleration or deceleration

These motions have long periods (greater than one second) with extreme values of pitch and roll reported as much as 20 and 40 degrees, respectively.

In extremely rough water the bow of the ship rises out of water and falls back again. The resulting forces exerted on the hull excite free-free vibration modes of the ship's longitudinal gird, which is called whipping. In the fundamental two-node mode, both the bow and stern move up and down in phase. Although whipping can occur in either the pure vertical or pure horizontal plane, it may also occur simultaneously in both planes to create a torsional vibration mode. Another hydrodynamically caused force on the hull is due to pounding of waves on the hull, similar to slamming, but in which the ship's bow does not rise out of the water. Finally, there are all the other wave impacts occurring more frequently but at less intense levels.

### **Air Transportation Hazard**

Designing packaging systems suitable for air transport has been recognised by Lambert, (1964) as follows:

- Cargo and its restraining system should be capable of withstanding all the aircraft vibrations occasioned for a time period consistent with the maximum range of the aircraft.
- The shock acceleration normally occasioned by landing should be based on a velocity at touchdown for the aircraft of 10 feet per second and any safety factors should be applied by increasing the number of shocks rather than the severity.
- Envelopes of the maximum data recorded are shown in Figure 2-14. These data are from tests in which short recording duration were used and where high input loadings were simulated consistent with test safety.

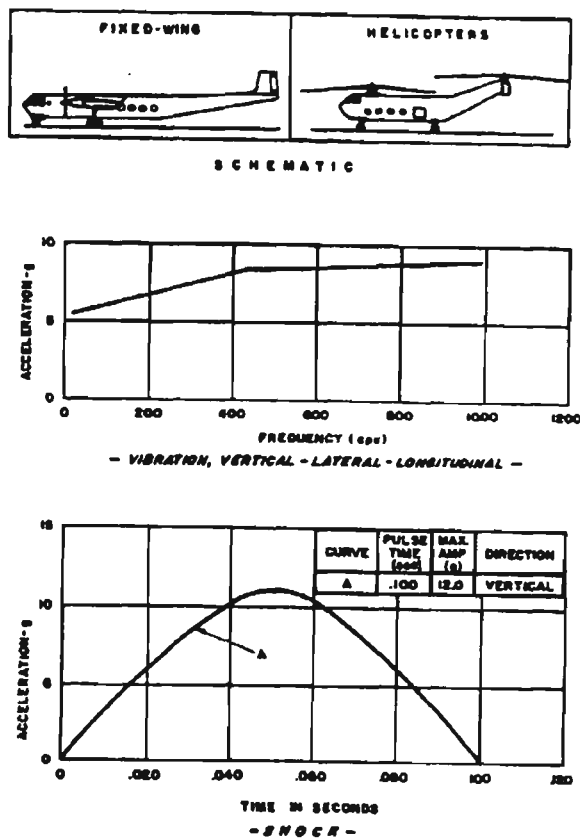


**Figure 2-14 Cargo environments for air transport**

The vibration in aircraft is generally random with superimposed excitation originating from the propulsive system, Tevelow (1983). For turbojets, the amplitude of the vibration spectra depend on the aircraft flight phase. Other vibrations in aircraft may result from or be compounded by unbalance in propellers, aerodynamic forces caused by the air flow fields, fluctuations in turbine air-fuel mix etc.

Trost (1986) compared air transportation with other means of transport and with regard to the stresses to which transported products are exposed. The induced shock and vibration for air transportation are considered the least severe to cargo and its restraining system:

- More specifically, the movements of the aircraft can be divided into a number of phases: taxiing, take-off, climb, cruise, descent, landing (touch down and roll-out) and subsequent taxiing. However whether the aircraft has ground contact or is airborne, the shock levels are higher during ground contact, but the time of

exposure is considerably shorter. The "real ground contact", i.e. when the product are handled and transported on their way between terminal and aircraft, shocks are more severe.

- Considerably lower vibration levels exist than for other means of transport in frequency range of importance, as far as product movement is concerned (e.g. up to 30-50 Hz), besides that the maximum acceleration occur less frequency during transport and for short periods of time (e.g. at landing, including touch-down ).

The stresses transferred to the product and its packaging system in the form of accelerations, during air transport have been measured and summarised as follows:

- As far as the shock and vibration levels are concerned, the ground transport phases of air transport are the severest, next come take-off and landing and then airborne.
- The vertical accelerations generally are the greatest.
- The transversal and longitudinal accelerations are generally smaller than the vertical acceleration. The relation between them is dependent on the phase of the flight. In phases where the aircraft is markedly inclined, such as climb and descent, the longitudinal stresses are greatest. This is also the case during the acceleration at take-off and braking after touch-down. During the cruise phase the transversal acceleration are normal somewhat larger than the longitudinal accelerations.
- The largest maximum acceleration levels have been recorded during landing, where touch-down gave 0.42g .

### **2.1.3 Experimental Analysis**

According to Ewins (1984) the experimental observations have been made for two major objectives

- Determining the nature and the extent of vibration response levels and
- Verifying theoretical models and predictions.

The two measurement objectives indicated above represent two corresponding types of test. The first is one where vibration force or, more usually, response are measured during 'operation' of the machine or structure under study. The second test is where the structure or component is vibrated with known excitation, often out of its normal service environment. This second type of test is generally made under more closely controlled conditions than the former and consequently yield more accurate and detailed information. This type of test is called 'Modal Testing' and the objective is to obtain a mathematical description of the dynamic or vibration behaviour i.e. natural frequency, damping factor, mode shape and frequency response function, for the purpose of verifying theoretical models and predictions.

### **2.1.4 Frequency Response Function Method**

Randall et al (1988) stated that the most commonly used experimental approach to determine the modal parameters is the Frequency Response Function (FRF) method. The FRF is the ratio of output response to input excitation as a function of frequency for a single input and a single output. The FRF usually are used to describe the input-output force-displacement relationship of a system. Most often, the system is assumed to be linear and time invariant. This method originated as a testing technique as a result of the use of FRF in the forced normal mode excitation method to determine natural frequencies, mode shape and the effective number of degree of freedom.

In this method, FRF are measured using excitation at single or multiple points. This excitation may be narrow band or broad band as well as being random or deterministic.

A curve fitting procedure is used to evaluate the model parameters (material properties, boundary conditions etc). In order to ensure that all modal vectors have been found experimentally, a number of excitation points must be utilised, one at a time or simultaneously.

The computation of the theoretical FRF depends upon the transformation of data from the time to the frequency domain. The FT is used for this computation. The integral FT definition requires time histories from negative infinity to positive infinity. Since this is not possible experimentally, the computation is performed digitally using a FFT algorithm which is based upon only a limited time history. In this way the theoretical advantages of the FFT can be implemented in digital computation scheme.

Randall suggested that data presentation should represent the physical interpretation of the modal parameters. It may simply be the numerical tabulation of the frequency, damping, and modal vectors, along with the associated geometry of the measured degrees of freedom.

### Frequency Response Function (FRF) Estimates

Probably the most common application of two channel analyser is to measure Frequency Response Functions (FRF) of physical systems. Referring to Figure 2-15, the FRF describing the system in the frequency domain is defined by

$$H(f) = \frac{B(f)}{A(f)}, \quad 2.8$$

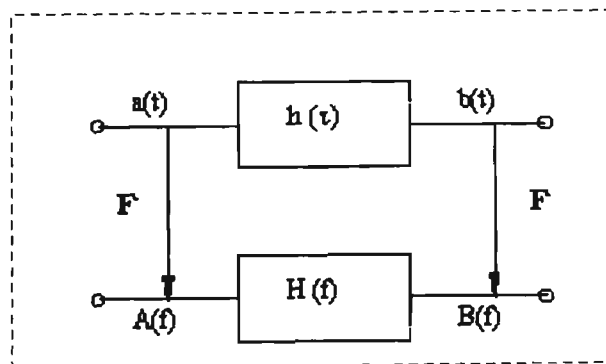


Figure 2-15 System with input signal  $a(t)$  and output signal  $b(t)$

A number of assumptions about the system have to be made before the system can be described in terms of a FRF:

1- the system must be physically realistic. It cannot respond to an input before it is applied, or  $h(\tau) = 0$  for  $\tau < 0$

2- The system must be time invariant. Its properties may not change with time,

$$h(\tau, t) = h(\tau) \quad 2.9$$

and  $H(f, t) = H(f), -\infty < t < \infty \quad 2.10$

3- The system must be stable. It can only respond with a limited amount of energy when excited with a finite amount of energy at the input. This is also true if

$$\int_{-\infty}^{\infty} |h(\tau)| d\tau < \infty \quad 2.11$$

4- The system must be linear. This means that if the inputs  $a_1(t)$  and  $a_2(t)$  produce the outputs  $b_1(t)$  and  $b_2(t)$  respectively, then the input  $a_1(t) + a_2(t)$  must produce the output  $b_1(t) + b_2(t)$ , and the input  $c \cdot a_1(t)$  must give the output  $c \cdot b_1(t)$ , where  $c$  is an arbitrary constant. The assumption of linearity is probably the requirement which is most often violated in practical applications. The input signal may have such high amplitude levels that the system will be excited beyond its range of linear behaviour. Also some systems are inherently non-linear and the system function description will not be valid except for very limited ranges of input signal levels.

The time variations can also cause severe problems in practice. The system characteristics might depend upon environmental conditions.

The FRF of the ideal system in Figure 2-15 fulfilling the requirements of equations (2.12) - (2.15) can be estimated using the two channel FFT analyser. The fundamental equation relating the input spectrum and output spectrum is

$$B(f) = H(f) \cdot A(f) \quad 2.12$$

Multiplying by the complex conjugate of  $A(f)$  ie.  $A^*(f)$  on both sides of the equation.

$$A^*(f) B(f) = H(f) \cdot A^*(f) \cdot A(f) \quad 2.13$$

$$S_{AB}(f) = H(f) S_{AA}(f) \quad 2.14$$

$S_{AB}(f)$  and  $S_{AA}(f)$  or  $G_{AB}(f)$  and  $G_{AA}(f)$  which are measured with the dual channel analyser.

The ratio of these estimates therefore gives a measure of the FRF and is called  $H_1(f)$  using the one-side spectra we get from equation (2.13)

$$H(f) = \frac{G_{AB}(f)}{G_{AA}(f)} \equiv H_1(f) \quad 2.15$$

Multiplying equation (2.8) by  $B^*(f)$  instead of  $A^*(f)$  we get

$$B^*(f) B(f) = H(f) \cdot B^*(f) \cdot A(f) \quad 2.16$$

$$S_{BB}(f) = H(f) S_{BA}(f) \quad 2.17$$

Using this equation the ratio of estimates of  $S_{BB}(f)$  and  $S_{BA}(f)$  or  $G_{BA}(f)$  and  $G_{BB}(f)$  also gives a measure of the FRF  $H(f)$ . This estimate called  $H_2(f)$  will in many practical cases give a different result than  $H_1(f)$ . In terms of the one sided spectra estimates therefore

$$H(f) = \frac{G_{BB}(f)}{G_{BA}(f)} \equiv H_2(f) \quad 2.18$$

Note that the phase of  $H_1(f)$  is the same as the phase of  $H_2(f)$  since  $G_{BA}^*(f) = G_{AB}(f)$

$$\text{Also note that } \frac{H_1(f)}{H_2(f)} = \frac{G_{AB}(f) G_{BA}(f)}{G_{AA}(f) G_{BB}(f)} = \gamma^2(f) \quad 2.19$$

Coherence  $\gamma^2$  of the signals  $a(t)$  and  $b(t)$  is a function which on scale from 0 to 1 measure the degree of linear relationship between the two signals at any given frequency.

## **2.2 Finite Element Method**

### **2.2.1 The Finite Element Method**

Clough et al (1993) stated that the FE method is a numerical procedure for analysing structures. Usually the analysis is too complicated to be solved satisfactorily by standard analytical methods. The problem may concern stress analysis, heat conduction, or several other areas. The FE procedure produces addition algebraic equations, which solved numerically on personal computers or mainframes, and all sizes in between, result are rarely exact. However, errors are decreased by processing more equations, and the results obtained are accurate enough for engineering purposes at reasonable cost

The FE method models a structure as assembly of small elements, each element is of simple geometry and therefore is much easier to analyse than the actual structure.

The solution is an approximate, but the approximation can be improve as the model is refined so that the analysis whether static or dynamic will produce the exact answer as the number of elements tends to infinity. This refinement usually involves dividing the element into successively larger number of smaller elements. The process of approximation in the analysis leads to sets of algebraic equations for which matrix provide a convenient short hand, even that the process is complicated in some cases. However introducing computer modelling makes modelling easier, therefore most of the effort will be directed to analysing the result rather than rechecking very lengthy mathematical operations.

A finite element analysis for stress and transfer analysis involves the following steps.

1. Divide the structure into finite elements, using mesh generation.
2. Formulate the material properties of each element. In stress analysis, this means determining nodal loads associated with all element deformation states that are allowed.
3. Assemble elements to obtain the finite element model (FEM) of the structure.
4. Apply the known load: nodal forces and/or moments in stress analysis.
5. In stress analysis, specify how the structure is supported. This step involves setting several nodal displacements to known values (which often are zero).

6. Solve simultaneous linear algebraic equation to determine nodal d.o.f. (nodal displacements in stress analysis).
7. In stress analysis, calculate element strains from the nodal d.o.f. and the element displacement field interpolation and finally calculate stress from strain.

Steps 1, 4, and 5 require decisions by the analyst and provide input data for the computer program. Steps 2, 3, 6 and 7 are carried out automatically by the computer program.

The power of FE method dwells in its flexibility. The method can be applied to various physical problems. The body analysed can have arbitrary shape, load and support conditions. The mesh can mix elements of different types, shapes and physical properties. The input data controls the selection of problem type, geometrical condition, element selection, etc.

An additional attractive feature of FE is the close physical similarity between the actual structure and its FEM. The model is not simply an hypothesis. This seems especially true in structural mechanics. The FE method also has disadvantages. A specific numerical result is found for a specific problem: FEA provides no closed-form solution that permits analytical study of the effects of changing various parameters.

## 2.2.2 Finite Element Static and Dynamic Analysis

### Finite Element Packages

Information was obtained for the purpose of evaluation and recommendation on PC based Finite Element packages, to be used by HEC manufacturing engineering department, Atkinson (1992). Three of software packaging have been selected and are shown in Table 2-2

**Table 2-2 PC based finite element packages**

Package	Vendor	Price
MSC/PAL	MacNeal Schwendler Corporation	\$ 1,800
ALGOR	ALGOR Inc.	\$ 2,150
STRAND 6.0	G + D Computing	\$ 4,000

A copy of each package was obtained and fully evaluated. All three packages proved to be reliable PC based analysis packages and because of their low prices, can be considered an excellent value. The capabilities of these packages are however limited by the PC configuration on which they run. It is difficult to compare the three packages, as the philosophies behind their design are completely different. The Algor tries to emulate the features found on workstation based packages, while Strand and MSC/PAL utilise techniques which require more thought from the operator, but are well suited for the PC environment. Table 2-3 attempts to grade the three packages in various area. In each case, the base configuration for each package is considered, as this is what the above prices are based on. Each score is out of 10.

**Table 2-3 PC based finite element packages comparison**

Function	STRAND	ALGOR	MSC/PAL
Pre-Processing	5	8	5
Solver	8	2	7
Post-Processing	5	8	5
Speed	5	7	5
Other Features	8	4	7
Data Translation	5	6	5
Accuracy	10	10	10
Growth path	10	7	0
Compatibility	6	5	6
Local Support	8	0	10
Local skills base	8	1	8

The recommendation was to purchase the STRAND package from G+D Computing. Although the STRAND package is currently weaker than the ALGOR package in the area of modelling and result interpretation, it wins out in almost every other area. It would have been possible to increase ALGOR's score in various areas by purchasing extra modules, however this would have meant purchasing over \$7,000 worth of software in order to outscore STRAND. In addition STRAND will be upgraded and will surpass the capabilities of both ALGOR and MSC/PAL

An added benefit of STRAND is the cost of additional licences. If STRAND has already been purchased for any workstation, additional copies of STRAND can be bought for one quarter of the original price.

The deciding factor for purchasing STRAND is it comes with its own graphical pre- and post-processors and is integrated into one package and it's ease of upgrade. For example, the package can be purchased to operate on a PC and will provide a more than adequate PC package. If and when it is deemed necessary to upgrade to workstation, STRAND can be transferred to a workstation, free of charge. Once on a workstation STRAND will take advantage of the extra processing power and graphics capabilities of workstation making the modelling and analysis tasks faster and easier.

Also, When STRAND is operating on a workstation, it will be capable of becoming the solver portion of the Unigraphics G/FEM plus finite element software. This means that the solver portions of G/FEM plus will not need to be bought, allowing considerable savings in the long term.

STRAND software presented the basic theoretical analysis as

### 2.2.3 Structural Static Analysis

The structural static analysis is used to determine the displacements, stresses, strain, and forces that occur in a structure or component as a result of applied loads. Static analysis is used to solve problems in which the time-dependent effects of inertia and damping do not significantly affect the structure's response. This analysis can be used for many applications, such as determining the stress concentration in fillets of mechanical components or predicting the stresses in a structure resulting from temperature distribution.

Most software programs solve static analysis problems by applying numerical techniques to these same traditional engineering concepts. The governing equation for static analysis is

$$[K] \{x\} = \{F\}$$

2.20

## 2.2.4 Modal

Experimental modal analysis is used to extract the natural frequencies and mode shapes of structure. This process is important as a preprocessor to any dynamic analysis because knowledge of structure's fundamental modes and frequencies can help to characterise its dynamic response. The results of this analysis also help determine the number of modes or the integration time step to be used in transient dynamic analyses.

## 2.2.5 Natural Frequency

Natural frequency is the frequency of free vibration of a system. For a multiple degree-of-freedom system, the natural frequencies are the frequencies of the normal modes of vibration. Normal mode of vibration is a mode of vibration that is uncoupled from (i.e. can exist independently of) other modes of vibration of a system. When vibration of the system is defined as an eigenvalue problem, the normal modes are the eigenvectors and the normal mode frequencies are the eigenvalues. Mode of vibration, is a characteristic pattern assumed by the system in which the motion of every particle is simple harmonic with the same frequency. Two or more modes may exist concurrently in a multiple degree-of-freedom system.

### Natural Frequencies and the Eigenvalue problem

One of the most distinguishing features of a body's dynamic behaviour is its undamped and unforced response to external excitation. The motion is assumed to be simple harmonic and is an important physical attribute. The equation of motion with no damping and no external force is,

$$[M]\{\ddot{x}\} + [K]\{x\} = \{0\} \quad 2.21$$

## 2.2.6 Harmonic Response

Harmonic response analysis is used to determine the steady state response of a linear structure to a sinusoidally varying forcing function. This analysis type is useful for studying the effects of load conditions that vary harmonically with time, such as those experienced by housing, mountings, and foundations of rotating machinery. The governing equation for harmonic response analysis is a special case of the general equation of motion, in which the forcing function  $\{F(t)\}$  is a known function of time varying sinusoidally with a known amplitude  $F_0$  at a known frequency  $\omega$  and phase angle,  $\phi$ :

$$\{F(t)\} = \{F_0 (\cos (\omega t + \phi ) + i \sin (\omega t + \phi ))\} \quad 2.22$$

The displacements vary sinusoidally at the same frequency  $\omega$  but are not necessarily in phase with the forcing function. Loading can be in the form of nodal forces or imposed displacements. The displacement can be obtained at specified frequencies.

### Phase Angle

The various load cases can have a phase angle  $\phi$  specified such that the force applied to the model at any time is

$$\{P\} \cos(\omega t + \phi ) \quad 2.23$$

The displacements in the structure may not always be in phase with the applied force. This means that the maximum response may not necessarily correspond to the maximum value of applied load. In order to determine the maximum displacements etc. it is necessary to investigate the response when the loads are applied at phase angles. The analysis normally carried out as a function of frequency and only the state of the structure at instant when the load is at the specified phase angle is considered. On large complex structures it may be necessary to carry out many analysis at different angles to fully capture the peak response of all parts of the structure. The phase angle is specified in degrees.

### 2.2.7 Transient Dynamics

Structural dynamic analysis is used to determine the effects of time-varying loads on a structure or component. Unlike static analysis, a dynamic analysis takes into account damping and inertia effects of time-varying loads, examples of such loads are as rotating machinery, impact or explosion, random forces, base excitation and any other transient forces, such as moving loads on a bridge.

Most problems in structural dynamics analysis fit into two broad classes.

- The natural frequencies and mode shapes and steady state response (harmonic response) of structure to cyclic loads.
- A complete detailed time history of transient motion, i.e. Immediately following a shock loading. This loading may produce a very localised effect and it would not be known in advance which were the significant eigen modes involved, it would certainly not be the lower ones.

In many cases a finite element static analysis is not sufficient, when the maximum acceleration or velocity of a system is required or when the response of a system to time varying load is needed. In these cases it is necessary to carry out a dynamic analysis of the system, the equations to be solved are of the form

$$[M]\{\ddot{x}\} + [C]\{\dot{x}\} + [K]\{x\} = \{F(t)\} \quad 2.24$$

In this form of analysis the inertia forces are included in the calculation through the mass matrix  $[M]$ , the effect of the inertia forces being proportional to the acceleration. Damping is included in the analysis through the damping matrix  $[C]$  and  $[K]$  is the system stiffness matrix. To carry out this form of analysis the direct integration method is used. Using the direct integration method the above equation is integrated using a numerical step by step procedure where the conditions at time 't' are assumed to be known and are required after a discrete time step ' $\Delta t$ ', at time ' $t + \Delta t$ '. It is also assumed that the variation of the displacement, velocity and acceleration are known over the time step. Repeating this method yields the response of the system at a finite number of points through time. To carry out this form of analysis the required information is therefore the initial conditions at time ' $t = 0$ ',

the mass, damping and stiffness matrices and some description of the variation of the applied load with time.

### Choice of time step

The choice of time step is of importance as far as the solution time is concerned. It is important to capture the low frequency response of the structure but in most cases if the time set was chosen to capture the behaviour of the highest frequency it would be prohibitively small. A good choice of time step is '  $\delta t = 0.01T$  ' where '  $T$  ' is the fundamental period of the system, this will adequately capture the low frequency response of the system and much of the higher frequency response. In fact if the low frequency response is required a time step size of a quarter of condition to be specified.

### 2.2.8 Finite Element Damping

The type of practical damping that can be included in a finite element formulation are the spectral methods. Viscous damping is introduced by specifying some fraction of the critical damping. Critical damping for a structure marks the transition between oscillatory and nonoscillatory response. For critical damping the ratio is  $\xi = 1$ .

If damping is to be included, a viscous damping matrix  $[C]$  is defined using Rayleigh or proportional damping. Rayleigh damping is the most popular form of spectral damping. The viscous damping matrix  $[C]$  is formed from a linear combination of the stiffness  $[K]$  and mass  $[M]$  matrices. This takes the form:

$$[C] = \alpha [M] + \beta [K] \quad 2.25$$

where  $\alpha$  and  $\beta$  are called the stiffness and mass proportional damping constants. The matrix  $[C]$  is an orthogonal damping matrix because it permits modes to be uncoupled. The relationship between  $\alpha$ ,  $\beta$  and the damping ratio  $\xi$  at some specified frequency  $\omega$  is given by:

$$\xi = \frac{1}{2} \left( \alpha \omega + \frac{\beta}{\omega} \right) \quad 2.26$$

The constant  $\alpha$  and  $\beta$  are determined by choosing the damping ratios ( $\xi_1, \xi_2$ ) at two different frequencies ( $\omega_1$  and  $\omega_2$ ) and solving simultaneously for  $\alpha$  and  $\beta$  :

$$\alpha = \frac{2\omega_1\omega_2(\xi_2\omega_1 - \xi_1\omega_2)}{(\omega_1^2 - \omega_2^2)} \quad 2.27$$

$$\beta = \frac{2(\xi_1\omega_1 - \xi_2\omega_2)}{(\omega_1^2 - \omega_2^2)} \quad 2.28$$

Usually  $\omega_1$  and  $\omega_2$  are chosen such that they cover all the frequencies of interest in the design. The  $\omega_1$  would normally be chosen as the lowest natural frequency of the structure and  $\omega_2$  would be the maximum frequency of interest in design.

### 2.2.9 Response Spectrum

A response spectrum analysis can be used to determine the response of a structure to shock loading conditions. This analysis type uses the result of a modal analysis along with a known spectrum to calculate actual displacement and stresses that occur in the structure at each of its natural frequencies. A typical response spectrum application is base acceleration analysis, which is used to study the effect of vibration transmitted from road to a packaging or from a packaging to products, seismic which study the effect of earthquakes on structures such as piping system, tower, and bridges.

#### Spectral Response

The spectral analysis calculates the linear elastic response of a structure subjected to a random dynamic loading. Usually it is used instead of transient dynamic analysis as a quicker alternative, also seismic technique can be adopted for analysis of lateral transportation vibration.

Two types of spectrum response analysis may be obtained:

- Response Spectrum

- Power Spectral Density (PSD).

The dynamic loading can be either base excitation represented by its response spectrum or a general dynamic load applied on the structure given by a load spectrum. In both cases the excitation is defined with a spectral curve:

- Spectral value or Spectral Density.
- Cyclic Frequency versus Spectral value.

The base excitation spectrum is applied equally at all supports. Also may act in the three global X-Y-Z directions simultaneously. Three types of base excitation spectral are available : acceleration spectrum, velocity spectrum, and displacement spectrum. The base excitation spectrum is used in the calculation of the maximum structural response to seismic action. The load spectrum simulates the situation when some random dynamic load is applied on the structure at a number of nodes away from the supports. The applied load has the same frequency content at each of the nodes but the magnitude may differ, its typical application is in response analysis to wind load, ocean wave loads or machinery vibration

The result of a spectral analysis is given as envelope of maximum values of nodal displacements, element and nodal stress, element and nodal strain and recovered reactions at constrained nodes, including elastic forces at all other nodes. The maximum values are calculated by combining the maximum response of all modes included in the analysis. Two methods for modal combination may be used: SRSS (Square Root of Sum of the Squares) and CQC (Complete Quadratic Combination). Maximum response values of nodal deformation, stresses and reactions are automatically calculated. The maximum values are usually sufficient for most applications.

In the case of a response spectrum the response of the structure is deterministic and thus the peak response of the structure to the applied load can be calculated. The situation with the power spectral density spectrum is different. The PSD curve represents an averaged random loading condition and thus an actual value of maximum response cannot be determined. The PSD method adopts a statistical approach and presents the output as a probabilistic response. The output displacements, stresses and strains are one standard deviation ( $\sigma$ ) values. From statistical theory this means that the actual response will be less than the calculated values

68.3 % of the time. The response at  $2\sigma$  and  $3\sigma$  can be calculated by scaling the results by a factor of 2 or 3 using the Combine Result module. The meaning of the response at  $2\sigma$  and  $3\sigma$  is that the calculated response will not be exceeded for 95.4 % and 99.7 % of the time respectively.

## Response Spectrum

The response spectrum is typically used in earthquake and shock analysis. For each mode and corresponding frequency the Spectral Solver calculates one spectral value (S) from the associated spectral tables. If the modal frequency is outside the table range the spectral value will be set to zero. In the case of seismic spectrum, the seismic excitation factor for each mode included in the analysis is calculated by the expression:

$$L_i = \{\phi\}_i^T [M] \{r\} \quad 2.29$$

In the case of load spectrum, the load excitation factor for each mode included in the analysis is calculated by the expression:

$$L_i = \{\phi\}_i^T \{R\} \quad 2.30$$

Modal displacement amplitude is calculated for each mode separately by one of the following expression:

$$\text{For seismic acceleration} \quad : \quad Y_i = \frac{L_i S_i}{\omega_i^2} \quad 2.31$$

$$\text{For seismic velocity} \quad : \quad Y_i = \frac{L_i S_i}{\omega_i} \quad 2.32$$

$$\text{For seismic displacement} \quad : \quad Y_i = L_i S_i \quad 2.33$$

$$\text{For load spectrum} \quad : \quad Y_i = \frac{L_i S_i}{\omega_i^2} \quad 2.34$$

Maximum displacement for each mode is calculated by :

$$\{X\}_i = \{\phi\}_i Y_i \quad 2.35$$

The maximum response  $\{x\}$  is calculated by combining modal responses by two alternative methods:

$$SRSS \quad \{x\} = \sqrt{\{x\}_1^2 + \{x\}_2^2 + \{x\}_3^2 + \dots + \{x\}_n^2} \quad 2.36$$

$$CQC \quad \{x\} = \left[ \sum_i \sum_j \alpha_{ij} \rho_{ij} |\{x\}_i| |\{x\}_j| \right]^{1/2} \quad ij = 1,2,3,\dots,n \quad 2.37$$

where 
$$\alpha_{ij} = \frac{L_i L_j}{|L_i| |L_j|}$$

### Interpretation of Spectral Curves and Applied loads

When the response spectrum is used, the spectral curves define a dynamic amplification factor as a function of the frequency of the structure for a particular level of damping and input load frequency or loading condition. The spectral values in the curves are basically a ratio between the peak dynamic response and an equivalent static response when a steady state load, of the same magnitude as the dynamic load, is applied, normally the spectral tables will express the dimensionless amplification factor as a function of cyclic frequency. These tables may also contain the magnitude of the applied load and in this case the table will have units appropriate to the spectrum type selected (i.e. m for displacement spectrum m/s for velocity spectrum,  $m/s^2$  for acceleration spectrum or N for load spectrum). The actual load applied to the model depends on whether a base excitation spectra or the applied load spectra are used.

In the case of a base excitation spectrum the direction vector defines the direction of the acceleration, velocity or displacement as three components in the global axis system. The direction vector may be normalised, in which case the magnitude of the loading must be included in the table . More commonly the vector is not normalised in which case both the magnitude and direction of the excitation are defined by the direction vector. In such case the load applied is Spectral Value \* Direction Vector. In the case of base excitation spectrum the loading is employed to the base of the structure, that is all nodes with freedom conditions applied in the direction of the excitation. The excitation is applied equally to all base nodes. Other loads such as point loads, global acceleration, etc. have no effect when one of the base excitation spectra is selected.

When the Applied Load Spectrum is used the load on the model is = Applied Load \* Spectral Value \* Load Factor.

In this case the loads applied in the spectral analysis include nodal loads, element pressures and global accelerations etc. A load factor multiply all the loads applied to the mode in a particular load case.

### **Finite Element PSD**

The power spectrum is typically used when a structure or mechanical component is subjected to random vibration. Examples are buildings subjected to wind loads or mechanical components subjected to random base acceleration such as accessories attached to an internal combustion engine.

PSD analysis is commonly used to determine the response of structure subjected to a statistically averaged random excitation. The random excitation can be a force, acceleration, velocity or displacement. Because the excitation is random, we cannot determine the structure's response at any particular time . However, given a sufficiently large time interval, we can find the statistical (or probability) distribution of the response of the structure over this period.

When the PSD option is selected the spectral solver estimates the response of a structural model subjected to stationary random dynamic excitation given in the form of a single PSD curve. The results are given as one standard deviation ( $\sigma$ ) of the response. Here, the PSD function is a Fourier Transform of the Autocorrelation Function of the random process considered. The process is assumed to be stationary.

The standard deviation of the response, assuming the mean value of the response is equal to zero, is given by the formula:

$$\sigma^2 = \int_0^{\infty} [H(\omega)]^2 S(\omega) d(\omega) \quad 2.38$$

Where	$\sigma$	-	standard deviation of the dynamic response (displacement or stress)
	$H(\omega)$	-	frequency response function
	$S(\omega)$	-	PSD input
	$\omega$	-	$2 \pi f$ where $f$ is frequency in Hz

The spectral solver employs an approximate procedure for the evaluation of the above integral. The major assumptions are:

- The excitation is a single PSD curve representing a random stationary process.
- Modal damping ratios are less than 0.10 (narrowband system).
- Modal responses are statistically independent.

Most structures conform with these assumptions.

The input PSD curve is converted into a Response Spectrum curve, and then the modal responses are calculated. The total response is determined as a combination of the modal responses using either the SRSS or the CQC method.

### Interpretation of Spectral Curves and Applied Loads

The interpretation of the curves, direction vectors, load factors and applied loads is identical to that for the response spectrum in the manner in which these are combined to produce the

loading condition on the models. The only difference between the two spectrum types is the units of the applied loads.

In the case of PSD the loads applied to the model are expressed in  $\text{m}^2/\text{Hz}$  for displacement,  $(\text{ms}^{-1})^2/\text{Hz}$  for velocity,  $(\text{ms}^{-2})^2/\text{Hz}$  for acceleration and  $\text{N}^2/\text{Hz}$  for load spectra. Another common system of units in which the acceleration spectra is expressed in  $\text{g}^2/\text{Hz}$ . In this case the actual magnitude of  $\text{g}^2$  i.e.  $96.2361(\text{ms}^{-2})^2$  must be included in the direction vector.

## **2.3 Finite Element Verification and Validation**

### **2.3.1 Finite Element Verification**

Bongardt, (1993) confirmed that many vibration problems are analysed by comparing finite element and experimental modal models. Often, an initial FEM is modified based upon experimental data results until the FEM can successfully predict the parameter of the structure's dynamic and static response to the operational environment. Bongardt presented a study of the FEA and the verification testing for ship structure for developing a FEM to accurately assess the dynamic behaviour of a structure in the early stages of design before experimental data is available to fine tune the FEM. Result from this experimental case history are then applied to developing the FEM for a more complex structure. The results of the "blind" analysis are then presented to demonstrate the effectiveness of implementing these modelling techniques.

Bongardt concluded that

- Natural frequency obtained from FEM results when compared with experimental results were compatible.
- Forced vibration levels were calculated by FEM Direct Frequency Response algorithm and compared to the FRFs obtained during modal testing, depended upon the accuracy of the natural frequency and mode shape predictions.
- Structural damping was applied to the FEM using a single uniform damping coefficient. This damping coefficient is not necessarily the best for all resonances

since damping varies with frequency, however it would have been extremely difficult and time consuming to predict an accurate damping as a function of frequency.

The results of the "blind" foundation analysis were validated using the machinery pallet. These techniques were also used in the analysis of several other structures with similar results. However the use of validated finite element analysis techniques can provide immeasurable benefits when properly applied to difficult design problems, the proper use of these complex tools generally requires the incorporation of varied level of engineering judgement and mathematical assumptions.

Also Li Runfang et al (1992) present a finite element modelling approach by mixed formula for the dynamic response of three-dimensional impact-contact system. In his approach, the Coulomb's law of friction is employed in the surface description of contact regions in the system, and boundary conditions on the contact regions are formulated into coefficient matrices. A modified Cholesky elimination algorithm is introduced to form the effective flexibility matrix of contact surface in the impact-contact system. In the process of iterations at each time step of direct Newmark integration, the computation is condensed to the solution of the effective flexibility matrix equation on the contact surface. Li Runfang present an example for the dynamic contact problem of semi-infinite elastic surface and an elastic hexahedron body under a sudden distributed loading. The FEM and the dimensions of the system are shown in Figure 2-16 the material in the system has modulus of elasticity  $E = 2.1 \times 10^{11} \text{ N/m}^2$ , mass density  $\rho = 7.8 \times 10^3 \text{ kg/m}^3$  and Poisson's ratio  $\nu = 0.3$ . The transient contact force of the centre node point on contact surface is shown in Figure 2-17 and the transient velocity response of the centre node point is shown in Figure 2-18. The time step of integration is  $\Delta t = 0.1 \text{ ms}$ .

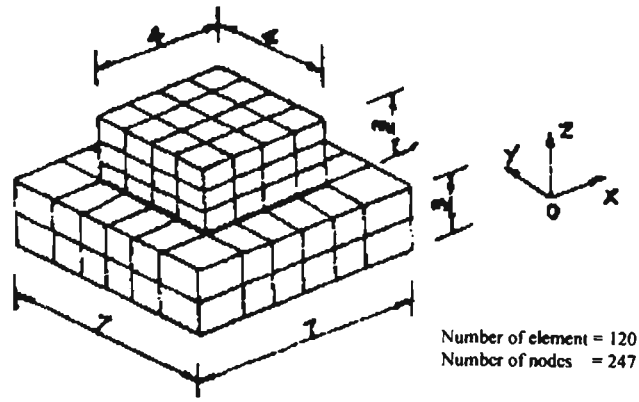


**Figure 2-16 Finite element model**

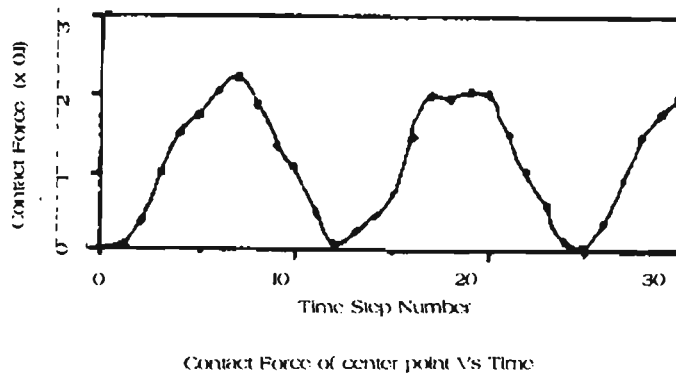


**Figure 2-17 Transient contact force**

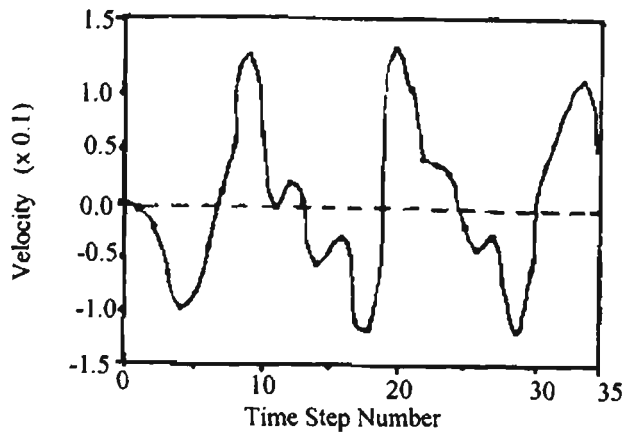


**Figure 2-18 Transient contact velocity response**

### 2.3.2 The Finite Element Validation

Dobson et al (1982) commented that finite element models are widely used to investigate the dynamic behaviour of structures. These models can predict the natural frequencies and the associated mode shapes and the response of the structure to different types of excitation. While finite element models may produce reliable dynamic and static predictions there are many cases in which some form of validation against experimental data is necessary. This is particularly important where a structure is to be analysed under severe loading conditions that may prevent a direct experimental study. In these cases the finite element model must be validated against practical experimental results obtained from standard modal tests and benchmark test such as frequency response curves, natural frequencies and mode shapes.

Ewins (1984) confirms that the most commonly used application to validate a model is the measurement of vibration modes in order to compare these with corresponding data produced by finite element or other theoretical model. This application is often born out of need or desire to validate the theoretical model prior to its use for predicting response level to complex excitation, such as shock, or other further stages of analysis. It is generally felt that affirmation of major modes of vibration by tests can provide reassurance of the basic validity

of the model which may then be put to further use. For this specific application, all that is required from the test is:

- accurate estimates of natural frequencies and
- descriptions of mode shapes using just sufficient detail and accuracy to permit their identification and correlation with those from the theoretical model. At this stage accurate mode shape data is not essential, it is generally not possible to predict the damping in each mode of vibration from a theoretical model and so there is nothing with which to compare measurements of modal damping from the test.

However, such information is useful as it can be incorporated into the theoretical model, as an approximation, prior to that being called upon to predict specific response level.

Also many cases of experiment - theory comparison stop at the stage of obtaining a set of results by each route and simply comparing them. Sometimes, an attempt will be made to adjust or correct the theoretical model in order to bring its modal properties into line with the measured results.

### **Comparison of Predicated and Measured Modal Properties**

Dobson et al (1982) have described and illustrated (Appendix A.4) a method for relating finite element and experimental result through the spatial parameters of mass and stiffness. In particular he has shown that incomplete experimental data may be used to locate specific regions within the structural model at which the stiffness has been incorrectly specified. It was suggested that the difference noted resulted from point defects at welded connections within the structure. However, the differences appeared to be systematic their interpretation was not clear. In general, stiffness variations between finite element models and real structures may result from a number of causes. These include overall effects (e.g. incorrect values of Young's modulus), local effects (stiffness or mass errors within an element or group of elements), point effects (joints or cracks) and, for fixed systems, errors resulting from incorrectly modelled boundary conditions.

### **2.3.3 Identification of Differences between Finite Element Analysis and Experimental data**

Lawrence (1987) states that the dynamic characteristics of a structure systems are often predicted using FEA and then later verified experimentally with dynamic analysis.

The increased demands for reliability, minimal vibration, optimum performance and low cost design, among other criteria, have increased designers needs for sophisticated dynamic analysis test techniques. An important problem that has emerged from these combined analytical / experimental investigations is the task of identifying and quantifying the differences between results predicted by FEA and results obtained from the experiment. Although both the FE and experimental methods can be accurate from a theoretical standpoint, inaccuracies do exist in their applications to real structural problems. In the case of FE modelling there is considerable uncertainty in the modelling of items such as boundary conditions, joint flexibility and damping. Because of this, the FE results are not exact since the input data itself is approximated. Also, it is not possible to completely eliminate experimental error.

A communication gap can exist between the experimentalist and FE modeller when the experimentalist cannot provide the quantitative data required by the analyst to identify the differences between the experimental data and the FEM. The gap exists because the experimentalist normally measures frequencies and mode shapes in a vibration test, while the analyst requires a mass, damping, and stiffness matrix for describing the FEM.

One possible way to compare the experimental result to the FEM is to compute the analytical frequencies and mode shapes from the FE equation of motion and to compare them to the frequencies and mode shapes obtained from the experiment. The limitation of making a comparison at this level is that even though disagreements can be identified, the cause of disagreements, namely differences in the mass, damping, and stiffness matrices, cannot be identified or quantified.

A more useful comparison between FE and experimental can be made through the equations of motion. By using the original FE equations and the equations of motion derived from the experimental data, differences between experiment and FE coefficients can be identified and

corrected. Unfortunately, the procedure of deriving an equation of motion from the experimental frequencies and mode shapes is not straightforward. To derive the equation of motion from experimental data requires that the same number of modes as degrees of freedom in the FEM be experimentally measured and that the experimental data does not contain any measurement error or noise. If both of these requirements are not met the experimental data cannot be used to construct a correct equation of motion. Since the coefficients for the equations of motion are computed by inverting matrices containing the experimental mode shapes, these matrices must be square. In a typical experiment, the number of measured modes will not be equal to the number of degrees of freedom so the modal matrices will be rectangular instead of square. Another difficulty is that the experimental data will always contain some amount of experimental error and noise which makes the outcome of a matrix inversion questionable. Also, if the highest modes in the structure are not included in the experimental data, the stiffness matrix computed from a modal matrix inversion will be incorrect, Berman (1971). Moreover, it is difficult to measure the values of the mode shapes corresponding to every degree of freedom used in the FEM. This causes the order of experimental matrices to be less than those in the FE equations.

Lawrence (1987) concluded that in a general procedure for identifying and quantifying the differences between FEM and experimental data, when the differences are computed in terms of mass, damping, and stiffness coefficient, possible modelling problems can be identified in the FE or analytical model. In practice, it will be required to measure the experimental frequencies and mode shapes very accurately before the differences can be attributed to shortcomings in the analytical model. If the experimental data is not accurate, the computed differences can still provide considerable insight into the possible locations of deficiencies. The difference is that the deficiencies may be in the experiment and some decision will be required to decide whether to modify the experiment or the analytical model.

Previous research in this area has focused on using experimental data to improve FEM rather than on identifying the differences. Most of the techniques have been based on some form of a least squares fit. In the work by Barman and Flannelly (1971) the analytical matrices are assumed to be close to the actual solution and then the smallest change in the analytical model that makes the experimental and analytical frequencies and mode shapes identical is

found. This assumption will not necessarily lead to an analytical model that is physically representative of the actual structure. The only assurance is that the revised model will correctly predict the modes that were measured. The problems arising from using "incomplete" data (data containing fewer modes than there are in the FE model) are discussed by Fuh, Chen and Berman (1984) who use similar approach for correcting structures with viscous damping.

Chen, Peretti and Garba (1984) refined a FEM of the Galileo spacecraft by first performing static test to improve the stiffness matrix and the dynamic tests for correcting the mass matrix. The mass matrix corrections of this approach are that two independent sets of tests must be run and again, there is no guarantee that actual physical characteristics will result from the least squares approach.

Hart and Yao (1977) discuss the advantages of using weighted least squares and Bayesian estimation. By using these extension of least squares methods, uncertainties in both the experimental data and analytical model can be included in the updating procedure. It can be very important to define the uncertainty in the experimental data since this data often contains more error than the FE description. It does not make much sense to attempt to improve a FEM with experimental data that is less certain than the FEM. By including relative uncertainties in the procedure, change to the analytical model will not be applied indiscriminately and the possibility exists for retaining the physical meaning of the structure in the updated model.

Dobb et al (1981) and Blakely et al (1984) applied the Bayesian estimation procedure to FEM of an offshore platform and dam. In their study the effects of a change in the uncertainties in both the experimental data and FE parameters were investigated. Unfortunately, well defined procedures do not exist for quantifying uncertainties so they had to be estimated using engineering judgement. Sidhu (1983) developed a procedure for approximating the difference between experimentally measured frequencies and mode shapes and FE parameters in terms of differences in mass, damping, and stiffness matrices. This approach has the potential for providing a direction to correct a FEM while retaining the physical characteristics of the real structure. The objective of this work is to extend the procedure developed by Sidhu for

correlation of linear finite element and modal test data to include structures with viscous damping. In this study, the derivation of the extended procedure and several case studies which use simulated experimental data are presented. The purpose of developing this procedure is to formalise a process for identifying the differences between experimentally measured frequencies and mode shapes and FEM in terms of differences in mass, damping and stiffness.

### 2.3.4 Methods of Model Updating

Many methods to improve the quality of analytical models using experimental data have been proposed and this process is often referred to as model updating. The report by Dornier Systems (1985) contains the following literature studies

#### Methods using Lagrange Multipliers.

The method proposed by Baruch (1997) assume that the mass matrix is correct and updates the stiffness matrix by minimising the distance  $\varepsilon$

$$\varepsilon = \left\| [K_A]^{-0.5} ([K_{AU}] - [K_A]) [K_A]^{-0.5} \right\| \quad 2.39$$

between the updated and the analytical stiffness matrices using Lagrange multipliers

Applying the following constraint equations:

$$[K_{AU}] - [K_A]^T = 0 \quad 2.40$$

$$[\phi_x]^T [K_{AU}] [\phi_x] [\omega_x^2] = 0 \quad 2.41$$

the updated stiffness matrix can be obtained as:

$$[K_{AU}] = [K_A] + [\Delta K] \quad 2.42$$

where

$$\begin{aligned}
[\Delta K] = & -[K_A][\phi_X][\phi_X]^T[M_A] - [M_A][\phi_X][\phi_X]^T[K_A] \\
& + [M_A][\phi_X][\phi_X]^T[K_A][\phi_X][\phi_X]^T[M_A] \\
& + [M_A][\phi_X][\omega_X^2][\phi_X]^T[M_A]
\end{aligned} \tag{2.43}$$

Berman and Nagy (1983) use the same approach to update the mass matrix by minimising

$$\varepsilon \dots = \left\| [M_A]^{-0.5} ([M_{AU}] - [M_A]) [M_A]^{-0.5} \right\| \tag{2.44}$$

using Lagrange multipliers and the orthogonality condition as the constraint equation. The updated mass matrix is obtained as

$$[M_{AU}] = [M_A] + [\Delta M] \tag{2.45}$$

where

$$\begin{aligned}
[\Delta M] = & -[M_A][\phi_X] \left( [\phi_X]^T [M_A] [\phi_X] \right) \\
& \left( [I] - [\phi_X]^T [M_A] [\phi_X] \right) \left( [\phi_X]^T [M_A] [\phi_X] \right) \\
& [\phi_X]^T [M_A]
\end{aligned} \tag{2.46}$$

For the updated stiffness matrix there are two additional constraint equation, namely the eigen value equation and the symmetry condition.

$$[K_{AU}] = [K_A] + [\Delta K] + [\Delta K]^T \tag{2.47}$$

Where

$$\begin{aligned}
[\Delta K] = & 0.5 [M_{AU}][\phi_X] \left( [\phi_X]^T [K_A] [\phi_X] + [\omega_X^2] \right) [\phi_X] [M_{AU}]^T \\
& - [K_A][\phi_X][\phi_X]^T [M_{AU}]
\end{aligned} \tag{2.48}$$

Caesar (1983) uses the same approach as Berman by applying the same three constraints but also includes the preservation of the system's total mass and that of the interface forces. A more detailed formulation of the problem is considered at the expense of increased computational effort and applicability to small and banded matrices only.

Similar updating techniques with different Lagrange multipliers have been proposed by Wei (1989) and O'Callahan and Chou (1988). It has since been suggested that these methods are applicable to special cases only, Lin et al (1990). A detailed review of methods based on Lagrange multipliers is given by Caesar (1987).

### Direct Method Based on Matrix Perturbation

Chen, Kuo, Garba (1983) define the updated mass and stiffness matrices as

$$[M_{AU}] = [M_A] + [\Delta M] \quad 2.49$$

$$[K_{AU}] = [K_A] + [\Delta K] \quad 2.50$$

with

$$[\Delta M] = [M_A][\phi_A] \left( 2[I] - [\phi_A]^T [M_A][\phi_x] - [\phi_A]^T [M_A][\phi_A] \right) [\phi_A]^T [M_A] \quad 2.51$$

$$[\Delta K] = [M_A][\phi_A] \left( 2[\omega_A^2] + 2[\omega_A][\omega_x] - [\phi_A]^T [K_A][\phi_x] - [\phi_A]^T [K_A][\phi_A] \right) [\phi_A]^T [M_A] \quad 2.52$$

where matrix perturbation theory has been used. A modified version of this method, Dorinier (1985), is based on response data rather than modal data and it also includes a procedure to update the damping matrix.

## Error Matrix Methods

The error matrix between two experimental and analytical matrices is defined as follows:

$$[\Delta S] = [S_x] - [S_A] \quad 2.53$$

where [S] can be the stiffness or the mass matrix.

The error matrix method proposed by Sidhu and Ewins (1984), is defined as

$$[\Delta K] \cong [K_A] \left\{ [K_A]^{-1} - [K_x]^{-1} \right\} [K_A] \quad 2.54$$

where  $[\Delta K]$  is assumed to be a small matrix such that

$$\lim_{n \rightarrow \infty} [\Delta K]^n = [0] \quad 2.55$$

Estimating the two pseudo-flexibility matrices using modal data yield

$$[\Delta K] \cong [K_A] \left\{ [\phi_A][\lambda_x]^{-1} [\phi_A]^{-1} - [\phi_x][\lambda_x]^{-1} [\phi_x]^T \right\} [K_A] \quad 2.56$$

$$[\Delta M] \cong [M_A] \left\{ [\phi_A][\phi_A]^T - [\phi_x][\phi_x]^T [\phi_x]^T \right\} [M_A] \quad 2.57$$

Further work on error matrix method was carried out by He and Ewins (1986), Ewins and Lieven (1988).

Some of the publications focusing around the error matrix method include a number of case studies where the success of the method is discussed when applied to a practical example Gysin (1986), Lawrence(1987) and Park et al (1988). A modified version of the error matrix method Lieven (1990) defines the stiffness matrix as

$$[\Delta K] = \left( [\phi_x][\lambda_x]^{-1} [\phi_x]^T \right)^{-1} - \left( [\phi_A][\lambda_A]^{-1} [\phi_A]^{-1} \right) \quad 2.58$$

and uses the singular value decomposition technique. Maia (1989) obtains slightly changed formulation by including the orthogonally condition. Gaukroger (1984) obtains a partly changed formulation by including the orthogonally condition.

$$[\Delta K] = \left( [I] - [K_A] \sum_{r=1}^m \left( \{ \phi_{x_r} \} \omega_{Ar}^{-2} \{ \phi_{x_r} \}^T - \{ \phi_{Ar} \}^T \right) \right)^{-1} [K_A] - [K_A] \quad 2.59$$

$$[\Delta M] = \left( [I] - [M_A] \sum_{r=1}^m \left( \{ \phi_{x_r} \} \{ \phi_{x_r} \}^T - \{ \phi_{Ar} \}^T \{ \phi_{Ar} \}^T \right) \right)^{-1} [M_A] - [M_A] \quad 2.60$$

Brown (1985) makes use of the vector space theory to obtain further error matrix formulation that depend on the chosen projection of the matrices used. The final expressions are quite similar to the basic formulation of error matrix method. Brown (1988) propose also an error location method based on non-zero values of matrix  $[\Delta]$  defined as

$$[\Delta] = 0.5 \left( 2 [M_A] [\phi_x] [\lambda_x]^{-1} [\phi_x]^T [M_A] - [K_A] [\phi_x] [\phi_x]^T [M_A] - [M_A] [\phi_x] [\phi_x]^T [K_A] \right) \quad 2.61$$

where a large element  $\Delta_{ij}$  indicates the location of the error. This cursor type formulation identifies both mass and stiffness errors concurrently, but it cannot distinguish between the two.

### Statistics and Sensitivity Methods

Collins et al (1974) use statistics as the basis for updating. The variance associated with the structural parameters is minimised to determine those that reproduce the measured modal properties. Measurement errors are also included as known uncertainties. This technique was developed further into a sensitivity type analysis where an iterative process to determine the structure parameters that reproduce the measured modal data is proposed. Chen and Wada (1975) introduced a similar approach for both correlation and updating purposes.

In recent years, sensitivity-based methods have increased in popularity due to their ability to reproduce the correct measured natural frequencies and mode shapes. Almost all sensitivity - based methods compute sensitivity matrix  $[S]$  by considering the partial derivatives of modal parameters with respect to structural parameters via a truncated Taylor's expansion. The resulting matrix equation is of the form

$$\{\Delta w\} = [S] \{\Delta p\} \quad 2.62$$

where the elements of  $\{\Delta p\}$  are the unknown changes in structural elements that are required to produce the changes in modal data vector  $\{\Delta w\}$  such that

$$\{\Delta w\} = \left\{ \{\Delta \phi_1\}, \{\Delta \phi_2\}, \{\Delta \phi_3\}, \dots, \{\Delta \phi_m\}, \{\Delta \lambda_1, \dots, \Delta \lambda_m\} \right\}^T \quad 2.63$$

The matrix equation above is solved for the unknown vector  $\{\Delta p\}$  to obtain the solution vector  $\{\Delta w\}$  and in the process the analytical mass and stiffness matrices are updated. A new

eigensolution is calculated and the process is repeated until the target modal properties are obtained. It should be noted that the formulation of the sensitivity matrix is based on a Taylor expansion and hence the method is an approximated one. It is customary to retain the first term only in the series, Kim (1983) (first order sensitivity method), but some researchers also consider the effect of the second order term (second order sensitivity method).

The sensitivity methods differ in the selection of parameters and the definition of the optimisation constraints (natural frequencies and modes shapes and orthogonally conditions). For the parameter selection the options can be elements of the [M] and [K] matrices, subdomain matrices, Lallement (1990), or macro elements, Jung (1990), or geometric and material properties used as input data to the FE model, Zhang et al (1987), Janter et al (1987), Wie et al (1988), Lallement and Zang (1988), discuss some of the difficulties related to sensitivity analysis. Janter et al (1988) offer a comparison of the interpretability, controllability and compatibility of the sensitivity techniques, but all these techniques are CPU intensive as a new eigensolution has to be computed for each iteration.

The sensitivity-based methods provide an updated analytical model capable of recreating the measured modes, but if applied directly, they have the advantage of modifying the most sensitive element rather than that in error. It is therefore recommended to localise the error first and allow for changes in the associated elements only. Heylen and Janter (1988) use MAC and spatial MAC calculation to locate the errors and they also include a MAC sensitivity equation in their analysis Wie and Janter (1988), which used also by Fillod et al (1986). user controllability is ensured by applying weighting factors and upper and lower bounds on adjustments Janter, Heylen (1988) and Janter, Heylen (1990).

Dascotte and Vanhonacker (1989) consider the sensitivity approach also in combination with confidence estimations on the experimental data and illustrate the relative merits of this method when applied to a practical example, Dascotte (1990). Slater et al (1988) used statistical analysis on different mode shape vectors to localise the error, which can then be corrected using a sensitivity approach. Chen (1987) also combines statistical considerations with other updating methods to achieve an optimally corrected model.

## Updating Techniques using Frequency Response Function Data

The updating methods reviewed so far make use of modal data only and hence frequency response function (FRF) measurements are not used directly since they have to be analysed first to obtain the required modal data. Lin and Ewins (1990) propose a technique that makes direct use of the measured FRF data. Starting from the mathematical identity

$$[[A] + [B]]^{-1} = [A]^{-1} - [[A] + [B]]^{-1} [B] [A]^{-1} \quad 2.64$$

$$\text{let } [A] = [Z_A(\omega)] \quad \text{and} \quad [A] + [B] = [Z_X(\omega)]$$

where  $[Z]$  is the dynamic stiffness matrix. Hence

$$[Z_X(\omega)]^{-1} = [Z_A(\omega)]^{-1} - [Z_X(\omega)]^{-1} [[Z_X(\omega)] - [Z_A(\omega)]] [Z_A(\omega)]^{-1} \quad 2.65$$

Substituting  $[Z]^{-1} = [\alpha]$  where  $[\alpha]$  is the receptance FRF matrix and taking the  $i^{\text{th}}$  column only:

$$\{\alpha_A(\omega)\}_i^T - \{\alpha_X(\omega)\}_i^T = \{\alpha_X(\omega)\}_i^T [\Delta Z(\omega)] [\alpha_A(\omega)] \quad 2.66$$

which can be rewritten into the form

$$[C(\omega)] \{\Delta p\} = \{B(\omega)\} \quad 2.67$$

where matrix  $[C(\omega)]$  and vector  $[B(\omega)]$  are known in terms of measured or predicted response properties or both and the elements vector  $\{\Delta p\}$  indicate the position of error in the original system matrices. It should be noted that  $[C(\omega)]$  and  $\{B(\omega)\}$  can be formed using any combination of discrete FRF data and the system is over determined.

Creamer and Junkins (1988) use a combination of analytical modal data and experimental frequency response data to find the model normalisation factors and subsequently update the system matrices using the orthogonally condition. Using the frequency response functions directly without having to have a priori knowledge of the analytical system matrices leads into the area of structure identification using a frequency filter based on a least squares method that has been suggested by Mottershead (1990). The technique has been applied also to improve reduced finite element models by Foster et al (1990).

## Concluding Remarks

A vast amount of research has been dedicated to the area of model updating. Results so far suggest that the problem remains largely unsolved and a very substantial amount of work is still needed. The sheer volume of techniques proposed and the number of variations tried also suggest that this research field is far from reaching maturity.

The error predictions using matrix updating methods of the section on model updating methods depend largely on the reduction or expansion technique used and there is little agreement between the various methods suggested.

Sensitivity based methods seem quite promising in the sense that they reproduce the desired modal properties. Some of the serious limitations lie in the fact that the most sensitive element (rather than that in error) is changed and knowledge of the element mass and stiffness matrices, as well as those of the subdomains that constitute the model, are required. The latter would, in turn, necessitate a different (and much more tedious) modeling route for finite element analysis, a hardly realistic proposition when the size of the finite element model is large.

The FRF based methods are perhaps even more promising since each individual FRF measurement contains information on out of range modes as well as on those within the frequency range of interest, and it is possible to specify measurement and excitation points to ensure maximum efficiency. Another advantage may well lie in the direct use of raw measured data thus simplifying lengthy modal analysis procedures.

The use of true experimental data is rather an exception, almost all reported cases deal with theoretically generated data only. Some of the anticipated additional difficulties which will render the formulation of successful model updating process even more elusive than it is now are:

- Mapping problem. The test coordinated grid is very often different from the finite element mesh. It would be very expensive, if at all possible, to measure at all finite

element nodes and in all coordinate direction. Also, there may be some physical constraints on the actual structure rendering some points totally inaccessible.

- Effect of damping and complex modes. Experimental and analytical data sets are incompatible because the analytical model usually yields real undamped modes while the modal tests lead to complex modes with damping. Often the normal mode approach is used in which case the complex modes are converted to real ones, Zhang et al (1987), Baruch and Itzhack (1977) and Niedbal (1984).
- Experimental and modal analysis errors. It is often conveniently ignored that the measured data also contain systematic and random errors. Also the reliability of analysed data may further be put into question by inaccuracies introduced during modal analysis, computational or superfluous modes being one of the side effects of some curve fitting techniques used.
- Algebraic manipulation of noise polluted matrices can give rise to large errors, especially during inversion, Barman (1984).

### **3. Aims**

The dynamic characteristics of the loaded engine rack can be predicted using finite element analysis at the design stage or design modification. Whilst finite element analysis may produce reliable static and dynamic predictions, there are some cases in which some form of validation against experimental data is necessary due to physical and behaviour modelling approximation and environmental simulation.

The following research will examine the engine rack that Holden's Engine Company intend to use for the shipment of its engines.

The general aims of the research project include:

- theoretically analyse and experimentally evaluate the loading induced in the rack/engine system by the transportation environment;
- investigation of the interaction between the rack structure and the engine under dynamic excitation; and
- recommendations regarding potential improvements to the design of the rack.

A specific aim of this study is to validate the FEM by predicting the dynamic characteristics such as the natural frequency and frequency response function of the engine rack and compare it with the experimentally tested prototype, and to modify the FEM until the FEM can accurately predict the rack response to a similar type of excitation. Usually the modifications include the selection of the element type, the size of meshing, material properties, boundary conditions. etc.

If the predicted FEA natural frequencies and the harmonic response to a unit force input using a uniform damping coefficient to approximate the rack damping coefficient compare well with the experimentally determined resonant frequencies, and the measured FRF, then the FEM can be used to predict the behaviour of the loaded engine to environment simulated condition.

## **4. Results and Discussion of Finite Element Analysis**

### **4.1 Experimental Evaluation**

The dynamic characteristics of the engines rack and similar structures are often predicted using FEA. While finite element models may produce reliable static and dynamic predictions there are many cases in which some form of validation against experimental data is necessary, often the processes involve comparing the FEM with experimental model and modifying the FEM until it can accurately predict the structure response to a similar type of excitation. Usually modification includes the selection of the element type, the size of meshing, material properties, boundary conditions etc. If the natural frequencies predicted FEA and the harmonic response to a unit force input using a uniform damping coefficient to approximate the structural damping compare well with the experimentally determined natural frequencies, and the measured frequency response function, then the FEM can be used to predict the behaviour of the structure and consequently develop an improved design.

A number of different methods have been developed in order to update FEM using vibration test data.

According to Randall (1988) the most common experimental analysis methods are:

- Forced normal mode excitation
- Frequency response function
- Damped complex exponential response
- Mathematical input-output model

However the FRF method is the most commonly used technique to estimate the structural parameters. This method has been developed using the FRF in forcing the normal mode to determine the natural frequencies of the structure and curve overlay procedure is used to evaluate the modal parameters. In order to ensure that the modal vectors at the point of interest have been found experimentally, the rack prototype will be excited where the environment excitation points are expected and the response will be measured at the contact points between the rack and the engine.

Thus this thesis will deal with updating the FEM using an incomplete set of measured frequency response function data, where FRF data and natural frequencies are employed.

#### 4.1.1 Excitation Signal

In most of FRF system analysis where input-output relationships have to be measured, it is necessary to excite the system with a controlled and measurable input, Randall (1988). A number of different types of excitation signals are available for the analysis, each has its own advantages and disadvantages. The choice of the signal depend upon the test application, non-linear behaviour of the system and time available for the analysis. It is also possible to use either an impact hammer or shaker.

The following are the most common types of excitation signal:

- The slow swept sine wave signal is a periodic deterministic signal with a frequency that is an integer multiple of the fast Fourier transform frequency increment. Sufficient time is required in the measurement procedure for any transient response to decay so that the resultant input and response histories will be periodic with respect to the sample period. Therefore, the total time needed to compute an entire FRF will be a function of the number of frequency increments.  
The periodic chirp is a fast swept sine wave signal that is a periodic deterministic signal and is formulated by sweeping a sine wave signal up or down within a frequency band of interest during a single sample period.
- An impact (impulse) excitation is a transient deterministic signal which is formed by applying to a system an input pulse lasting only a very small part of the sample period. The width, height, and shape of this pulse will determine the useable spectrum of the impact. The width of the pulse determine the frequency band width, the height and shape of the pulse controls the level of the spectrum. Impact signals are applied with instrumented hammer.
- The step relaxation excitation is a transient deterministic signal which is

formed by releasing a previously applied static input. The sample period begins at the instant that the release occurs.

- Pure random excitation is a stationary random signal which has a Gaussian probability distribution. In general the frequency content of the signal contains all frequencies (not just integer multiples of the fast Fourier transform frequency increment) but may be filtered to include only information in a frequency band of interest.
- Pseudorandom excitation is a stationary random signal consisting only of integer multiples of the fast Fourier transform frequency increment. The frequency spectrum of this signal has a constant amplitude with random phase. If sufficient time is allowed in the measurement procedure for any transient response to the initiation of the signal to decay, the resultant input and response histories are periodic with respect to the sample period. The number of averages used in the measurement procedure is only a function of the variance error. In a noise free environment, only one average may be necessary.
- Periodic random excitation is a stationary random signal consisting only of integer multiples of the fast Fourier transform frequency increment. The frequency spectrum of this signal has random amplitude and random phase distribution.
- A random transient ( random burst ) is neither a completely transient deterministic signal nor a completely stationary random signal but contains properties of both signals. The frequency spectrum of this signal has random amplitude and random phase distribution and contains energy throughout the frequency spectrum. The difference between this signal and the periodic random signal is that the random transient history is truncated to zero after some percentage of the sample period ( normally 50 to 80 % ) The measurement procedure duplicates the periodic random procedure, but without the need to wait for the transient response to decay. The point at which the input history is truncated is chosen so that the response history decay to zero within the sample period.

Table 4-1 shows a summary of characteristics of excitation signals used for frequency response function estimates

**Table 4-1 Characteristics summary of excitation signals**

	Type of Excitation							
	Steady state sine	Pure random	Pseudo random	Random	Fast sine	Impact	Burst sine	Burst random
Minimise leakage	No	No	Yes	Yes	Yes	Yes	Yes	Yes
Signal to noise ratio	Very high	Fair	Fair	Fair	High	Low	High	Fair
RMS to peak ratio	Very high	Fair	Fair	Fair	High	Low	High	Fair
Test measurement time	Very long	Good	Very short	Fair	Fair	Very good	Very good	Very good
Controlled frequency content	Yes	Yes	Yes	Yes	Yes	No	Yes	Yes
Controlled amplitude content	Yes	No	Yes	No	Yes	No	Yes	No
Removes distortion	No	Yes	No	Yes	No	No	No	Yes
Characterise nonlinearity	Yes	No	No	No	Yes	No	Yes	No

#### 4.1.2 Excitation of the Structure

Various devices are available for exciting the structure and several of these are in widespread use. They can be divided into two types: contacting and non contacting. The first of these involves some form of connection of the exciter which remains attached to the structure throughout the test, whether the excitation type is continuous (sinusoidal, random, etc.) or transient (pulse, chirp). The second type includes devices which are either out of contact throughout the vibration (such as provided by a non contacting electromagnet) or which are only in contact for a short period while the excitation is being applied (such as a hammer blow). The most common available exciters are:

- Mechanical (out-of-balance rotating masses)
- Electromagnetic (moving coil in magnetic field)
- Electrohydraulic.

- **Mechanical Exciters**

The mechanical exciter is capable of generating a prescribed force at a variable frequency although there is relatively little flexibility or control in its use. The magnitude of the force is restricted by the out-of-balance and is only variable by making adjustments to this quantity. The disadvantage of this type is its ineffectiveness at low frequencies because of the speed-squared dependence, unless the amplitude caused by the exciter becomes large relative to the orbit of the out-of-balance masses. The advantage of the mechanical exciters is that its magnitude and phase of the excitation force is known quite accurately and does not need further measurement.

- **Electromagnetic Exciters**

The electromagnetic exciters supplies input signals converted from an alternating magnetic field in which is placed a coil which is attached to the drive part of the device, and the structure. The advantage of using the electromagnetic exciter is that its frequency and amplitude of excitation are controlled independently of each other. The disadvantage of this system is the electrical impedance of these devices varies with the amplitude of motion of the moving coil and so it is not possible to deduce the excitation force from a measurement of the voltage applied to the shaker. It is appropriate to deduce the excitation force by measuring the current passing through the shaker because this measures the force applied not to the structure itself, but to the assembly of the structure and shaker driver.

- **Electrohydraulic Exciters**

In electrohydraulic exciters, the power amplification to generate substantial forces is achieved through the use of hydraulics. These exciters do have one

potentially significant advantage. That is ability to apply simultaneously a static load as well as a dynamic vibratory load which is useful when testing structures or materials whose normal vibration environment is combined with a major static load which may well change its dynamic properties or even its geometry. Another advantage of this type is the possibility of providing a relatively long stroke, therefore permitting the excitation of structures at low frequencies and large amplitudes. On the other hand the electrohydraulic exciters tend to be limited in operational frequency range to below 1 kHz, whereas electromagnetic exciters can operate well into the 30 - 50 kHz region, depending on their size.

- **Impact Exciters**

Impact excitation using an impact hammer is a convenient excitation method for mechanical structure. When the structure is excited by the hammer, energy is transferred to the structure in a very short period of time giving an input force signal. The shape of this force signal depends upon the type of the hammer tip, mass of the hammer and dynamic characteristics of the structure under investigation.

The advantages of using an impact hammer test are:

- It is very fast, only a few averages are needed.
- There is no mass loading.
- No fixture is required as for shaker excitation.
- Easy to use in the field.

The disadvantages are:

- The force signal has a high crest factor which can make this technique unsuitable for non linear system.
- Limited control of excitation bandwidth.

### **4.1.3 Experimental Equipment**

The main objective of the following analysis is to measure input-output relationships (FRF). A dual channel FFT analyser will permit the calculation of a function that will describe the engine rack dynamic behaviour. The system should be linear and time

invariant. The validity of the result will depend upon the quality of the model linearity. Coherence provides a measure of the degree of linear relationship between the two signals at any given frequency.

The estimated FRF's will represent the best linear fit (in the least squares sense) to the system. This is very important in analysing nonlinear systems where the best linear fit is needed for mathematical modelling.

The estimated FRF will depend upon the type of signals involved in the analysis and their level. Secondly, it is possible to measure the FRF even though the input signal or output signal is contaminated with extraneous noise, e.g. in situations where other inputs than the measured are present.

#### **4.1.4 Experiment Setup and Results**

The natural frequency and frequency response function (FRF) of the rack prototype, No H4185, shown in Figure 4-11, was experimentally determined by using incomplete sets of data techniques. These techniques involved acquiring the natural frequencies and FRF data at the points of interest where the rack is in contact with the engine only. This data was compared with the FE data to obtain the FE validation.

The data comparisons was limited to:

- The natural frequency of the spring suspended rack.
- The FRF curves overlay.
- The receptance values in the Y-direction with different damping coefficients.

#### **Note:**

- The receptance (displacements per unit force) comparison has been selected because it is more accurate than mobility and inertance as far as finite element analysis is concerned.
- Phase and coherence comparison are not available on strand software and will not be included in the comparison.
- Icats software was used to identify the model damping factors.

## Rack Impact Test

PCB modally tuned impact hammer with sensitivity of 2.1 mV/N, an accelerometer with voltage sensitivity 23.4 mv/g model No BK4333 and the dual channel FFT analyser Brüel & Kjær, model No 2032 were used to acquire the experimental frequency response functions of the rack. Figure 4-1 shows the schematic diagram of the test arrangement.

To simulate a freely supported condition with minimal effect of the rigid body mode the rack was suspended by four low stiffness springs.

The rack was excited at one location in the vertical direction and response was measured in the vertical direction as this direction has most influence upon the energy transferred to the engine. The response was measured at four points where the engine was in contact with the rack. The FRF was measured by averaging 20 samples and the frequency span was set to 800 Hz with 1 Hz resolution.

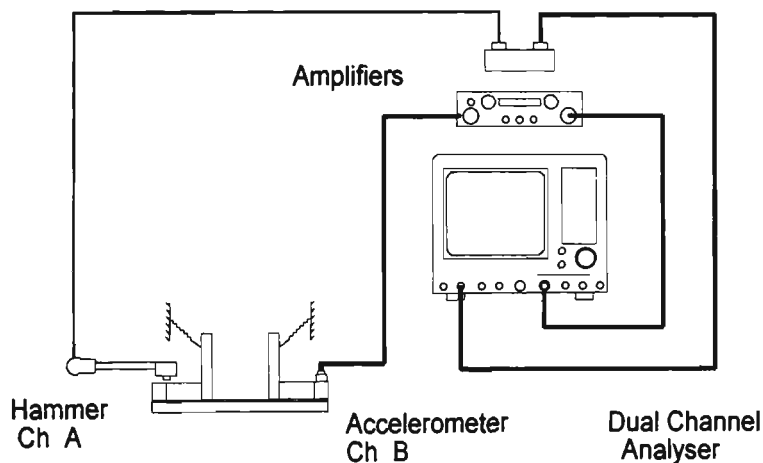


**Figure 4-1 Schematic diagram to the test arrangement**

### Test setup

Measurement : Dual spectrum averaging

Trigger	: Ch. A	+ slope	level : +0.10 max input
Delay	:Trig → A :	-9.76 ms	Ch. A → B : 0.00ms
Averaging	:Lin	20	
Freq. span	:800 Hz	$\Delta F$ : 1Hz	T: 1s $\Delta T$ : 488 $\mu$ s
Center Freq.	:Baseband		
Weight Ch. A	:Transient	shift : 0.00 ms	length : 100.09 ms
Weight Ch. B	:Exponential	shift :0.00 ms	length : 250.00 ms

Figure 4-2 shows the layout of the tested prototype No H4185, which has been built for the purpose of experimental evaluation to the rack dynamic properties.

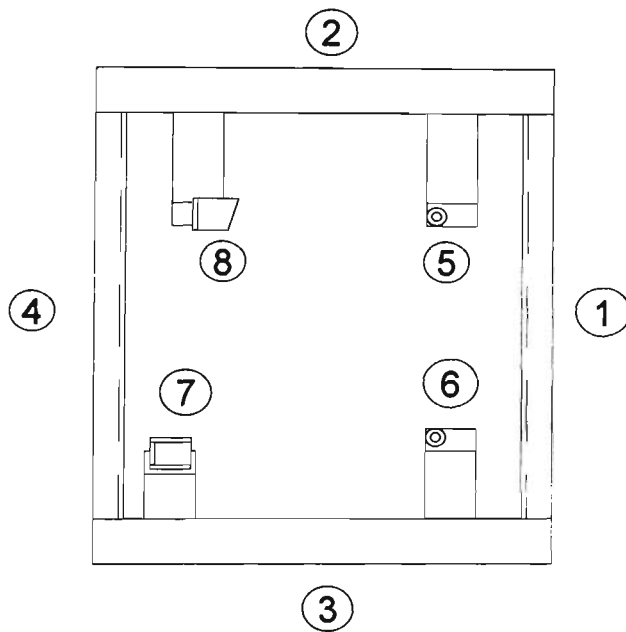


**Figure 4-2 Prototype No H4185 layout**

## Frequency Response Function Analysis

The following curves Figure 4-3, Figure 4-4, Figure 4-5 and Figure 4-6 are the Receptance FRF. Using hammer excitation at node No 1 as input, the output was measured at nodes No 5, 6, 7 and 8 respectively and  $H_{jk}$  is the FRF at  $j$  - response node,  $k$  - excitation node

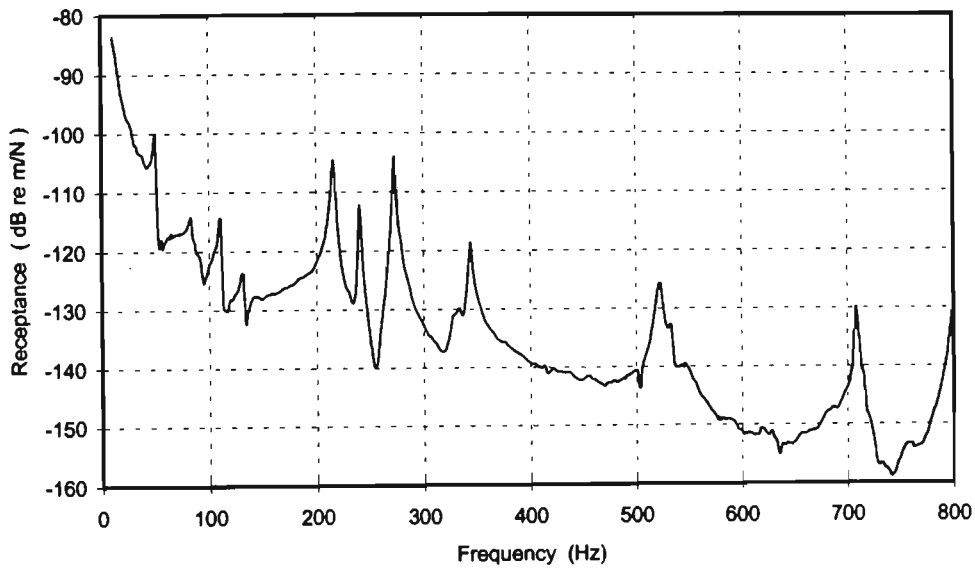


**Figure 4-3 Experimental FRF ( $H_{5,1}$ )**

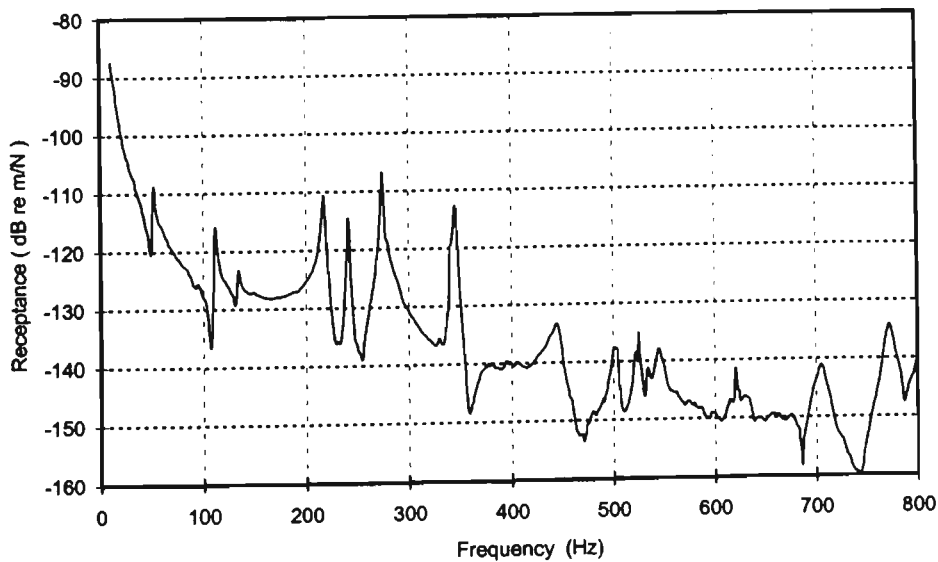


**Figure 4-4 Experimental FRF ( $H_{6,1}$ )**

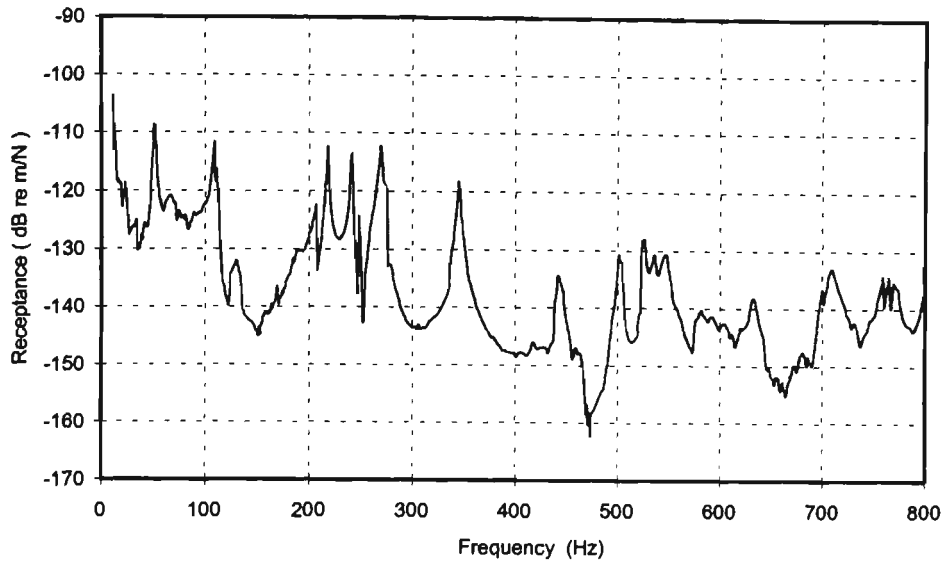


**Figure 4-5 Experimental FRF ( $H_{7,1}$ )**

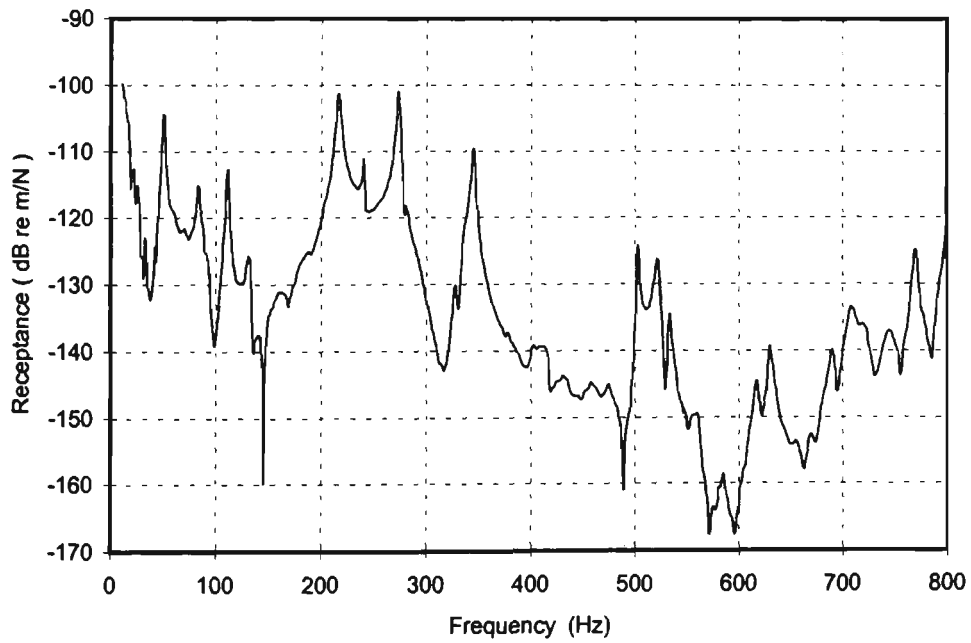


**Figure 4-6 Experimental FRF ( $H_{8,1}$ )**

Figure 4-7, Figure 4-8, Figure 4-9 and Figure 4-10 show the receptance FRF's in linear scale.

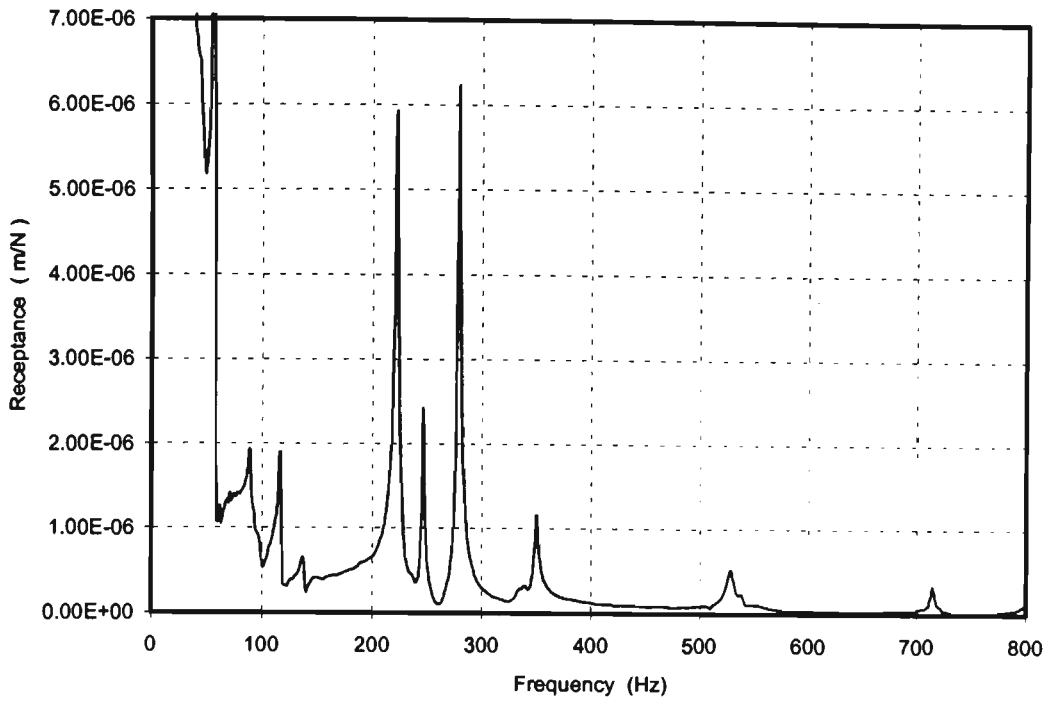


**Figure 4-7 Experimental FRF ( $H_{5,1}$ )**

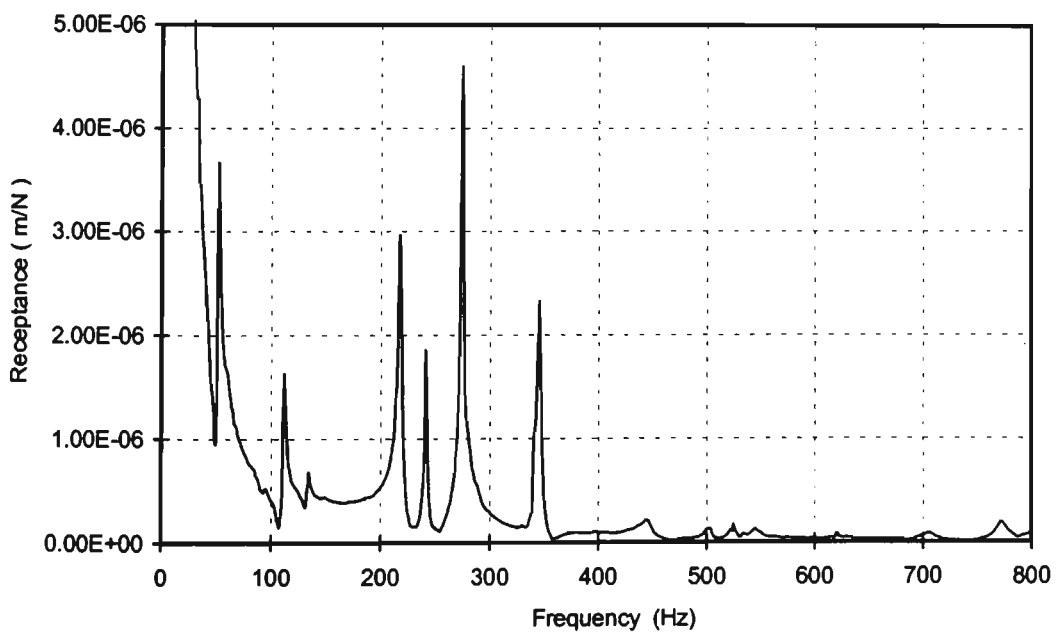


**Figure 4-8 Experimental FRF ( $H_{6,1}$ )**

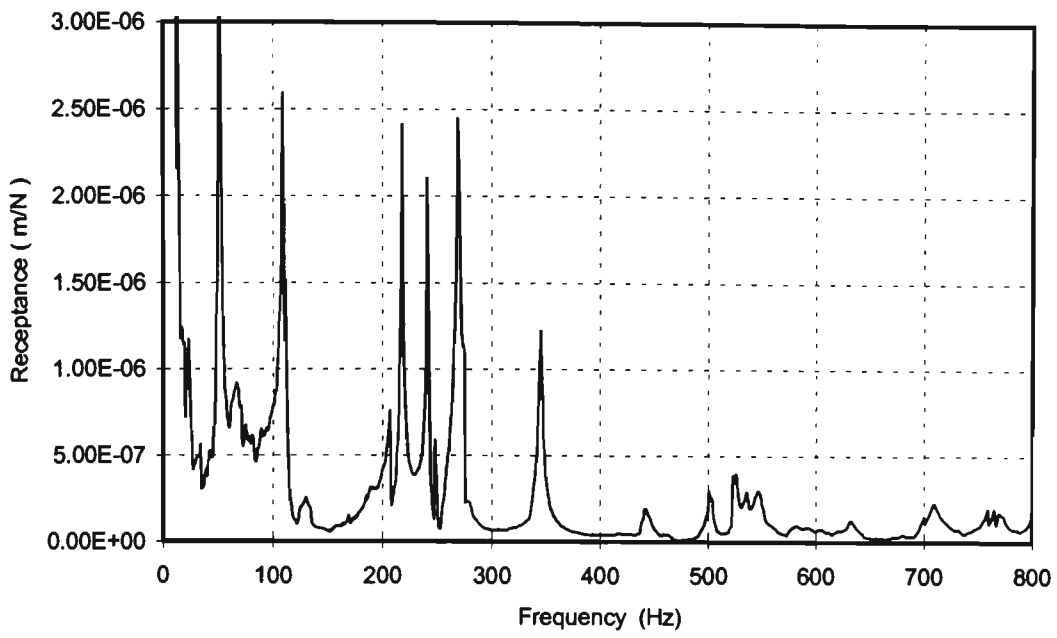


**Figure 4-9 Experimental FRF ( $H_{7,1}$ )**

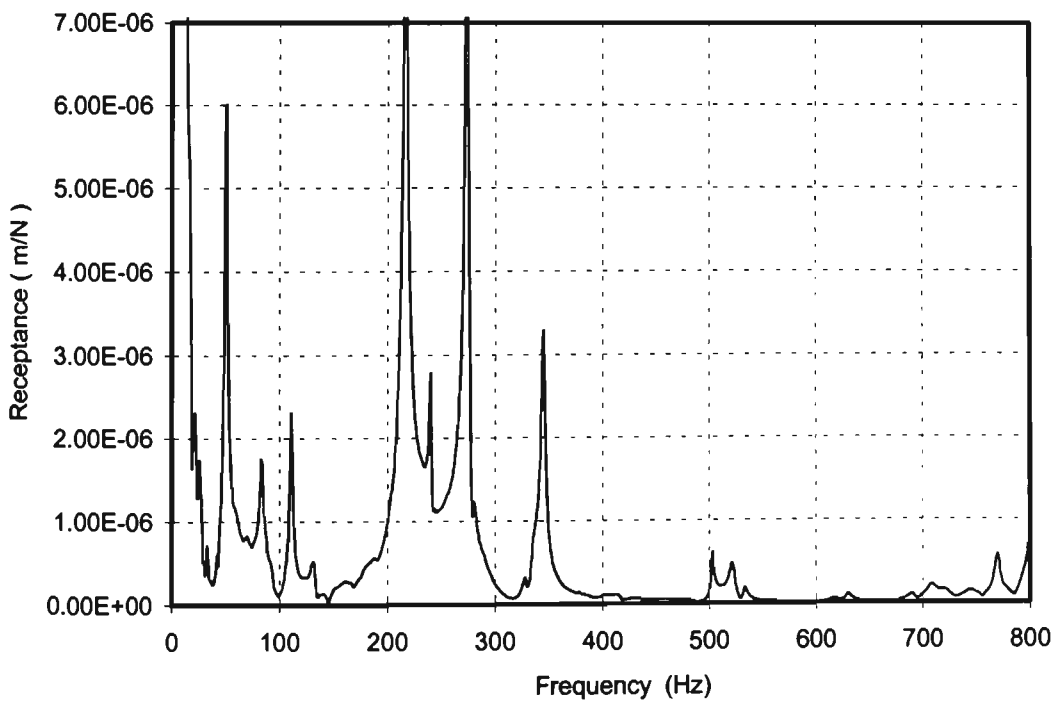


**Figure 4-10 Experimental FRF ( $H_{8,1}$ )**

Table 4-2, Table 4-3, Table 4-4 and Table 4-5 show the receptance, coherence of nodes 5, 6, 7 and 8 vs resonant frequency as well as the damping ratio as identified by the I cats software circle fit.

**Table 4-2 Receptance relationships for  $H_{5,1}$**

Node 5 Frequency Hz	Receptance $H_{5,1}$ m/N	Coherence $\gamma$ %	Damping factor circle fit
50	1.00E-05	98.5	0.0260
110	1.90E-06	99.4	0.0150
216	5.92E-06	99.8	0.0142
240	2.40E-06	96.3	0.0069
273	6.20E-06	99.9	0.0066
344	1.17E-06	99.4	0.0078
522	5.12E-07	97.6	0.0115
545	9.94E-08	96.2	0.0093
708	3.20E-07	96.8	0.0105

**Table 4-3 Receptance relationships for  $H_{6,1}$**

Node 6 Frequency Hz	Receptance $H_{6,1}$ m/N	Coherence $\gamma$ %	Damping factor circle fit
52	3.66E-06	99.1	
112	1.63E-06	99.3	0.0214
217	2.96E-06	99.8	0.0107
241	1.85E-06	96.8	0.0113
274	4.58E-06	99.8	0.0086
345	2.33E-06	99.8	0.0074
503	1.31E-07	97.3	0.0055
523	1.20E-07	96.8	0.0078
705	8.75E-08	98.2	0.0156
772	1.94E-07	99.2	0.0104

**Table 4-4 Receptance relationships for  $H_{7,1}$** 

Node 7 Frequency Hz	Receptance $H_{7,1}$ m/N	Coherence $\gamma$ %	Damping factor circle fit
51	3.65E-06	97.1	0.038
109	2.58E-06	99.3	0.023
218	2.41E-06	99.6	0.014
241	2.10E-06	96.5	0.008
269	2.44E-06	99.3	0.008
345	1.22E-06	93.6	0.018
442	1.91E-07	99.6	0.010
501	2.92E-07	96.8	0.005
523	3.81E-07	92.3	0.005
536	2.91E-07	85.9	0.008
547	2.95E-07	96.8	0.013
771	1.55E-07	97.3	0.006

**Table 4-5 Receptance relationships for  $H_{8,1}$** 

Node 8 Frequency Hz	Receptance $H_{8,1}$ m/N	Coherence $\gamma$ %	Damping factor circle fit
51	6.00E-06	89.2	0.0380
83	1.75E-06	98.4	0.0440
111	2.30E-06	99.2	0.0172
131	5.16E-07	98.2	0.0256
216	8.64E-06	98.7	0.0212
240	1.96E-06	95.2	0.0081
273	5.98E-06	96.7	0.0083
345	2.12E-06	92.5	0.0108
503	6.16E-07	89.9	0.0038
521	4.80E-07	83.9	0.0074
533	1.86E-07	85.6	0.0066
630	1.08E-07	48.2	0.0062
706	1.93E-07	82.6	0.0150
770	5.74E-07	95.9	0.0062

## 4.2 FEA Modelling Strategy

Finite element models are widely used to investigate the dynamic behaviour of structures. These models can predict the natural frequencies and the associated mode shapes, and the response of the structure to different types of excitation. This is important particularly when the structure is to be analysed under severe loading conditions that may prevent a direct experimental test. In these cases the finite element model must be validated against practical experimental results obtained from standard modal tests and benchmark test such as frequency response curves, natural frequencies and mode shapes, Ewins (1995).

The finite element model has an important function in static and dynamic analysis. It may be used to find the structure response, loading capability, design changes and stability of the structure. However, for a structure the precise analytical solution does not in general exist. Nevertheless, before creating a model, a decision has to be made as to which type of element, [beam, plate, or bricks] material properties, boundary condition, loading etc., will describe better the physical properties and parameters of the structure being analysed.

Considerations for approximation in any FEA would include:

- Approximation to the physical behaviour.
- Approximates the physical shape of the structure.

Such an approximate model can be considered as a good model if it will not only predict responses over the frequency range of interest, but also represent the physical characteristics. Thus it must have the capability to reflect and predict the effects of changes in physical parameters and to represent correctly not only the prototype but also the actual structure. However the solution will improve with mesh refinement and as the number of elements is increased.

The computer memory and central processing time to complete the solution increase as the number of elements is increased. Therefore the FE mesh used is usually a compromise between accuracy, computing time and memory.

### 4.2.1 Type of Elements

The type of element selected should represent the physical structure, application, conditions of the problem and the length of the analysis. Different types of elements are available for modelling, such as beam, plate, thin shell plate, Constant Strain Triangle (CST), linear quad and brick element.

### 4.2.2 Size and Number of Elements

The size and number of elements directly influence the convergence of the solution. If the size of the elements is small, the final solution is expected to be more accurate. Also, the use of smaller size elements will lead to greater computation times. Different elements size may be used. For example, in those regions where a precise solution is required finer meshes may be employed. Another characteristic is related to the size of elements. The aspect ratio, describes the shape of the element in the assembly of elements. The aspect ratio is taken as the ratio of the largest dimension of the element to the smallest dimension. Elements with nearly unity aspect ratios generally yield best results.

### 4.2.3 Finite Element Analysis

The aim of the finite element calculation is to establish the best approach to model the rack and to define the modal parameters, such as natural frequency, FRF for curve overlay of the engine rack prototype and compare them with the experimental results.

#### Natural Frequency Solver :

Determination of the vibration characteristics including natural frequencies and mode shapes is by calculating the eigenvalues and eigenvectors of :

$$[K]\{\bar{\chi}\} = \lambda.[M]\{\bar{\chi}\} \quad 4.1$$

where [K] the banded stiffness matrix.  
{ $\bar{\chi}$ } the eigenvector.  
 $\lambda$  the eigenvalue.  
[M] the mass matrix.

As the state of stress in a structure is changed the natural frequencies vary. This effect can be taken into account in the natural frequency analysis by the inclusion of the stress stiffening matrix [Kg]. The equation to be solved for the eigenvalues corresponding to the natural frequencies becomes:

$$([K] + [Kg])\{\bar{\chi}\} = \lambda.[M]\{\bar{\chi}\} \quad 4.2$$

The stress stiffening matrix [Kg] is the same size as the global stiffness matrix [K] and is assembled from individual elements [kg]. It is based on elements geometry, properties, displacements and state of stress.

#### 4.2.4 Material Properties Selection

The following listing is the material properties selected to model the engine rack built specifically to test and validate the FE model as shown in Figure 4-11. The prototype layout shown in Figure 4-12.

<u>Beam Properties</u>		<u>Type 1</u>	<u>Section</u>		
Standard Circular		OD = 2.50E-02 m			
Beam Type:		Normal Beam			
E	=	2.00E+11 N/m <sup>2</sup>	A	=	4.91E-04 m <sup>2</sup>
J	=	3.84E-08 m <sup>4</sup>	G	=	8.00E+10 N/m <sup>2</sup>
I <sub>11</sub>	=	1.92E-08 m <sup>4</sup>	I <sub>22</sub>	=	1.92E-08 m <sup>4</sup>
Density	=	7.85E+03 Kg/m <sup>3</sup>			

<u>Beam Properties</u>		<u>Type 2</u>	<u>Section</u>		
Standard Circular		OD = 1.25E-02 m			
Beam Type:		Normal Beam			
E	=	2.00E+11 N/m <sup>2</sup>	A	=	1.23E-04 m <sup>2</sup>
J	=	2.40E-09 m <sup>4</sup>	G	=	8.00E+10 N/m <sup>2</sup>
I <sub>11</sub>	=	1.20E-09 m <sup>4</sup>	I <sub>22</sub>	=	1.20E-09 m <sup>4</sup>
Density	=	7.85E+03 Kg/m <sup>3</sup>			

The property of beam type 3 has been selected to represent the spring used to suspend the prototype during the experimental test.

<u>Beam Properties</u>		<u>Type 3</u>	<u>Section</u>		
Standard Circular		OD = 3.00E-03 m			
Beam Type:		Normal Beam			
E	=	2.00E+02 N/m <sup>2</sup>	A	=	7.07E-06 m <sup>2</sup>
J	=	7.9521E-12 m <sup>4</sup>	G	=	8.00E+01 N/m <sup>2</sup>
I <sub>11</sub>	=	3.98E-12 m <sup>4</sup>	I <sub>22</sub>	=	3.98E-12 m <sup>4</sup>
Density	=	7.80E+00 Kg/m <sup>3</sup>			

Plate Properties      Type 1

Isotropic      Element :      Thin Shell, Plate Shell, von Mises  
E                =      2.00E+11 N/m<sup>2</sup>      Poisson Ratio =      3.00E-01  
Memb. Thick =      5.00E-03 m      Bend Thick    =      2.50E-03 m  
Density        =      7.85E+03 Kg/m<sup>3</sup>

Plate Properties      Type 2

Isotropic      Element :      Thin Shell, Plate Shell, von Mises  
E                =      2.00E+11 N/m<sup>2</sup>      Poisson Ratio =      3.00E-01  
Memb.Thick =      2.50E-03 m      Bend Thick    =      2.50E-03 m  
Density        =      7.85E+0 Kg/m<sup>3</sup>

Plate Properties      Type 3

Isotropic      Element :      Thin Shell, Plate Shell, von Mises  
E                =      2.00E+11 N/m<sup>2</sup>      Poisson Ratio =      3.00E-01  
Memb.Thick =      5.00E-03 m      Bened Thick   =      5.00E-03 m  
Density        =      7.85E+03 Kg/m<sup>3</sup>

Plate Properties      Type 4

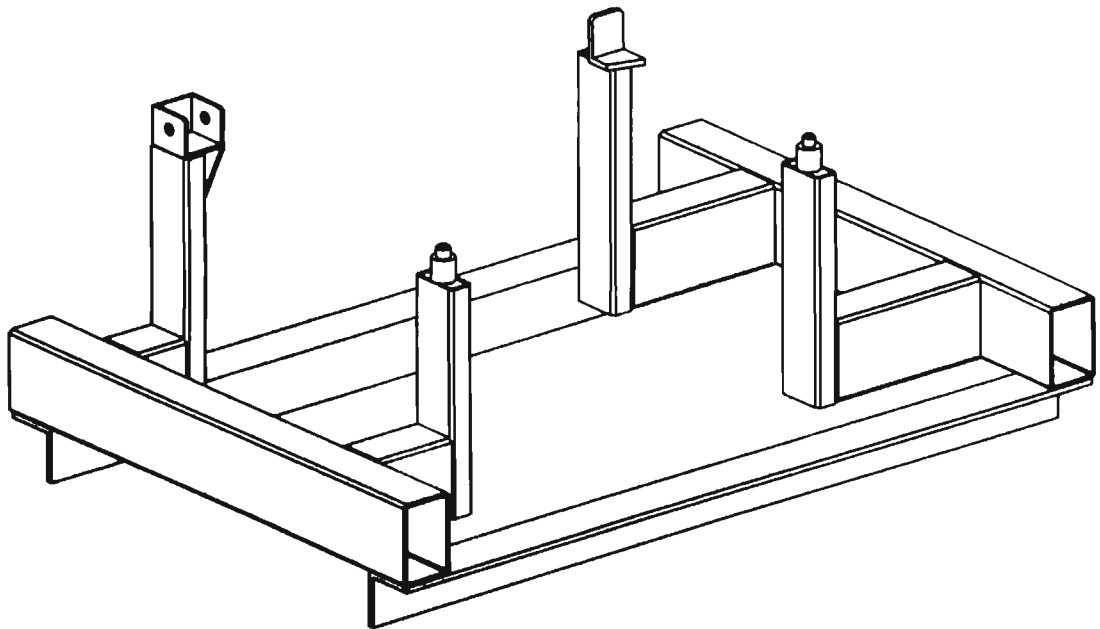
Isotropic      Element :      Thin Shell, Plate Shell, von Mises  
E                =      2.00E+11 N/m<sup>2</sup>      Poisson Ratio =      3.00E-01  
Memb.Thick =      3.00E-03 m      Bend Thick    =      3.00E-03 m  
Density        =      7.85E+03 Kg/m<sup>3</sup>

Plate Properties      Type 5

Isotropic      Element :      Thin Shell, Plate Shell, von Mises  
E                =      2.00E+11 N/m<sup>2</sup>      Poisson Ratio =      3.00E-01  
Memb. Thick =      3.00E-03 m      Bend Thick    =      3.00E-03 m  
Density        =      7.85E+03 Kg/m<sup>3</sup>

Plate Properties      Type 6

Isotropic	Element :	Thin Shell, Plate Shell, von Mises		
E	=	2.00E+11 N/m <sup>2</sup>	Poisson Ratio =	3.00E-01
Memb. Thick	=	5.00E-03 m	Bend Thick =	5.00E-03 m
Density	=	7.85E+03 Kg/m <sup>3</sup>		



**Figure 4-11 Prototype No H4185**

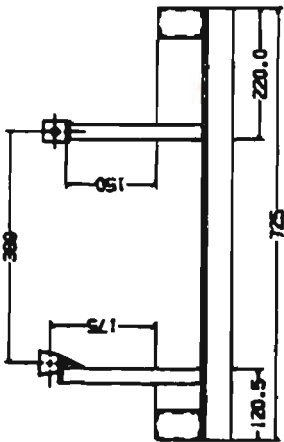
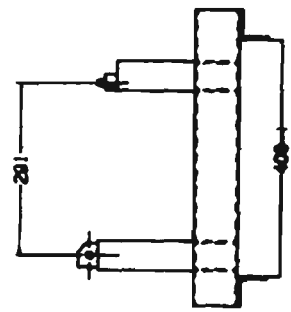
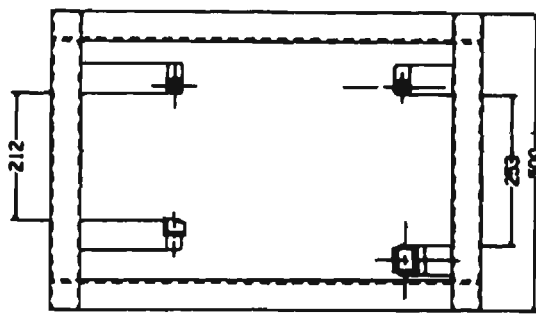
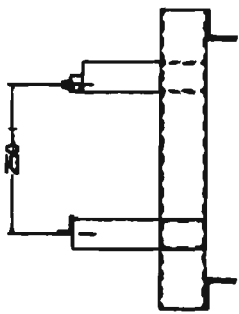
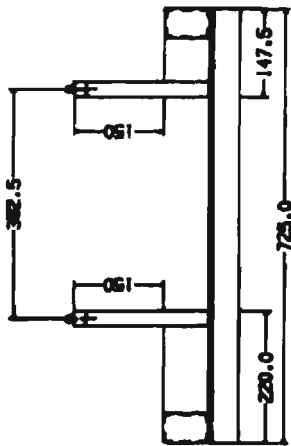


Figure 4-12 Prototype No H4185 layout

**Element Selection:**

Several trials have been conducted to decide on the modelling method used for the engine rack structure.

Table 4-6 shows natural frequencies for different types of elements and the comparison to the results obtained experimentally. The natural frequencies experimental nominal values were obtained from the average of 16 experimentally determined nodes.

**Table 4-6 Natural frequency comparison of different type of elements**

Mode No.	Experiment nominal, Hz	Beam Hz	Error %	Linear Quad, Hz	Error %	CST Hz	Error %	Thin Shell Hz	Error %
1	50	----		51	2.00	53	6	49.9	-0.20
2	84	81.4	-4.1	89.5	5.30	93	10.7	86.9	3.45
3	110	103	-6.3	109	-0.9	114	3.6	106	-3.60
4	131	----		133	1.5	----		134	2.20
5	217	220	1.3	----		----		214	-1.38
6	240	236	-1.6	246	2.5	225	-3.7	242	0.80
7	272	----		275	1.1	286	5.15	270	-0.70
8	338	332	-1.7	340	0.6	363	7.3	335	-0.89
9	448	463	3.3	438	-2.2	460	2.7	434	-3.10
10	503	----		----		----		510	1.39
11	522	----		524	0.38	----		521	-0.20
12	533	----		535	0.37	529	0.75	536	0.56
13	545	546	0.18	539	-1.1	553	1.46	543	-0.50
14	629	630	0.16	619	-1.6	----		613	-2.00
15	691	----		692	0	----		697	0.86
16	706	710	0.56	----		714	1.1	----	
17	744	755	1.47	----		----		762	-1.00
18	770	755	-1.9	760	-0.5	765	-0.65	----	
19	786	846	7.6	----		----		790	0.50

## Remarks

- The rack structure has been constructed from welded rectangular hollow section RHS beams, which are available from the standard beam menu of the strand software which also calculates the cross-section area, the second moment of area, the torsion constant and shear centre. However, the missing modes were responsible for the large errors associated with this type of element compared to the experimental results.
- Linear Quad and CST type elements have been tested and compared with the experimental results. The missing modes and high errors associated with these type of elements were again evident. Moreover, Linear Quad and CST elements are sensitive to warping problems which are related to the mesh size and consequently to the time required to perform a solution.
- The final decision was to build the rectangular hollow section from Thin Shell Plates element in modelling the prototype, since this type of element yields more accurate and stable results, because the element has six degrees of freedom active at each node when the element is used to model a flat plate. In other words, it has both in-plane and out-of-plane stiffness and does not have drilling freedom problems and no special consideration is needed if the surface is curved or if the elements are used to model a structure consisting of intersecting plates. It will be used to perform the harmonic response analysis, also the same model will be used to perform the field simulated conditions. The only unusual feature in the implementation of the Thin Shell is that boundary conditions which suppress the rotational degrees of freedom at selected nodes should be prescribed across at least two neighbouring nodes since an averaging of the elements means that the rotation about the normal to the surface is described midway between the nodes. Drilling freedom at two such nodes must be fixed for plates.

#### 4.2.5 Finite Element Natural Frequency

Figure 4-13 shows the FE model simulated arrangement of the prototype that has been experimentally tested to obtain the natural frequencies and mode shapes.

Appendix B.1 shows a typical printout from the strand 6.16 Natural Frequency solver.

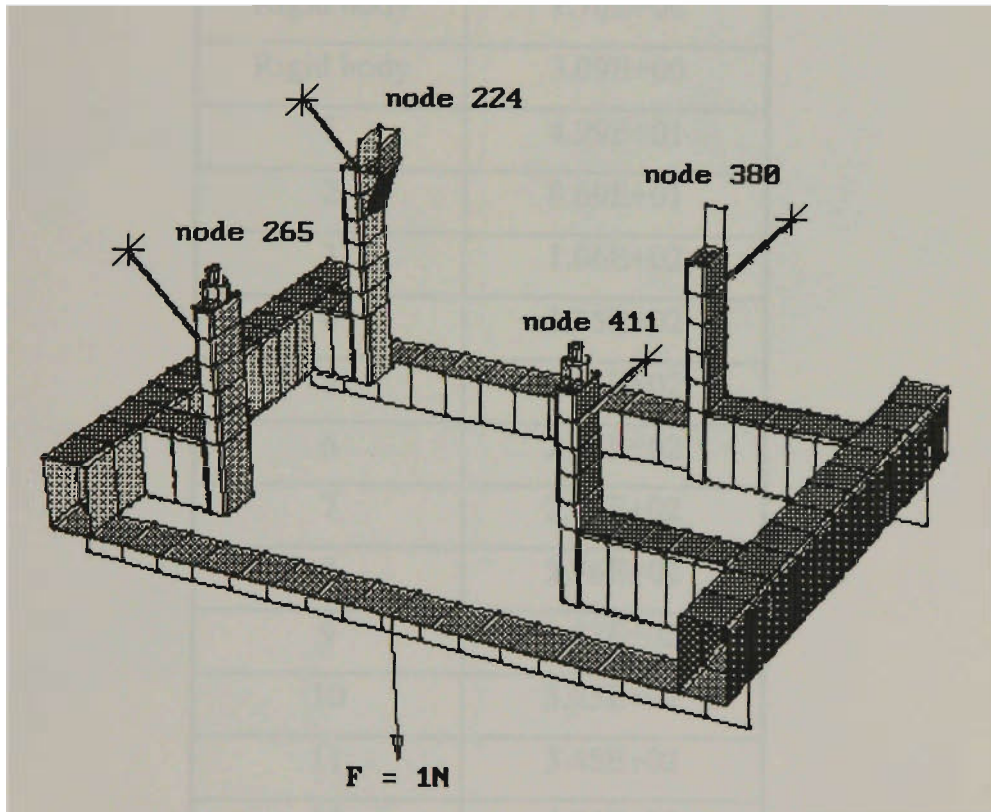


**Figure 4-13 FE model arrangement**

Table 4-7 shows the first 20 natural frequencies that have converged solving equation (4.1).

**Table 4-7 The FE predicted natural frequencies**

Mode No.	Natural Freq. Hz
Rigid body	9.78E-01
Rigid body	1.70E+00
Rigid body	3.09E+00
1	4.99E+01
2	8.69E+01
3	1.06E+02
4	1.35E+02
5	2.14E+02
6	2.43E+02
7	2.71E+02
8	2.76E+02
9	2.82E+02
10	3.35E+02
11	3.45E+02
12	4.34E+02
13	5.11E+02
14	5.22E+02
15	5.36E+02
16	5.43E+02
17	6.14E+02

## 4.2.6 Finite Element Mode Shapes

Figure 4-15, Figure 4-16, Figure 4-17, Figure 4-18 and Figure 4-18 show the engine rack mode shapes from mode 4 to 17. The first three natural frequencies has been omitted and considered as rigid body modes.

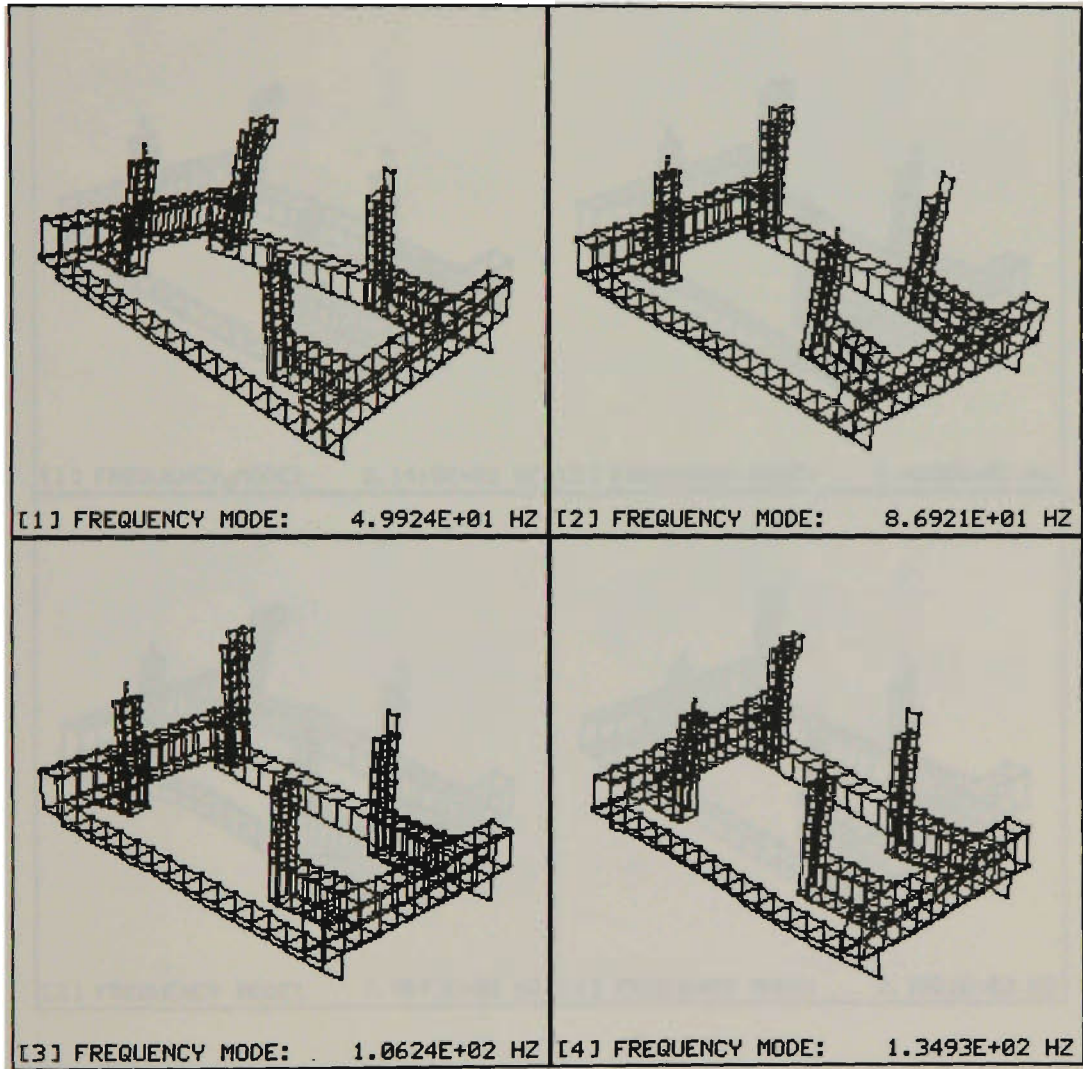


**Figure 4-14 Engine rack mode shapes from : Mode 1 to 4**

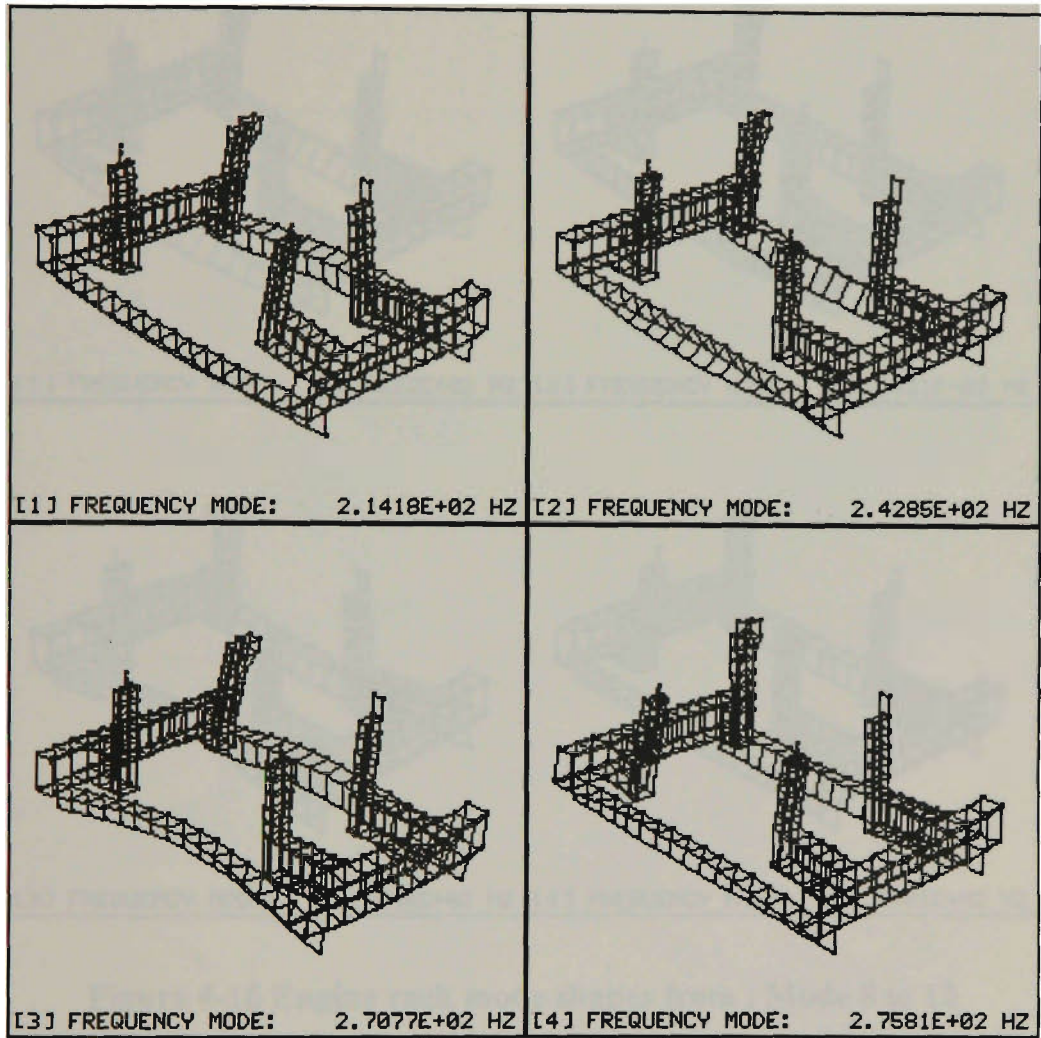


**Figure 4-15 Engine rack mode shapes from : Mode 5 to 8**

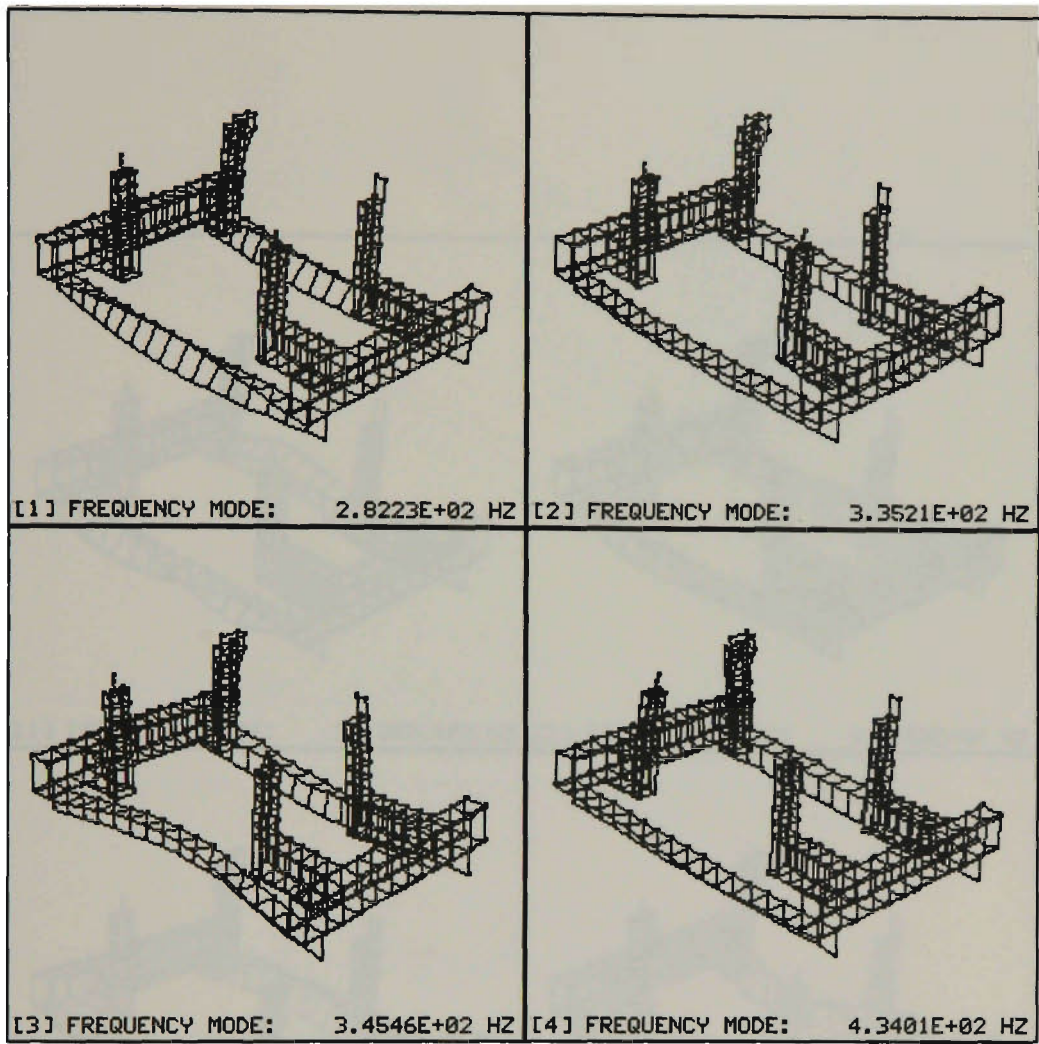


**Figure 4-16 Engine rack mode shapes from : Mode 8 to 12**

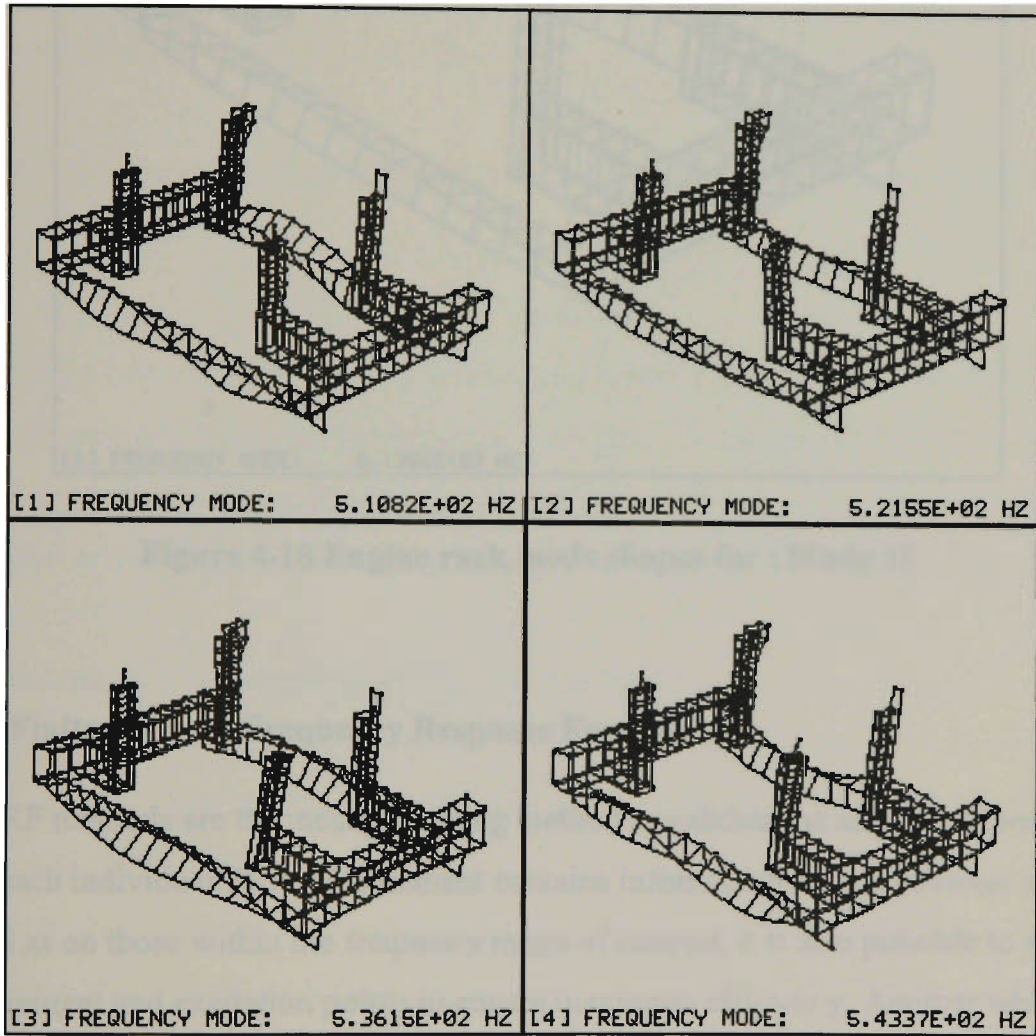


**Figure 4-17 Engine rack mode shapes from : Mode 13 to 16**

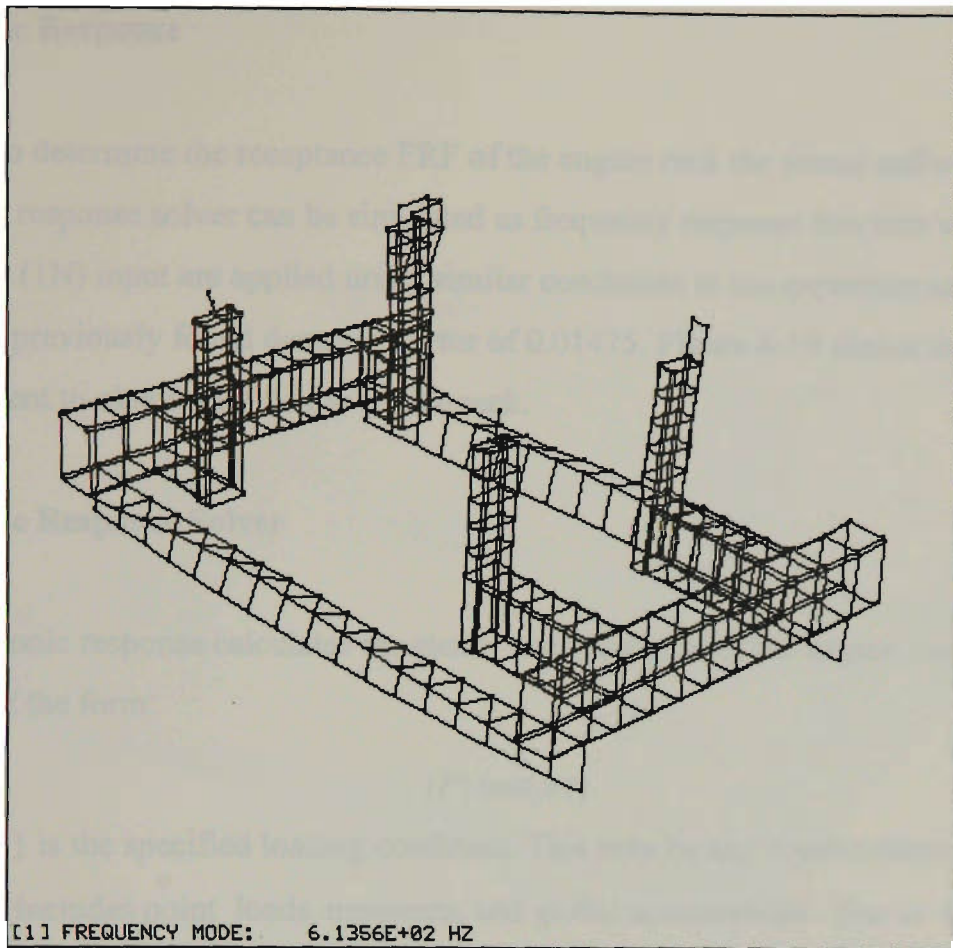


**Figure 4-18 Engine rack mode shapes for : Mode 17**

#### **4.2.7 Finite Element Frequency Response Function**

The FRF methods are the most promising method to validate the analytical model since each individual FRF measurement contains information on out-of-range modes as well as on those within the frequency range of interest, it is also possible to specify measurement and excitation points to ensure maximum efficiency. Another advantage is the direct use of the measured data, thus simplifying lengthy modal analysis procedures. The frequency response functions are compared by overlaying experimental and FE curves on the same frame.

## Harmonic Response

In order to determine the receptance FRF of the engine rack the strand software harmonic response solver can be simulated as frequency response function when 1 unit force (1N) input are applied under similar conditions to the experimental test, using the previously found damping factor of 0.01475. Figure 4-19 shows the FE arrangement to obtain FRF of the engine rack.

### Harmonic Response Solver

The harmonic response calculates the steady state response of the engine rack to loading of the form:

$$\{P\} \cos(\omega t) \quad 4.3$$

Where  $\{P\}$  is the specified loading condition. This may be any combination of load cases and includes point loads, moments, and global accelerations. The  $\omega$  is the frequency at which load is applied and  $t$  is the time. The response of the rack is calculated as a function of frequency for a specific phase angle of applied load.

The harmonic response determines the receptance of the model as a function of frequency. A frequency range of interest is specified and the response of the structure determined at a finite number of points within this range, up to 100. The solution begins at the lowest frequency and steps upward to the upper frequency specified. The stability and accuracy of the solution is not dependent on the number of steps however if the steps are large, some significant modes behaviour will either be missed or inadequately represented.

### Harmonic Response Result

Harmonic response generates a receptance FRF plot for a structure that is subjected to a sinusoidally varying load which act at the specified frequencies.

Figure 4-19 shows the simulated experimental arrangement used to obtain the FE model frequency response function of the engine rack using the harmonic response

solver. Appendix B.2 show a typical print out for the strand 6.16 harmonic response solver.

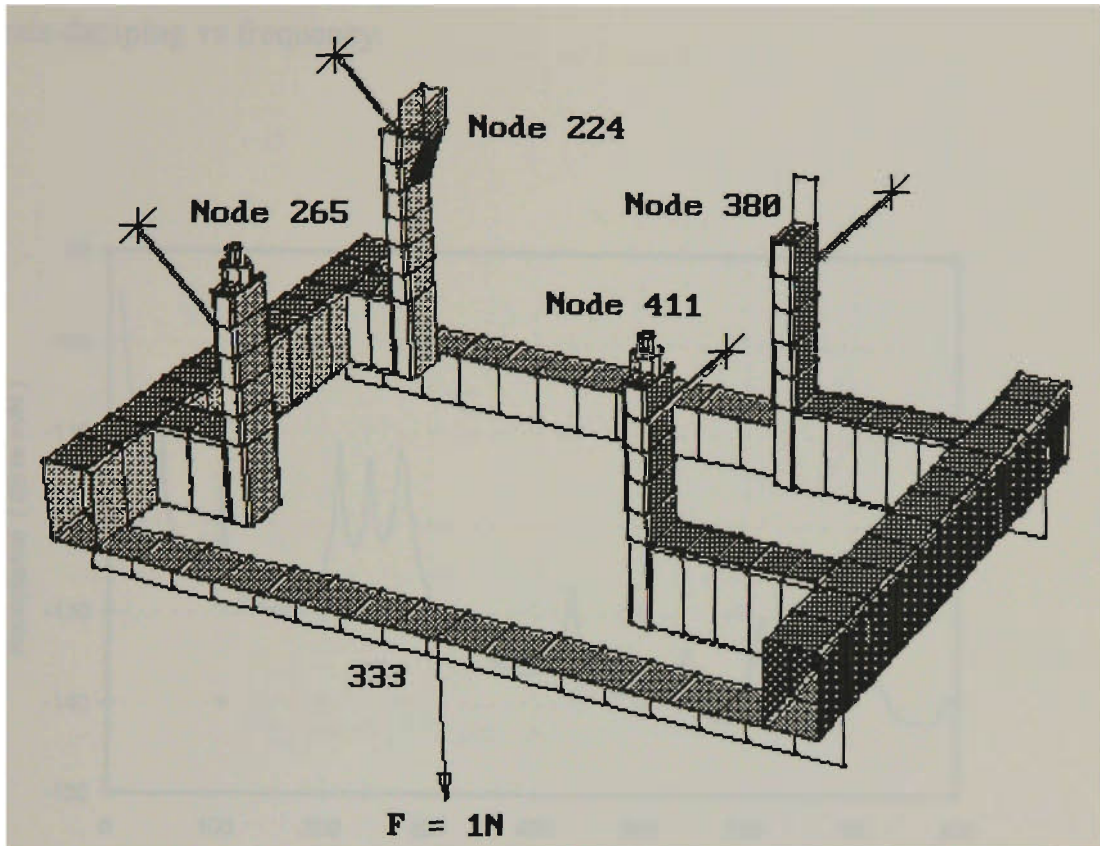


**Figure 4-19 FE arrangement to obtain FRF of the engine rack**

Note:

- FEM node No 333 correspond node No 1 experimental model
- FEM node No 224 correspond node No 5 experimental model
- FEM node No 265 correspond node No 6 experimental model
- FEM node No 380 correspond node No 7 experimental model
- FEM node No 411 correspond node No 8 experimental model

The curves in Figure 4-20, Figure 4-21, Figure 4-22 and Figure 4-23 show receptance FRF in the vertical (Y-direction) where the engine contacts the rack. Using the excitation at node No 333 as input, the output was measured at nodes 224, 265, 380 and 411 respectively.  $H_{jk}$  is the FRF at j - response node, k - excitation node. The FE results were obtained by digitising the response to the same resolution as the experimental test analyser and at 1N input force, setting the default general damping

factor to 0.01475 which has been obtained as an arbitrary figure close to the Nyquist circle fit damping factor average. This damping coefficient is not necessarily the best for all resonances, however it is extremely difficult and time consuming to predict an accurate damping vs frequency.

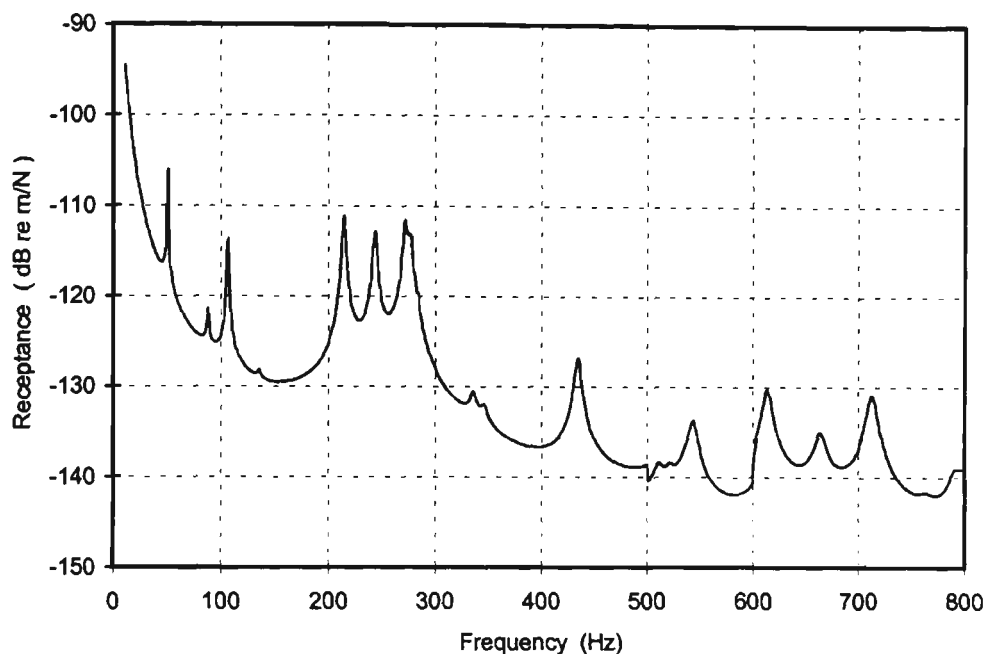


**Figure 4-20 Finite element FRF ( $H_{224,333}$ )**

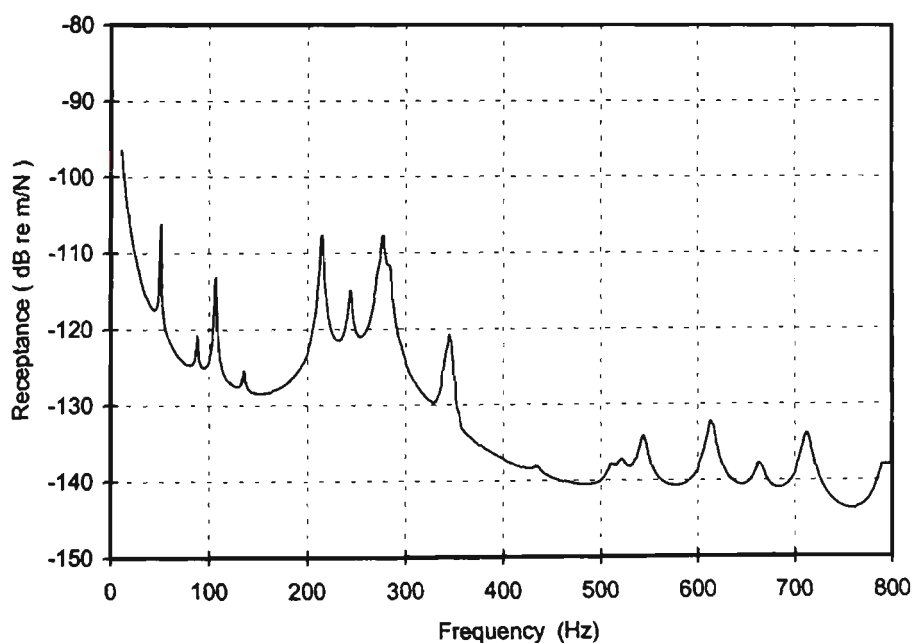


**Figure 4-21 Finite element FRF ( $H_{265,333}$ )**

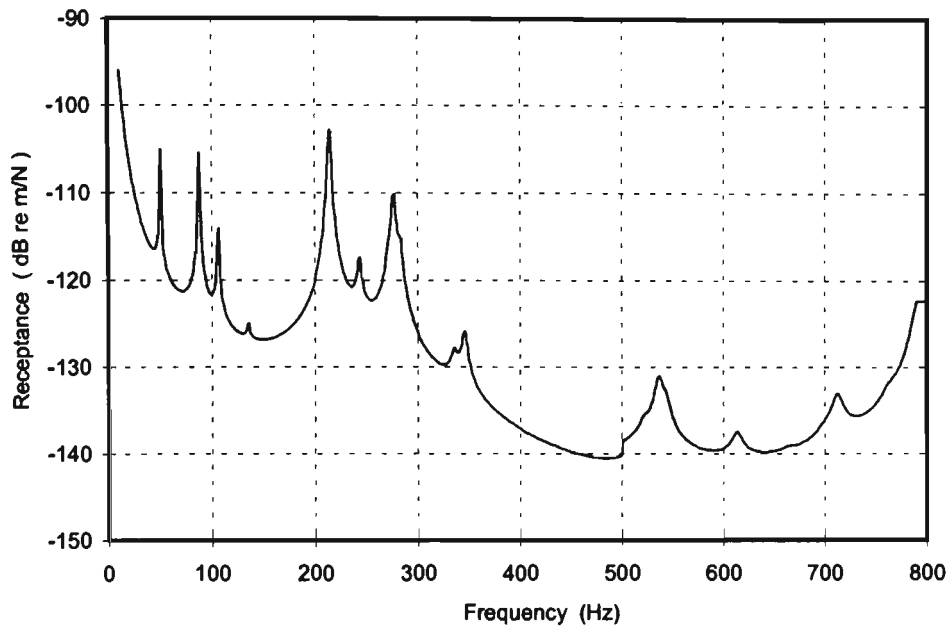


**Figure 4-22 Finite element FRF ( $H_{380,333}$ )**

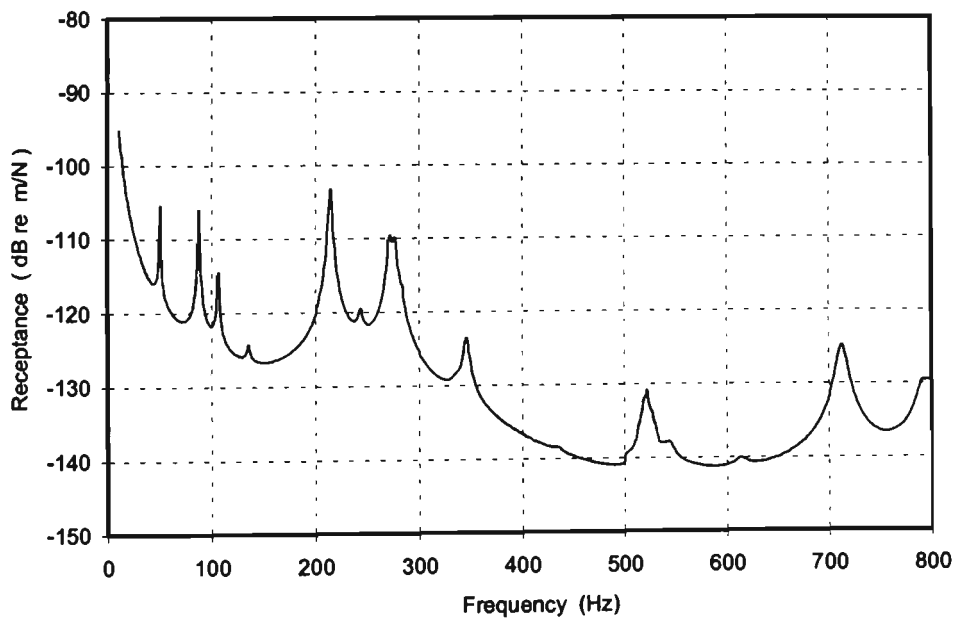


**Figure 4-23 Finite element FRF ( $H_{411,333}$ )**

Figure 4-24, Figure 4-25, Figure 4-26 and Figure 4-27 show the receptance FRF at the nodes 224, 265, 380 and 411, respectively, in linear scale.

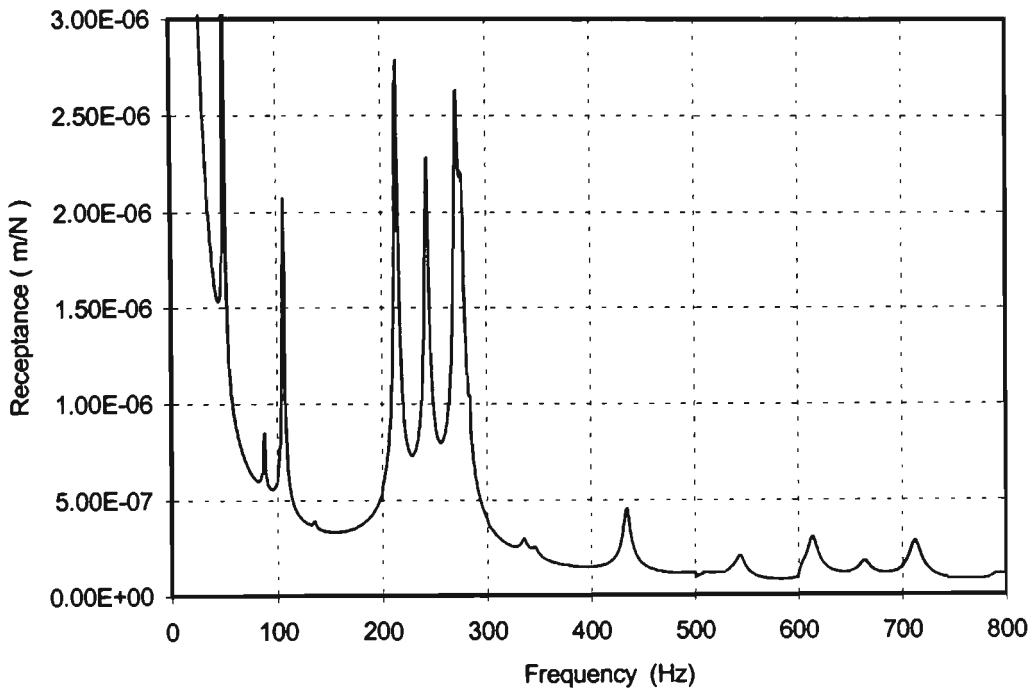


**Figure 4-24 Finite element FRF ( $H_{224,333}$ )**

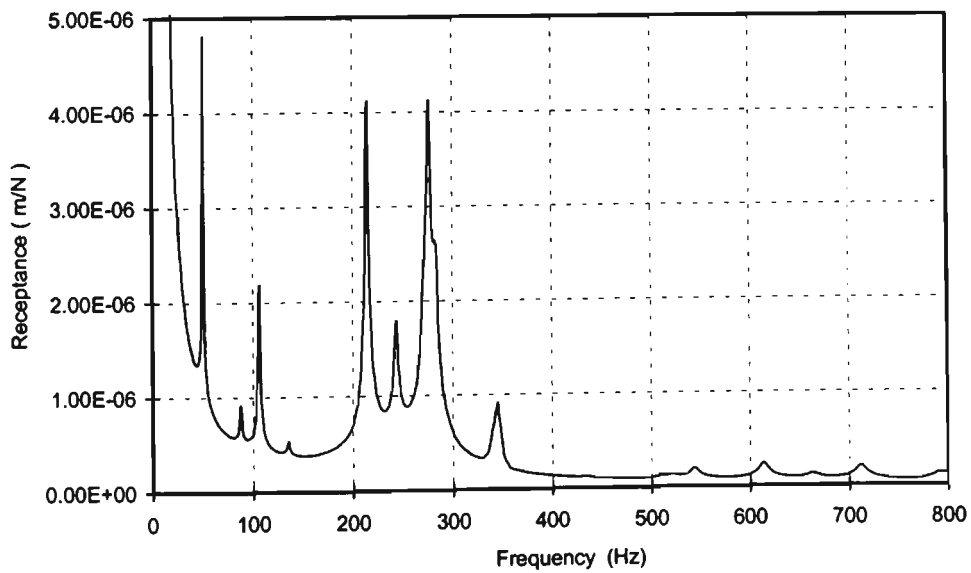


**Figure 4-25 Finite element FRF ( $H_{265,333}$ )**

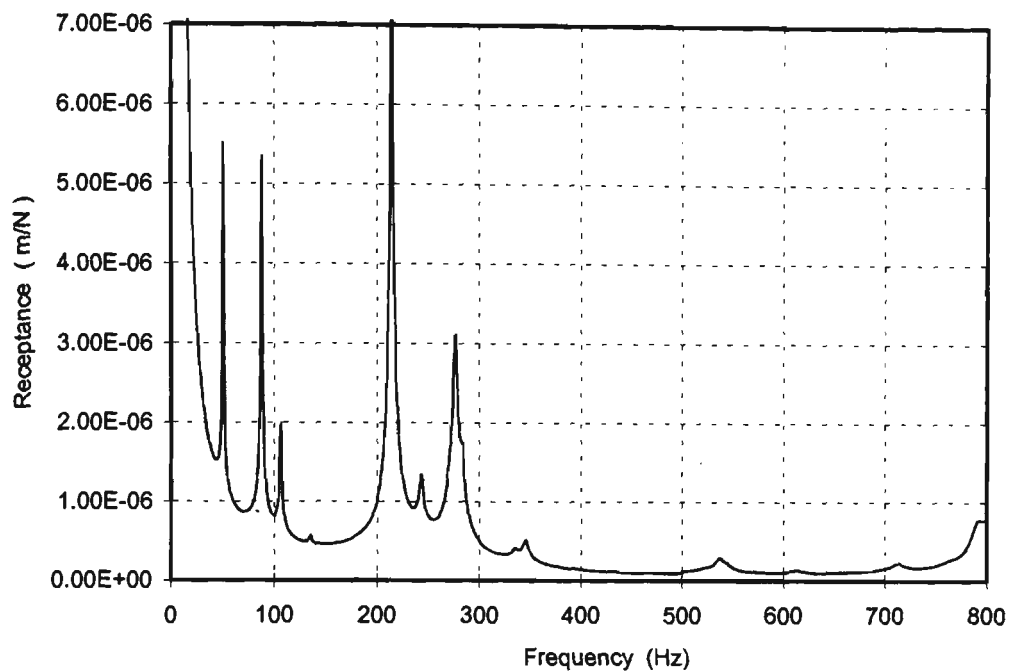


**Figure 4-26 Finite element FRF ( $H_{380,333}$ )**

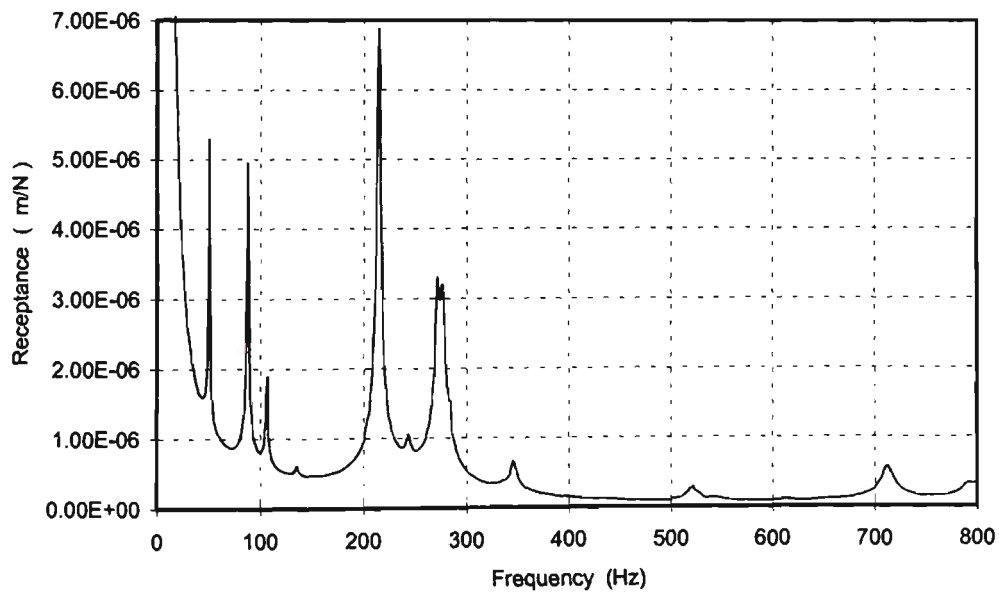


**Figure 4-27 Finite element FRF ( $H_{411,333}$ )**

Table 4-8 shows the receptance values at resonant frequencies for the FEM at the nodes where the engine assembly contacts the rack. This result was obtained from the harmonic response solver to 1 N input force and damping factor of 0.01475.

**Table 4-8 Receptance at resonant modes for the FEM**

Freq. Hz	(H <sub>224.333</sub> ) m/N	Freq. Hz	(H <sub>265.333</sub> ) m/N	Freq. Hz	(H <sub>380.333</sub> ) m/N	Freq. Hz	(H <sub>411.333</sub> ) m/N
51	4.86E-06	51	4.76E-06	51	5.45E-06	51	5.24E-06
107	2.06E-06	107	2.17E-06	107	1.97E-06	107	1.88E-06
215	2.78E-06	215	4.11E-06	136	5.62E-07	215	6.87E-06
244	2.28E-06	244	1.79E-06	213	7.24E-06	244	1.05E-06
272	2.63E-06	277	4.11E-06	244	1.43E-06	272	3.30E-06
336	2.96E-07	345	9.15E-07	277	4.61E-06	346	6.63E-07
435	2.53E-07	522	1.37E-07	346	9.09E-07	522	1.64E-07
500	1.17E-07			537	2.82E-07	544	1.29E-07
522	1.20E-07			713	5.72E-07		
544	2.07E-07						
664	1.78E-07						

### 4.3 Comparisons and Validation

#### 4.3.1 Comparisons of Natural Frequencies

Ewins (1984) stated that the most common method of comparing natural frequencies from two different models is to plot experimental values against FE model for all available modes. The points of the resulting curve should lie on a straight line of slope  $\pm 1$  for perfectly correlated data. A systematic derivation suggests a consistent error (e.g., in material properties) while a large random scatter suggests poor correlation. Table 4-9 and curve Figure 4-28 show a comparison of the experimental nominal natural frequency against finite element model. The FE model results obtained by using thin shell element, all rigid body modes has been omitted.

**Table 4-9 Comparison of the natural frequency of experimental vs FEA**

Experimental nominal - Hz	Finite Element Hz
50	49.9
84	86.9
110	106
131	135
217	214
240	243
272	271
	276
	282
338	335
	345
448	434
503	511
522	522
533	536
545	543
629	614
691	697
706	
744	762
770	
786	790
800	800

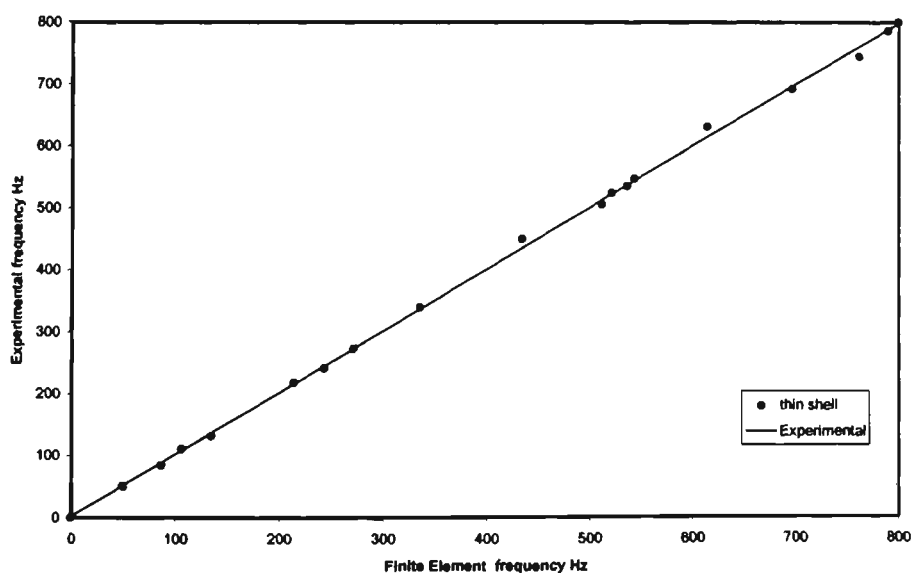


**Figure 4-28 Comparison of the natural frequency of experimental vs FEA**

### 4.3.2 Comparison of FRF's

Figure 4-29, Figure 4-30, Figure 4-31 and Figure 4-32 show the overlay of the receptance FRF at nodes [7 vs 224], [6 vs 265], [8 vs 380] and [5 vs 411] respectively.

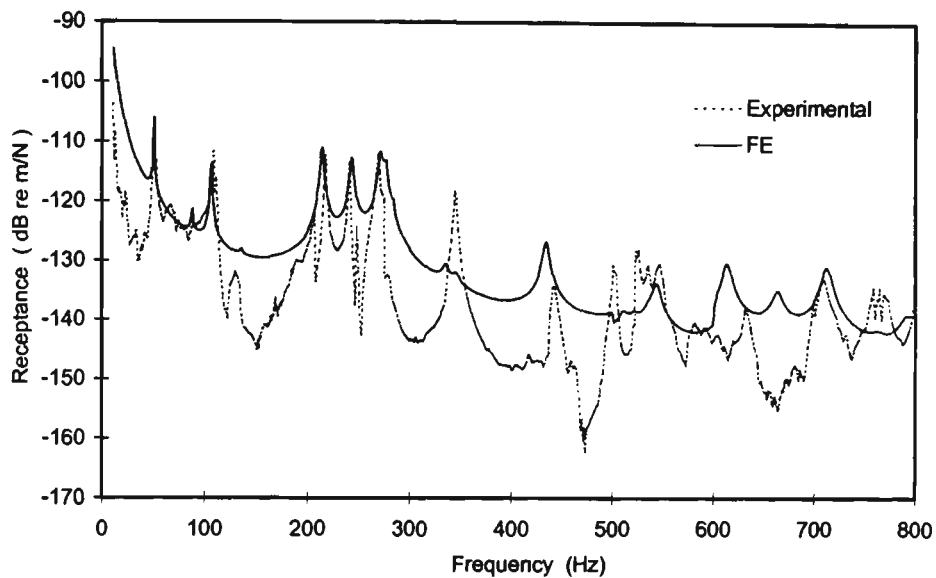


**Figure 4-29 FRF overlay experimental and FE ( $H_{7,1}$ ) and ( $H_{224,333}$ )**

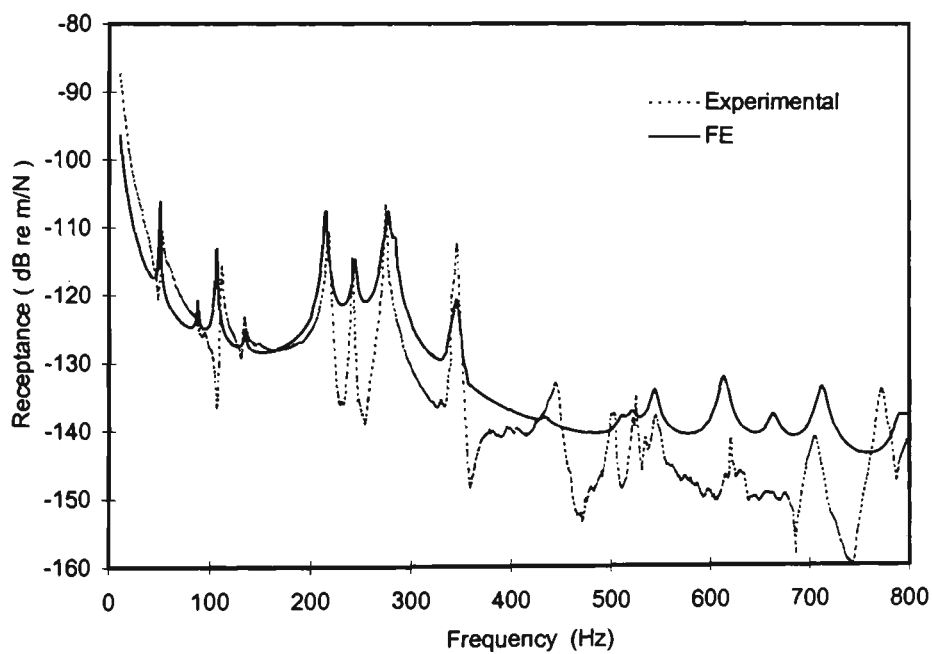


**Figure 4-30 FRF overlay experimental and FE ( $H_{6,1}$ ) and ( $H_{265,333}$ )**

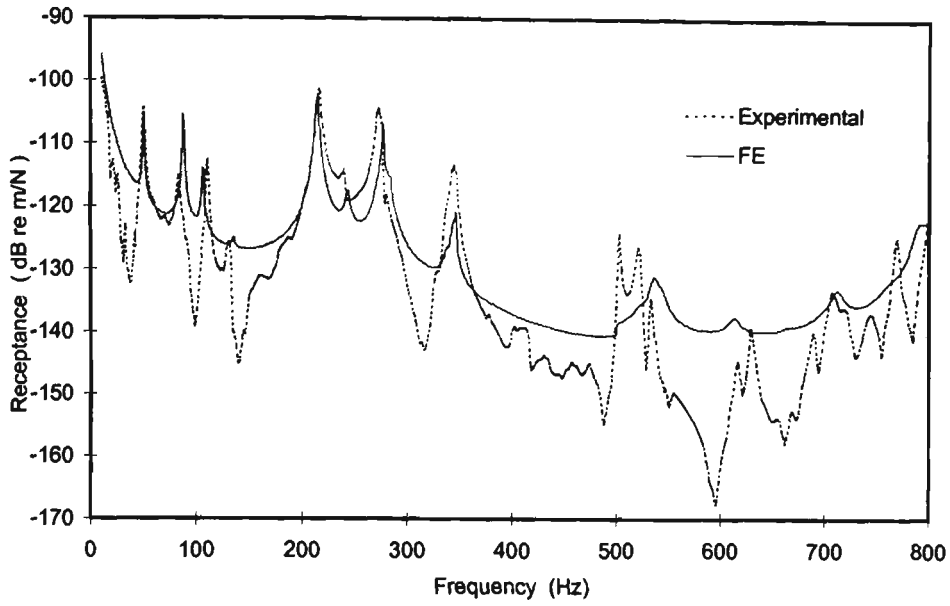


**Figure 4-31 FRF overlay experimental and FE ( $H_{8,1}$ ) and ( $H_{380,333}$ )**

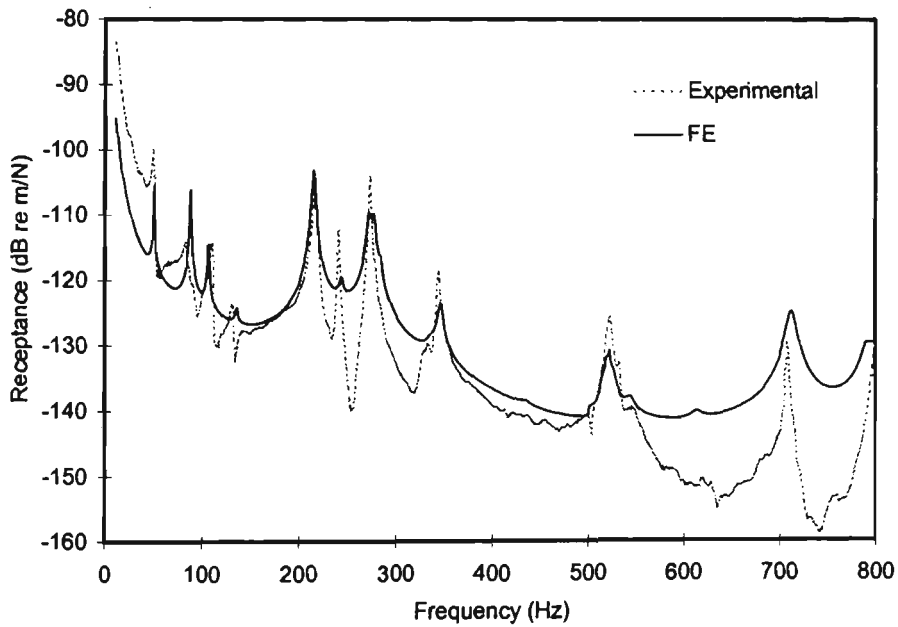


**Figure 4-32 FRF overlay experimental and FE ( $H_{5,1}$ ) and ( $H_{411,333}$ )**

Examining the curves in Figure 4-29, Figure 4-30, Figure 4-31 and Figure 4-32 show that there is no systematic discrepancy or a steady frequency shift between the two curves. Also indicating a high degree of correlation in the receptance axis.

Investigating the antiresonances shows discrepancies which may be due to localised errors (loss of stiffness at joints etc.) or due to more general factors such as incorrect values of elastic modulus or material density, etc.

Another factor has an effect on the accuracy of the curve comparison, the FRF can be very sensitive to the exact location of the response point and possibly to the excitation point, i.e. if the location of the measured response point used in the modal test does not coincide exactly with any of the mesh points used in the FE model.

Figure 4-33, Figure 4-34, Figure 4-35 and Figure 4-36 show the overlay of the FRF's Experimental vs FE in linear scale at nodes [7 vs 224], [6 vs 265], [8 vs 380] and [5 vs 411] respectively.

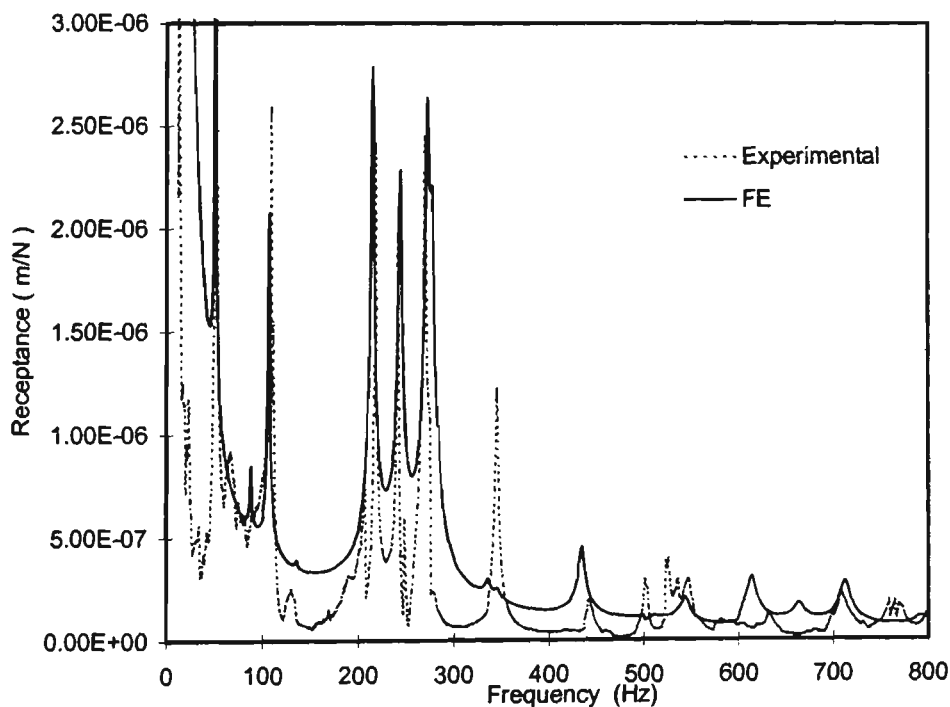


**Figure 4-33 FRF overlay experimental and FE ( $H_{7,1}$ ) and ( $H_{224,333}$ )**

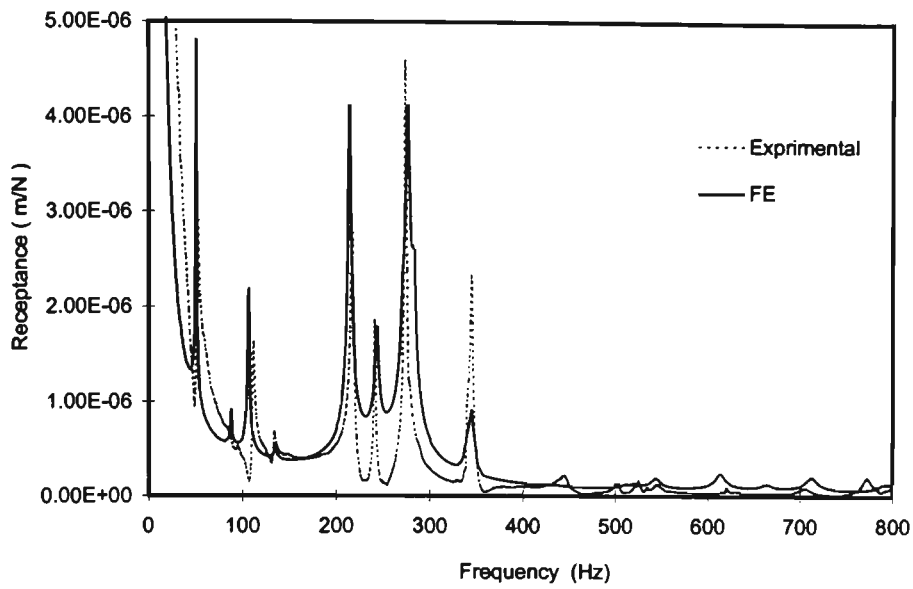


**Figure 4-34 FRF overlay experimental and FE ( $H_{6,1}$ ) and ( $H_{265,333}$ )**

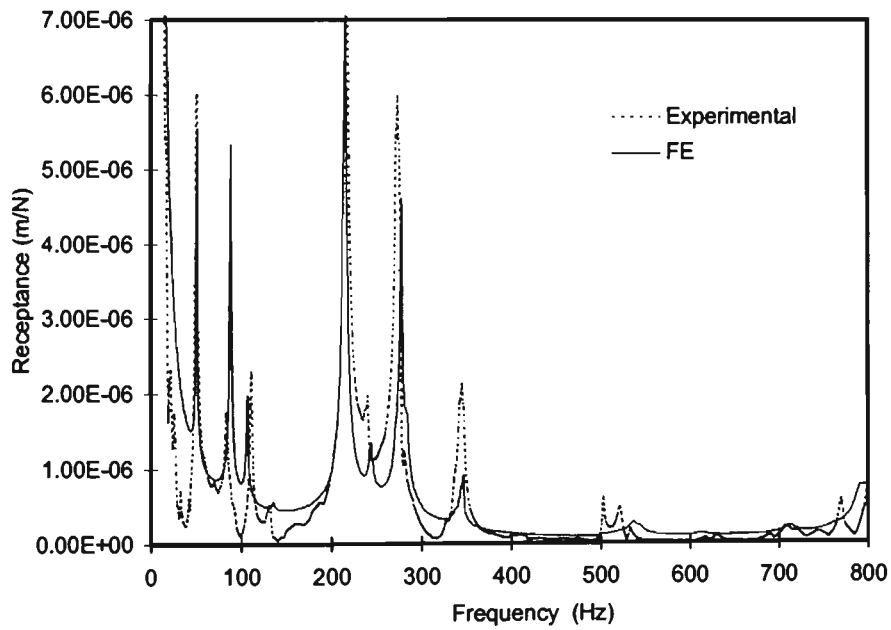


**Figure 4-35 FRF overlay experimental and FE ( $H_{8,1}$ ) and ( $H_{380,333}$ )**

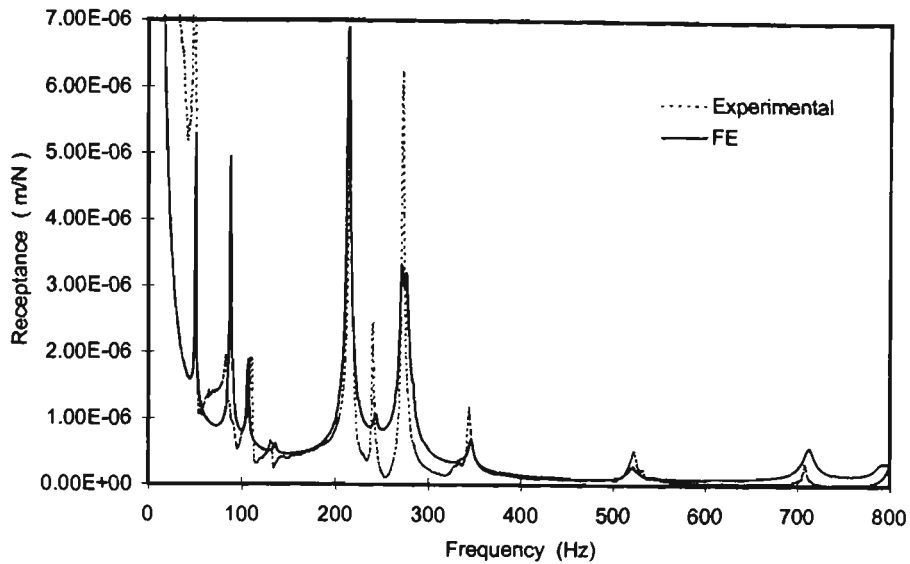


**Figure 4-36 FRF overlay experimental and FE ( $H_{5,1}$ ) and ( $H_{411,333}$ )**

### 4.3.3 Displacement Comparisons

Table 4-10, Table 4-11, Table 4-12 and Table 4-13 show the receptance comparison between the tested prototype model at node 5, 6, 7 and 8 and finite element model at node 224, 265, 380 and 411, respectively. The finite element model has been examined under two different modes of damping, the software default damping factor of 0.01 and the proposed general default damping factor of 0.01475.

The receptance of the finite element model under the condition of 0.01 damping factor was much higher than the experimental receptance, while the 0.01475 damping factor yielded more realistic and closer receptance to the experimental one.

**Table 4-10 Receptance comparison : Node 7 vs 224**

Node 7-224 Hz.	Experimental $H_{7,1}$	FE $H_{224,333}$ D =.01475	FE $H_{224,333}$ D =0.01
50	3.65E-06		
51		4.86E-06	6.68E-06
107		2.06E-06	2.86E-06
109	2.58E-06		
215		2.78E-06	3.94E-06
218	2.41E-06		
240	2.10E-06		
241		2.28E-06	3.16E-06
269	2.44E-06		
272		2.63E-06	3.55E-06
336		2.96E-07	3.35E-07
345	1.22E-06		
435		4.52E-07	6.21E-07
442	1.91E-07		
500		1.17E-07	1.87E-07
501	2.92E-07		
522		1.20E-07	2.87E-07
523	3.81E-07		
536	2.91E-07		
544		2.07E-07	4.69E-07
547	2.95E-07		
664		1.78E-07	1.97E-07
771	1.55E-07		

**Table 4-11 Receptance comparison : Node 6 vs 265**

Node 6-265 Hz.	Experimental $H_{7,1}$	FE $H_{265,333}$ D =.01475	FE $H_{265,333}$ D =0.01
52	3.66E-06	4.76E-06	6.59E-06
107		2.17E-06	3.02E-06
112	1.63E-06		
215		4.11E-06	5.9E-06
217	2.96E-06		
241	1.85E-06		
244		1.79E-06	2.36E-06
274	4.58E-06		
277		4.11E-06	5.65E-06
336		9.15E-07	4.13E-06
345	2.33E-06		
503	1.31E-07		
523	1.20E-07	1.37E-07	1.52E-07
705	8.75E-08		
772	1.94E-07		

**Table 4-12 Receptance comparison : Node 8 vs 380**

Node 8-380 Hz.	Experimental $H_{8,1}$	FE $H_{380,333}$ D =.01475	FE $H_{380,333}$ D =0.01
51	6.00E-06	5.45E-06	7.55E-06
83	1.75E-06		
88		5.33E-06	7.60E-06
107		1.97E-06	2.64E-06
111	2.30E-06		
131	5.16E-07		
136		5.62E-07	6.11E-07
213		7.24E-06	6.81E-06
216	8.64E-06		
240	1.96E-06		
244		1.34E-06	1.67E-06
273	5.98E-06		
277		4.61E-06	3.31E-06
345	2.12E-06		
346		9.09E-07	6.44E-07
503	6.16E-07		
521	4.80E-07		
533	1.86E-07		
537		2.82E-07	3.58E-07
630	1.08E-07		
706	1.93E-07		
770	5.73E-07		

**Table 4-13 Receptance comparison : Node 5 vs 411**

Node 5-411 Hz.	Experimental $H_{7,1}$	FE $H_{411,333}$ $D = .01475$	FE $H_{411,333}$ $D = 0.01$
50	1.00E-05		
51		5.24E-06	7.20E-06
107		1.87E-06	2.52E-06
110	1.90E-06		
215		6.87E-06	1.00E-05
216	5.92E-06		
240	2.40E-06		
244		1.05E-06	1.21E-06
272		3.30E-06	4.39E-06
273	6.20E-06		
344	1.17E-06		
346		6.63E-07	8.74E-07
522	5.12E-07	2.96E-07	3.21E-07
544		1.29E-07	1.92E-07
545	9.94E-08		
708	3.20E-07		
713		5.72E-07	7.36E-07

#### 4.4 Summarising Remarks

The physical and behavioural approximations used in FE modelling leads to considerable uncertainty in modelling of items such as boundary conditions, joint flexibility. The finite element results are not exact, since the input data itself is approximate. Also it is not possible to eliminate the experimental error such as measurement errors, equipment sensitivity and noise.

Different approaches have been considered to update the finite element model, such as improved connectivity, the effect of hammer excitation method on damping and changing strand default damping ratio.

It was found that Thin Shell Plates element yielded more accurate and stable result than Linear Quad, CST and Beam element. The investigation of the natural frequencies results shows that both the experimental and FEM were close and within the acceptable limits of variation and shift (less than 4%). Other errors were due to experimental inaccurate conduct and the approximation contained in the FE model.

It was possible that the experimental 50 Hz mode was due to interference from the electrical mains. However in this case the FEA has confirmed that there is a true mode at 50 Hz. Investigating the FRF overlay curves found that both the experimental and FEM were close and acceptable. A damping factor of 0.1475 was introduced during FRF analysis to the FE model because 0.01 the default damping factor of the strand software resulted in higher amplitudes compared with the experimental results.

Since both the experimental and finite element models yielded correlated amplitude values, the choice of damping factor of 0.01475 which has been obtained as an arbitrary figure close to Nyquist circle fit damping factor average is a reliable factor and can be used in subsequent calculations. Figure 4-29, Figure 4-30, Figure 4-31 and Figure 4-32 show a comparison between experimental and FEM of FRF of the engine rack. The plots show a discrepancy between the two sets of data, while at the time indicating a high degree of correlation in the amplitude axis. Also of interest are the relative values of the frequencies of resonance and of antiresonance. Close

examination of which can indicate whether the discrepancies are due to localised errors (loss of stiffness at joints etc) or to more general factors ( such as incorrect values of elastic modulus, material density, residual stresses due to welding and imperfection of the thickness regularity of cold roll RHS, etc.)

For both experimental and FE data, when the engine rack receptance was measured, if the location of the response point used in the experimental test did not coincide exactly with the mesh of grid point used in the FE model, making a direct comparison proved impossible. This observation is very useful when we consider how to assess the degree of correlation between the experimental and FE models. Because the particular parameter being measured (FRF) can be very sensitive to the exact location of the response point and possibly to the excitation point.

The differences noted in this study probably resulted from point defects at welded connections within the structure. In general, stiffness variations between the FEM and real rack may result from a number of causes. These include overall effects (e.g. incorrect values of Young's modulus), local effects (stiffness or mass errors within an element or group of elements), point effects (joints or cracks) and for fixed systems, errors resulting from incorrectly modelled boundary conditions.

## 5. Results and Discussion of Dynamic Analysis

The aim of this chapter is to predict the response of the engine rack and its content to shock and vibration, as loaded and used in a simulated environment in terms of :

- Engine rack response to the random vibration when exposed to a simulated transportation environment. The random vibration that has been used in this analysis contains simulated averages, vibration intensities and frequencies for truck under severe conditions, refer to section 2.1.2 and ASTM D4728 (1994).

- Energy transfer from transient vibration to engine rack and its content.

However the shock received from a drop during handling is greater than that experienced in being transported in a vehicle. Such shock usually determines the severity of the shock test and simulation. These shock characteristics define a fast transfer of kinetic energy which take place in sudden and short duration compare with the natural period of oscillation of the loaded rack. The shock spectrum that has been used in this analysis is a theoretical spectrum that has the acceleration varying with time and equal to the acceleration that develop in the rack during the impact.

The FEM that has been used in this environmental simulated condition was similar to the prototype No H4182 model used for the validation with some loading and freedom condition variation, specifically:

- Loading method : A heavy plate with special shape to represent an approximate engine shape and weight distribution on the four engine supports. Figure 5-1 shows the simulated FEM.
- Freedom condition : For transient and spectral response solution in which the rack is subject to acceleration which varies with time, this acceleration will be downward and equal to the acceleration that develops in the rack during impact, therefore the rack should be fixed at the base where it contact the ground.
- The global acceleration in the downward (y - direction) equal to the gravitational acceleration.

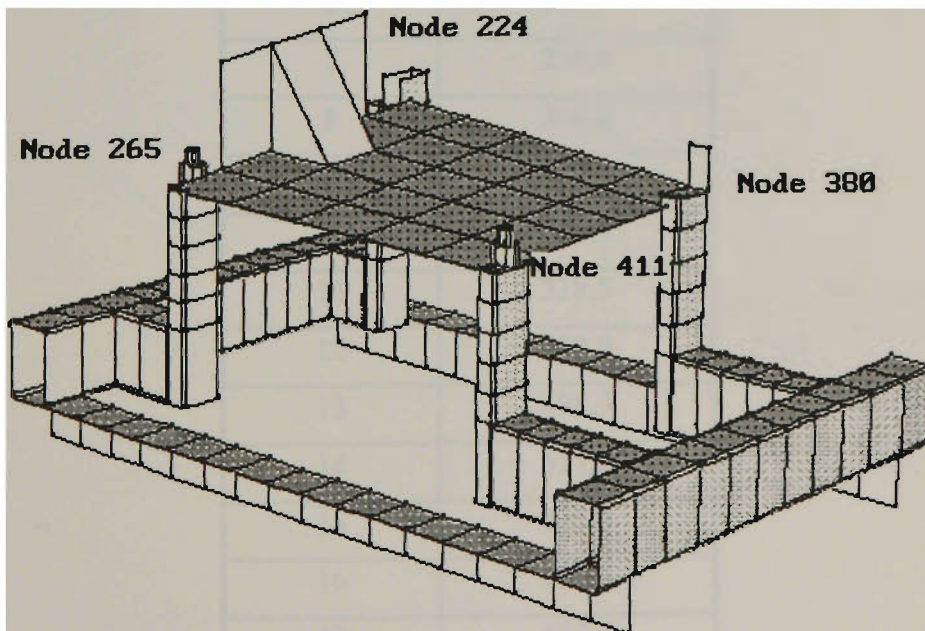


**Figure 5-1 FEM used for simulation**

## 5.1 Natural Frequency

It was necessary to calculate a new set of natural frequencies and mode shapes for the loaded engine rack.

### 5.1.1 Natural Frequency Analysis

Table 5-1 shows the first 20 natural frequencies converged that reflect the simulated environment conditions.

**Table 5-1 The first 20 natural frequencies**

<b>Mode No</b>	<b>NATURAL FREQ. Hz</b>
1	17.4
2	34.6
3	68.5
4	81.9
5	131.8
6	199.5
7	230.8
8	246.2
9	267.1
10	285.8
11	318.5
12	392.9
13	498.3
14	517.9
15	522.0
16	603.5
17	689.6
18	705.6
19	747.4
20	775.7

Appendix C.1 shows a typical printout from the strand 6.16 natural frequency solver

Figure 5-2, Figure 5-3, Figure 5-4, Figure 5-5 and Figure 5-6 show the first 20 mode shapes of the loaded rack as calculated from the FEM.

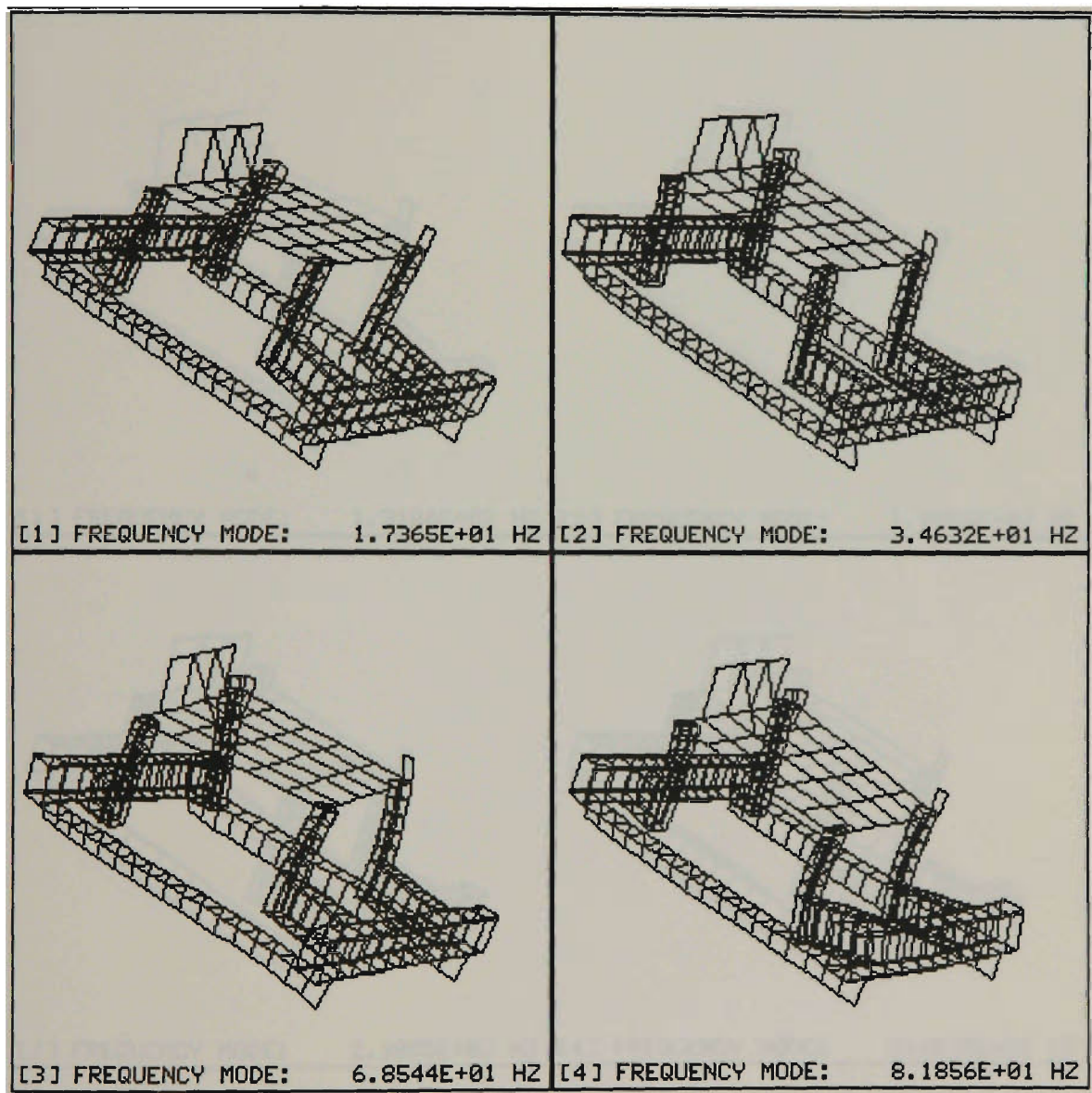


**Figure 5-2 Mode shapes of the loaded rack : Mode 1 to 4**

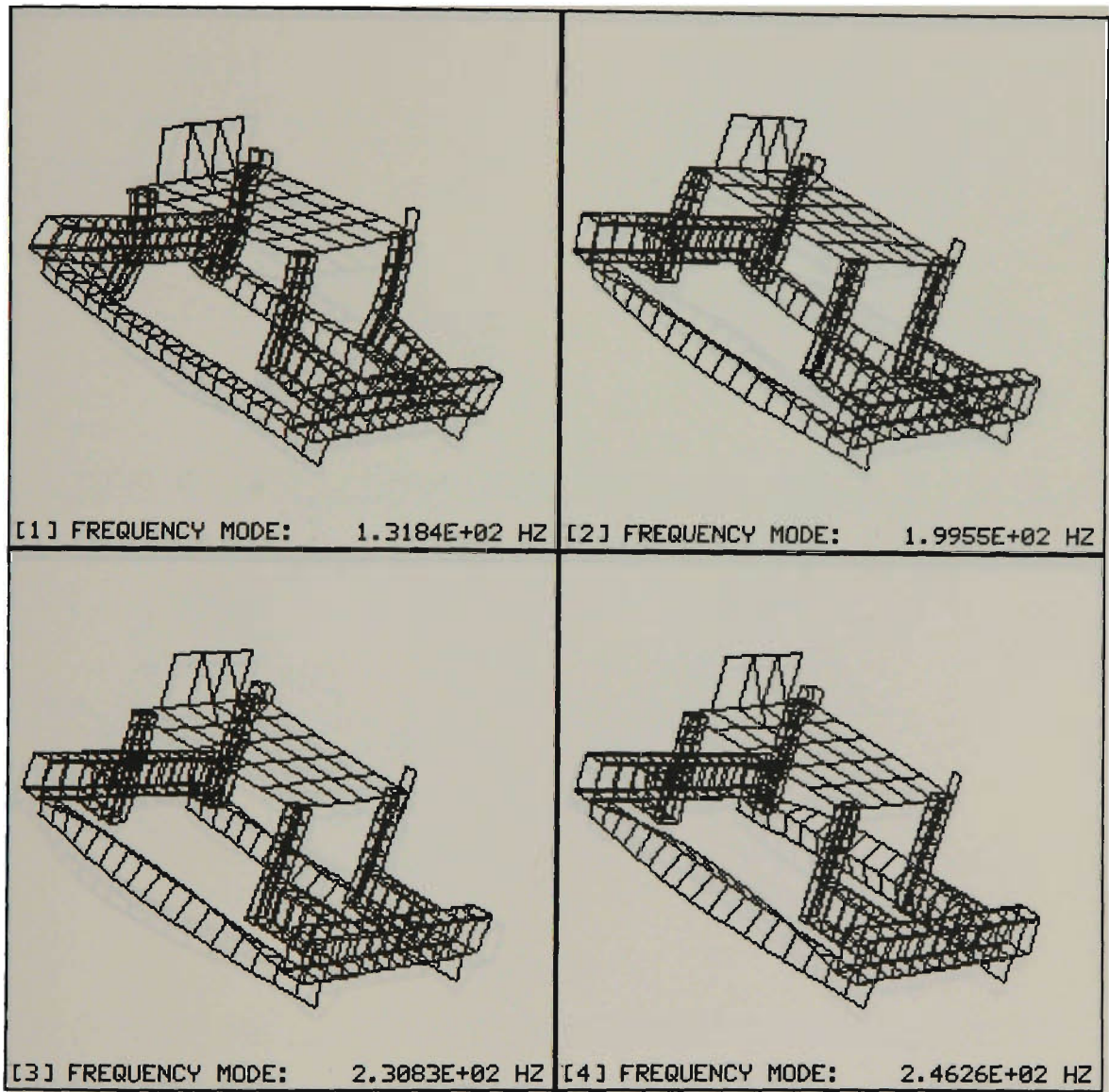


**Figure 5-3 Mode shapes of the loaded rack : Mode 5 to 8**

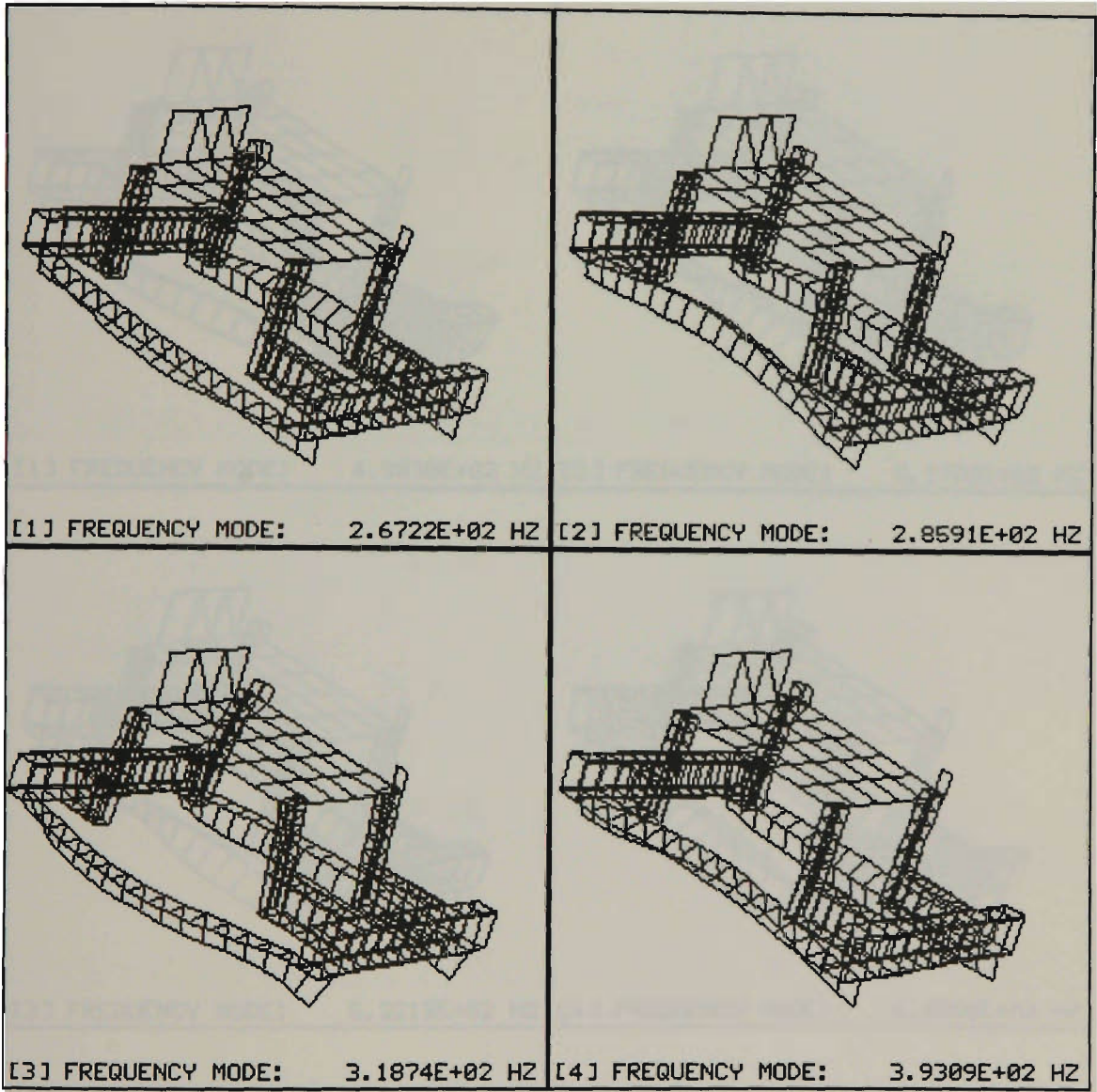


**Figure 5-4 Mode shapes of the loaded rack : Mode 9 to 12**

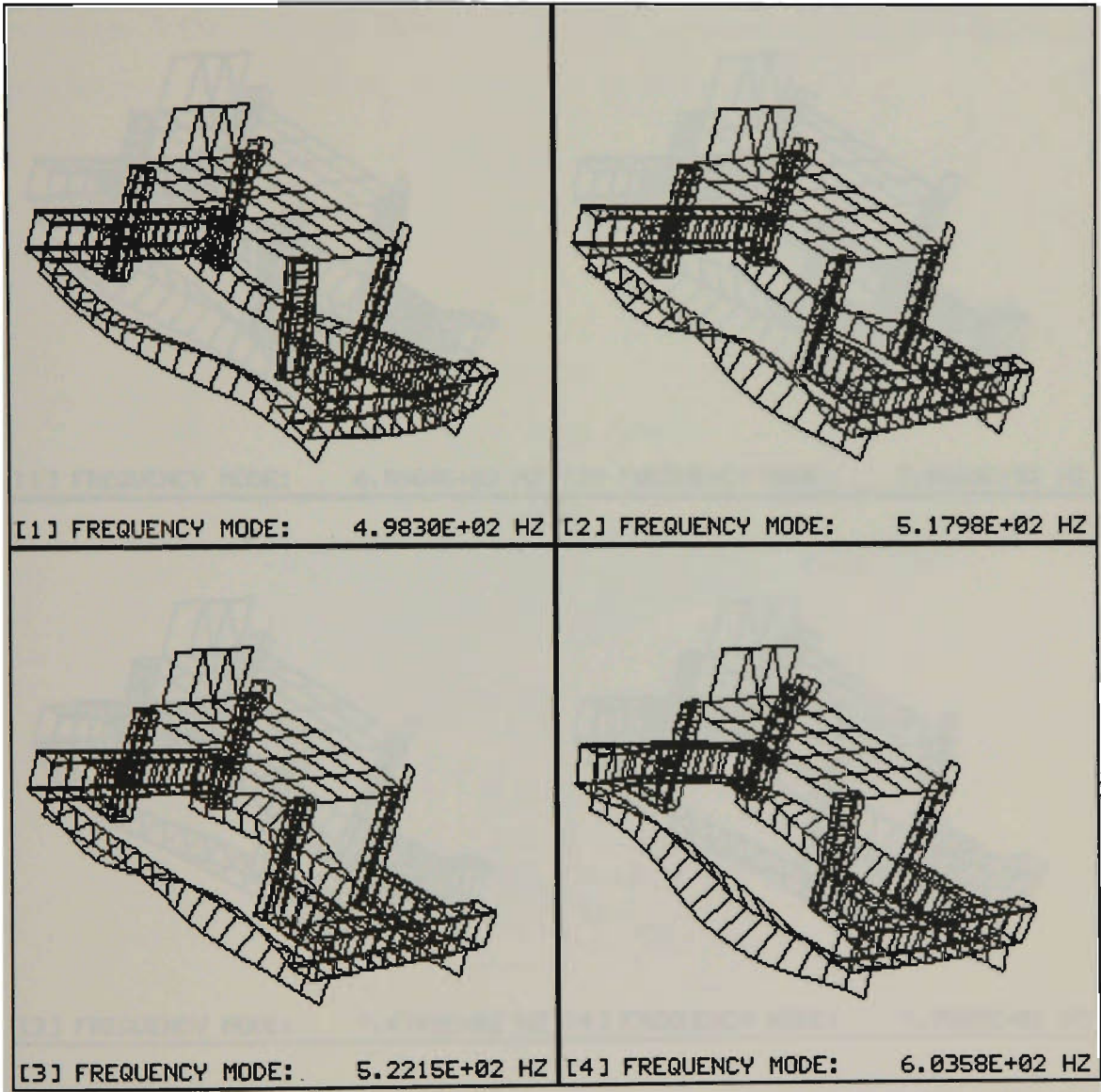


**Figure 5-5 Mode shapes of the loaded rack : Mode 13 to 16**

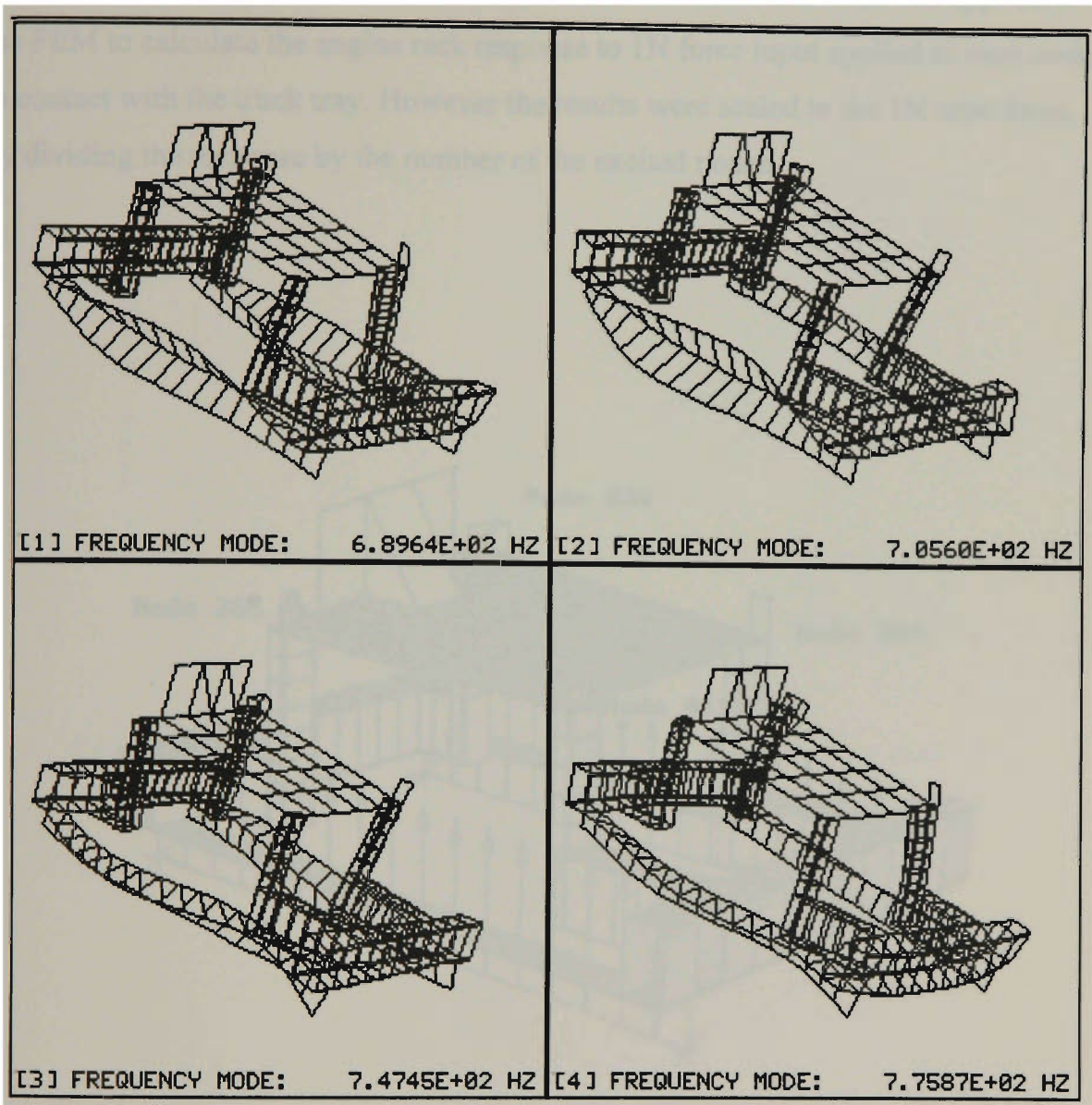


**Figure 5-6 Mode shapes of the loaded rack : Mode 17 to 20**

## 5.2 Harmonic Response

The previously defined parameters were used with the harmonic response solver to obtain the engine rack displacement magnitude at the nodes of contact with the engine. Figure 5-7 shows the excitation direction and freedom conditions applied to the FEM to calculate the engine rack response to 1N force input applied to each node in contact with the truck tray. However the results were scaled to the 1N total force, by dividing the response by the number of the excited nodes.

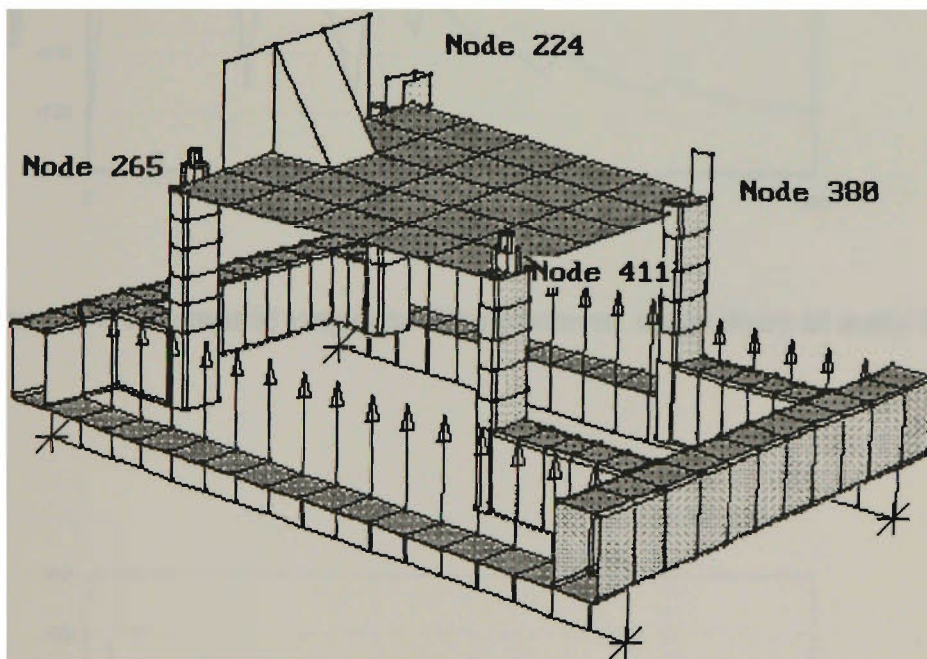


**Figure 5-7 FE harmonic response loading simulation**

## 5.2.1 Harmonic Response Analysis

Figure 5-8, Figure 5-9, Figure 5-10 and Figure 5-11 show the displacement magnitude as a function of Frequency at various modes in dB scale.

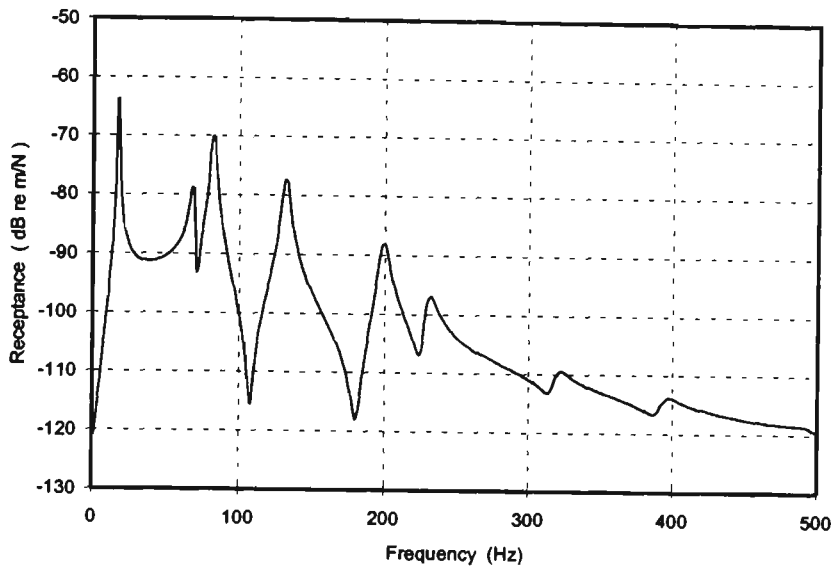


**Figure 5-8 Harmonic response displacement magnitude at node 224**

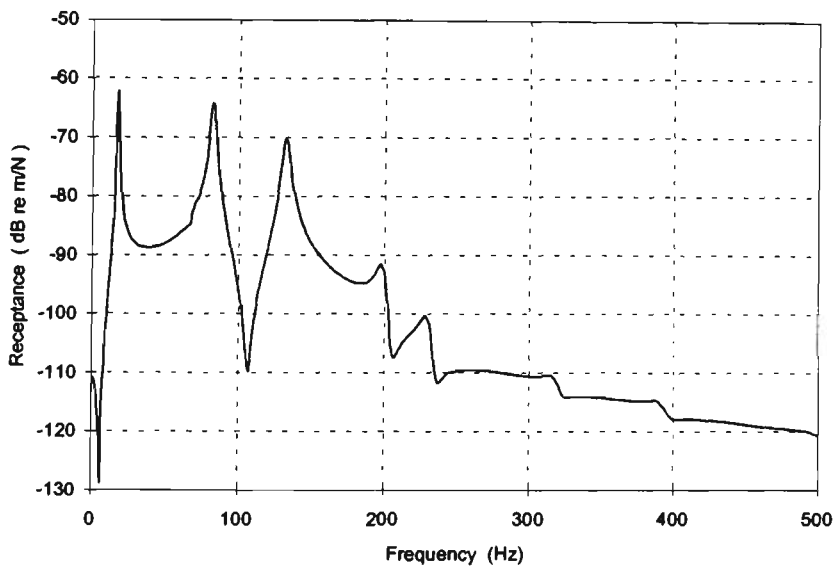


**Figure 5-9 Harmonic response displacement magnitude at node 265**

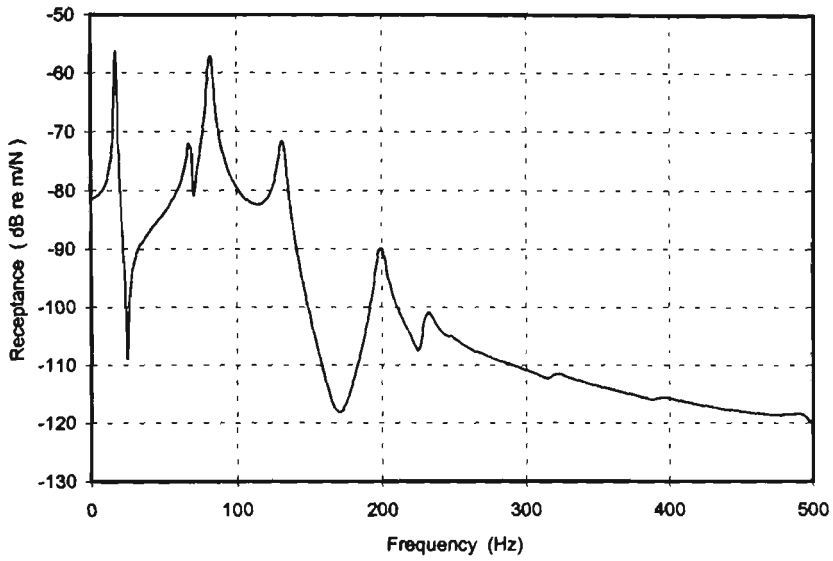


**Figure 5-10 Harmonic response displacement magnitude at node 380**

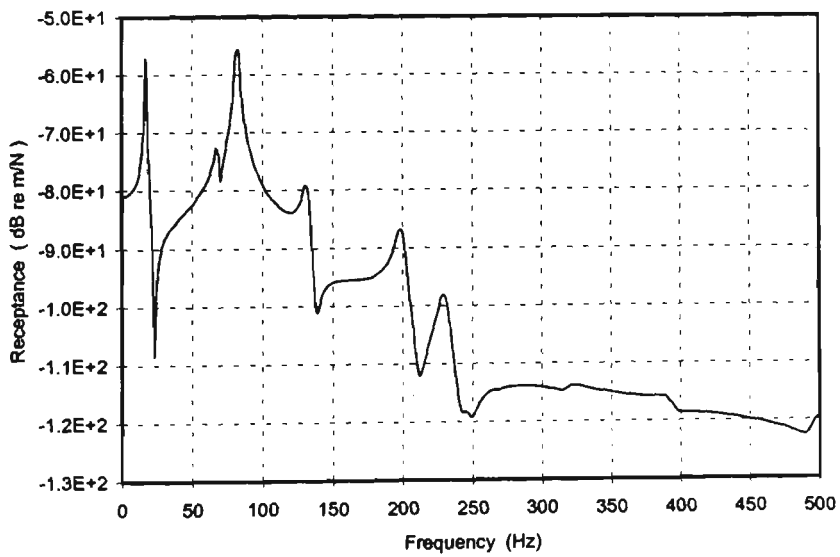


**Figure 5-11 Harmonic response displacement magnitude at node 411**

Figure 5-12, Figure 5-13, Figure 5-14 and Figure 5-15 show the displacement magnitude as a function of frequencies at various modes in linear scale.

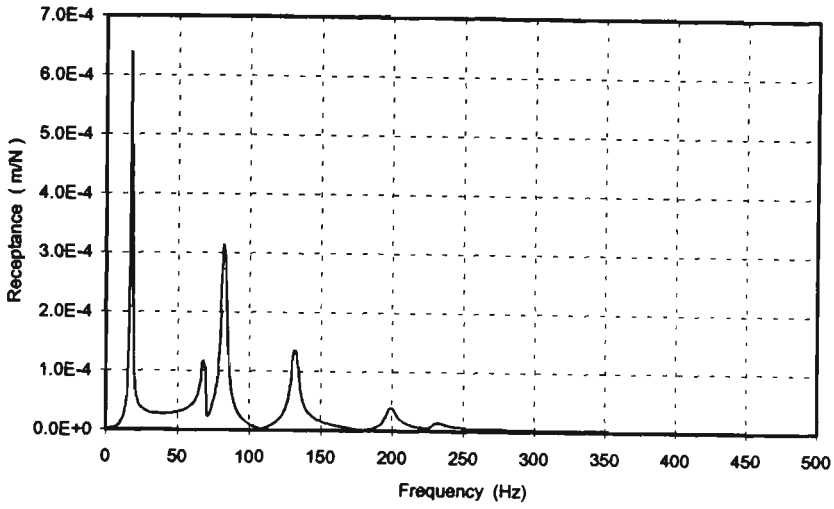


**Figure 5-12 Harmonic response displacement magnitude at node 224**

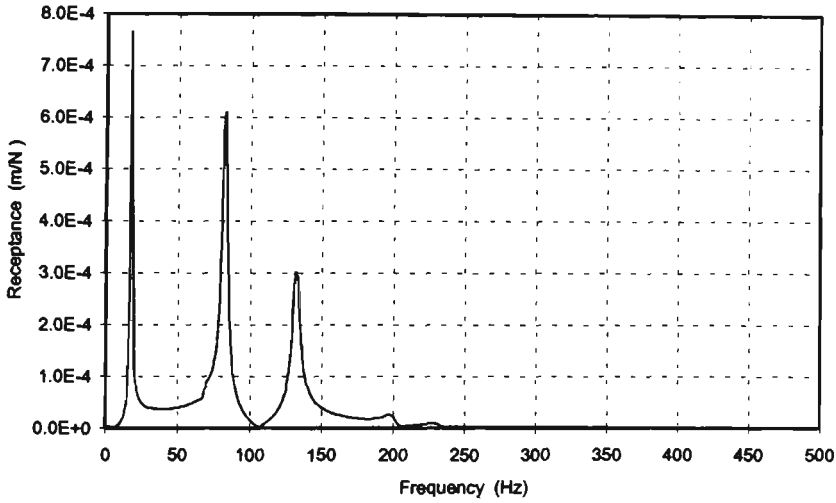


**Figure 5-13 Harmonic response displacement magnitude at node 265**

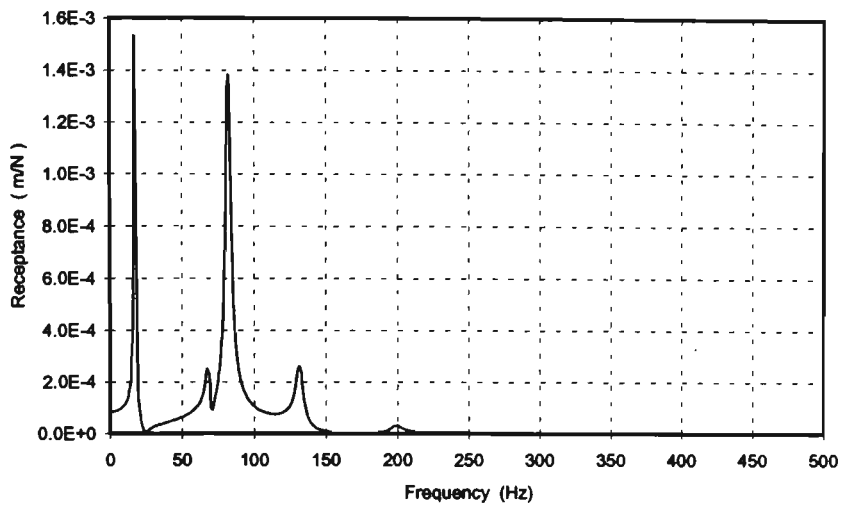


**Figure 5-14 Harmonic response displacement magnitude at node 380**

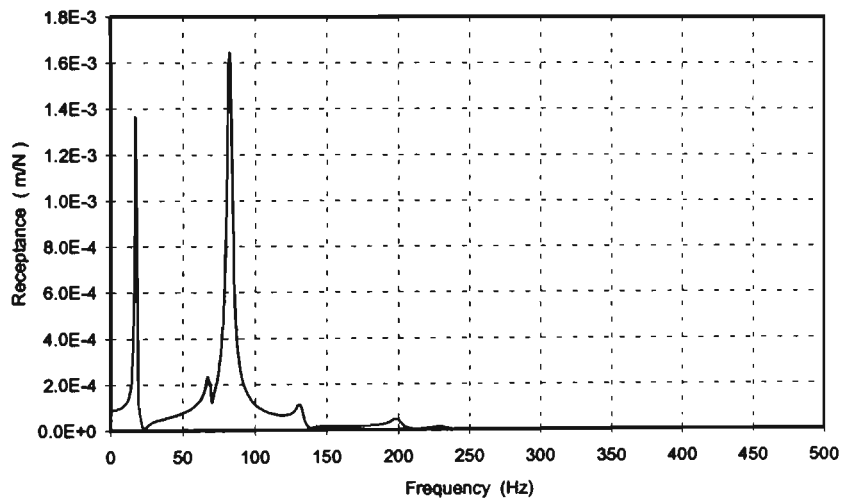


**Figure 5-15 Harmonic response displacement magnitude at node 411**

Table 5-2 shows the relationship between modes and displacement magnitude at the nodes of contact between the engine rack and engine. Small frequency variation for the same mode found by natural frequency solver at different nodes are also found. It is significant that the first and fourth modes have the highest displacement magnitude at each node, with maximum displacement of 5.14E-05 m/N at node 411 caused by the fourth mode.

**Table 5-2 Modes and displacement relationship at nodes of contact**

Mode No	Mode Hz	Node 224 m/N	Node 265 m/N	Node 380 m/N	Node 411 m/N
1	17	1.98E-05	2.37E-05	4.77E-05	4.26E-05
2	34				
3	68	3.63E-06		7.56E-06	6.76E-06
4	82	9.81E-06	1.90E-05	4.32E-05	5.14E-05
5	132			8.04E-06	3.28E-06
5	133	3.97E-06	9.66E-06		
6	197		8.19E-07		
6	198				1.42E-06
6	200	1.23E-06		9.86E-07	
7	229				3.87E-07
7	230		2.70E-07		
7	232	4.44E-07		2.79E-07	
8	245				3.81E-08
9	260		1.05E-07		
10	287				
11	314		9.34E-08		
11	322	1.05E-07		8.26E-08	
11	323				6.39E-08
12	386				5.11E-08
12	394				
12	397	6.37E-08		5.14E-08	
13	499				

Appendix C.2 shows a typical printout from the strand 6.16 harmonic response solver

## 5.3 Random Vibration

### 5.3.1 Spectral Response:

Spectral analysis available in strand is an approximate method that allows the calculation of the peak response to a specified acceleration loading. strand software allows use of different spectra types: Seismic acceleration, seismic velocity, seismic displacement and force spectrum. The first three types are assumed to excite the structure by movement of the base. The force spectrum applies a more general spectral loading at any point on the structure. All the different spectra are used in a similar manner. The acceleration response spectra are used for most shock problems.

There are three factors which are combined to give the spectral acceleration applied to the base of the structure. These are:

- The global acceleration applied to the model.
- Spectral value.
- Direction factors.

For the acceleration response spectrum, the spectral acceleration applied to the model is:

Spectral acceleration = global acceleration x direction factor x spectral value

In random vibration the product of the global acceleration and the direction factor vector defines the maximum amplitude of the applied acceleration. The spectral value is a factor that defines the effect of the acceleration on the different modes of vibration of the structure. The components of the direction vector are simply factors that multiply the applied loads. They define the direction of the seismic acceleration and may be either normalised or non-normalised.

The spectral value is defined by a spectral curve input in the tables module and it is a function of the frequency of the structure. This value defines the response ratio between the dynamic response and an equivalent static response when the structure is loaded with the peak acceleration.

In case of the engine rack loaded with an engine with 20 frequencies contributing to the response, a spectral curve is required that covers the entire frequency range and the spectral analysis should include all of these. A spectral value may then be calculated for each of the frequencies and used to excite the corresponding mode. The response for each of the modes has been combined to get the total response using the SRSS method.

Figure 5-16 shows a typical commercial truck transport random vibration spectral to which a package would be exposed during transportation phase, ASTM D4728-95 (1995). The data is an average vibration intensities measured under various loading, condition, suspension types, road conditions, weather condition, travel speed, etc. and does not represent the environment that exists in any specific transportation environment. Figure 5-17 shows the linear scale of the same random vibration PSD in the format required for input to strand load vs time table.

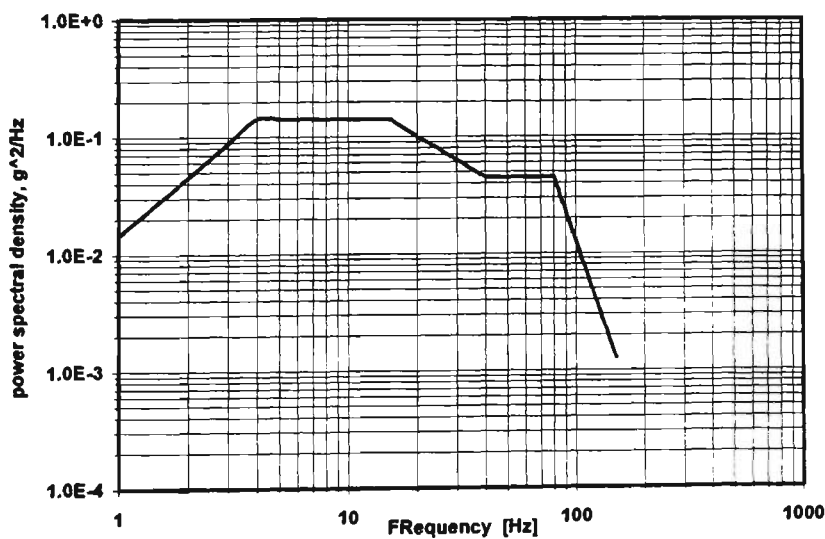


**Figure 5-16 Commercial transport random vibration PSD**

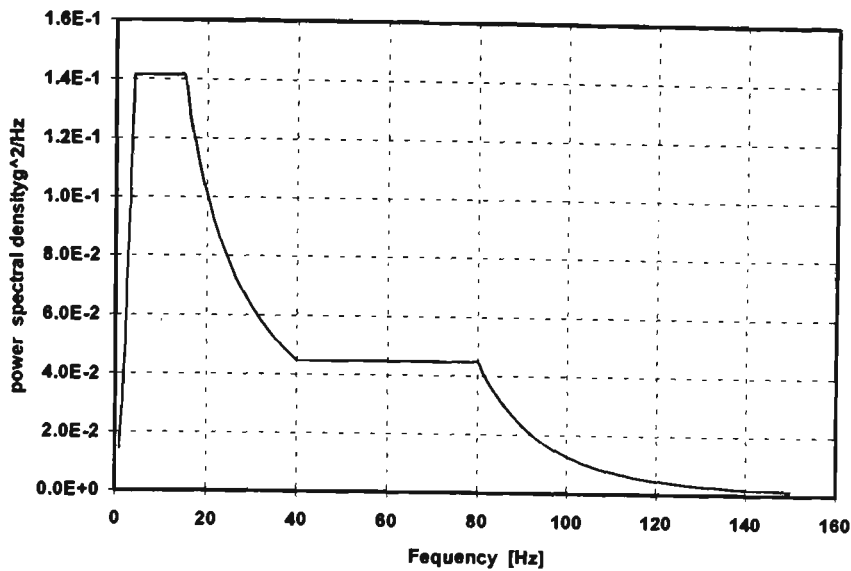


**Figure 5-17 Commercial transport random vibration PSD**

### 5.3.2 Spectral Response Analysis

Two solutions have been obtained of the spectral response solver to the previously found transport random vibration excitation spectra for the truck.

- When the full amount of excitation is acting in the Y direction only.
- When the full amount of excitation is acting in each of X, Y and Z direction.

### 5.3.3 Spectral Response in Vertical Direction only

#### Spectral Response Analysis to Vertical Excitation

A standard truck vibration spectrum Figure 5-16 was employed to act in the vertical direction (Y) only. Also it was limited to the engine rack first 6 modes.

In the spectral solver panel the direction vector will be  $V_x = 0$ ,  $V_y = 1$ ,  $V_z = 0$

and spectrum type should be set to Seismic Acceleration (Base Acceleration). For modal combination, the Square Root of the Sum of the Squares (SRSS) method was chosen as the most common approach.

Table 5-3 shows the spectral value for different modes and the spectral curve in the table module of strand. Table 5-4 shows loaded rack mass participation factors and the seismic random vibration excitation factors as a function of rack natural frequencies.

**Table 5-3 Spectral Value**

<b>Mode No</b>	<b>Frequency Hz</b>	<b>Spectral Value</b>
1	17.4	0.12
2	34.6	0.05
3	68.5	0.04
4	81.9	0.04
5	131.8	0.00
6	199.5	0.00

**Table 5-4 Seismic excitation factors and mass participation factors**

<b>Mode No</b>	<b>Frequency Hz</b>	<b>Excitation <math>g^2</math></b>	<b>Mass Partic. %</b>
1	17.4	8.82E-01	0.48
2	34.6	3.87E-03	0
3	68.5	3.37E+00	6.96
4	81.9	1.08E+01	71.44
5	131.8	4.66E+00	13.27
6	199.5	1.98E+00	Negligible

Total mass participation factor: 92.15 %

Appendix C.3 shows a typical printout from the strand solver for truck spectral response in the vertical direction (Y) only.

Table 5-5 shows the modal maximum displacement amplitude due to vertical excitation for the first six modes using modal combination SRSS method

**Table 5-5 Maximum displacements amplitude due to vertical excitation**

Mode No	Frequency Hz	Amplitude m
1	17.4	7.78E-04
2	34.6	7.87E-07
3	68.5	2.33E-04
4	81.9	5.35E-04
5	131.8	2.91E-05
6	199.5	0.00E+00

The mass participation factors indicate that the fourth and the fifth modes contribute most significantly to the response. The total mass participation factor is greater than 93%, which indicates that a sufficient number of modes was included in the analysis. The modal displacement amplitude shows that the most significant contribution to the response in the vertical direction is from the first and fourth modes. If the analysis were carried out by including only these two modes the results would be almost identical. If more analysis in the vertical direction is required then the first and fourth modes need to be included. The maximum displacement amplitude given will not occur simultaneously, these are only an envelope of the maximums which occurred during the dynamic action at different time. Also, the maximum displacements do not correspond to the maximum stresses.

Table 5-6 shows the displacement at each node where the engine in contact with the rack for each mode using SRSS. It is significant that the first and fourth modes were causing the highest displacement.

**Table 5-6 Nodal displacement at natural frequencies**

Mode No	Frequency Hz	Node 224 m	Node 265 m	Node 380 m	Node 411 m
1	17.4	-1.99E-05	-2.38E-05	4.79E-05	4.28E-05
2	34.6	-2.80E-09	-2.63E-11	3.19E-09	1.25E-10
3	68.5	4.10E-06	-8.48E-07	7.59E-06	5.38E-06
4	81.9	-1.24E-05	-2.40E-05	-5.45E-05	-6.49E-05
5	131.8	-1.78E-06	-3.94E-06	3.36E-06	1.30E-06
6	199.5	0.00E+00	0.00E+00	0.00E+00	0.00E+00

Table 5-7 shows the maximum combined nodal stress, i.e. the sum of the linear static stress and the stress resulted from the vertical excitation at the natural frequencies

**Table 5-7 Maximum nodal and plate stress for vertical excitation**

Mode No	Frequency Hz	Max. Stress $\sigma_{T_r}$ MPa	Node No	Adjacent Plates No
1	17.4	25.54	254	569, 568, 569, 570
2	34.6	1.31	46	11, 12, 20, 21
3	68.5	8.26	459	412, 413, 420, 421
4	81.9	23.21	457	371, 372, 379, 380
5	131.8	2.07	234	531, 532, 539, 540
6	199.5	Negligible	Not included	Not included

### 5.3.4 Spectral Response in Three Orthogonal Directions

#### Spectral Response Analysis (X, Y and Z Direction)

At this analysis truck vibration spectrum Figure 5-16 is acting at the three directions (X, Y and Z). In the spectral solver panel the direction vector will be  $V_x = 1$ ,  $V_y = 1$ ,  $V_z = 1$  and spectrum type should be set to Seismic Acceleration (Base Acceleration), SRSS method for modal combination.

#### Spectral Response Analysis(X, Y, and Z)

Table 5-8 shows the spectral value for different modes and the spectral curve in the table module of strand. Table shows the loaded rack mass participation factors and the seismic random vibration excitation factors as a function of rack natural frequencies.

**Table 5-8 Spectral Value**

<b>Mode No</b>	<b>Frequency Hz</b>	<b>Spectral Value</b>
1	17.4	0.12
2	34.6	0.05
3	68.5	0.04
4	81.9	0.04
5	131.8	0.003
6	199.5	0.000

**Table 5-9 Seismic excitation factors and mass participation factors**

<b>Mode No</b>	<b>Frequency Hz</b>	<b>Excitation <math>g^2</math></b>	<b>Mass Partic. %</b>
1	17.4	1.25E+01	31.95
2	34.6	1.26E+01	32.59
3	68.5	2.39E+00	1.16
4	81.9	8.66E+00	15.27
5	131.8	7.94E+00	12.85
6	199.5	1.44E+00	negligible

Total mass participation factor: 93.82 %

Appendix C.4 shows a typical printout for the strand solver for truck spectral response in three directions (X, Y and Z).

Table 5-10 shows the modal maximum displacement amplitude due to three orthogonal directions excitation for the first six modes using modal combination SRSS method.

**Table 5-10 Maximum displacements amplitude due to three orthogonal excitation directions**

<b>Mode No</b>	<b>Frequency Hz</b>	<b>Amplitude m</b>
1	17.4	1.09E-03
2	34.6	2.65E-03
3	68.5	1.64E-04
4	81.9	4.28E-04
5	131.8	4.97E-05
6	199.5	0.00E+00

The mass participation factors indicate that the first and second modes contribute most significantly to the response. The total mass participation factor is greater than 93% which indicates that sufficient number of modes was included in the analysis.

The modal displacement amplitude shows that the most significant contribution to the response in the three direction is from first and second modes. If the analysis were carried out by including only these two modes the result would be almost identical. For more analysis in the X, Y and Z direction first, second and fourth modes need to be included. The maximum amplitude values will not occur simultaneously, these are only an envelope of the maximums which occurred during the dynamic action at different time. Also, the maximum displacements do not correspond to the maximum stresses.

Table 5-11 shows the maximum displacement at each node where the engine in contact with rack for each mode using SRSS method. It is significant that first and second modes were causing the highest displacement at nodes 380 and 411, respectively.

**Table 5-11 Nodal maximum displacement at natural frequencies**

<b>Mode No</b>	<b>Frequency Hz</b>	<b>Node 224 m</b>	<b>Node 265 m</b>	<b>Node 380 m</b>	<b>Node 411 m</b>
1	17.4	-2.81E-04	-3.36E-04	6.75E-04	6.04E-04
2	34.6	-9.37E-06	-4.37E-08	1.07E-05	3.95E-07
3	68.5	-2.91E-06	5.94E-07	-5.36E-06	-3.79E-06
4	81.9	9.88E-06	-1.92E-05	-4.37E-05	-5.20E-05
5	131.8	3.04E-06	6.72E-06	-3.37E-06	-2.22E-06
6	199.5	0.00E+00	0.00E+00	0.00E+00	0.00E+00

Table 5-12 shows the maximum combined nodal stress i.e. the sum of the linear static stress and the stress resulted from three orthogonal directions excitation, at the natural frequencies.

**Table 5-12 Maximum nodal and plate stress for X, Y, and Z**

Mode No	Frequency Hz	Max. Stress $\sigma_{T_r}$ Mpa	Node No	Adjacent Plates No
1	17.4	124.9	254	569, 568, 569, 570
2	34.6	21.0	46	11, 12, 20, 21
3	68.5	5.9	459	412, 413, 420, 421
4	81.9	16.33	457	371, 372, 379, 380
5	131.8	2.81	234	531, 532, 539, 540
6	199.5	Negligible	Not included	Not included

### Material Strength

Material strength for the Rectangular Hollow Section as per AS 1163

Hot roll Rectangular Hollow Section

Minimum yield Strength = 250 MPa ( $\sigma_y$  Stress = 250 N/mm<sup>2</sup>)

Minimum Ultimate Strength = 345 MPa ( $\sigma_{ult}$  Stress = 345 N/mm<sup>2</sup>)

## 5.4 Transient Dynamic

The FE static analysis is not a sufficient analysis, especially when the maximum acceleration, velocity or displacement of a system is required to calculate the maximum energy and power, when the response of a system to time varying load is required. In these cases it is necessary to carry out a transient dynamic analysis of the system, the equations used are of the form

$$[M]\{\ddot{x}\} + [C]\{\dot{x}\} + [K]\{x\} = \{F(t)\} \quad 5.1$$

Where  $\{F(t)\}$  is the time dependent load vector.

Appendix C.5 shows Strand transient dynamic capability and condition required to execute the transient solver

### 5.4.1 Simulated Half-Sine Shock

There are several ways of specifying a shock environment simulation, including the acceleration - time history, the pulse shock, the Fourier integral spectrum and the acceleration response spectrum.

The transient dynamic analysis in which the engine rack is subject to some acceleration that varies with time. This acceleration was downward and equals the acceleration developed in the rack during impact. The rack was fixed at base (i.e. the degree of freedom is zero) where the engine rack contacts the ground.

The following is a brief outline of the shock modelling procedure that was applied.

- 1- Build the model, including all point masses, material properties, etc.
- 2- Apply freedom condition to the parts of the structure that contact the ground during the impact.

3- Apply a global acceleration in the downward (-Y) direction equal to 1 g. This will be factored by a time table as detailed below.

4- Calculate the acceleration of the frame as function of time during the impact.

If a structure is dropped from a given height then the velocity at the instant before impact is:

$$V_i = \sqrt{2 g h} \quad 5.2$$

where:

h drop height

g gravitational acceleration

$V_i$  the velocity at the instant before impact.

The following discussion is applicable to a drop height of which corresponds to the drop height recommended by the ASTM-D 4169 for testing of container with a similar condition to the loaded rack at an assurance level III. Figure 5-18 shows simulated half sine shock pulses for various coefficient of restitution and shock duration.

The following equation has been used to calculate the maximum acceleration (G) at variable coefficient of restitution (e) and shock duration ( $\tau$ ).

Appendix C.6 shows the derivation of the equation used to calculate the maximum acceleration at impact.

$$G = \frac{\pi}{2} \left( \frac{1+e}{\tau} \right) \sqrt{2 g h} \quad 5.3$$

where.

e is the coefficient of restitution.

G is the acceleration at which the object travel before impacting with the ground

$\tau$  is the shock duration measured in sec.

The necessary data files have been build in the format compatible with strand load vs time table.

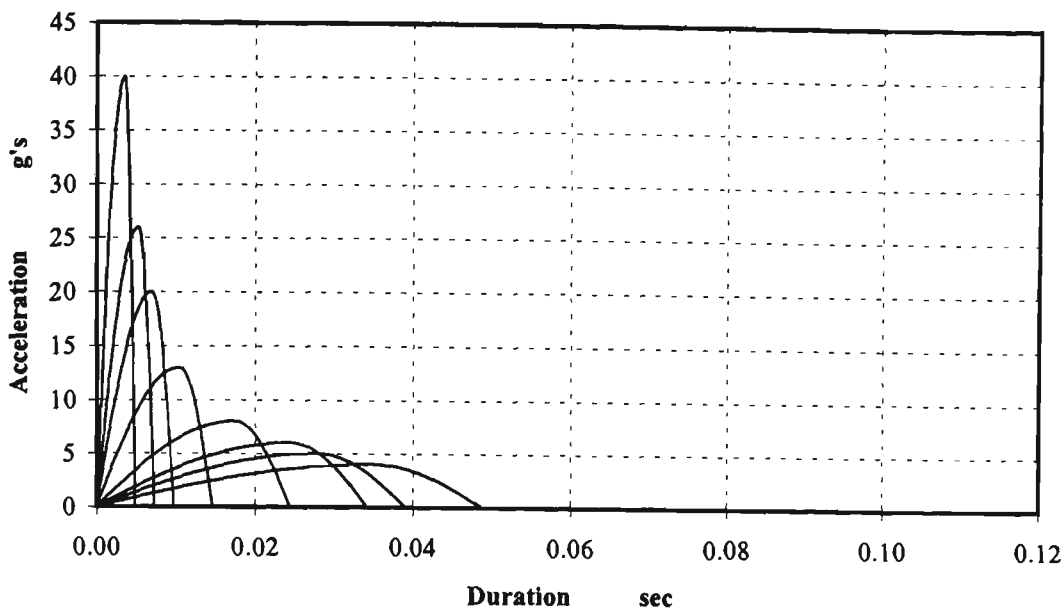


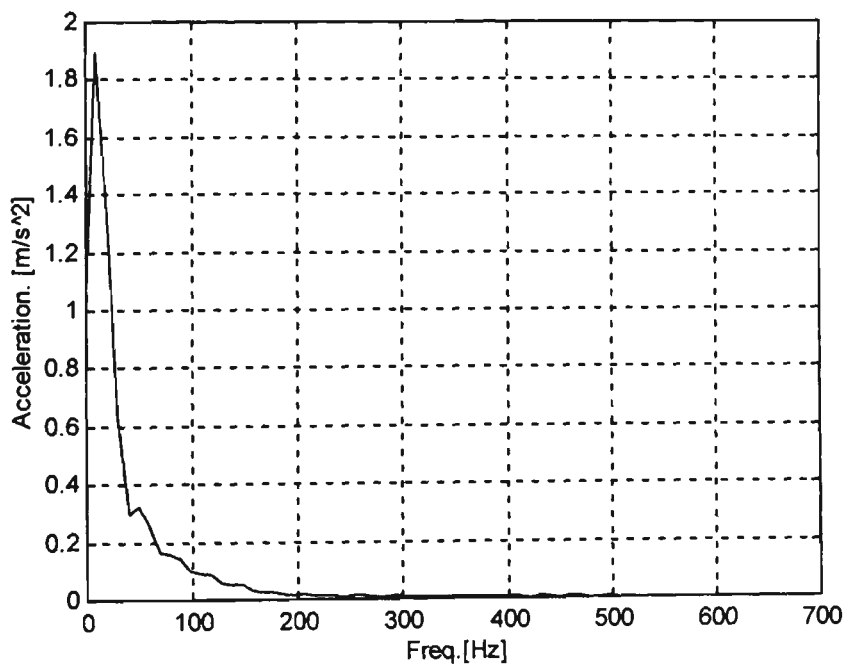
**Figure 5-18 Various shock pulses**

When the table option selected and load vs time option is chosen. The shock pulses were zero padded so that the period of time included in the table was greater than that for which the solution was carried out.

- The values in the table are the multipliers for the acceleration applied to the model.
- The graph of time table should be exactly the same as the plot of acceleration vs time shown above. The only difference is the 9.81 scaling factor.
- The transient solver used an initial velocity equal to the calculated impact velocity. Also impact problems require the use of a small time step due to the rapid rates of loading. It is important to use a time equal to approximately 1/100th of the period of the mode of the structure that will be excited during the impact. If the time step is too large, the analysis will not capture the full response of the structure.
- To define the frequency range that will be considered in the solution, the time history of the input excitation signal is required to be defined.
- Fourier spectrum decomposition is a widely used procedure for the analysis of shock data. Appendix C.7

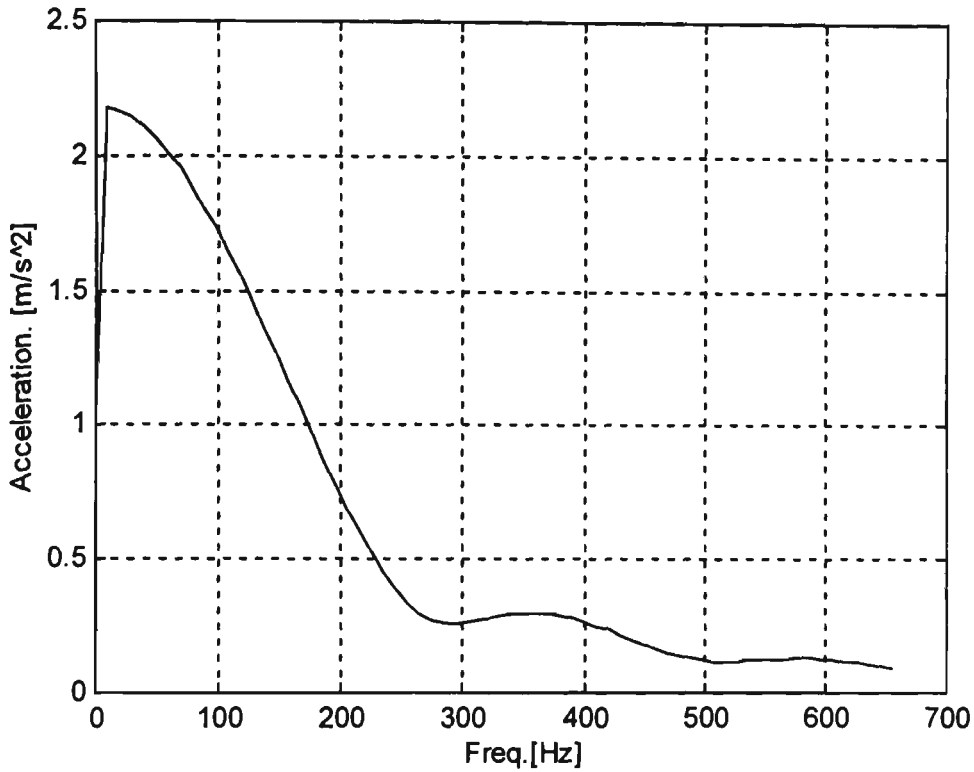
The rack was subjected in strand to several half-sine shocks whose pulses are shown in Figure 5-18. Number of modes to include in the analysis were determined from the spectral bandwidth of the shock pulses. As an example Figure 5-19 demonstrates a spectrum of a half-sine shock with the peak acceleration of 5 g, duration of 70 ms and the coefficient of restitution of 0.2, for which the effective bandwidth was less than approximately 300 Hz, Figure 5-20 corresponds to a shock with peak acceleration of 36 g, duration 10 ms and coefficient of restitution of 0.3 the effective bandwidth is significantly wider which required an inclusion of more modes in comparison to the pervious shock.

Figure 5-19 shows the acceleration spectrum of the input shock signals that have 5 g and duration of 70 ms with coefficient of restitution of 0.2.



**Figure 5-19 Acceleration spectrum of a shock signals (5 g,70 ms, e=0.2)**

Figure 5-20 shows the acceleration spectrum of the input shock signals that have 36 g and duration of 10 ms with coefficient of restitution of 0.3.

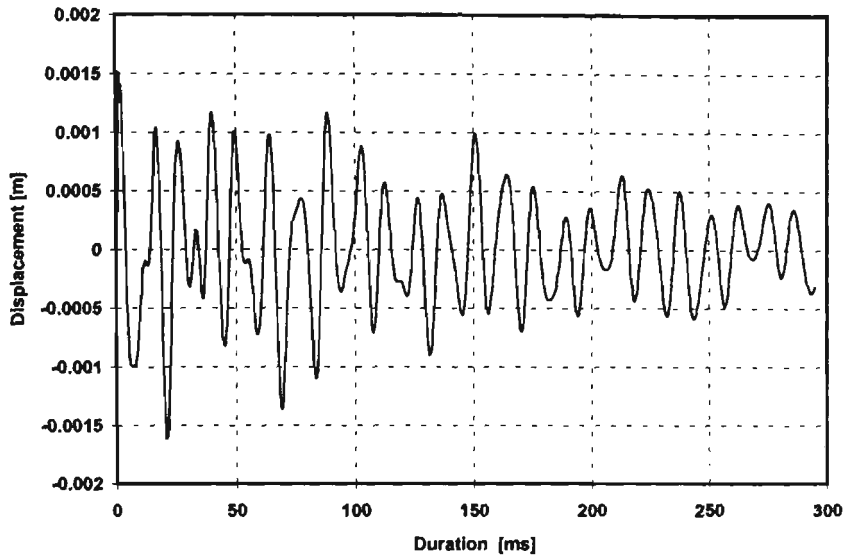


**Figure 5-20 Acceleration spectrum of a shock signal (36 g, 10 ms,  $e=0.3$ )**

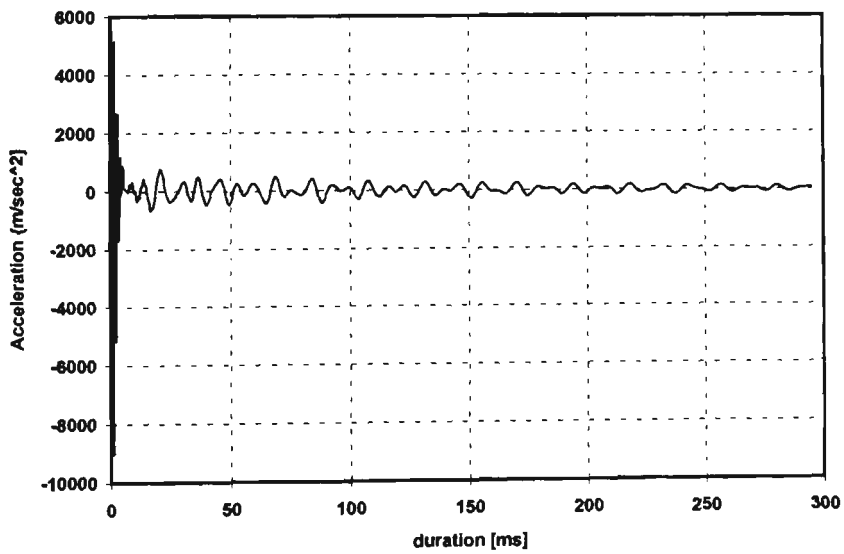
#### 5.4.2 Transient Response Analysis

The transient dynamic analysis rack response to the excitation spectrum curve that was previously defined in Figure 5-18. Also the frequency range of every spectrum has been limited to the range defined by the FFT analysis to every excitation spectrum.

Figure 5-21 and Figure 5-22 are examples of the displacement and acceleration Response respectively at the point of contact (node 224) between the rack and the engine to a half-sine excitation impulse whose spectrum is shown in Figure 5-20.

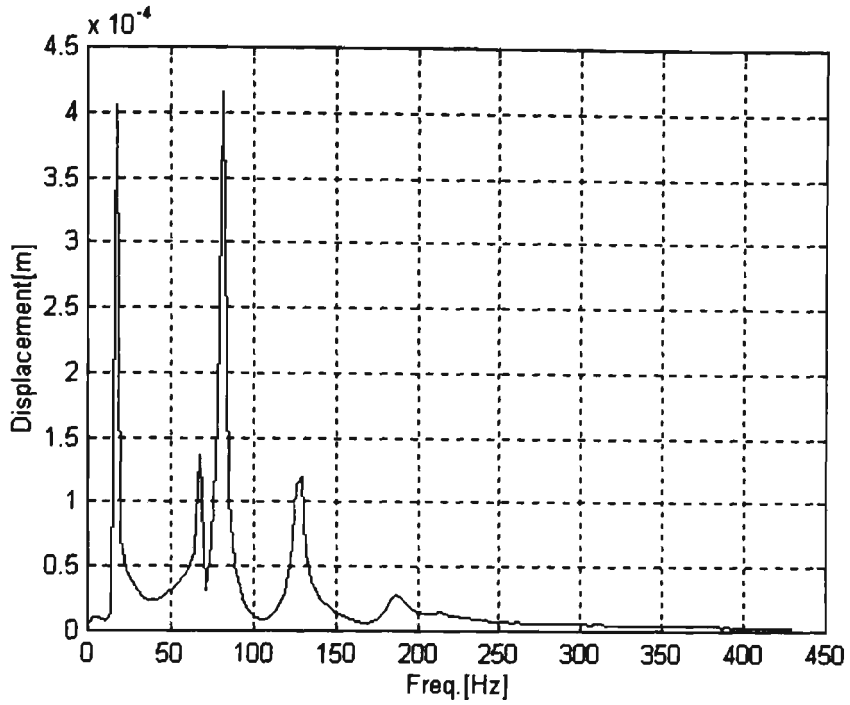


**Figure 5-21 Displacement response at node 224 to a shock (36 g, 10 ms, e=0.3)**



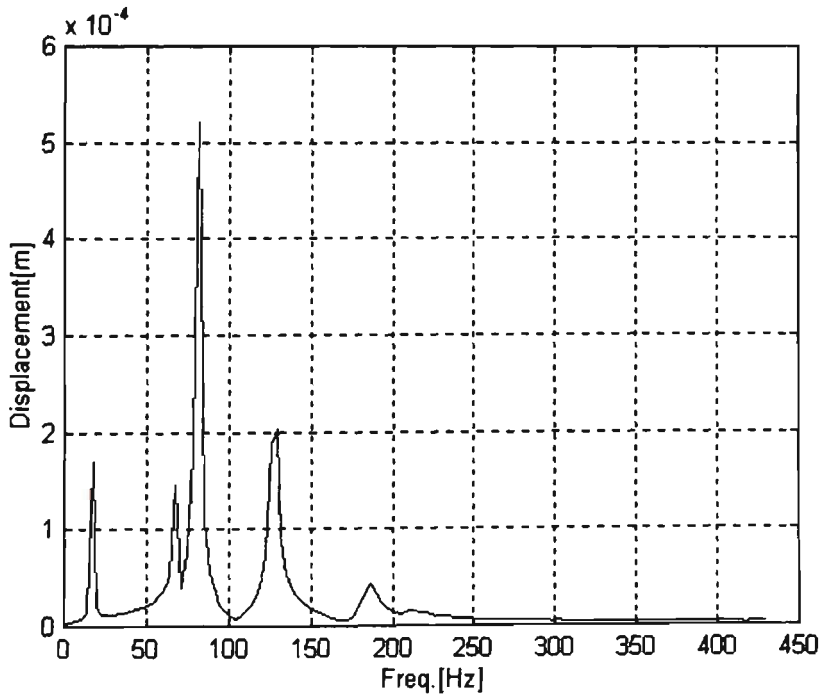
**Figure 5-22 Acceleration response at node 224 to a shock (36 g, 10 ms, e=0.3)**

Figure 5-23 shows the displacement response at node 224 to an input shock signal with peak acceleration of 5 g, duration of 70 ms and coefficient of restitution of 0.2.



**Figure 5-23 Displacement response of node 224 to 5 g,70 ms, e=0.2**

Figure 5-24 shows the displacement response at node 224 to an input shock signal with peak acceleration of 36 g, duration of 10 ms and coefficient of restitution of 0.3.



**Figure 5-24 Displacement response of node 224 to 36g, 10 ms, e=0.3**

Matlab program was written to calculate from the magnitude of the displacement response, the values of RMS, power and energy transferred to the engine assembly through the point of contact with the rack. Appendix C.8

From the displacement response curve Figure 5-23 at node 224 to 5g, 70ms, e=0.2

RMS	=	4.87E-04	m
Power	=	2.7E-07	m <sup>2</sup>
Energy	=	7.00E-08	m <sup>2</sup> s

From the displacement response curve Figure 5-24 at node 224 to 36g, 10ms, e=0.3

RMS	=	4.97E-04	m
Power	=	2.47E-07	m <sup>2</sup>
Energy	=	7.30E-08	m <sup>2</sup> s

Table 5-13 shows the energy transferred to the nodes of contact between the rack and the engine (nodes 224, 265, 380 and 411) due to different shock excitation similar to ones shown in Figure 5-18.

**Table 5-13 Displacement energy transferred at nodes 224, 265, 380 and 411**

Acc. g	Duration $\tau$ ms	Ceoff of rest. e	Freq. range Hz	Energy $m^2s$			
				224	265	380	411
32	10	0.2	600	7.33E-08	2.65E-07	1.07E-06	1.42E-06
22	15	0.2	600	9.61E-08	3.38E-07	1.50E-06	2.04E-06
16	20	0.2	500	9.18E-08	3.09E-07	1.43E-06	1.94E-06
11	30	0.2	400	6.54E-08	2.06E-07	8.47E-07	1.11E-06
7	50	0.2	300	7.48E-08	2.26E-07	9.66E-07	1.26E-06
5	70	0.2	200	7.00E-08	1.95E-07	8.39E-07	1.06E-06
4	80	0.2	150	6.42E-08	1.74E-07	7.45E-07	9.31E-07
3	100	0.2	100	5.53E-08	1.46E-07	6.35E-07	7.87E-07
36	10	0.3	600	7.30E-08	2.67E-07	1.07E-06	1.42E-06
24	15	0.3	600	9.75E-08	3.46E-07	1.52E-06	2.06E-06
18	20	0.3	500	9.55E-08	3.24E-07	1.50E-06	2.05E-06
12	30	0.3	400	6.75E-08	2.14E-07	8.84E-07	1.16E-06
17	50	0.3	300	7.42E-08	2.25E-07	9.63E-07	1.26E-06
5	70	0.3	200	6.88E-08	1.91E-07	8.20E-07	1.04E-06
4	80	0.3	150	6.41E-08	1.74E-07	7.48E-07	9.36E-07
3	100	0.3	100	5.53E-08	1.45E-07	6.30E-07	7.78E-07
40	10	0.4	600	7.29E-08	2.69E-07	1.07E-06	1.42E-06
26	15	0.4	600	9.90E-08	3.54E-07	1.55E-06	2.10E-06
20	20	0.4	500	9.93E-08	3.39E-07	1.58E-06	2.15E-06
13	30	0.4	400	6.95E-08	2.21E-07	9.24E-07	1.22E-06
8	50	0.4	300	7.48E-08	2.27E-07	9.70E-07	1.27E-06
7	70	0.4	200	7.04E-08	1.93E-07	8.22E-07	1.03E-06
5	80	0.4	150	6.65E-08	1.78E-07	7.63E-07	9.50E-07
4	100	0.4	100	5.81E-08	1.49E-07	6.47E-07	7.92E-07
41	10	0.5	600	7.13E-08	2.64E-07	1.04E-06	1.39E-06
27	15	0.5	600	9.87E-08	3.54E-07	1.54E-06	2.09E-06
21	20	0.5	500	9.95E-08	3.52E-07	1.59E-06	2.19E-06
14	30	0.5	400	7.16E-08	2.29E-07	9.66E-07	1.28E-06
8	50	0.5	300	7.36E-08	2.23E-07	9.56E-07	1.25E-06
6	70	0.5	200	6.98E-08	1.92E-07	8.17E-07	1.03E-06
5	80	0.5	150	6.60E-08	1.77E-07	7.56E-07	9.43E-07
4	100	0.5	100	5.81E-08	1.49E-07	6.46E-07	7.91E-07

Table 5-13 Cont.

Acc. g	Duration $\tau$ ms	Ceoff of rest. e	Freq. range Hz	Energy $m^2s$			
				224	265	380	411
44	10	0.6	600	7.11E-08	2.65E-07	1.04E-06	1.38E-06
29	15	0.6	600	1.00E-07	3.61E-07	1.57E-06	2.12E-06
22	20	0.6	500	1.02E-07	3.53E-07	1.63E-06	2.23E-06
15	30	0.6	400	7.37E-08	2.37E-07	1.01E-06	1.34E-06
9	50	0.6	300	7.40E-08	2.24E-07	9.57E-07	1.25E-06
6	70	0.6	200	6.93E-08	1.91E-07	8.15E-07	1.03E-06
5	80	0.6	150	6.56E-08	1.76E-07	7.52E-07	9.38E-07
4	100	0.6	100	5.81E-08	1.49E-07	6.46E-07	7.91E-07
47	10	0.7	600	7.12E-08	2.67E-07	1.05E-06	1.39E-06
31	15	0.7	600	1.02E-07	3.68E-07	1.60E-06	2.16E-06
23	20	0.7	500	1.03E-07	3.58E-07	1.65E-06	2.26E-06
16	30	0.7	400	7.59E-08	2.45E-07	1.05E-06	1.40E-06
9	50	0.7	300	7.31E-08	2.22E-07	9.46E-07	1.23E-06
7	70	0.7	200	7.13E-08	1.95E-07	8.28E-07	1.04E-06
6	80	0.7	150	6.79E-08	1.80E-07	7.66E-07	9.50E-07
5	100	0.7	100	6.10E-08	1.54E-07	6.65E-07	8.08E-07
49	10	0.8	600	7.08E-08	2.66E-07	1.04E-06	1.38E-06
33	15	0.8	600	1.03E-07	3.75E-07	1.62E-06	2.19E-06
25	20	0.8	500	1.07E-07	3.71E-07	1.71E-06	2.35E-06
16	30	0.8	400	7.67E-08	2.48E-07	1.07E-06	1.43E-06
10	50	0.8	300	7.39E-08	2.23E-07	9.52E-07	1.24E-06
7	70	0.8	200	7.09E-08	1.94E-07	8.27E-07	1.04E-06
6	80	0.8	150	6.75E-08	1.79E-07	7.63E-07	9.48E-07
5	100	0.8	100	6.08E-08	1.53E-07	6.63E-07	8.06E-07
52	10	0.9	600	7.14E-08	2.69E-07	1.05E-06	1.40E-06
35	15	0.9	600	1.05E-07	3.76E-07	1.65E-06	2.23E-06
26	20	0.9	500	1.08E-07	3.82E-07	1.73E-06	2.37E-06
17	30	0.9	400	7.87E-08	2.55E-07	1.10E-06	1.48E-06
10	50	0.9	300	7.34E-08	2.22E-07	9.46E-07	1.23E-06
7	70	0.9	200	7.04E-08	1.94E-07	8.25E-07	1.04E-06
6	80	0.9	150	6.71E-08	1.79E-07	7.61E-07	9.47E-07
5	100	0.9	100	6.06E-08	1.53E-07	6.60E-07	8.04E-07

Figure 5-25, Figure 5-26, Figure 5-27 and Figure 5-28 show the energy transferred at nodes 224, 265, 380 and 411, respectively, due to different shock excitation spectrum similar to Figure 5-18 and Table 5-13. Appendix C.9 shows listing of the matlab program to plot the energy transfer curves.

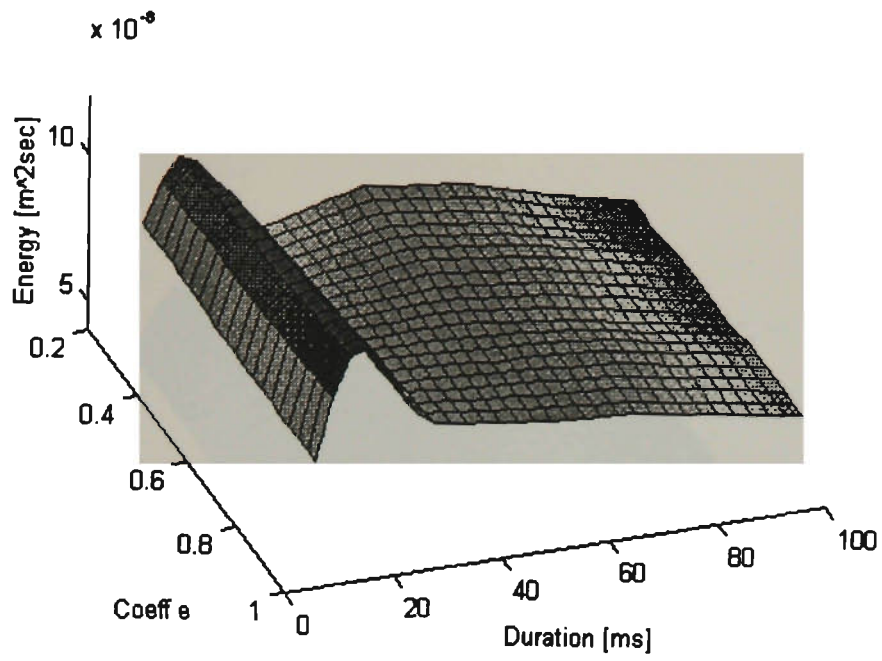


**Figure 5-25 Displacement energy transferred at node 224**

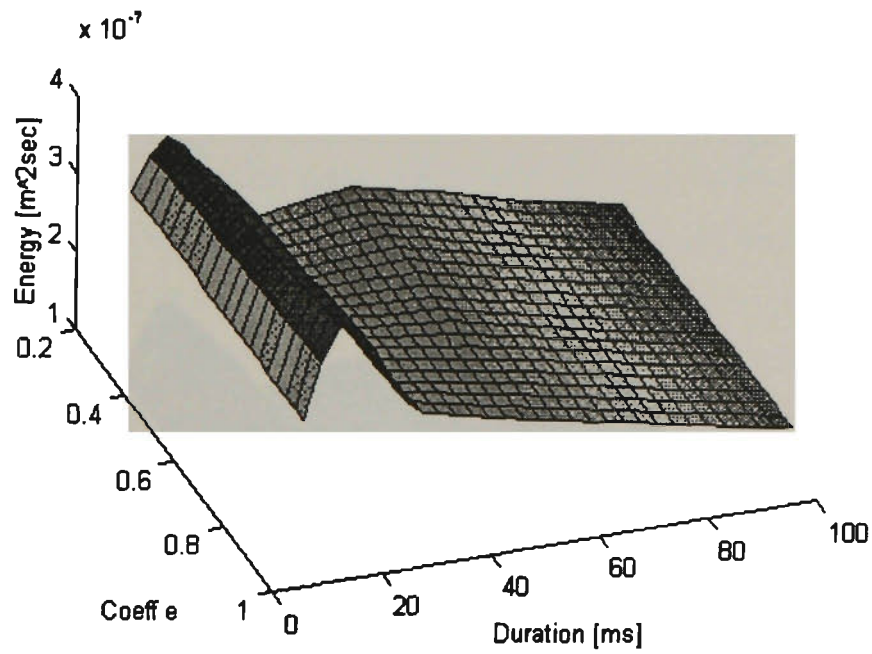


**Figure 5-26 Displacement energy transferred at node 265**

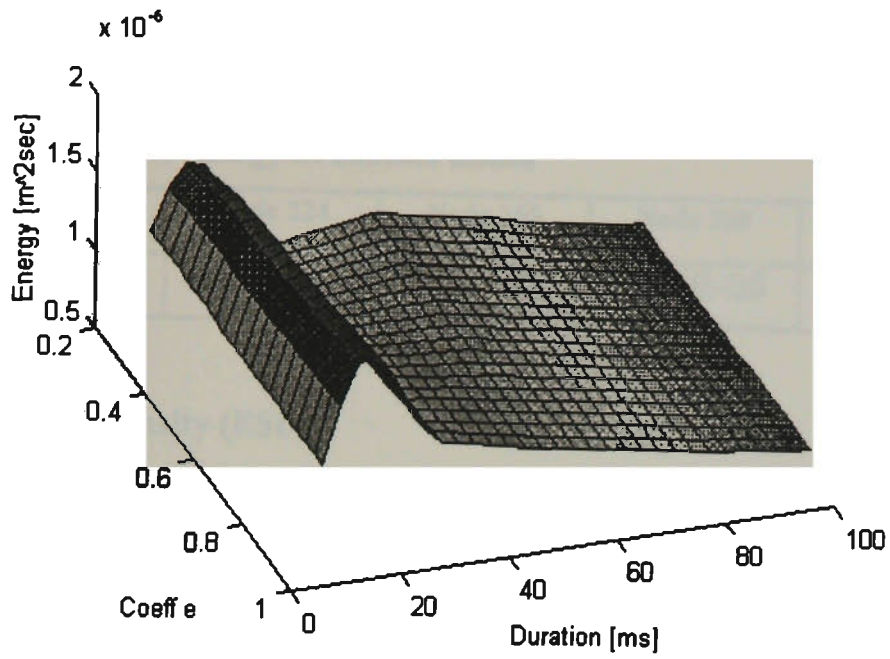


**Figure 5-27 Displacement energy transferred at node 380**

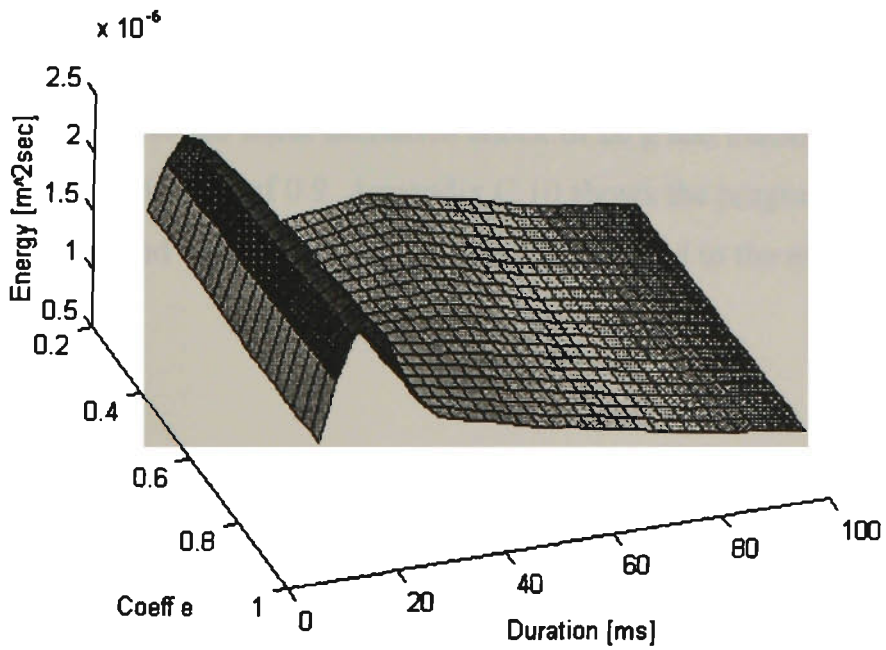


**Figure 5-28 Displacement energy transferred at node 411**

Table 5-14 shows the values of Energy Transferred to the engine assembly through Node 224, 265, 380 and 411, due to an input excitation signal that had parameters of

Acceleration	=	26	g's
Duration	=	20	ms
Coefficient of Restitution	=	0.9	

**Table 5-14 Maximum energy at contact nodes**

	Node 224	Node 265	Node 380	Node 411
ENERGY	1.08E-07	3.82E-07	1.73E-06	2.37E-06

### Energy Spectral Density (ESD)

- Short transients are one of the classes of nonstationary signal that can be defined as signals of finite duration which are to be analysed as an entity with no regard to how they varied with time. Therefore they are considered to have a finite amount of energy (amplitude squared integrated over time) and the spectrum is expressed in terms of ESD. Their length would be of the order of, or even shorter than the impulse response of the system to which they are applied or from which they result. To define the ESD distribution across the range of the frequency band, it is valid to convert the transient response signal to ESD employing FFT and PSD to calculate ESD. Figure 5-29, Figure 5-30, Figure 5-31 and Figure 5-32 show displacement ESD values transferred to the engine assembly through nodes 224, 265, 380 and 411 to the input excitation shock of 26 g and duration of 20 ms with coefficient of restitution of 0.9. Appendix C.10 shows the program used with Matelab to plot and calculate the ESD values transferred to the engine assembly.

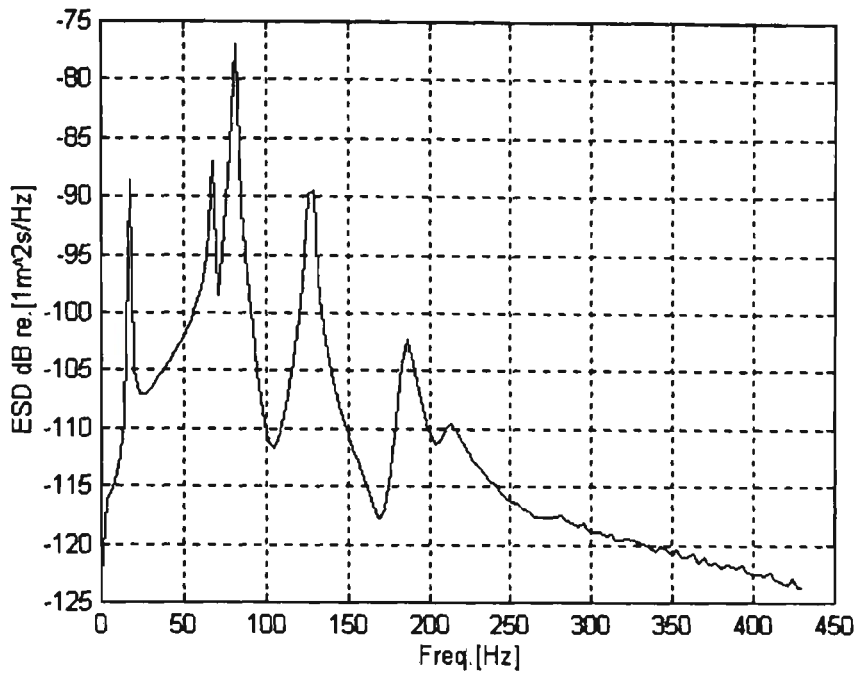


**Figure 5-29 Displacement ESD values transferred through node 224**

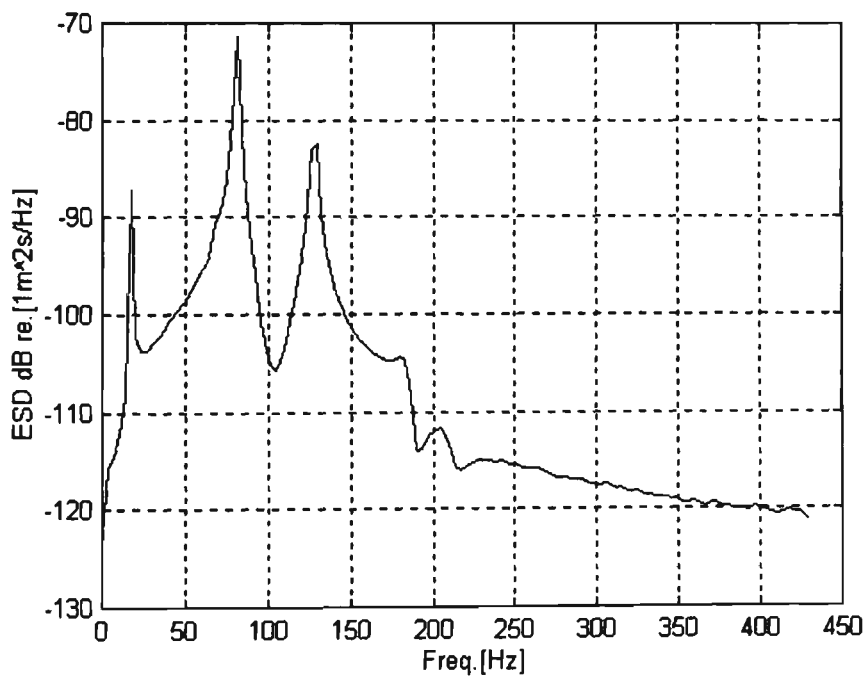


**Figure 5-30 Displacement ESD values transferred through node 265**

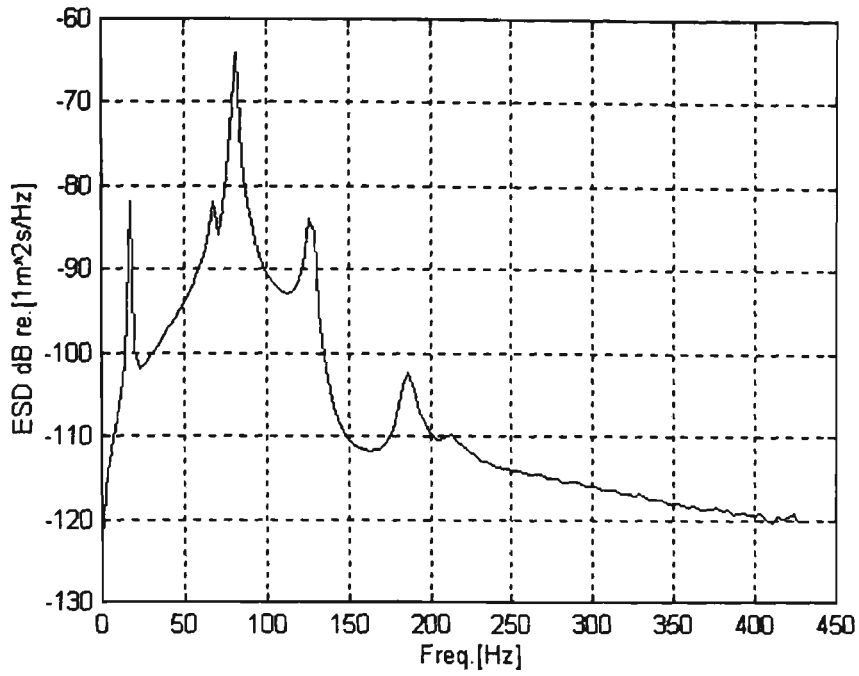


**Figure 5-31 Displacement ESD values transferred through node 380**

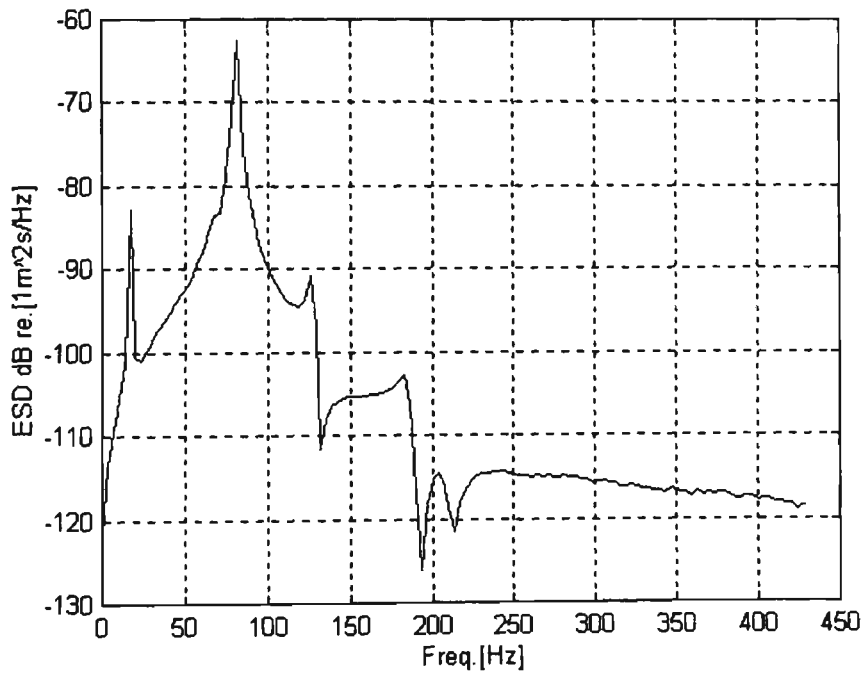


**Figure 5-32 Displacement ESD values transferred through node 411**

Figure 5-33, Figure 5-34, Figure 5-35 and Figure 5-36 show the Maximum Displacement Magnitude Response at nodes 224, 265, 380 and 411 due to an input excitation signal with parameters in the vicinity of 20 ms duration and 26 g acceleration.

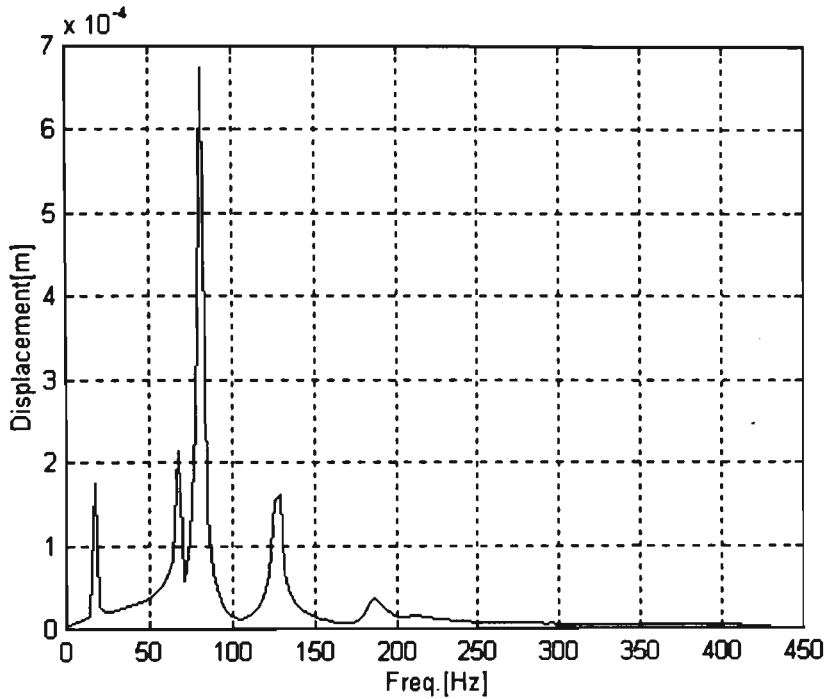


**Figure 5-33 Maximum displacement response at node 224**

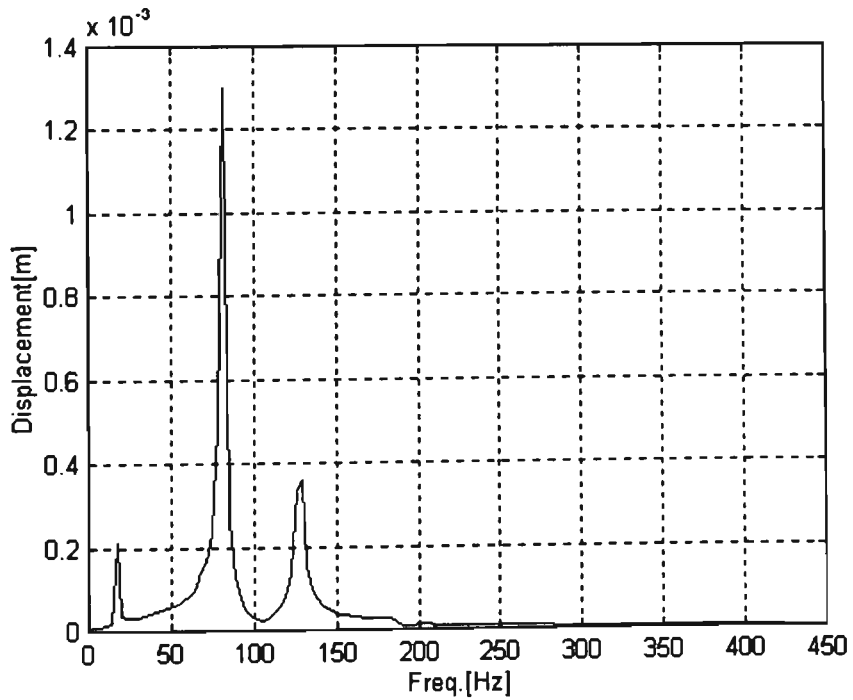


**Figure 5-34 Maximum displacement response at node 265**

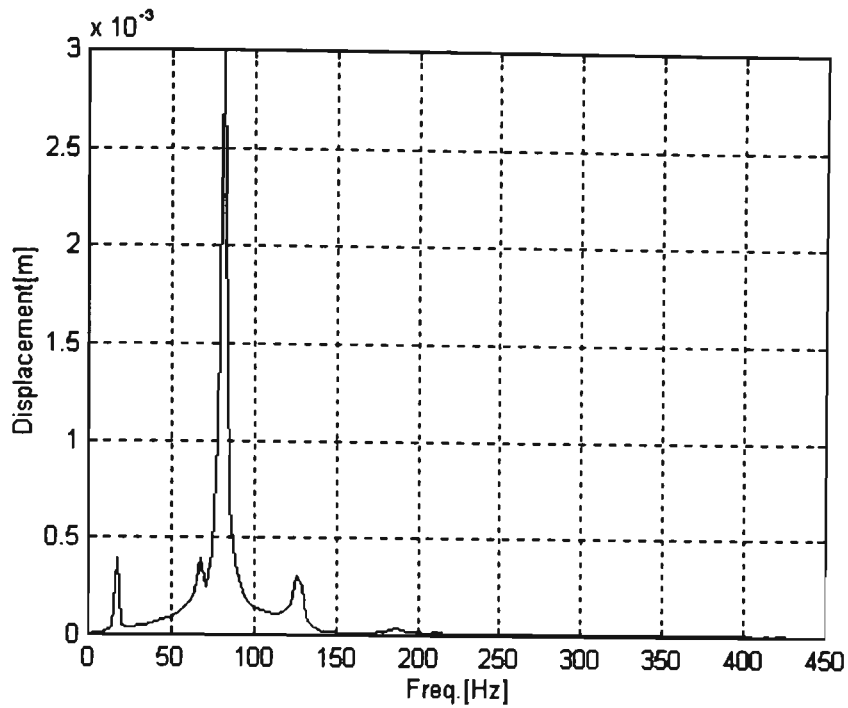


**Figure 5-35 Maximum displacement response at node 380**

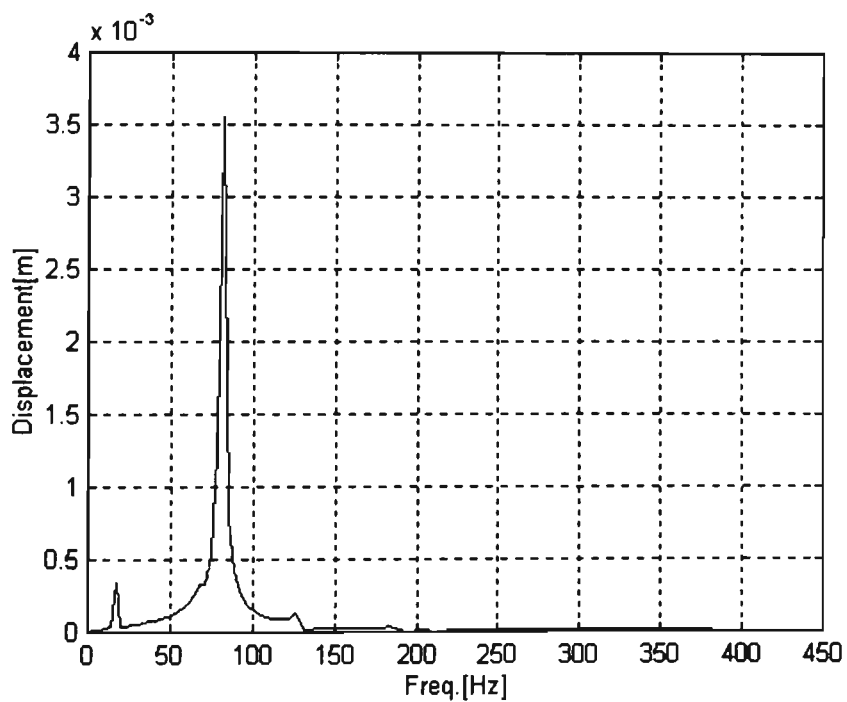


**Figure 5-36 Maximum displacement response at node 411**

Table 5-15 shows the maximums of displacement of ESD response at nodes 224, 265, 380 and 411 due to an excitation shock with parameters in vicinity of 20 ms duration.

**Table 5-15 ESD values at natural frequencies**

Mode No	Frequency Hz	ESD $\frac{m^2}{Hz}$			
		Node 224	Node 265	Node 380	Node 411
1	17.4	1.35E-08	0.66E-08	2.30E-08	1.80E-08
2	34.6	2.01E-08	0.82E-08	2.30E-08	4.40E-08
3	68.5	2.61E-08	3.52E-08	1.53E-07	2.23E-07
4	81.9	1.98E-07	2.50E-07	1.33E-006	1.87E-06
5	131.8	1.13E-08	1.91E-08	1.40E-08	0.30E-09
6	199.5	0.00E+00	0.00E+00	0.00E+00	0.00E+00

Table 5-16 shows the Maximum Displacement Magnitude Response at nodes 224, 265, 380 and 411 due to an input excitation signal with parameters in the vicinity of 20 ms duration and 26 g acceleration.

**Table 5-16 Nodal displacement at natural frequencies**

Mode No	Frequency Hz	Node 224 m	Node 265 m	Node 380 m	Node 411 m
1	17.4	1.76E-04	0.22E-03	0.40E-03	0.30E-03
2	34.6	2.15E-04	0.10E-03	0.10E-04	0.01E-04
3	68.5	2.45E-04	0.22E-03	0.40E-03	0.3E-03
4	81.9	6.74E-04	1.30E-03	3.00E-03	3.60E-03
5	131.8	1.61E-04	0.39E-03	0.30E-3	0.20E-03
6	199.5	0.00E+00	0.00E+00	0.00E+00	0.00E+00

## 5.5 Summarising Remarks

The aim of the Harmonic Response Analysis was to calculate the engine rack response to a 1N force input applied to all nodes in contact with the truck tray during the course of transport. The significance of this analysis was that it showed that the first and fourth modes had the highest displacement magnitude at each node in contact with the engine, with a maximum displacement of  $5.14E-5$  m/N at node 411, caused by fourth mode (81.9 Hz).

### Random Vibration Environment

Random vibration analysis was carried out to simulate two different environmental conditions:

- When the full power of the spectrum was acting in the vertical direction only. The analysis showed that the first and fourth modes contributed most to the displacement magnitude. However the fourth mode caused a displacement of  $-1.24E-5$ ,  $-2.4E-05$ ,  $-5.45E-05$  and  $-6.49E-05$  m/N at nodes 224, 265, 380 and 411, respectively. A maximum combined nodal stress of 25.54 MPa was found at node 254 and the surrounding plates No 569, 568, 569 and 570 at first mode (17.4 Hz).
- When the full power of the spectral was acting in three orthogonal directions. The analysis showed that the first and second modes contributed most to the displacement magnitude. However, the first mode (17.4 Hz) caused a maximum displacement of  $2.81E-04$ ,  $-3.36E-04$ ,  $-6.75E-04$  and  $-6.04E-04$  m/N at nodes 224, 265, 380 and 411, respectively. A maximum combined nodal stress of 124.9 MPa was found at node 254 and the surrounding plates No 569, 568, 569 and 570 at first mode (17.4 Hz), in comparison with Hot roll Rectangular Hollow Section (RHS).  
Minimum Yield Strength = 250 MPa ( $\sigma_y$  Stress = 250 N/mm<sup>2</sup>)

- The maximum displacement values given in both cases will not occur simultaneously, these are only an envelope of the maximums which occurred during the dynamic action at a different time. Also, it is not necessary that the

maximum displacement corresponds to the maximum stress.

### **Transient Dynamic Analysis**

Transient dynamic analysis was carried out to obtain the energy, energy spectral density (ESD) and the engine displacement response at the nodes of contact between the engine and the engine rack. The maximum total energy values found to be transferred to the engine assembly through nodes 224, 265, 380 and 411 were 1.08E-07, 3.82E-07, 1.73E-06 and 2.37E-06  $\frac{\text{m}^2\text{s}}{\text{Hz}}$  and displacement magnitude response of 4.74E-04, 1.30E-03, 3.00E-03 and 3.60E-03 m, respectively were transferred to the engine assembly at the fourth mode (81.9 Hz). As a result of an shock excitation with parameters in the vicinity of 20 ms duration.

## 6. Conclusions and Recommendations

### 6.1 Conclusions

The study of the engine rack system resulted in the following conclusions:

1. Thin Shell Plate elements yields more accurate and stable result than Linear Quad, CST and Beam elements.
2. Examination of the natural frequency results show that both the experimental and FEM results agreed within the acceptable limits of variation.
3. The finite element models correlated the FRF's with the experimental results as a consequence of simulating with the damping factor of 0.01475 which can be used in subsequent calculations.
4. The FRF experimental and FEM results were comparable.
5. FRF can be very sensitive to the exact location of the excitation and response points used in the experimental test and to the corresponding excitation and response points used in the FEA.
6. The FRF-based methods for updating the FE model are useful since each individual FRF measurement contains information on out-of-range modes as well as on those within the frequency range of interest and it is possible to specify measurement and excitation points to ensure maximum efficiency.
7. Implementing the environmental simulated condition revealed that the **Spectral Analysis** results is an approximate solution. The solution depended on the number of modes included in the analysis and maximum response is approximated as an average response of all modes. The results should be considered as a probable maximum response of the rack to the dynamic action given by the input spectral

curve. In this type of analysis the sign of all result quantities is not significant. The maximum displacement values given as results will not occur simultaneously.

8. The maximums which occurred during the dynamic action are only an envelope at different times. Also, the maximum displacements do not correspond to the maximum stress.
9. The most significant contribution to the response in the three direction (X, Y and Z) is from first and second modes. The displacement was much less than the height of the locating pin (12 mm).
10. The stress induced by the base acceleration in the three directions loading showed that the most influential modes on the randomly vibrated rack were the first, second and fourth mode, a maximum combined nodal stress of half the yield stress of the hot roll Rectangular Hollow Section (RHS) found at node 254 and the surrounding plates No 569, 568, 569 and 570 at first mode (17.4 Hz).
11. The transient dynamic analysis revealed that the maximum energy transfer to the engine assembly through nodes 224, 265, 380 and 411, due to input shock excitation with duration in the vicinity of 20 ms.
12. The FE model was shown to represent the dynamic characteristic of the rack and can be used to simulate the rack response to transportation environment

## 6.2 Recommendations

- The severe field simulation conditions used in this study are acceptable theoretically and for design purposes, but more work is required in this field to estimate the service life of the rack.
- More work is required in the finite element modelling of the shock after impact with emphasis on the nonlinear material behaviour.
- It is significant that the fourth mode is the most critical mode for transient conditions and, further investigation is required to shift this mode outside the transportation input excitation.
- Additional recommendation concerning designing for impact and vibration loading can found in Appendices D.1 and D.2.

## References

Argyris J.H. and Kelsey, S. (1960) Energy Theorems and Structural Analysis, Butterworth, London, (Collection of papers published in Aircraft Engineering in 1954 and 1955).

ASCEJ. Eng. Mech. Div.,103(6), pp 1089 -1104.

ASTM, D4728 (1995/97) Standard Test Method for Random Vibration Testing of Shipping Containers.

ASTM, D4003 (1991) Methods of Controlled Horizontal Impact Test for Shipping Containers, Selected ASTM Standards on Packaging, Third Edition.

ASTM, D4169 (1991) Practice for Performance Testing of Shipping Containers and Systems, selected ASTM Standards on Packaging. Third Edition.

ASTM, D5276 (1992) Standard Test Method for Drop Test of Loaded Container by Free Fall.

Atkinson, R. (1992) PC Based Finite Element Analysis Package, EDS, Internal Report Holden's Engine Company.

Baruch, M. and Itzhack, T. (1979) Optimal Weighted Orthogonalization of Measured Modes, TAE Report. 297.

Baruch, M. (1978) Optimisation Procedure to Correct Stiffness and Flexibility Matrices Using Vibration Test, AIAA J. 16 (11), pp 1208-1210.

Berman, A. and Fannelly, W. G. (1971) Theory of Incomplete Models of Dynamic Structures. AIAAJ., 9 (8), pp 1481 - 1487.

Berman, A. and Nagy, E.Y. (1983) Improvement of a Large Analytical Model Using Test Data, *AIAA J.*, 21 (8), pp 1168-1173.

Berman, A. (1984) Limitations on the Identification of Discrete Structural Dynamic Models, *Proc. 2nd Intl. Conference Recent Advances in Structures*, pp 427-435.

Bird, I. and Freeman, M. (1993) Current Method of Packaging and Shipping Engines, Holden's Engine Company Quality Assurance Department Report.

Blakely, K.D. and Walton, W.D. (1984) Selection of Measurement and Parameter Uncertainties for Finite Element Model. Revision. *Proceedings of the 2nd Intl. Modal Analysis Conference and Exhibit, Vol 1*, P. B. Juhl and D. J. Demichele, eds.

Bongardt, J.E. Jr. (1993) Newport News Shipbuilding. 11th IMAC Intl. Modal Analysis Conference Volume II. Kissimmee, Florida.

Broch, J.T. (1988) *Mechanical Vibration and Shock Measurements*. Brüel & Kjær

Brown, T.A. (1985) A Unified Approach to the Identification of Dynamic Behaviour Using the Theory of Vector Spaces, Ph.D. Thesis.

Brown, T.A. (1988) A Matrix Cursor for Dynamic Model Improvement Using Experimental Modes of Vibration, *GEC J. Res.*, 6 (3) pp 139-393.

Bull, K.W. and Kossack, C.F. (1963) Measuring Field Handling and Transportation Conditions, WADD Tech. Report. 60-4.

Caesar, B. (1987) Update and Identification of Dynamic Mathematical Models, *Proc. 5th Intl. Modal Analysis Conference, London, UK*. pp 453-459.

Chen, J.C., and Wada, B.K. (1975) Criteria for Analysis --Test Correlation of Structural Dynamic Systems, *J. Appl. Mech.*, pp 471-477.

Chen, J.C., Kuo, C.P. and Gaba, J.A. (1983). Direct Structure Parameter Identification by Modal Test Results, AIAA/ASME/AMS Proc. 24th Struc. Dynamic. and Material Conference, pp 44-49.

Chen, J.C., Peretti, L.F. and Garba, J.A. (1984) Spacecraft Structure System Identification by Modal Test. 25th Structures, Structural Dynamics, and Materials Conference, Pt. 2, AIAA, pp 478 - 489.

Chen, T.Y. (1987) Finite Element Model Refinement Using Analysis Data, Ph.D. Thesis, Univ. of Texas at Arlington.

Clough, R.W. (1980) The Finite Element Method after Twenty-Five Years a Personal View, Computers & Structures, 12 (4) pp. 361-370.

Collins, J.D., Hart, G.C. Hasselman, T.K. and Kennedy, B. (1974) Statistical Identification of Structures, AIAA J., 12 (2), pp 471-477.

Courant, R. (1943) Variational Methods for the Solution of Problems of Equilibrium and Vibration, Bulletin of the American Mathematical Society, Vol. 49, pp 1-23.

Creamer, N.G. and Junkins, J.C. (1988) Identification Method for Lightly Damped Structures, AIAA J. Guidance, 11 (6), pp 571-576.

Crowford, A.R. and Crowford, S. (1992) The Simplified Handbook of Vibration analysis. Computational System, Incorporated.

Cutter Information Corporation (1993) EC Packaging Debate Heats up, Environment Watch - Western Europe, 2 (7).

Dagel, Y. (1961) Ermittlung der Falholhen von Packstucken beim Verladen auf einem Guterbahnhof mit Hilfe einer Filmmethde, Verpackungs - Rundschau No. 6.

Dascotte, E. and Vanhonacker, P. (1989) Development of an Automatic Model Updating Program, Proc. 13th Intl. Modal Analysis Conference, K.U. Leuven, pp 596-602.

Dascotte, E. (1990) Practical Applications of Finite Element Tuning Using Experimental Modal Data, Proc. 8th Intl. Modal Analysis Conference, Kissimmee, Florida, pp 1032-1037.

Dobbs, M., Blakely, K. D. and Gundy, W. E. (1981) System Identification of Large - Scale Structures SAE Paper 811050.

Dobson, B. J. et al (1982) Comparison of Predicted and Measured Modal Properties 1st IMAC, Orlando, Florida, USA.

Dornier Systems (1985) Procedures for Updating Dynamic Mathematical Models, Tech. Report.

Ewins, D. J. (1979) The Whys and Wherefores of Modal Testing. J Soc. Env. Engrs, 18(3).

Ewins, D. J. (1981) State of the Art Assessment of Mobility Measurements - A Summary of European Results. Shock and Vibration Bulletin, 51 (1), pp15 - 35.

Ewins, D.J. (1984) Model Testing: Theory and Practice. John Wiley & Sons Limited.

Ewins, D.J. (1995) Modal Testing Theory and Practice. Research Studies Press Ltd.

Fillod, R., et al (1986) Parametric Correction of Regular Non-Dissipative Finite Element Models, Proc. 11th Intl. Modal Analysis Seminar, K.U. Leuven.

Foley, J.T., et al (1973b) Transportation Dynamic Environment Summary, Sandia Laboratories, EDB 1354.

Foster, C.D. and Mottershead, J.E. (1990) A Method for improving Finite Element Models by Using Experimental Data: Application and Implications for Vibration Monitoring , Intl. J. Mech. Sci., 32 (3), pp 191-203.

Fuh, J. S. , Chen, S.Y. and Beerman, A. (1984) System Identification of Analytical Models of Damped Structures. 25th Structures, Structural Dynamics, and Materials Conference, Pt. 2, AIAA, pp 112 - 116.

Gaukroger, D.R. (1984) A Note on Using Measured Vibration Modes to Modify an Analytical Model of a Structure, Tech. Memo MAI/SIR 1018.

General American Research Division Final Report. MR 1262.

Glotzbach, R.W., Wentz, R.A. and Mehta, N.C. (1977) Passenger Vibration in Transportation Vehicle, presented at Design Engineering. Tech. Conference Applied Mechanics Division Vol. 24, ASME.

Goodwin D.L., Goyal S.K. (1997) Accuracy in the Testing Protocol for Measured Drop Height in Distribution Environment. 10<sup>th</sup> IAPRI World Conference on Packaging, Melbourne, pp 201-209.

Gysin, H.P. (1986) Critical Application of the Error Matrix Method for Location of Finite Element Modeling Inaccuracies, Proc. 4th Intl. Modal Analysis Conference, pp 1339-1351..

Harrison, V.G.W. (1963) Evaluation of Package Performance, Proc. PATRA Packaging Conference, Oxford, England, pp 250-264.

Hart, G. C. and Yao, J. T. P. (1977). System Identification in Structure Dynamics.

He, J. and Ewins, D.J. (1986) Location of Damping Elements in Vibration Structure, Proc. 11th Intl. Modal Analysis Seminar, K.U. Leuven, A-2.

Heylen, W. and Janter, T. (1988) Application of the Modal Assurance Criterion in Dynamic Model Updating Proc. 13th Intl. Modal Analysis Seminar, K.U. Leuven, I-18.

Heylen, W. and Sas, P. (1987) Review of Model Optimisation Techniques, Proc. 5th Intl. Modal Analysis Conference, London, UK. pp 1177-1182.

Hoppmann, W.H. II. (1988) Shock and Vibration Handbook, chapter 9 third edition Cyril M. Harris. McGraw-Hill.

Ibrahim, S.R. (1983) Computation of Normal Modes from Identified Complex Modes, AIAA J. 21 (3), pp 446-451.

Janter, T., Heylen, W. and Sas, P. (1987) QA-model Updating Proc. 12th Intl. Modal Analysis Seminar, K.U. Leuven.

Janter, T., Heylen, W. and Sas, P. (1988) A Comparison Between Modal Optimisation Procedures Based On the Model Optimisation Parameter Set, Proc. 6th Intl. Modal Analysis Conference, Kissimmee, Florida, pp 87-92.

Janter, T., Heylen, W. and Sas, P. (1988) QA-model Updating, Proc. 13th Intl. Modal Analysis Seminar, K.U. Leuven, C-13.

Janter, T., Heylen, W. and Sas, P. (1990) Practical Application of the UA Model Updating Scheme, Proc. 8th Intl. Modal Analysis Conference, Kissimmee, Florida, pp 173-179.

Jung, H. (1990) Sensitivity Analysis Using Macro Elements, Proc. 15th Intl. Modal Analysis Seminar, K.U. Leuven.

Kim, K.O., Anderson, W.J. and Sandstrom R.E. (1983) Nonlinear Inverse Perturbation Methods in Dynamic Analysis, AIAA J. 21 (9), pp 1310-1316.

Lallement, G. and Zhang, Q., (1988) Inverse Sensitivity Based on the Eigensolution: Analysis of Some Difficulties Encountered in the Problem of Parametric, Proc. 13th Intl. Modal Analysis Seminar, K.U. Leuven, I-16.

Lallement, G. and Piranda (1990) Localisation Methods for Parametric Updating of FE Models, Proc. 8th Intl. Modal Analysis Conference, Kissimmee, Florida, pp 579-585.

Lambert, J.C. (1964) Transportability Criteria Shock and Vibration Department of the Army Technical Bulletin [ TB 55 - 100 ]. Headquarters, Department of the Army, Washington, D.C.

Lawrence, C. (1987) Identification of Differences between FiniteElement Analysis and Experimental Vibration Data, Proc.5th Intl. Modal Analysis Conference, London,UK. pp 1681-1691.

Levy, S. (1953) Structural Analysis and Influence Coefficient for Delta Wings, J.Aero. Sci., 20,(7), pp. 449-454.

Li Runfang (1992) 10th IMAC, San Diego, California.

Lieven, N.A.J. and Ewins, D.J. (1990) Error Location and Updating the Finite Element Model Using Singular Value Decomposition, Proc.8th Intl. Modal Analysis Conference, Kissimmee, Florida, pp 769-773.

Lin, R.M. and Ewins, D.J. (1990) Modal Updating Using FRF Data, Proc. 15th Intl. Modal Analysis Seminar, K.U. Leuven.

Link M. (1986) Identification of Physical System Matrices Using Incomplete Vibration Test Data, Proc. 4th Intl. Modal Analysis Conference, pp 386-393.

Lox, F. (1992) Packaging and Ecology, Pira Intl., Letherhead, Surrey.

Maia, N.M.M. (1989). An Introduction to the Singular Value Decomposition Technique (SVD), Proc. 7th Intl. Modal Analysis Conference, Las Vegas, Nevada, pp 335-339.

McAlees, J. (1962) Study of Test and Test Procedures for Packed Electronic Equipment. Packaging Consultants, Inc., Washington, D. C.

Mottershead, J.E. (1990) Theory for the Estimation of Structural Vibration Parameters from Incomplete Data, AIAA J., 28 (3), pp 559-561.

Niedbal, N. (1984) Analytical Determination of Real Modes from Measured Complex Responses, Proc. 25th Structures, Struc. Dynam. Materials Conference, pp 292-295.

O'Callahan, J.C. and Chou, C.M. (1988) Localisation of Model Errors in Optimised Mass and Stiffness Matrices Using Modal Test Data, Proc. 6th Intl. Modal Analysis Conference, Kissimmee, Florida, pp 49-55.

Ostrem, F.E. (1965) Transportation Shock and Vibration Design Criteria Manual.

Park, Y.S., Park, H.S. and Lee, S.S., Weighted (1988) Error Matrix Application to detect Stiffness Damage by Dynamic Characteristic Measurement, Intl. J. Analytical. Experimental. Modal Analysis, 3 (3).

Randall, J. A. and David, L. B. (1988) Shock and Vibration Handbook, Chapter 21, Experimental Modal Analysis, third edition Cyril M. Harris, McGraw-Hill.

Ray, W. and Cough, J.P. (1993) Dynamic of Structures, McGraw-Hill.

Richmond, R. (1993) Report on engine transport rack testing, Packaging Centre, Victoria University of Technology.

Robert, S.A. (1988) Shock and Vibration Handbook, Chapter 8, Transient Response to Step and Pulse Function third edition Cyril M. Harris. McGraw-Hill.

Robinson J. (1985) Early FEM Pioneers, Robinson & Associates, Dorset, England.

Rouillard, V., Sek M. A. and Perry, T. (1996) Analysis and Simulation of Road Profiles. ASCE Journal of Transportation Engineering, 122 (3), pp 241-245.

Rummler, T. and Schutt, W. (1993) The German Packaging Ordinance, B.Behr's Verlag, Hamburg.

Schiff, D. (1990) Assurance Technology Corporation. Carlisle, Massachusetts. Wiley - Interscience.

Sharp, A. (1992) Report of Inspection, Probable Cause of Carton Failure and Moisture Damage, and Recommendations for Future Practice", CSIRO Report No HEC2.

Sheldon, R. (1988) The Aerospace Cooperation. Shock and Vibration Handbook, chapter 23, third edition Cyril M. Harris. McGraw-Hill.

Sidhu, J. (1983) Reconciliation of Predicted and Measured Modal Properties of Structures. PhD Thesis, Department of Mechanical Engineering, Imperial College of Science and Technology, London.

Sidhu, J. and Ewins, D.J. (1984) Correlation of Finite Element and Modal Test Studies of a Practical Structure, Proc.2nd Intl. Modal Analysis Conference, Kissimmee, Florida, pp 756-762.

Sidhu, J. and Ewins, D.J. (1984)"Correlation of Finite Element and Modal Tests - Study of a Practical Structure" 2nd IMAC, Orlando, Florida.

Singh, S.P., Gary J. Burgess and Paween R. (1995). School of Packaging, Michigan State University, East Lansing, MI 48824 - 1223, USA Packaging Technology and Science Vol 8 33-41. John Wiley & Sons.

Singh, S.P., Marcondes, J. (1992) Vibration Levels in Commercial Truck Shipments as a Function of Suspension and Payload. Journal of Testing and Evaluation. JTEVA. Vol. 20. No 6. pp 466-469.

Singh, S.P., Marcondes, J. (1992) Vibration Level in Commercial Truck Shipments as a Function of Suspension and Payload. ASTM JOTE.

Singh, S. P., Voss T. (1992) Drop Heights Encountered in the United Service Small Parcel Environment in the United States, Journal of testing and Evaluation, JTEVA, Vol. 20, No 5, pp382-387.

Slater, J.C., Johnson, A.R., Fatemi, B. and Wiederrich, J.L. (1988) Model Refinement through a Statistical Analysis of a Mode Shape Difference Vector, Proc. 6th Intl. Modal Analysis Conference, Kissimmee, Florida, pp 93-99.

Tawfik, N. (1992) Redesign of the Engine Packaging system, Holden's Engine Company Design Group report.

To, W. M., Lin, R.M. and Ewins, D.J. (1990) A Criterion for the Localisation of Structure Modification Sites Using Modal Data, Proc.8th Intl. Modal Analysis Conference, Kissimmee, Florida, pp 961-967.

Turner, M.J., Clough, H.C., Martain and Topp, L.J. Stiffness and Deflection Analysis of Complex Structures, J.Aero. Sci., 23 (9), pp.805-823.

Wei, F.S. (1989) Structure Dynamic Model Modification using Vibration Test Data, Proc.7th Intl. Modal Analysis Conference, Las Vegas, Nevada, pp 562-567.

Wei, M.L. and Jantre, T. (1988) Optimisation of Mathematical Model via Selected Physical Parameters, Proc. 6th Intl. Modal Analysis Conference, Kissimmee, Florida, pp 73-79.

## Appendices

### Appendix A.1

#### Finite Element History

Beginning in 1906, research suggested a "lattice analogy" for stress analysis. The concept was replaced by a regular pattern of elastic bars. Properties of the bars were chosen in a way that caused displacements of joints to approximate displacements of points. The method sought to capitalise on well-known method of structure analysis. Courant appears to have been the first to propose the finite element method as we know it today. In 1943 mathematics lecture, published the principle of stationary potential energy and piecewise polynomial interpolation over triangular subregions to study the Saint-Venant torsion problem. Courant's (1943) work was ignored until engineers had independently developed it. None of the work was of much practical value at the time because there were no computers available to generate and solve large sets of simultaneous algebraic equation. It is no accident that the development of finite elements coincided with major advances in digital computers and programming languages.

By 1953 engineers had written stiffness equations in matrix format and solved the equations with digital computers, Levy (1953). Most of this work took place in the aerospace industry. At the time, a large problem was one with 100 d.o.f. In 1953, at the Boeing Airplane company, Turner suggested that triangular plane stress elements be used to model the skin of delta wing, Clough (1980). This work, published almost simultaneously with similar work done in England, Turner et al (1965), Argyris, Kelsey (1955). Marks the beginning of widespread use of finite elements. Much of this early work went unrecognised because of company policies against publication, Robison (1985).

The name "finite element method" was coined by Clough in 1960. The practical value of the method was soon obvious. New elements for stress analysis applications were developed, largely by chance and physical argument. 1963, the finite element method gained respectability when it was recognised as having a sound mathematical foundation, then was regarded as the solution of a variational problem by

minimisation of functional. Consequently the method was seen as applicable to all field problems that can be cast in a variational form.

General purpose finite element computer programs emerged during the late 1960s and early 1970s. Examples include ANSYS, ASKA, and NASTRAN. Each of these programs included several kinds of elements and could perform static, dynamic, and heat transfer analysis. Additional capabilities were soon added. Also added were preprocessors (for data input) and postprocessors (for results evaluation). These processors rely on graphics and make it easier, faster, and cheaper to do finite element analysis. Graphics development became intensive in the early 1980s as hardware and software for interactive graphics became available and affordable.

However, in the mid 1980s adaptation of general purpose programs began to appear on personal computers, and hundreds of analysis programs are now available.

## Appendix A.2

### The Finite Element Validation

Dobson et al (1982) describes the results obtained from a fixed system (a simple cantilever beam) in which a point defect was introduced.

#### Theory:

##### Modal Analysis and Finite Element Model

The modal analysis method assume a mathematical model for the structure of the form:

$$[M] \{\ddot{X}\} + i[H] \{\dot{x}\} + [K] \{x\} = \{F\} \quad (A.2.1)$$

The free response solution of equation (1) will yield complex natural frequencies and associated mode shapes. In particular the mode shapes may be scaled such that:

$$[\phi]^T [M] [\phi] = I \quad (A.2.2)$$

where  $[\phi]$  is the mass-normalised modal matrix. It follows that:

$$[\phi]^T [K + iH] [\phi] = \begin{bmatrix} \lambda^2 & & \\ & \lambda^2 & \\ & & \lambda^2 \end{bmatrix} \quad (A.2.3)$$

Where  $\begin{bmatrix} \lambda^2 & & \\ & \lambda^2 & \\ & & \lambda^2 \end{bmatrix}$  is the diagonal matrix of eigenvalues obtained from the free

response solution of equation (A.2.1)

Using single point harmonic excitation at coordinate (j) and measuring the response at coordinate (i) and applying equation (1) leads to the general expression for the ratio ( $x_i / f_j$ ) referred to as receptance ( $\alpha_{ij}$ ):

$$\alpha_{ij} = \frac{x_i}{f_j} = \sum_{r=1}^N r^{\phi_i} r^{\phi_j} / \omega_r^2 - \omega^2 + i \eta_r \omega_r^2 \quad (A.2.4)$$

$\omega_r$  = Natural frequency of rth mode

$\eta_r$  = Damping loss factor of rth mode

$$\lambda^2 = \omega_r^2 (1 + i \eta_r)$$

Equation (A.4.4) may be used to compute values within the modal matrix, the natural frequencies and the damping loss factors (17). This may be achieved using multi-mode curve fitting or single mode analysis through Nyquist plots (3).

Finite element analysis generally assume an undamped system represented by a mathematical model of the form:

$$[M] \{\ddot{x}\} + [K] \{x\} = \{F\} \quad (A.2.5)$$

The free response solution will yield the undamped natural frequencies ( $\bar{\omega}$ ) and associated mass normalised mode shapes  $[\bar{\phi}]$ . Unlike the modal analysis model these quantities will be real. However, for lightly damped systems with proportional damping the eigen solutions for equations (A.2.1) and (A.2.5) will be very similar:

$$\bar{\omega} \equiv \omega \quad \text{or} \quad \begin{bmatrix} \backslash & \\ & \bar{\lambda} \\ & & \backslash \end{bmatrix} \equiv \begin{bmatrix} \backslash & \\ & \lambda \\ & & \backslash \end{bmatrix} \quad (A.2.6)$$

$$[\bar{\phi}] \equiv [\phi]$$

Thus, if the complexity of the experimental results is shown to be small, comparisons of the modal parameters is possible.

Frequency response curves in the form of receptance may be computed for the finite element model using equation (A.2.4). Damping may either be ignored or experimental values may be substituted at this point.

#### Calculation of Spatial Parameters

Having obtained the experimental modal parameters it is theoretically possible to deduce the mass, stiffness and damping matrices. For a system containing N coordinates and assuming the complete set of N natural frequencies and associated N x N modal matrix have been measured, equations (A.2.2) and (A.2.3) yield:

$$[M] = [\phi]^{-T} [\phi]^{-1} = \left( [\phi] [\phi]^T \right)^{-1} \quad (A.2.7)$$

$$\text{and} \quad [K + iH] = [\phi]^{-T} \begin{bmatrix} \backslash & \\ & \lambda \\ & & \backslash \end{bmatrix} [\phi]^{-1} = \left( [\phi] \begin{bmatrix} \backslash & \\ & \lambda \\ & & \backslash \end{bmatrix} [\phi]^T \right)^{-1} \quad (A.2.8)$$

In the absence of damping equation (A.2.7) and (A.2.8) will reduce to :

$$[M] = ([\bar{\phi}][\phi]^{-T})^{-1} \quad (A2.9)$$

$$[K] = ([\bar{\phi}] \begin{bmatrix} \backslash & & \\ & \bar{\lambda} & \\ & & \backslash \end{bmatrix}^{-1} [\bar{\phi}]^T)^{-1} \quad (A.2.10)$$

However, in general whilst the finite element model will contain N coordinates, the measured data will be incomplete and may only contain 'n' coordinates at 'm' natural frequencies. Thus, the experimental modal matrices are not square and cannot be immediately inverted. It was also found during this study that the products on the right hand sides of equations (A.2.9) and (A.2.10), which are square, are often singular or ill-conditioned unless many modes are included. Further, for the complete

matrices, since:  $[\bar{\phi}] \begin{bmatrix} \backslash & & \\ & \bar{\lambda} & \\ & & \backslash \end{bmatrix}^{-1} [\bar{\phi}]^T$  represents flexibility.

From equation (A.2.9) and (A.2.10) it is possible to compute inverse mass and stiffness (flexibility) matrices:

$$[M]^{-1} = [\bar{\phi}][\phi]^{-T} \quad (A.2.11)$$

$$[K]^{-1} = [A] = [\bar{\phi}] \begin{bmatrix} \backslash & & \\ & \bar{\lambda} & \\ & & \backslash \end{bmatrix}^{-1} [\bar{\phi}]^T \quad (A.2.12)$$

If  $[\bar{\phi}]$  represent the complete N x N modal matrix it may be partitioned to the form:

$$[\bar{\phi}] = \begin{bmatrix} \phi_1 & \phi_2 \\ \phi_3 & \phi_4 \end{bmatrix} \quad (A.2.13)$$

in which  $[\phi_1]$  contains the measured mass normalised mode shape terms and is of dimensions (n x m).

$[\phi_2]$ ,  $[\phi_3]$  and  $[\phi_4]$  contain the un-measured data.

Similarly  $\begin{bmatrix} \backslash & & \\ & \lambda & \\ & & \backslash \end{bmatrix}$  may be partitioned to yield:

$$\begin{bmatrix} \backslash & & \\ & \bar{\lambda} & \\ & & \backslash \end{bmatrix} = \begin{bmatrix} \lambda_1 & 0 \\ 0 & \lambda_2 \end{bmatrix} \quad (A.2.14)$$

in which  $\begin{bmatrix} \backslash & & \\ & \lambda_1 & \\ & & \backslash \end{bmatrix}$  contains the measured eigenvalues ( $\bar{\omega}_r^2$ ) and is of dimensions (m x n).

Substituting (A.2.13) and (A.2.14) into (A.2.12) leads to the following expression for flexibility:

$$\begin{bmatrix} \left( [\phi_1][\lambda_1]^{-1} [\phi_1]^T + [\phi_2][\lambda_2]^{-1} [\phi_2]^T \right) & ; & \left( [\phi_1][\lambda_1]^{-1} [\phi_3]^T + [\phi_2][\lambda_2]^{-1} [\phi_4]^T \right) \\ \left( [\phi_3][\lambda_1]^{-1} [\phi_1]^T + [\phi_4][\lambda_2]^{-1} [\phi_2]^T \right) & ; & \left( [\phi_3][\lambda_1]^{-1} [\phi_3]^T + [\phi_4][\lambda_2]^{-1} [\phi_4]^T \right) \end{bmatrix} = [A] \quad (A.2.15)$$

Thus, the experimental values may be used to compute the contribution of the measured data to a part of the flexibility matrix. As n and m tend to N the properties of the overall flexibility calculated from incomplete data will increase. Also, since  $[\lambda_1]$  is a diagonal matrix the effects of individual modes will be strongly reflected in the computed flexibility. From equation (A.2.15) it is possible to compare finite element predictions with experimental result in terms of differences in "pseudo" flexibilities obtained from:

$$[A_e] = \left( [\phi_1][\lambda_1]^{-1} [\phi_1]^T \right)_{fe} - \left( [\phi_1][\lambda_1]^{-1} [\phi_1]^T \right)_{exp} \quad (A.2.16)$$

(nxn)                      (nxn)                      (nxn)

The resulting difference matrix may be plotted as a three - dimensional surface in order to locate regions at which large variations exist and to observe overall trends within the matrix. Sidhu (1983) has suggested an alternative approach in which the approximate error in the stiffness matrix may be evaluated from a knowledge of the "pseudo" flexibility matrices. If the error in the finite element stiffness matrix is expressed in the form:

$$[K_e] = [K_m] - [K_f] \quad (A.2.17)$$

where

$[K_m]$  represents the "correct" stiffness corresponding to measured data and  $[K_f]$  is the stiffness computed from the finite element idealisation, then:

$$[K_f] [K_m]^{-1} = (I + [K_e] [K_f]^{-1})^{-1} \quad (\text{A.2.18})$$

Under certain conditions this equation may be expanded using the binomial theorem, convergence being ensured provided that the product:

$$[K_e] [K_f]^{-1} \leq \pm 1$$

(This is generally true for a stiff, fixed structure containing small errors).

Neglecting second-order terms leads to the equation:

$$[K_e] = [K_f] ( [K_m]^{-1} - [K_f]^{-1} ) [K_f] \quad (\text{A.2.19})$$

For incomplete data the specific contribution of the measured data to the overall result may be calculated. The terms within the brackets correspond to equation (A.2.16).

$[K_f]$  which is (NxN) may be partitioned to:

$$[K_f] = \begin{bmatrix} K_1 & K_2 \\ \text{nxn} & \\ K_2^T & K_4 \end{bmatrix} \quad (\text{A.2.20})$$

$$\text{Thus : } [K_{1e}] = [K_1] ( [A_e] ) [K_1] \quad (\text{A.2.21})$$

$[K_1]$  may be obtained from the full finite element stiffness matrix by simply removing rows and columns corresponding to coordinates at which measurements were not obtained. Again, the resulting error matrix may be plotted as a three dimensional surface.

The error matrices generated from equation (A.2.16) and (A.2.21) may be computed in two ways; using all of the measured modes or using the measured modes separately. Since particular defects may only affect specific modes this latter method should enable the detection of several errors with a given structure.

## Appendix B.1

### Natural Frequency as obtained by strand software

Strand 6.15 Natural Frequency solver

File : C:\HOS11\H-4185-1\H-4185-1

678 Nodes    8 Beams.    604 Plates.    0 Bricks.

Consistent element mass matrices.

Plate Drilling Freedoms are Suppressed.

Sorting Nodes : Tree method

Initializing Graph for Mesh Sorting.

Forming Beam List.

Forming Plate List.

Pass number 1

Maximum Beam Bandwidth	=	84
at Beam Number	=	1
Maximum Plate Bandwidth	=	246
at Plate Number	=	234
Maximum half bandwidth	=	246
Avarage bandwidth	=	102
Number of equations	=	4044
Matrix vector length	=	413790

Creating Matrix.    104 Blocks.

Sorting Elements.

Assembling    8 Beams.

Beam Assembly Complete.

Assembling    604 Thin Shells.

Thin Shell Assembly Complete.

Detection of Singularity in Stiffness Matrix and

Automatic Suppression of Drilling Freedoms.

No Singularity Detected.

Executing Eigenvalue Solver.

Shifting matrix.

Degrees of freedom excited by starting vector

3333	1065	3326	2223	3057	2991	2619	2217
1755	1569	1863	2133	2349	2457	2571	3189
2234	1293	2043	2139	2355	2463	2757	2859
2925	3123	1179					
Reducing		4044	Equations.				

## Appendix B.2

### Strand 6.16 Harmonic Response solver

File : D:\HOS6\H4185-2\H4185-2

678 Nodes. 8 Beams. 604 Plates. 0 Bricks.

Load Cases = 1

Consistent Load Vector for Beam UDLs.

Consistent Load Vector for Plate Pressure.

Mesh is NOT SORTED

PASS NUMBER 1

Maximum Beam Bandwidth = 12

at Beam Number = 1

Maximum Plate Bandwidth = 2574

at Plate Number = 598

Sorting Elements.

Assembling PoIntl Load Case : 1

PoIntl Load Assembly Complete.

Assembling 8 Beams.

Beam Assembly Complete.

Assembling 604 Thin Shells.

Thin Shell Assembly Complete.

Calculating Total Applied Loads

Summation of Loads Applied to Structure

Load Case : 1

Direct summations

FX FY FZ MX MY MZ

0.00000E+00 0.14563E+03 0.00000E+00 0.00000E+00 0.00000E+00 0.74115E-21

Moments about the origin

MX MY MZ

-0.36045E+02 0.00000E+00 0.52537E+02

Calculating 100 steps

## Appendix C.1

### Strand 6.16 Natural Frequency Solver

File : C:\TRANST-1\TRAN6\TRAN6

710 Nodes. 4 Beams. 635 Plates. 0 Bricks.

Consistent element mass matrices.

Plate Drilling Freedoms are Suppressed.

Sorting Nodes : TREE METHOD

Initializing Graph for Mesh Sorting.

Forming Beam List.

Forming Plate List.

#### PASS NUMBER 1

Maximum Beam Bandwidth	=	390
at Beam Number	=	4
Maximum Plate Bandwidth	=	408
at Plate Number	=	477
Maximum half bandwidth	=	408
Avarage bandwidth	=	192
Number of equations	=	4236
Matrix vector length	=	811830

Creating Matrix. 203 Blocks.

Sorting Elements.

Assembling 4 Beams.

Beam Assembly Complete.

Assembling 2 Plates.

Plate Assembly Complete.

Assembling 633 Thin Shells.

Thin Shell Assembly Complete.

Detection of Singularity in Stiffness Matrix and  
Automatic Suppression of Drilling Freedoms.

No Singularity Detected.

Executing Eigenvalue Solver.

Degree of freedom excited by starting vector

2889	387	2882	147	2085	1803	879	357
39	3	33	1017	861	681	141	2529
58	1509	1263	1077	687	585	363	279
111	2295	105					

Reducing 4236 Equations.

The first 20 eigenvalues have converged.

## Appendix C.2

### Strand 6.16 Harmonic Response Solver

File : C:\TRANST-1\TRAN6\TRAN6

710 Nodes. 4 Beams. 635 Plates. 0 Bricks.

Load Cases = 1

Lumped Load Vector for Beam UDLs.

Lumped Load Vector for Plate Pressure.

Mesh is not sorted

Pass number 1

Maximum Beam Bandwidth = 12

at Beam Number = 1

Maximum Plate Bandwidth = 2772

at Plate Number = 609

Sorting Elements.

Assembling PoIntl Load Case : 1

PoIntl Load Assembly Complete.

Assembling 4 Beams.

Beam Assembly Complete.

Assembling 2 Plates.

Plate Assembly Complete.

Assembling 633 Thin Shells.

Thin Shell Assembly Complete.

Calculating Total Applied Loads

Summation of Loads Applied to Structure

Load Case : 1 Direct summations

FX	FY	FZ	MX	MY	MZ
0.00E+00	1.61E+03	0.00E+00	0.00E+00	0.00E+00	0.00E+00

Moments about the origin

MX	MY	MZ
.39536E+3	0.00E+00	4.67E+03

### Appendix C.3

#### Strand 6.16 Spectral Response in Orthogonal Direction (Y) solver

File : C:\TRANST-1\TRAN6\TRAN6

710 Nodes. 4 Beams. 635 Plates. 0 Bricks.

Load Cases = 1

Lumped Load Vector for Beam UDLs.

Lumped Load Vector for Plate Pressure

Consistent element mass matrices

Plate Drilling Freedoms are Suppressed.

Sorting Nodes : Tree method

Initializing Graph for Mesh Sorting.

Forming Beam List.

Forming Plate List.

Pass number 1

Maximum Beam Bandwidth = 390

at Beam Number = 4

Maximum Plate Bandwidth = 408

at Plate Number = 477

Creating Matrix. 203 Blocks.

Sorting Elements.

Calculating Spectral Values

Beam Assembly Complete.

Assembling 2 Plates.

Plate Assembly Complete.

Assembling 633 Thin Shells.

Thin Shell Assembly Complete.

Executing Spectral Response Solver.

Mass matrix: Consistent

## Appendix C.4

File : C:\TRANST-1\TRAN6\TRAN6

Heading : STRAND6.16

10 Nodes.      4 Beams.      635 Plates.      0 Bricks.

Load Cases = 1

Lumped Load Vector for Beam UDLs.

Lumped Load Vector for Plate Pressure.

Consistent element mass matrices.

Plate Drilling Freedoms are Suppressed.

Sorting Nodes : Tree method

Initializing Graph for Mesh Sorting.

Forming Beam List.

Forming Plate List.

Pass number 1

Maximum Beam Bandwidth            =      390

at Beam Number                        =      4

Maximum Plate Bandwidth            =      408

at Plate Number                        =      477

Creating Matrix.      203 Blocks.

Sorting Elements.

Calculating Spectral Values

WARNING! Frequency of 1.996E+0002 is outside the range of Table: 1

Value set to zero      Assembling      4 Beams.

Beam Assembly Complete.

Assembling      2 Plates.

Plate Assembly Complete.

Assembling      633 Thin Shells.

Thin Shell Assembly Complete.

Executing Spectral Response Solver.

Mass matrix :      Consistent

## Appendix C.5

### Transient Dynamic

transient dynamic equations used are of the form

$$[M]\{\ddot{x}\} + [C]\{\dot{x}\} + [K]\{x\} = \{F(t)\} \quad (C.5.1)$$

Where  $\{F(t)\}$  is the time dependent load vector.

A transient analysis can be performed by selecting the Transient Dynamics option in the solver menu. It is important that an eigen analysis must be performed on the structure before commencing a transient analysis since the fundamental eigenvalue is required for determining the time step for the solution. Transient solver allows to re-select whether the Wilson- $\theta$  or Newmark- $\beta$  method is used. Time Step Increment, the time step size used for Integration, the default and recommended value is automatically selected, but this may be altered if required. The number of time steps that the solution proceeds for is then selected. The time step Interval should be chosen depending upon how much of the analysis is required.

Strand also allows several other initial condition to be specified. If required the analysis can be started with the structure already having an initial displacements, which may occur when a structure is displaced and then released. It is also possible to specify initial overall velocities and accelerations in the x, y and z directions, these allow the possibility of carrying out impact analysis.

Applies a time-stepping algorithm to determine the response of a structure to a time dependent loading defined by a load vs time table or mathematical equation. In addition to this steady loads such as load point, pressures and global accelerations can be applied. The response of the structure can be calculated when it is released from some initially displaced condition; defined by reference to the results of a linear static load case. Combinations of applied loads and initial conditions can also be considered. Modal damping may be applied.

**Time Step Increment :**

The choice of time step is of importance as far as the resolution of solution is concerned. As the frequency increases the time step should be made finer so that details of the response are not missed by the solution.

**Solution Method:**

The two solution methods available are the Wilson- $\theta$  and the Newmark- $\beta$  methods. The two constants  $\theta$  and  $\beta$ , are used to control the stability of the solution process. By choosing the correct value, both methods are unconditionally stable.

**Calculate Stress:**

The nodal and elemental stresses can be calculated and saved for every time step in the structure.

**Calculate Velocity :**

The velocities of each node in the global coordinate system can be calculated. Since these are obtained by differentiating the calculated displacements, the accuracy is not as good as for displacement.

**Calculate Acceleration :**

The acceleration of each node in the global coordinate system can be calculated. These are obtained by taking the double derivative of the calculated displacements and hence the error will be greater than for the velocity.

**Damping Factor:**

If damping selected to ON, software gives the option to modify any or all of  $\xi_1$ ,  $\xi_2$ ,  $\omega_1$  and  $\omega_2$  (Hertz) by editing the following parameters:

Damp. Fact. 1, Frequency. 1, Damp. Fact. 2 and Frequency. 2.

Frequency 1 default to the lowest mode determined by the natural frequency solver and Frequency 2 default to the highest mode.

Damping can be included in the analysis automatically or through manual input. If a sufficient number of eigenvalues have been selected (normally three is sufficient), the default damping ratios are set to 0.01 and the two frequencies at which these damping ratio occur correspond to the lowest and highest eigenvalues from the eigen analysis, all these values may be altered manually.

**Initial Condition- Load Case :**

If required the analysis can be started with the structure already having an initial displacement, which may occur when structure is displaced and then released.

**Initial Velocity :**

Three real values, VX, VY, and VZ are required here to define the initial velocity vector for the structure in global coordinates. Every free node is assigned these velocities instantaneously at time zero.

**Initial Acceleration :**

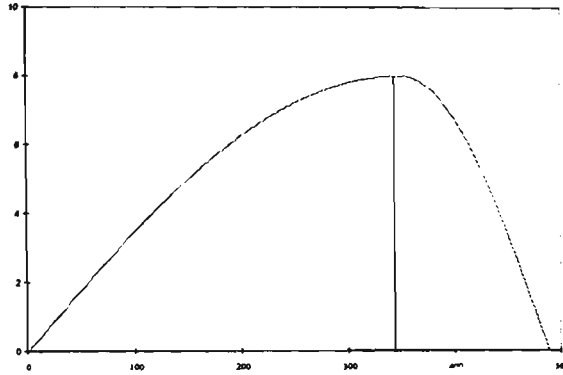
Three real values, AX, AY, and AZ are required here to define the initial acceleration vector for the structure in global coordinates. These accelerations have the same significance as the initial velocities, that is they are assigned to every node instantaneously at time zero.

**Case / LVT :**

Load case option allows the selection of the load case that is to be used for the analysis and the Load Vs Time Table specifies the table to be used to dictate how the loading on the structure varies with time.

## Appendix C.6

The following equation has been used to calculate the maximum acceleration ( $G$ ) at variable Coefficient of Restitution ( $e$ ) and shock duration ( $\tau$ ).



$$\Delta V = \frac{2}{\pi} G\tau$$

$$V_i = \frac{2}{\pi} G\tau_1 = \sqrt{2gh}$$

$$V_r = \frac{2}{\pi} G\tau_2$$

$$\Delta V = V_i - V_r = \frac{2}{\pi} (\tau_1 + \tau_2)$$

$$e = \frac{V_r}{V_i}$$

$$V_r = e V_i = \frac{2}{\pi} G\tau_1 e$$

$$\tau_2 = \tau_1 e$$

$$\tau_1 + \tau_1 e = \tau$$

$$\tau_1 = \frac{\tau}{1+e}$$

$$V_i = \frac{2}{\pi} G \frac{\tau}{1+e} = \sqrt{2gh}$$

then

$$G = \frac{\pi}{2} \left( \frac{1+e}{\tau} \right) \sqrt{2gh}$$

## Appendix C.7

The following Matlab program was used to calculate the magnitude spectrum a signal

```
load d:\mat-2\m057002.txt
t=m057002(:,1);
a=m057002(:,2);
dt=t(2)-t(1);
sfreq=1/dt;
npts=length(a);
spec=fft(a);
spec=spec/npts;
spec=spec(1:npts/2+1);
spec=abs(spec);
spec(2:npts/2)=spec(2:npts/2)*2;
df=sfreq/npts;
f=[0:df:(length(spec)-1)*df]';
plot(f(1:length(f)/15),spec(1:length(f)/15),'b');
grid on
xlabel('Freq.[Hz]')
ylabel('acceleration[m/s^2]')
```

## Appendix C.8

The following Matlab program was used to calculate from the parameters of a transient and its spectrum the Displacement Response magnitude the values of RMS, power, and energy transferred to the engine assembly through the point of contact with the rack.

```
load d:\mat\table25.txt
t=table25(:,1);
a=table25(:,2);
dt=t(2)-t(1);
sfreq=1/dt;
npts=length(a);
rms=sqrt(sum(a.^2) ./npts);
power=rms^2
energy=sum(a.^2).*dt*(npts-1)
spec=fft(a);
spec=spec/npts;
spec=spec(1:npts/2+1);
spec=abs(spec);
spec(2:npts/2)=spec(2:npts/2)*2;
df=sfreq/npts;
f=[0:df:(length(spec)-1)*df]';
clf
plot(f(1:length(f)/2),spec(1:length(f)/2),'b')
grid on
xlabel('Freq.[Hz]')
ylabel('Displacement[m]')
```

## Appendix C.9

The following Matlab program was used to generate Figures 5-25 to 5-28 representing the energy transferred to engine through rack due to different input excitation shock spectrum similar to Figure5-18

```
load d:\mat-2\energ2.txt
z=energ2(:,1);
z = reshape(z,8,8)
x= [0.2000  0.3000  0.4000  0.5000  0.6000  0.7000  0.8000  0.9000]
y= [10 15 20 30 50 70 80 100]
xi = linspace(x(1),x(length(x)),20)
yi = linspace(y(1),y(length(y)),30)
zi = Intlerp2(x,y,z,xi,yi);
grid on
surf(xi,yi,zi)
view(-290,50)
title('fft of node 224 table 42')
xlabel('Duration[ms]')
ylabel('Energy[m^2sec]')
zlabel('Coeff e')
```

## Appendix C.10

Show the formate used with Matlab to plot and calculate the ESD values transferred to the engine assembly.

```
load d:\bill-1\table92.txt
t=table92(:,1);
a=table92(:,8);
dt=t(2)-t(1);
sfreq=1/dt;
npts=length(a);
rms=sqrt(sum(a.^2) ./npts);
power=rms^2
energy=sum(a.^2).*dt
spec=fft(a);
spec=spec/npts;
spec=spec(1:npts/2+1);
spec=abs(spec);
spec(2:npts/2)=spec(2:npts/2)*2;
df=sfreq/npts;
f=[0:df:(length(spec)-1)*df]';
mag=spec
psd=mag.^2/2./df
duration = t(length(t));
esd = psd .* duration;
clf
plot(f(1:length(f)/2),10*log10(esd(1:length(f)/2)),'b')
grid on

xlabel('Freq.[Hz]')
ylabel('ESD dB re.[1m^2s/Hz]')
whitebg
system_dependent(40,'on')
```

## Appendix D.1

### Recommendations Related to Designing for Impact

- The rack members should be designed as an energy absorbing system. The aim is to have the maximum volume of material stressed to the highest working stress. This increases capacity to absorb energy.
- For any given cross-section of the member, have the maximum area subjected to the maximum allowable stress. The entire length of member should be subjected to this maximum stress.
- Stress concentrations should be reduced to a minimum and abrupt changes in section avoided.
- The impact formulas can be used as a guide in the proper design of a member rather than as the actual determinant of the impact stress or impact deformation.
- Use of steel with higher yield strength and higher values of modulus of resilience perform better under impact. i.e. material should have a high modulus of resilience  $U = \sigma_y^2 / 2E$ . This is the energy absorbed per unit volume. Although a lower modulus of elasticity (E) appears to be helpful, materials of lower (E) generally have correspondingly lower values of yield strength ( $\sigma_y$ ), and this latter value is more important because it is squared.
- The material should have high fatigue strength, although this is not considered to be so important as high yield strength.
- The material should be positioned so that the direction of hot rolling (sheet or bar in steel mill) is in line with the impact force, because the impact strength in this direction is higher than that at right angles to the direction of rolling.
- It is important to restrict the weight of the member and maintain optimum rigidity of the member for its particular use or service. This means that light-weight, well-stiffened members having adequate moment of inertia should be used.
- To build in protection against inertia forces caused by the rapid movement of a member due to explosions etc, it is important to decrease the possible acceleration and/ or deceleration of this member through some form of flexible support.
-

## **Appendix D.2**

### **Recommendations Relating to Designing for Vibration Loading**

- Careful fabrication and smooth transition of sections enhances fatigue loading capacity.
- Use simple butt welds rather than lap or T fillet welds.
- Avoid excessive reinforcement, undercut, overlap, lack of penetration, roughness of weld, sharp corners and weld placement in areas which are subjected to flexing.
- For designing under critical loading conditions, place material so that the direction of rolling (of sheet in steel mill) is in line with the loading force, because the fatigue strength may be higher in this direction than if placed at right angles to the direction of rolling.
- Where possible, form the member into the shape that it tends to assume under load, and hence prevent the resulting flexile movement.
- Avoid designing structures operating in the critical or resonant frequency of individual members or the whole structure in order to prevent excessive vibration.
- Prestressing a beam in axial compression will reduce the tensile bending stress and lessen the chance for fatigue failure even though the compressive bending stress is increased to some extent.
- Avoid designing involving eccentric application of loads which may cause additional flexing with each application of load.
- The use of stiffeners decreases flexibility of members and results in better fatigue strength.